Molecular Association in Biological and Related Systems

Published on June 1, 1968 on http://pubs.acs.org | doi: 10.1021/ba-1968-0084.fw001

Molecular Association in Biological and Related Systems

A symposium sponsored by
the Division of Colloid
and Surface Chemistry at
the 153rd Meeting of the
American Chemical Society,
Miami Beach, Fla.,
April 13-14, 1967.

E. D. Goddard, *Symposium Chairman*

ADVANCES IN CHEMISTRY SERIES 84

AMERICAN CHEMICAL SOCIETY
WASHINGTON, D. C. 1968

Library of Congress Catalog Card 68-59079

PRINTED IN THE UNITED STATES OF AMERICA

Advances in Chemistry Series

Robert F. Gould, *Editor*

AMERICAN CHEMICAL SOCIETY PUBLICATIONS

FOREWORD

ADVANCES IN CHEMISTRY SERIES was founded in 1949 by the American Chemical Society as an outlet for symposia and collections of data in special areas of topical interest that could not be accommodated in the Society's journals. It provides a medium for symposia that would otherwise be fragmented, their papers distributed among several journals or not published at all. Papers are refereed critically according to ACS editorial standards and receive the careful attention and processing characteristic of ACS publications. Papers published in ADVANCES IN CHEMISTRY SERIES are original contributions not published elsewhere in whole or major part and include reports of research as well as reviews since symposia may embrace both types of presentation.

PREFACE

Traditionally, colloid and surface chemists have displayed an active interest in studies of materials of biological origin. Pioneers of the concept of molecular orientation at interfaces, such as William Hardy and Irving Langmuir, were well aware of the biological implications of their work. In the decades preceding World War II, flourishing schools of colloid science were established, which were actively engaged in studies of interactions involving materials of biological interest. At E. K. Rideal's school in Cambridge, emphasis centered chiefly on interactions occurring at interfaces, and at Bungenberg de Jong's school in Leiden, emphasis was largely on the colloidal approach. This era saw the growing development and acceptance of the concept of monomolecular layers in membranes, as supported by the Gorter and Grendel analysis of the lipid content of red cells and the more complete hypothesis of the bimolecular leaflet structure of membranes advanced by Davson and Danielli. The tremendous upsurge in interest in these phenomena that has occurred since the war needs no emphasis. Investigators in the various realms of biology and medicine are now well aware of the important role that surface and colloid chemistry plays in the study of biological systems and their functions. It is thus no coincidence that many different disciplines are represented in the contributions that make up this volume.

It is impossible to write an introduction to a collection of such papers without being acutely aware of the pioneering contributions of J. H. Schulman, whose untimely death in June 1967 robbed surface and colloid chemistry of one of its most gifted investigators. His insight in the field of biology has been a source of inspiration to many and will long be remembered. We are indeed fortunate to have a paper coauthored by him as one of the contributions to this volume.

Edgewater, N. J.
February 1968

E. D. Goddard

Interaction of Water with Alkyl-Substituted Amides

P. ASSARSSON

Sterling Forest Research Center, Union Carbide Corp., Tuxedo, N. Y.

F. R. EIRICH

Polytechnic Institute of Brooklyn, Brooklyn, N. Y.

Phase diagrams from freezing point depressions show true compound formations for simpler amides—e.g., *water*-N-*methylacetamide forms a compound at a mole ratio of 2 to 1, water*-N,N-*dimethylacetamide at 3 to 2 and 3 to 1, and water*-N-*methylpyrrolidone at 2 to 1. The heats of mixing and heat capacities at 25°C. of a number of water-amide systems were determined. All mixing curves were exothermic and possess maxima at definite mole ratios, while the heat capacities for the most part show distinct curvature changes at the characteristic mole ratios. Both experimental results point to the stability of the particular complexes even at room temperature. This is further supported by absolute viscosity studies over the whole concentration range where large maxima occur at these same mole ratios for disubstituted amides and* N-*substituted pyrrolidones.*

Amides in general have been the subject of considerable discussion in the literature, prompted among other things by their versatility as solvents for organic and inorganic compounds, and serving as models in elucidating the physical properties of the peptide bond. Furthermore, amide-water mixtures are commonly used binary solvents or reaction media in chemical rate and equilibrium studies. The above applications are then ample reasons for taking a critical look at the physical properties of aqueous solutions of amides, trying to establish the mechanism and energetics of the interaction pattern throughout the complete concentration range. The solution process of any particular amide may be arbitrarily divided and discussed in terms of the amide dipole association

with water molecules, the influence of the hydrophobic alkyl substituents on the strength of the amide group, and the possible structural changes of water in the solvation sphere.

Those amides which are soluble in all proportions in water at room temperature follow a general trend in that the fully substituted amides are capable of bringing into solution a greater number of alkyl carbons than the mono- or unsubstituted ones—*e.g.*, the upper limit for *N*-disubstituted acetamides is a pair of propyl groups, while for the *N*-monosubstituted acetamide the butyl group appears to represent the maximum. Acetamide, on the other hand, is only partially soluble in water, and in contrast to most other amides, the heat of solution for this binary mixture is endothermic. It is evident that the breaking of hydrogen bonds in bulk and their reforming between the amide dipole in solution and water are the predominant features governing this particular solubility pattern.

The preference of the peptide group, found in *N*-methylacetamide, to associate selectively with water rather than with itself has been demonstrated through investigation in the near-infrared region by spectroscopic investigation following the N—H absorption band in the 1.5-micron region (*8*).

The atomic coordinates for the planar amide bond were first charted by Pauling and co-workers (*9*) in their investigation of the structure of proteins, and later confirmed in x-ray studies (*4*, *7*). Ample experimental evidence also exists, mainly from NMR data on *N*-alkyl substituted amides, in support of the partial double bond character of the N=—C

O

bond, although estimates of the amount of double bond character vary from the 40% originally proposed by Pauling to lower values of about 25% (*5*). The electrical moment of the amide bond calculated from the individually known bond polarities has a value of about 3.4 *D*, for *N*-methylacetamide, or roughly 1 *D* less than found experimentally. This discrepancy has been referred to as another indication of a double bond character in the nitrogen-carbon bond (*11*). The pertinent dimensions of the planar peptide bond in trans-configuration are shown opposite. [Actually the complete planarity of amides containing the —NH_2 group may be questioned in view of the shallow pyramid shape shown for formamide by microwave spectroscopy (*5*).]

The basicity of the amide bond, when the substituents are changed, remains almost constant or increases slightly with increasing size of the substituents. These results were obtained from infrared studies and potentiometric titrations of *N*,*N*-disubstituted amides in several organic solvents (*1*) and corroborated by the magnitude of the experimentally obtained electrical moments (*12*).

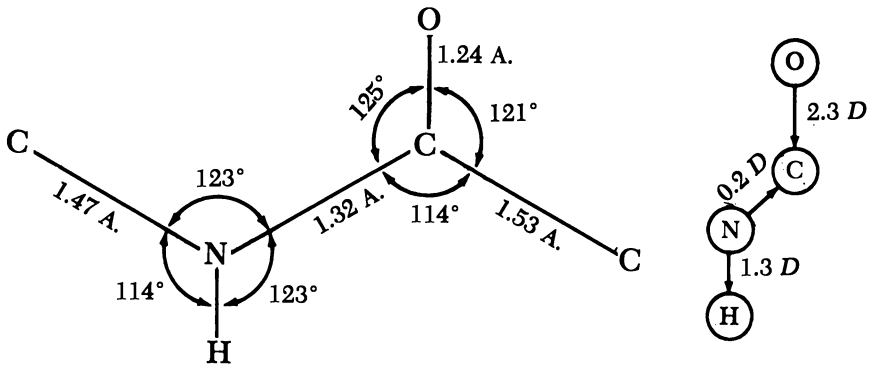

The work introduced here concerns the aqueous solutions of amide groups or peptide dipoles studied with the help of substituted amides which are soluble over the entire concentration region. Specifically, attention has been focused on *N,N*-disubstituted acetamides where the —R groups have been varied in pairs from methyl to propyl or isopropyl, *N*-monosubstituted acetamides with —R either a methyl or ethyl group, and *N*-substituted pyrrolidones with —R either a methyl or isobutyl group. These choices allow one to study the mechanism of hydration of the peptide dipole unaffected by coulombic charges. Various experimental techniques have been utilized, aimed at probing the energetics of water binding and possibly elucidating where "complexing" occurs between the amide group and water. Secondly, when possible, we have been looking for noticeable changes in the water structure which might accompany the solution process.

Results

Experimental. VISCOSITIES. The absolute viscosities in centipoises (cp.) for several amide-water systems at 25°C. were obtained using calibrated Ubbelohde viscometers and calculated from $\eta = \rho[Kt - L/t]$ where ρ is density of mixture, and K and L are instrument constants. The results, plotted against the mole fraction of water, are shown in Figures 1 and 8.

There are two rather striking features—the large magnitudes of the maxima in the case of the fully *N*-substituted acetamides or pyrrolidones which extend from about 1 to 2 cp. for the pure amides to between 4 and 5 cp. at the maxima, and the three families of curves, according to which specific mole fraction ratios the respective maxima occur. The fully *N*-substituted acetamides, *N,N*-dimethylacetamide (DMA), *N,N*-diethylacetamide (DEA), *N,N*-di-*n*-propylacetamide (Dn-PA), and *N,N*-diisopropylacetamide (Di-PA), together with *N,N*-diethylformamide with

a smaller maximum (no figure) have their maxima close to a mole ratio of 3 waters to 1 amide (3 to 1). These results may be compared with previously published data on DMA and are in fair agreement with respect to that maximum at a mole ratio of 2.7 to 1 (*10*).

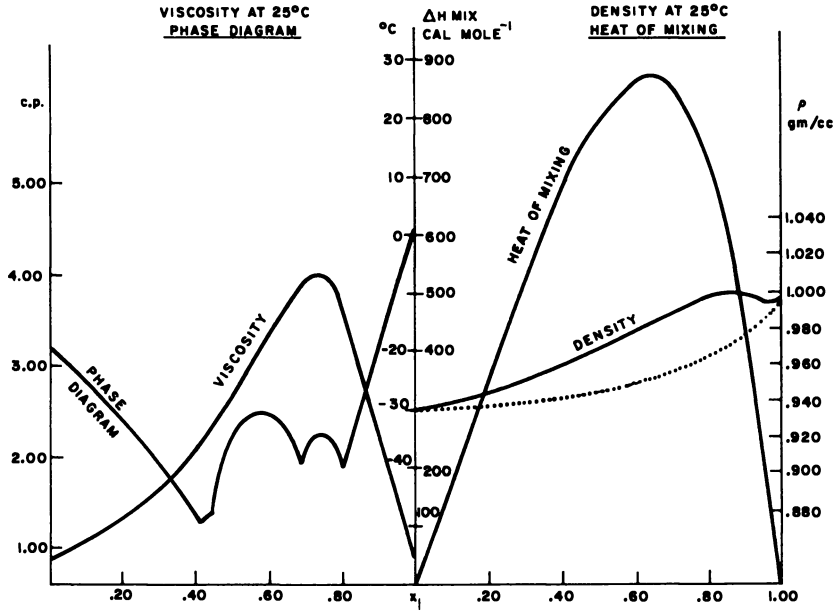

Figure 1. N,N-*Dimethylacetamide–water system*

The second family of curves are those of the *N*-substituted pyrrolidones, *N*-methylpyrrolidone (NMPy) and *N-tert*-butylpyrrolidone (NtBPy), with their respective maxima at a common mole ratio of 2 to 1. The third family are of the self-associating *N*-monosubstituted acetamides, *N*-methylacetamide and *N*-ethylacetamide, which show shallow maxima at a mole ratio of about 1 to 1.

The general nature of the curves shows strong, positive deviations from ideal behavior, as is often seen with associating binary liquid mixtures, in particular where one of the components is water. The interpretation of this phenomenon lacks a well founded theoretical treatment, but it is not too unreasonable to attribute the maxima of the fully substituted amides to discrete hydrodynamic entities. The unusual specificity of the maxima is a good indication that we are dealing with a highly associating or complexing system. On the other hand, the shallow maxima at 1 to 1, observed for the *N*-monosubstituted acetamides, appears to be more a sign of an optimum ratio in the process of forming

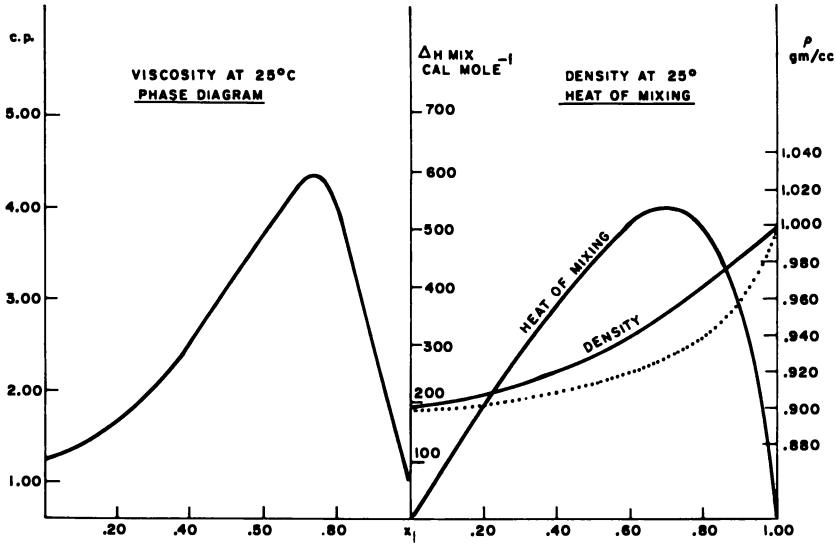

Figure 2. N,N-*Diethylacetamide–water system*

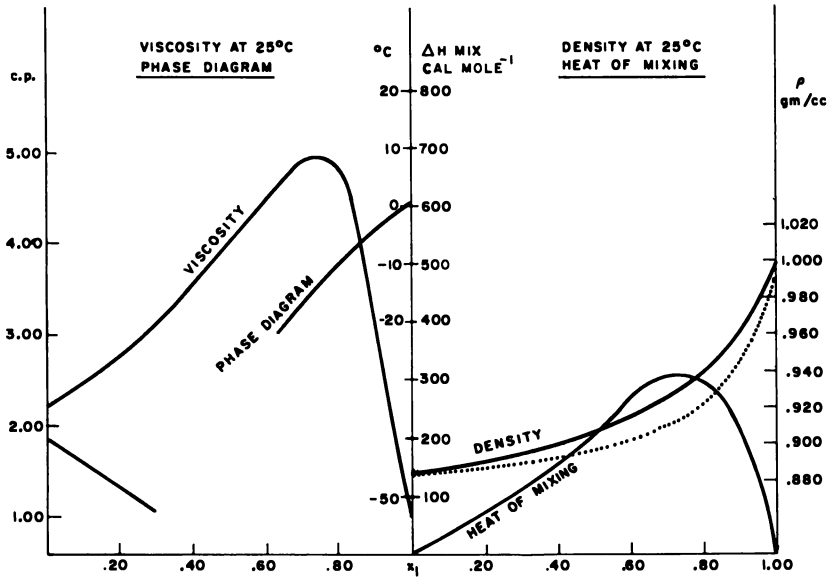

Figure 3. N,N-*Di*-n-*propylacetamide–water system*

polymeric species when chains are formed by interposing water molecules through hydrogen bonding between the amides.

VOLUME CHANGES. The density changes of several amide-water systems have been measured using 10-cc. specific gravity bottles. These experimental values were compared with an ideal density defined in terms of additive molar volumes and are shown as a dotted line in Figures 1 through 8 for the respective amide-water mixtures.

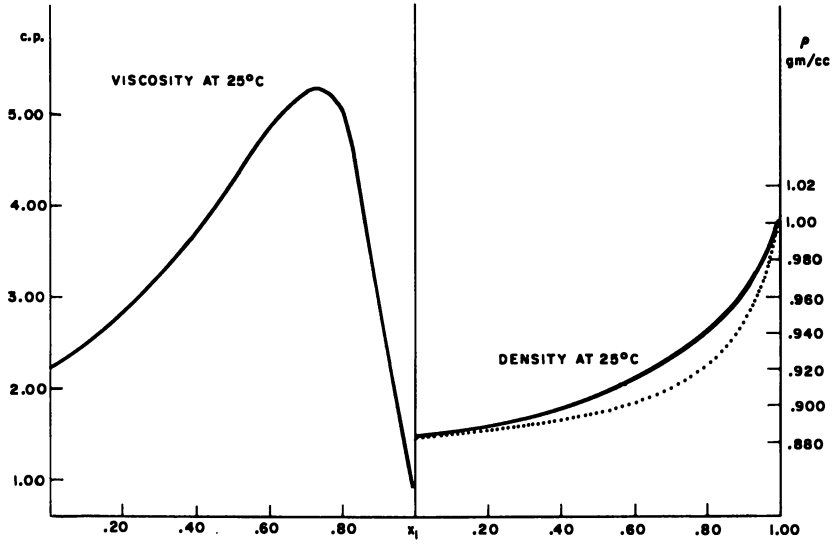

Figure 4. N,N-*Diisopropylacetamide–water system*

The positive deviations in the density changes, or conversely negative volume changes upon mixing, are consistent with what one would expect from the exothermic heats of mixing shown below. The maximum deviations of these changes are all of approximately the same order—*e.g.*, in terms of $\triangle V_{mix}$ they amount to about 1.46 cc. per mole for DMA. They decrease slightly within the homologous acetamide series to about 1.40 cc. per mole for DEA, 1.11 cc. per mole for Di-PA, and 1.05 cc. per mole for Dr-Pa. The greatest deviations are found around a mole ratio of 2 to 1 for all amide-water systems studied.

The partial molar volumes at infinite dilution of the amides show a consistent volume decrease for the amides on transfer into the aqueous phase, which becomes greater with increasing size of the substituents and amounts to about 2.5 cc. per mole per pair of methylenic groups in the case of the acetamide series. This value may be compared with that found in the alcohol series (*6*), where a more negative value of about 2.5 cc. per mole per methylenic group is found, and also to similar de-

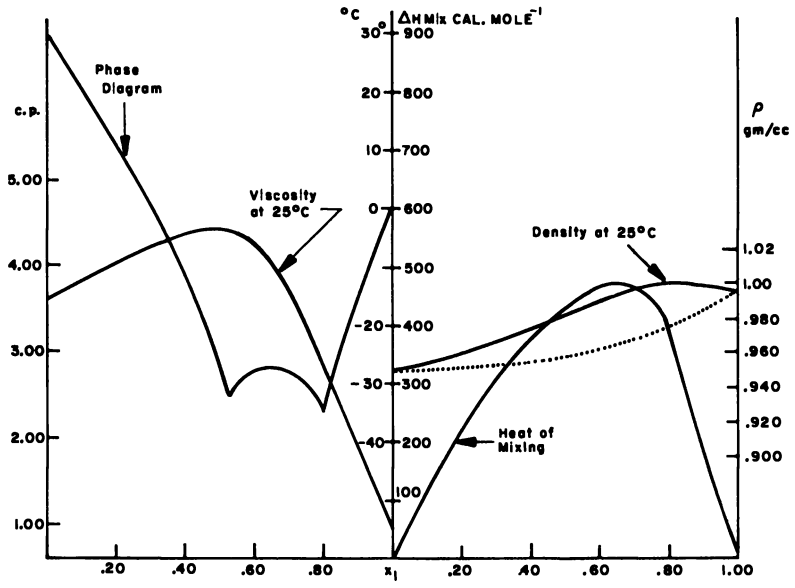

Figure 5. N-*Methylacetamide–water system*

creases in the tetraalkylammonium series (*13*). This volume deficiency has often been interpreted in terms of interstitial solvation—*i.e.*, fitting the hydrophobic portion into cavities supposed to exist in the liquid water structure. However, other explanations are possible, such as comparable "fitting" losses which can be approximated purely on the basis of geometrical considerations of the packing of spheres of different sizes (*2*).

HEATS OF MIXING. In order to obtain data on the energetics of the interaction between the amide group and water, the heats of mixing, $\triangle H_{mix}$, and associated heat capacities were determined on several systems. The experiments were conducted in a semimicro adiabatic calorimeter using a calibrated thermistor as one leg in a Wheatstone bridge circuit to sense the temperature changes. All the amides used in this study—DMA, DEA, Dn-PA, NMA, and NMPy—show exothermic heats over the entire concentration region, especially large for DMA and NMPy. It is suggestive, though possibly fortuitous, that the maxima again occur at the definite mole ratios found in either by viscosity or phase diagrams since the $\triangle H_{mix}$ values are also functions of the heats of evaporation, $\triangle H_{evap}$, of the two components. A better quantity to describe the molecular interaction would be the heat of solvation; however, most $\triangle H_{evap}$ values for the amides are unknown. Despite this, the large maximum of DMA at 2 to 1 and the skewed successively lower maxima at 3 to 1 for DEA and Dn-PA would seem to prove that two molecules of water interact strongly with the peptide dipole. Further

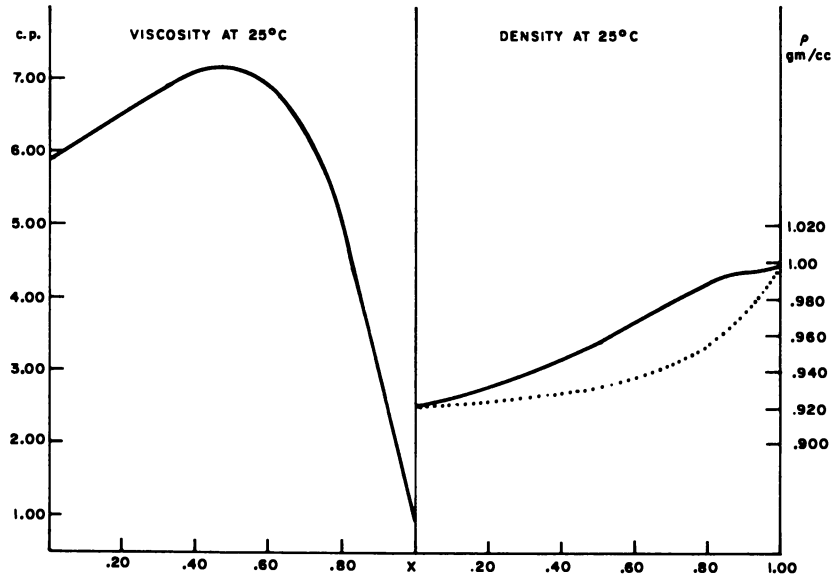

Figure 6. N-*Ethylacetamide–water system*

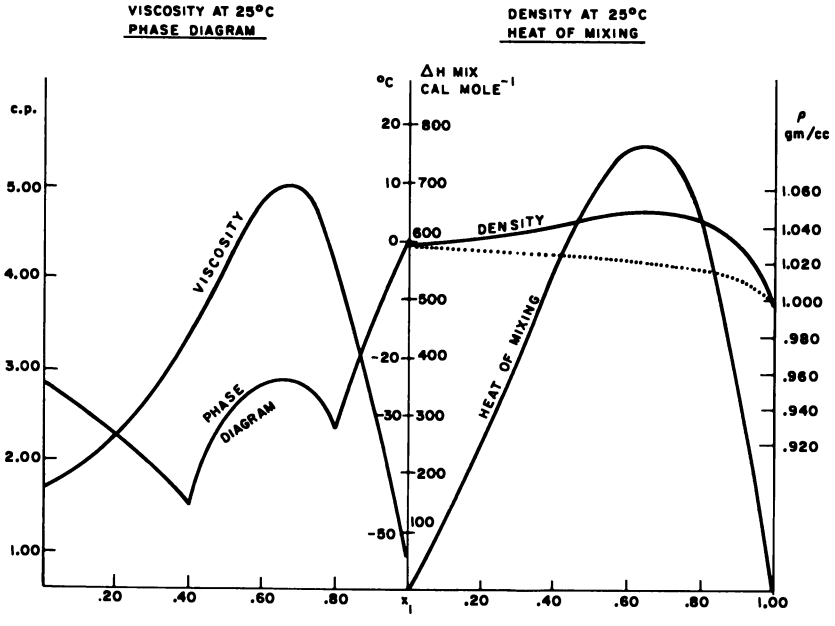

Figure 7. N-*Methylpyrrolidone–water system*

supporting this conclusion is the fact that the maxima for NMA and NMPy also occur at a mole ratio of 2 to 1.

HEAT CAPACITIES. The heat capacities (C_p in cal./mole-°C., not shown here) exhibit some unusual features, in that they show marked curvature changes at the characteristic mole ratios found thus far for each of the respective amides or pyrrolidones, again rendering it likely that definite stoichiometric complexes occur in the amide-water mixtures.

PHASE DIAGRAMS. In an endeavor to prove the reality of definite water binding or complexing in these systems, the phase diagrams for a few selected amide-water mixtures—*i.e.*, of NMA, DMA, Dn-PA, and NMPy—were studied. The freezing point depressions were measured with a conventional thermocouple circuit. Some of the resulting phase diagrams, shown in the figures, clearly establish that the simpler amides form compounds. The DMA-water system is complex, with a peritectic point at a mole fraction of about 0.44 of water, followed by maxima, interpreted as compounds, at mole ratios of 3 to 2 and 3 to 1. Both NMA and NMPy exhibit compound formation at mole ratios of 2 to 1, while, as in the case of DMA, there is a common eutectic point at 4 to 1. The 3 to 1 compound for DMA, and the 2 to 1 compound for NMPy, are of the same ratios as found for the viscosity maxima, perhaps indicating that a similar molecular association ratio is retained to some extent even at 25°C.

The same explanation or analogy should, of course, not be valid for NMA, where the viscosity maximum was interpreted as being caused by

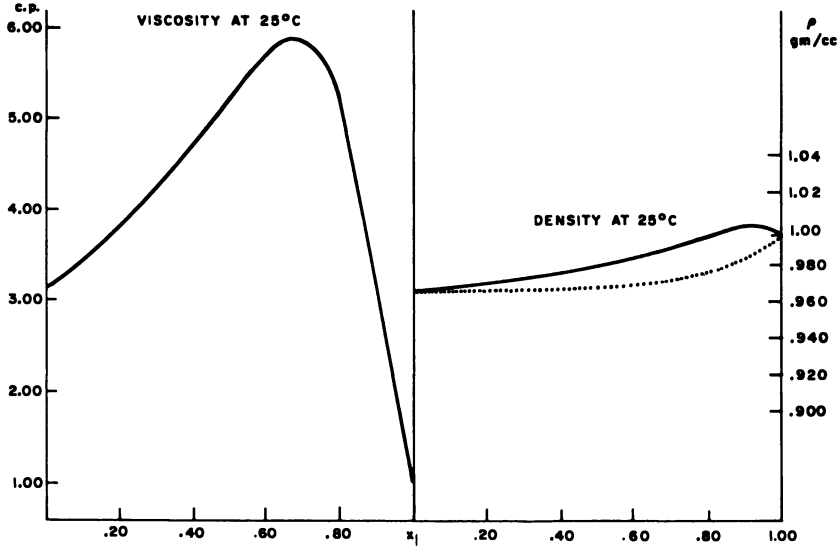

Figure 8. N-tert-*Butylpyrrolidone–water system*

polymeric species. The freezing point depression curve for Dn-PA fails to show any compound at 3 to 1 and is discontinuous in the middle region because of the formation of a noncrystallizable glass. The absence of any compound here is probably not so much caused by lack of specific association between the amide group and water, but the bulky *N*-propyl substituents may be incompatible in a simple crystal lattice, while yet short enough not to be able to participate in van der Waals associations which occur in the crystallization of longer hydrocarbon chains.

Conclusions

We conclude that a definite molecular interaction exists between the peptide dipole and water. The common feature among the amides and pyrrolidones investigated here is the evidence—thermodynamic and from viscosity data—that two molecules of water are being bound per NCO group. The logical site of this association is through hydrogen bonding with the lone electron pairs of the carbonyl oxygen; this argument runs parallel with spectroscopic studies from NMR data on the protonation of the amide group (3). The fully substituted amides appear to be able to hold also a third water molecule in the immediate solvation sphere by an apparently less energetic interaction. It is not possible on the basis of known bond angles and bond distances of the water molecule to bridge the first two hydrogen-bonded water molecules into a ring structure. It is more likely that there is interaction with the partially positive nitrogen. The fact that one does not find evidence of a third water molecule associated with the *N*-substituted pyrrolidones is probably caused by the presence of the ring with its special geometry as evidenced by the greater densities of these compounds.

Acknowledgment

The authors wish to express their gratitude for grants made available by the National Institutes of Health, Grant GM 09553, Research Grants Branch, and Grant DE 01769, National Institute of Dental Research, which also supported one of the authors (P.A.) through graduate school at Polytechnic Institute of Brooklyn.

Literature Cited

(1) Adelman, R., *J. Org. Chem.* **29**, 1296 (1963).
(2) Assarsson, P., Eirich, F. R., in press.
(3) Bunton, C. A., Figgis, B., Nayak, B., "Advances in Molecular Spectroscopy," Vol. 3, Macmillan, New York, 1962.
(4) Corey, R., Donohue, J., *J. Am. Chem. Soc.* **72**, 2899 (1950).
(5) Costain, C. C., Dowling, J. M., *J. Chem. Phys.* **32**, 158 (1960).

(6) Franks, F., *Ann. N. Y. Acad. Sci.* **125,** 277 (1965).
(7) Katz, J. L., Ph.D. Thesis, Polytechnic Institute of Brooklyn, 1957.
(8) Klotz, J., Franzen, J., *J. Am. Chem. Soc.* **82,** 5241 (1960).
(9) Pauling, L., *Proc. Natl. Acad. Sci. U.S.* **18,** 293 (1932).
(10) Petersen, R., *J. Phys. Chem.* **64,** 184 (1960).
(11) Smyth, C. P., "Dielectric Behavior and Structure," pp. 53, 73, McGraw-Hill, New York, 1955.
(12) Thompson, B., LaPlanche, L., *J. Phys. Chem.* **67,** 2230 (1963).
(13) Wen, W., Saito, S., *J. Phys. Chem.* **68,** 2639 (1964).

RECEIVED October 6, 1967.

2

Light-Scattering Study of the Interaction of β-Lactoglobulin Solvent Components in the System Water–2-Chloroethanol

HIDEO INOUE and SERGE N. TIMASHEFF[1]

Eastern Utilization Research and Development Division, U. S. Department of Agriculture, Philadelphia, Pa. 19118

The preferential binding of solvent components to the macromolecular solute has been investigated by light scattering for the system 2-chloroethanol–water–β-lactoglobulin A. In the presence of 0.02M NaCl and 0.01M HCl, 2-chloroethanol is bound preferentially to the protein up to ca. 60 volume % of that component. Above this concentration of the organic solvent, water is bound preferentially in the immediate domain of the β-lactoglobulin. The necessary working equations are developed.

Light scattering is a powerful tool for studying interactions of biological macromolecules in solution. Since the first theoretical analysis of light scattering in multicomponent systems by Zernike (*28*) in 1918, this theory has been extended in great detail by several investigators. Thus, at present, the thermodynamic interactions which take place between macromolecules and between macromolecules and solvent components can be rigorously characterized. Some of the more important contributions to this field can be found in the work of Ewart, Roe, Debye, and McCartney (*8*), Brinkman and Hermans (*5*), Kirkwood and Goldberg (*10*), Stockmayer (*18*), Shoenji (*14*), Ooi (*12*), Vrij and Overbeek (*26, 27*), Stigter (*16, 17*), Casassa and Eisenberg (*6, 7*), Strazielle and Benoit (*19*), Timasheff and Kronman (*21*), and others.

Using the combined notation of Stockmayer (*18*) and of Kirkwood and Goldberg (*10*), and expressing the chemical potential functions

[1] Present address, Graduate Department of Biochemistry, Brandeis University, Waltham, Mass. 02154.

according to Scatchard (*13*), we obtain the light-scattering equation for a three-component system:

$$\frac{H''V\Psi_2^2}{\Delta\tau} = \frac{a_{22} - a_{12}^2/a_{11}}{\left[1 + \frac{\Psi_1}{\Psi_2}\left(\frac{\partial m_1}{\partial m_2}\right)_{T,p,\mu_1}\right]^2} \qquad (1)$$

$$H'' = \frac{32\pi^3 n^2}{3N\lambda^4} \qquad \Psi_i = \left(\frac{\partial n}{\partial m_i}\right)_{T,p,m_j}$$

$$a_{ij} = \left(\frac{\partial \ln a_i}{\partial m_j}\right)_{T,p,m}$$

where n is the refractive index of the solution, N is Avogadro's number, λ is the wavelength of the light *in vacuo*, V is the volume of solution in milliliters containing 1000 grams of principal solvent, $\Delta\tau$ is the excess turbidity of the solution over that of the solvent, m_i is the molality of component i (moles per 1000 grams of principal solvent), and a_i is the activity of component i. The principal solvent is component 0, the added solvent or electrolyte is component 1, and the macromolecular solute is component 2. Subscript m denotes constancy of all the m_i not indicated as variables in the corresponding derivative.

Expressing activity a_2 in terms of the excess chemical potential (*13*), we obtain from Equation 1:

$$\frac{H''V\Psi_2^2 m_2}{\Delta\tau} = \left[1 + \frac{\Psi_1}{\Psi_2}\left(\frac{\partial m_1}{\partial m_2}\right)_{T,p,\mu_1}\right]^{-2}\left[1 + \left\{\beta_{22} - \frac{(a_{12})^2}{a_{11}}\right\} m_2\right]$$

$$\beta_{ij} = \frac{1}{RT}\left(\frac{\partial \mu_i^{(e)}}{\partial m_j}\right)_{T,p,m} \qquad (2)$$

where $\mu_i^{(e)}$ is the excess chemical potential of component i, defined by $\mu_i = RT\Sigma\nu_i \ln m_i + \mu_i^{(e)} + \mu_i^{\circ}(T,p)$, and $\Sigma\nu_i$ is the number of particles into which component i dissociates.

In practice, concentration measurements are done more easily on a volume basis than on a weight basis. Changing the concentration units from molality, m_i, to grams per milliliter of solution, C_i, results in

$$\frac{H''C_2}{\Delta\tau}\left(\frac{\partial n}{\partial C_2}\right)_{m_1}^2 = \frac{1}{M_2(1+D)^2} \times$$

$$\left[1 + \frac{C_2}{RT}\left\{\left(\frac{\partial \mu_2^{(e)}}{\partial C_2}\right)_{m_1} + \left(\frac{\partial \mu_1^{(e)}}{\partial C_2}\right)_{m_1}\left(\frac{\partial m_1}{\partial m_2}\right)_{T,p,\mu_1} + 2RT\bar{V}_2\right\}\right] + O(C_2^2)$$

$$D = \frac{M_1}{M_2} \frac{(1 - C_1\bar{V}_1)_{m_2}(\partial n/\partial C_1)_{m_2}}{(1 - C_2\bar{V}_2)_{m_1}(\partial n/\partial C_2)_{m_1}} \left(\frac{\partial m_1}{\partial m_2}\right)_{T,p,\mu_1} \tag{3}$$

$$\left(\frac{\partial m_1}{\partial m_2}\right)_{T,p,\mu_1} = -\frac{\beta_{12}}{\frac{\Sigma\nu_1}{m_1} + \beta_{11}} \doteq \frac{M_2}{M_1} \frac{(1 - C_2\bar{V}_2)_{\mu_1}}{(1 - C_1\bar{V}_1)_{\mu_2}} \left(\frac{\partial C_1}{\partial C_2}\right)_{T,p,\mu_1}$$

$$= \frac{[\mu_2^{(e)}/\partial m_2]_{T,p,\mu_1} - [\partial\mu_2^{(e)}/\partial m_2]_{m_1}}{(\partial\mu_2^{(e)}/\partial m_1)_{m_2}}$$

On extrapolation to zero concentration of the macromolecular component, the last of Equations 3 reduces to

$$\left(\frac{\partial m_1}{\partial m_2}\right)^{\circ}_{T,p,\mu_1} = \frac{M_2}{1000} \frac{m_1}{C_1(\bar{V}_o)_{m_1,m_2}} \left[\left(\frac{\partial C_1}{\partial C_2}\right)^{\circ}_{T,p,\mu_1} + C_1(\bar{V}_2)_{m_1}\right] \tag{3'}$$

where M_i is the molecular weight of component i, $\bar{V}_i$ is its partial specific volume measured at equal molality of component i in the solution and the reference solvent, R is the gas constant, and T is the thermodynamic temperature. The conditions for applicability of Equation 3 are that the molality, m_1, of component 1 be kept identical in solvent and solution in all the light-scattering and differential refractometric measurements. On the other hand, if both measurements are carried out at conditions at which the chemical potential of component 1 and the pressure are held fixed in the solvent and the protein solution, the light-scattering equation assumes a pseudo-two-component form (*7*, *12*, *16*, *26*):

$$\frac{H''C_2}{\Delta\tau}\left(\frac{\partial n}{\partial C_2}\right)^2_{\mu_1} = \tag{4}$$

$$\frac{1}{M_2}\left[1 + \frac{C_2}{RT}\left\{\left(\frac{\partial\mu_2^{(e)}}{\partial C_2}\right)_{T,p,\mu_1} + 2RT\left[\bar{V}_2 + \frac{M_1}{M_2}\bar{V}_1\left(\frac{\partial m_1}{\partial m_2}\right)_{T,p,\mu_1}\right]\right\}\right] + O(C_2^2)$$

While applicability of Equation 4 requires that all measurements be done at constant pressure, in practice it is much simpler to do the measurements in a state of dialysis equilibrium—*i.e.*, at constant T, μ_o, and μ_1. The error introduced by the practical approximation $(\partial m_1/\partial m_2)_{T,p,\mu_1} = (\partial m_1/\partial m_2)_{T,\mu_0,\mu_1}$ is minor (*16*). In this manner, light-scattering measurements on protein solutions in a mixed solvent, with and without dialysis, make possible the determination of both the molecular weight and the extent of preferential interaction of the protein with one of the solvent components (*21*).

Procedure. The molecular weight, M_2, of component 2, is obtained by Equation 4 from light-scattering and refractive index measurements

on protein solutions which have been dialyzed against the solvent. The extent of aggregation of the protein can be determined from this molecular weight. Next, the measurements are repeated on undialyzed protein solutions, and the left side of Equation 3 is plotted *vs.* the concentration, C_2. The deviation from $1/M_2$ of the intercept at $C_2 = 0$ makes it possible to evaluate D and, thus, $(\partial m_1/\partial m_2)_{T,p,\mu_1}$. The nonideality terms β_{ij} can be obtained then by combining D with the initial slope of the plot. If β_{11} is not known from other measurements, it can usually be assumed to be zero, as a first approximation.

A light-scattering study of this nature has been carried out on solutions of β-lactoglobulin A (β-A) dissolved in mixtures of water with 2-chloroethanol in the presence of 0.02*M* NaCl and 0.01*M* HCl. 2-Chloroethanol is known to be a structure-forming protein denaturant and can be expected to interact with proteins; freshly distilled, its refractive index at 436 mμ is 1.447, different from that of water, 1.340. This results in a large value of $\partial n/\partial C_1$.

Experimental

β-Lactoglobulin A was prepared by standard techniques (*1*) and recrystallized before use. Solvents were double-distilled in all-borosilicate glass stills and used immediately. Light-scattering measurements were performed in the Brice photometer (*4*) at 25°C. with the 436-mμ mercury arc line. Light-scattering measurements at constant concentration of 2-chloroethanol were carried out according to a modified Dintzis technique (*20*), as described previously (*23*). Solutions for operations at constant chemical potential of chloroethanol were prepared as follows. In each series, solutions (about 5 ml.) of β-A at different concentrations were made in a given water-chloroethanol mixture, dialyzed overnight against a large excess of the same solvent, and passed through an ultrafine sintered-glass filter (*2*) after centrifuging. Refractive index increments were measured on the Brice differential refractometer (*3*) at 25°C. and 436 mμ. Protein concentrations were measured on a Zeiss PMQ II spectrophotometer at 278 mμ. An absorptivity value of 0.96 liter/cm.-gram (*25*) was used.

Results

Light Scattering at Constant Chemical Potential. In these measurements the concentration of chloroethanol was varied from 5 to 60 volume %. The intensity of scattering of β-A dissolved in these media remained constant for at least 24 hours if the β-A concentration were less than 2 grams per liter. Typical results of experiments at constant chemical

potential are shown in Figure 1, where the values of $H''(\partial n/\partial C_2)_{T,\mu_0,\mu_1} C_2/\Delta\tau$ are plotted against the protein concentration, C_2; the straight lines were calculated by the method of least squares using the data below 2 grams per liter. It is evident that all the data extrapolate essentially to the same intercept. The average value of the molecular weight found in these experiments is 18,700. It is known that at pH below 3.5, native β-A dissociates to a monomer with a molecular weight of *ca.* 18,000 (*22*); this dissociation is enhanced by low salt concentration and a low dielectric constant of the medium (*24*). The present results extend these previous findings to β-A in water–2-chloroethanol mixtures in the presence of 0.02*M* NaCl and 0.01*M* HCl; in these solvents β-A exists in monomeric form.

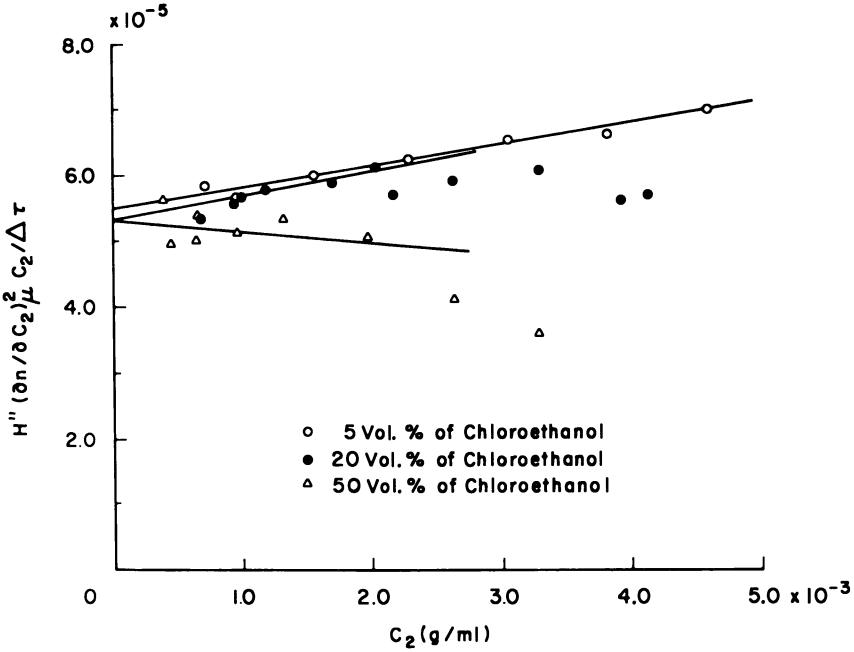

Figure 1. Light-scattering data on β-lactoglobulin A in various concentrations of 2-chloroethanol at constant chemical potential of 2-chloroethanol

Solvent components are water, 2-chloroethanol, 0.02M NaCl, and 0.01M HCl

Light Scattering at Constant Concentration. Measurements were carried out without previous dialysis in solvent mixtures containing up to 80 volume % of 2-chloroethanol. The scattered intensity showed no time dependence up to 24 hours at β-A concentrations below 6 grams per liter, except for the highest concentration of chloroethanol (80%), at which slow changes were seen at protein concentrations above 2 grams

per liter. Typical results are shown in Figure 2, where it can be seen that the intercept is a function of chloroethanol concentration. The variation of M_{app}/M_w, the ratio of the apparent molecular weight to the true molecular weight, with increasing chloroethanol concentration can be calculated from such data. This parameter first rises, then after passing a maximum at *ca.* 40% chloroethanol ($M_{app}/M_w = 1.7$), it drops, becoming less than unity above *ca.* 65% chloroethanol.

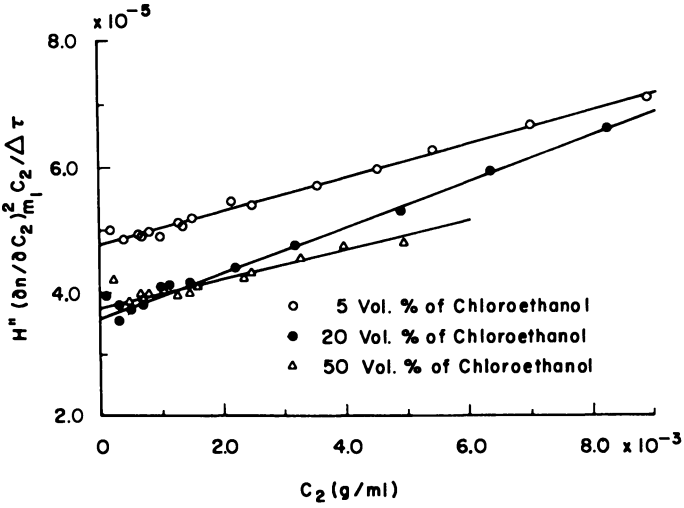

Figure 2. Light-scattering data on β-lactoglobulin A in various concentrations of 2-chloroethanol

Each series of experiments was carried out at constant concentration of 2-chloroethanol. Solvent components. Water, 2-chloroethanol, 0.02M NaCl, and 0.01M HCl

Preferential Solvation. Examination of the data of Figure 2 in terms of Equation 3 shows that below 65% chloroethanol, $(\partial m_1/\partial m_2)_{T,\mu_0,\mu_1}$ is positive, while above this point it becomes negative. Negative values of this interaction parameter indicate a deficiency of component 1 in the immediate vicinity of molecules of component 2—*i.e.*, preferential hydration of component 2. The extent of hydration is given by Equation 5.

$$\left(\frac{\partial m_0}{\partial m_2}\right)_{T,p,\mu_1} = -\frac{m_0}{m_1}\left(\frac{\partial m_1}{\partial m_2}\right)_{T,p,\mu_1} \tag{5}$$

The interaction between solvent components and the macromolecule is reflected also in the difference between the refractive index increments measured at constant concentration and those found at constant chemical

potential of component 1. The relation between these is given in Equation 6 (*6, 7, 12, 14, 16, 17, 26, 27*).

$$\left(\frac{\partial n}{\partial m_2}\right)_{\mu_1} = \left(\frac{\partial n}{\partial m_2}\right)_{m_1} + \left(\frac{\partial n}{\partial m_1}\right)_{m_2}\left(\frac{\partial m_1}{\partial m_2}\right)_{\mu_1} \tag{6}$$

Converting from molal to grams per milliliter concentration units, and extrapolating to $C_2 = 0$, gives:

$$\left(\frac{\partial m_1}{\partial m_2}\right)^0_{T,p,\mu_1} = \frac{M_2}{M_1(1-\bar{V}_1C_1)}\left\{\left(\frac{\partial n}{\partial C_2}\right)_{T,p,\mu_1} - \left(\frac{\partial n}{\partial C_2}\right)_{T,p,m_1}\right\}\Big/\left(\frac{\partial n}{\partial C_1}\right)_{T,p,m_2} \tag{7}$$

where superscript 0 indicates this extrapolation.

The values of the preferential binding of 2-chloroethanol to protein, obtained from light scattering and expressed in terms of moles of this component per mole of protein, are plotted in Figure 3 as a function of chloroethanol concentration. At low concentrations of chloroethanol, β-A has a higher affinity for this component than for water. This affinity

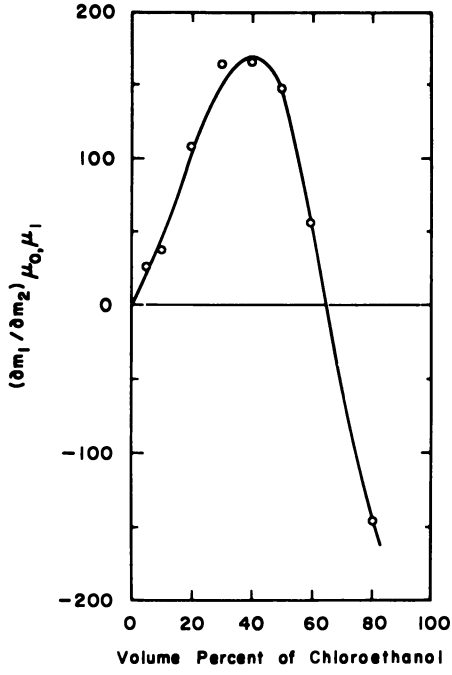

Figure 3. Variation of solvation of β-lactoglobulin A with increasing 2-chloroethanol concentration in water–2-chloroethanol mixtures

increases with an increase in C_2, reaching a maximum at *ca.* 40 volume %. Above this chloroethanol concentration, it decreases monotonically to negative apparent absorption of chloroethanol after passing through zero at *ca.* 65 volume %. Above this concentration, β-A is preferentially hydrated. Thus, the point at 80 volume % chloroethanol corresponds to the preferential binding of 140 moles of water per mole of protein. These results are similar to those obtained in the serum albumin–water–2-chloroethanol system (*15*).

Optical rotatory dispersion and circular dichroism measurements have been carried out on β-A in this solvent system; the details are published elsewhere (*9*). A progressive change in solvent composition from aqueous to 2-chloroethanol induces a gradual change from the native globular structure to one rich in α-helix. This conformational change, however, does not seem to be related in any simple fashion to the variation in the thermodynamic interaction parameters. Further investigations on the effects of such solvent components on this and other proteins are in progress (*11*).

Literature Cited

(1) Aschaffenburg, R., Drewry, J., *Biochem. J.* **65**, 273 (1957).
(2) Bier, M., "Methods in Enzymology," S. P. Colowick, N. O. Kaplan, eds., Vol. 4, p. 165, Academic Press, New York, 1957.
(3) Brice, B. A., Halwer, M., *J. Opt. Soc. Am.* **41**, 1033 (1951).
(4) Brice, B. A., Halwer, M., Speiser, R., *J. Opt. Soc. Am.* **40**, 768 (1950).
(5) Brinkman, H. C., Hermans, J. J., *J. Chem. Phys.* **17**, 574 (1949).
(6) Casassa, E. F., Eisenberg, H., *Advan. Protein Chem.* **19**, 287 (1964).
(7) Casassa, E. F., Eisenberg, H., *J. Phys. Chem.* **64**, 753 (1960).
(8) Ewart, R. H., Roe, C. P., Debye, P., McCartney, J. R., *J. Chem. Phys.* **14**, 687 (1946).
(9) Inoue, H., Timasheff, S. N., *J. Am. Chem. Soc.* **90**, 1890 (1968).
(10) Kirkwood, J. G., Goldberg, R. J., *J. Chem. Phys.* **18**, 54 (1950).
(11) Noelken, M., Timasheff, S. N., *J. Biol. Chem.* **242**, 5080 (1967).
(12) Ooi, T., *J. Polymer Sci.* **28**, 459 (1958).
(13) Scatchard, G., *J. Am. Chem. Soc.* **68**, 2315 (1946).
(14) Shogenji, H., *Busseiron Kenkyu* **62**, 1 (1953).
(15) Stauff, J., Mehrotra, K. N., *Kolloid Z.* **176**, 1 (1961).
(16) Stigter, D., *J. Phys. Chem.* **64**, 842 (1960).
(17) Stigter, D., "Electromagnetic Scattering," M. Kerker, ed., p. 303, Pergamon, New York, 1963.
(18) Stockmayer, W. H., *J. Chem. Phys.* **18**, 58 (1950).
(19) Strazielle, C., Benoit, H., *J. Chim. Phys.* **58**, 678 (1961).
(20) Timasheff, S. N., Dintzis, H. M., Kirkwood, J. G., Coleman, B. D., *J. Am. Chem. Soc.* **79**, 782 (1957).
(21) Timasheff, S. N., Kronman, M. J., *Arch. Biochem. Biophys.* **83**, 60 (1959).
(22) Timasheff, S. N., Townend, R., *J. Am. Chem. Soc.* **83**, 470 (1961).
(23) Townend, R., Timasheff, S. N., *J. Am. Chem. Soc.* **82**, 3168 (1960).
(24) Townend, R., Weinberger, L., Timasheff, S. N., *J. Am. Chem. Soc.* **82**, 3175 (1960).

(25) Townend, R., Winterbottom, R. J., Timasheff, S. N., *J. Am. Chem. Soc.* **82,** 3161 (1960).
(26) Vrij, A., Ph.D. Thesis, Utrecht, 1959.
(27) Vrij, A., Overbeek, J. Th. G., *J. Colloid Sci.* 17, 570 (1962).
(28) Zernike, F., *Arch. Néerl. Sci.* (III A) **4,** 74 (1918).

RECEIVED July 19, 1967. Work done during the tenure of a U. S. Department of Agriculture Resident Post Doctoral Research Associateship, by Hideo Inoue, 1965–1967.

Effect of Deuterium Oxide on Protein Aggregation in Deuterio and Protio Phycocyanin and Other Proteins

DONALD S. BERNS, JUNG JA LEE, and EDITH SCOTT

Division of Laboratories and Research, New York State Department of Health, and Department of Biochemistry, Albany Medical College, Albany, N. Y.

The effect of deuterium oxide on protein aggregation was investigated with trypsin, soybean trypsin inhibitor, catalase, α_s-casein B, phycocyanin, and fully deuterated phycocyanin. Enhancement of aggregation is found only in the proteins in which hydrophobic forces are of postulated importance in the aggregation phenomenon. The relative increase in aggregation in phycocyanin and in deuterated phycocyanin, produced by substitution of deuterium oxide for water as solvent, is confined to the 11S *species and is of the same magnitude in both proteins. The results are interpreted as supporting the suggestions that the* 11S *species is favored by hydrophobic forces and is further stabilized by dispersion forces and that deuteration at nonexchangeable sites has a minor effect on hydrophobic forces.*

In previous work on fully deuterated proteins (*16*), we demonstrated that *C*-phycocyanins extracted and purified from the blue-green algae *Plectonema calothricoides* and *Phormidium luridum*, grown in H_2O or D_2O, aggregate in a similar manner. The relative amounts of the several aggregates present as a function of pH, temperature, and ionic strength differ for the protio and fully deuterated proteins. (The term "protio" is used here to indicate the protein isolated from algae grown in H_2O in contrast with the "deuterio" or "deuterated" protein isolated from algae grown in D_2O. The deuterio protein has deuterium substituted at all proton sites when studies are performed in D_2O. In H_2O only exchangeable sites are populated by protons in the deuterated protein.)

The amount of aggregate sedimenting at *11S* is substantially less in the fully deuterated proteins. The secondary and tertiary structures of the comparable deuterated and protio proteins have been demonstrated to be identical by immunochemical techniques (*2*) and by optical rotatory dispersion criteria (*6*). The difference in aggregation properties in the fully deuterated protein was explained in terms of a decrease in dispersion forces, which, after hydrophobic forces bring the subunits in close contact, stabilize the *11S* hexameric aggregate. Another study on fully deuterated proteins (*8*) suggested that the general reduction in all aggregation in these proteins is explicable solely in terms of a decrease in hydrophobic forces.

This study demonstrates by a novel method the enhancement of hydrophobic forces. New data are presented to support the suggestion that dispersion forces specifically stabilize the *11S* aggregate and that hydrophobic forces are not substantially altered by deuteration at nonexchangeable sites.

Recent model compound studies by Kresheck *et al.* (*11*), using D_2O and H_2O, led to the postulate that hydrophobic interactions are greater in D_2O than in H_2O. The critical micelle concentration for detergents in D_2O is also reported to be lower than in H_2O. These experiments suggested the possible use of D_2O as a solvent to increase hydrophobic forces, which would be a good test of the type of major forces contributing to stabilization of protein aggregates. Consequently, studies of the effect of D_2O on aggregation in several proteins, including protio and deuterio phycocyanin, were undertaken.

It is also possible that if hydrophobic interactions were less in the deuterated than in the protio protein, the percentage increase in aggregates favored by hydrophobic interactions would be substantially smaller in deuterio than in protio proteins.

Experimental

Materials and Methods. Fully deuterated phycocyanin and protio phycocyanin from *Ph. luridum* were used. The method of purifying phycocyanin was identical to that used previously (*15, 16*). The purity of the phycocyanin preparations, the complete substitution of deuterium for hydrogen in the fully deuterated phycocyanin, and the reversibility of the aggregation phenomenon were ascertained as previously (*4, 16*). Purified bovine trypsin, soybean trypsin inhibitor, and bovine liver catalase were obtained from the Worthington Biochemical Corp., Freehold, N. J., and used without further purification. Bovine α_s-casein B was kindly supplied by Chien Ho of the University of Pittsburgh.

Sedimentation velocity measurements were made on a Beckman-Spinco Model E ultracentrifuge equipped with RTIC. The sedimentation coefficients were not measured as a function of concentration for

each protein. This extrapolation for phycocyanin and the other proteins was not deemed necessary. The areas under each sedimentation peak were evaluated from tracings with a Nikon microcomparator as reported previously (*15*). The velocity of sedimentation was always 59,780 r.p.m., and the rotor temperature was maintained close to 25°C. There was no more than a 1° temperature variance in all sedimentation experiments. This small variance had a negligible effect on the relative amounts of each sedimenting species. The sedimentation coefficients of each species were determined from photographic plates by measuring distances with a Nikon microcomparator. The appropriate viscosity and density corrections for D_2O and H_2O buffers were applied (*7*). Phosphate buffers, 0.1 ionic strength, were used in all phycocyanin experiments. The spectra of all phycocyanin samples in D_2O and H_2O were monitored by a Beckman DB spectrophotometer with periodic cross-checking with a Cary model 14 spectrophotometer. The concentrated solutions were examined without dilution by using appropriate spacer cells.

Protein solutions in D_2O were prepared by making up a protein solution in the appropriate H_2O buffer, pipetting 1 ml. of solution into each of two lyophilizing flasks, and lyophilizing. One sample was reconstituted with H_2O and one with D_2O; lyophilization was repeated, and the samples were reconstituted again immediately before use. The pH of each final solution was measured by a Radiometer TTT1A pH meter. In experiments with catalase and α_s-casein B, prior to lyophilization, the solutions were adjusted to a pH of 7.0 and were 0.01 or 0.1 ionic strength in KCl. The experiments with trypsin and soybean–trypsin inhibitor were performed in pH 6.0, $\mu = 0.1$ ionic strength, buffers.

Results

Sedimentation. The sedimentation experiments are tabulated in Tables I and II. In Table I typical sedimentation coefficients determined in H_2O and D_2O are in close agreement here and with previously reported values determined for both protio and deuterio phycocyanin from *P. calothricoides* (*15, 16*). Each of the tabulated coefficients is for a single experiment at an approximate protein concentration of 15 mg. per ml. Lyophilizing a phycocyanin preparation twice had little effect on the observed sedimentation coefficients. In calculating the S values the same partial specific volume of the protein was used for both D_2O and H_2O. This practice is consistent with the recent results of Edelstein and Schachman (*7*). Small increases in sedimentation coefficients from H_2O to D_2O are to be expected because of deuterium substitution on exchangeable positions. The slope of an S *vs.* concentration plot for phycocyanin in H_2O and D_2O would also probably differ. Consequently, small changes in S from H_2O to D_2O would be expected at a constant protein concentration.

In Table II the areas under the several peaks are tabulated as a function of pH and pD for both deuterio and protio proteins. The effect of

Table I. Typical Sedimentation Coefficients for Phycocyanin in H_2O and D_2O

H_2O		D_2O	
pH	S_{25}, H_2O	*pD*[a]	S_{25}, H_2O[b]
	Protio Protein		
6.0[c]	6.60	6.15	7.55
	11.2		12.8
	18.8		20.6
6.0	6.40	6.5	7.06
	11.7		11.6
	18.7		18.8
8.0	6.90	8.0	7.76
	12.6		13.45
	20.1		21.3
	Deuterated Protein[d]		
6.0	8.95	6.15	9.12
	15.0		15.3
	23.4		23.6
6.0[e]	4.69	6.5[e]	
	7.81		8.08
	14.6		15.3
8.0	5.07	8.0	
	8.04		8.26
	14.9		15.8
			22.6

[a] pD = observed pH + 0.4.
[b] As if sedimentation proceeded at solvent viscosity and density of water, at given protein concentration.
[c] All preparations except this one were lyophilized twice. This preparation was examined prior to lyophilization.
[d] Fully deuterated protein preparations were purified in pH 6.0 phosphate buffer to ensure presence of some *19S* material.
[e] This deuterated protein preparation was purified at pH 7.0 and used as a control experiment.

lyophilization on the relative amounts of each species is seen by comparison of the pH 5.6 and 6.0 unlyophilized and lyophilized preparations. There is some decrease in the amount of *11S* material and an increase in *7S* and *19S* species. This effect is to be compared with the effect of reconstituting the protein in D_2O. In all D_2O experiments there is a substantial increase in the amount of *11S* and decrease in the amount of *7S* material. It is of particular interest that the protio protein preparations in H_2O have distributions of *7S*, *11S*, and *19S*, close to those reported for purified *P. calothricoides* phycocyanin (*15*). The relative amounts of *7S* and *11S* in the deuterio protein preparations are comparable with those reported for deuterio phycocyanin from *P. calothricoides* (*16*). The *P.*

calothricoides deuterio preparations were purified at pH 7.0; consequently, little *19S* material was evident in those preparations. Similar H_2O and D_2O experiments were carried out with pH 7.0 purified deuterio *Ph. luridum* protein with results analogous to those presented in Table II. A typical example is included in Table II at pH 6.0. The pH 7.0 purified deuterio protein when lyophilized in H_2O had a tendency to disaggregate to 3S material; however, in D_2O at pD 6.5, no 3S material was evident. The relative amounts of *7S* and *11S* species present in the pH 7.0 purified sample at pH 6.0 were similar to those reported for deuterio *P. calothricoides* phycocyanin (*16*), except for the presence of substantial amounts of 3S material. Lyophilization of pH 6.0 purified deuterio protein resulted in the formation of 3S material but at a higher pH.

The data in Table II were analyzed for the relative change in amounts of *7S* and *11S* material (Table III). The relative amounts of each species at intermediate pH's not measured were calculated by interpolation. Comparison with previous results with protio and deuterio phycocyanins from *P. calothricoides* indicates that the relative error in this procedure

Table II. Sedimentation Behavior of Protio and Deuterio Phycocyanin in H_2O and D_2O

			H_2O, Relative Area under Peaks, %				*D_2O, Relative Area under Peaks, %*			
Protein	*pH*	*pD*[a]	*3S*	*7S*	*11S*	*19S*	*3S*	*7S*	*11S*	*19S*
Protio	5.6[b]			16	66	18				
	5.6			19	57	24				
	6.0[b]			18	70	12				
	6.0	6.15		22	55	23		13	69	18
		6.5						21	65	15
	7.0			64	25	11				
	7.4	7.5		80	16	4		43	41	17
	8.0	8.0		85	11	4		66	29	5
		8.4						66	28	1
Deuterio	5.6			46	38	17				
	6.0	6.15		46	26	28		30	49	21
	6.0[c]	6.5[c]	11	41	47			19	81	
		6.5						40	35	25
	7.0			73	19	8				
	7.4	7.5	1	92	8			61	25	14
	8.0	8.0		83	5			84	14	2
		8.4					10	86	4	

[a] pD = observed pH + 0.4.
[b] These preparations were not lyophilized; all other preparations were lyophilized twice.
[c] Purified at pH 7.0.

is small. The relative area measurements probably do not have a precision better than 10% in any event, and the tabulation in Table III is more of an indication of relative trends than a catalog of precise changes. The differences in the amount of *19S* material in H_2O and D_2O were not tabulated since no definite trend was noted. Furthermore, in experiments with pH 7.0 purified deuterio protein, although large increases in the amount of *11S* material were present (*see* pH 6.0, pD 6.5, Table II, for a typical example), no *19S* material was formed.

Other proteins were examined in H_2O and D_2O (Table IV). In all cases, except α_s-casein B, the behavior in H_2O and D_2O was similar, and no enhancement of aggregation was noted.

Table III. Percentage Change in *7S* and *11S* Species between H_2O and D_2O Solutions

Protein	*pH = pD*	*Change, %*
Decrease in *7S* from H_2O to D_2O		
Deuterio	6.0	35
	6.5	32
	7.0	32
	7.4	34
	8.0	13
Protio	6.0	36
	6.5	30
	7.0	50
	7.4	46
	8.0	29
Increase in *11S* from H_2O to D_2O		
Deuterio	6.0	50
	6.5	50
	7.0	58
	7.5	212
	8.0	180
Protio	6.0	25
	6.5	62
	7.0	112
	7.4	156
	8.0	160

Spectral Measurements. The spectral characteristics of the deuterio and protio phycocyanin were examined in H_2O and D_2O under comparable conditions. Changes in the position of the visible absorption maximum were noted. In general, these shifts were of the order of approximately 2 mμ. The increase in the relative concentration of *11S* resulted in a small red shift. Attempts at difference spectra of D_2O and H_2O solutions of protio phycocyanin under related conditions (pD =

Table IV. Sedimentation Behavior of Other Proteins in D_2O and H_2O

	H_2O		D_2O
Protein and pH	S_{25}, H_2O[a]	S_{25}, H_2O[b]	S_{25}, H_2O[a, c]
Trypsin (pH 6.0, pD 6.3)	2.6	2.9	3.0
Soybean trypsin inhibitor (pH 6.0, pD 6.3)	2.3	2.9	2.5
Trypsin inhibitor, 1:1 complex (pH 6.0, pD 6.3)	3.4	4.2	3.8
Catalase[d]			
pH 6.9	4.2	4.7	4.8
pD 6.6	8.3	8.5	6.8
	12.7	12.8	12.8
α_s-casein B[e]			
pH 7.3, pD 7.3, $\mu = 0.01$	1.71	1.48	3.98
pH 7.3, pD 7.7, $\mu = 0.1$	4.2	5.1	7.4

[a] Sedimentation coefficients determined in this study.
[b] Literature values of sedimentation coefficients: trypsin and soybean trypsin inhibitor (*17*); catalase (*18*); α_s-casein B (*10*).
[c] As if sedimentation proceeded at solvent viscosity and density of water, at given protein concentration.
[d] Relative area under the three catalase peaks unchanged in going from H_2O to D_2O.
[e] α_s-Casein B sedimentation results included experiments at protein concentrations of from 2 to ~ 10 mg./ml. with little variation in sedimentation coefficients. An α_s-casein B D_2O solution was also lyophilized and reconstituted in H_2O with a return to the S_{25}, H_2O value close to that in the literature.

pH) indicated that in D_2O there was an enhancement of absorption in the 625-mμ region. Deuterio phycocyanin when compared with protio phycocyanin in H_2O or D_2O showed the expected blue shift (*15*) and difference spectra indicated an enhancement of absorption in the 610-mμ region. The observed trends of the spectral shifts were entirely consistent with the previous postulate (*4, 8, 16*) that the visible absorption maximum represents the overlap of absorption maxima owing to each of the several species present, and enhancement of the percentage of large aggregates results in a red shift and disaggregation results in a blue shift.

Discussion

Our data seem to confirm the suggestion of Kresheck *et al.* (*11*) that hydrophobic interactions are enhanced in D_2O. A logical argument for the enhancement of hydrophobic forces in D_2O could be formulated simply from the more structured nature of D_2O. The term "hydrophobic forces" refers to the favorable entropic effect of squeezing together

apolar amino acid residues. With a more ordered structure, a greater ΔS contribution is to be expected.

The relative difference of aggregation in H_2O and D_2O seems to be a sensitive indicator of the presence of hydrophobic forces. Several proteins, in which a hydrophobic aggregation mechanism is not postulated, behave almost identically in H_2O and D_2O. These include the trypsin–soybean trypsin inhibitor complex, which has been characterized as proceeding by a mechanism in which protons are released (*12*). For α_s-casein B a greater degree of aggregation is favored in D_2O than in H_2O. The mechanism of the aggregation of α_s-casein B is reported to involve some electrostatic contributions (*9*) and is still under study; however, hydrophobic forces have been suggested in at least one genetic variant of α_s-casein (*13*).

In several recent publications (*5*, *15*, *16*), the *11S* species in *C*-phycocyanin from several different algal sources has been characterized; it is favored under conditions of high temperature, high ionic strength, and pH close to the isoelectric point. Mainly from electron micrographs (*3*), it was postulated that this species is a hexamer, a deduction corroborated by hydrodynamic measurements. The *7S* species, or trimer, appears to be favored under conditions that intensify electrostatic repulsive forces. The *3S* material is thought to be the monomeric species. It has been suggested that the *11S* species is stabilized by virtue of dispersion interactions that successfully compete with electrostatic repulsion. The water structure, entropy effect (*14*), pushes the subunits together, and dispersion forces stabilize the subunit interaction against the electrostatic repulsion. The conditions for formation of the *19S* species are evidently more complex and not well understood, except that they do not correspond exactly to those for the *11S*. There appear to be some charge interactions which favor *19S* formation. In studies to be published shortly, we have examined the effect of D_2O on phycocyanin samples with much larger amounts of *11S*, *19S*, and *25S* material. In all experiments the amount of *19S* material is never enhanced in D_2O. There is some enhancement of *11S*, but a consistent decrease in *19S* and a major increase in much higher aggregates. These findings seem to suggest that the *19S* aggregate is not stabilized by a simple hydrophobic mechanism. Studies with deuterated phycocyanin (*16*) indicated that less *11S* material is found under conditions comparable with those examined for protio protein. It was suggested that a decrease in dispersion interactions inferred from the work of Bartell and Roskos (*1*) was responsible for a less successful competition with the destabilizing electrostatic repulsion forces. Consequently, although the subunits were forced together by hydrophobic forces, the hexamer was less stable because of more efficient subunit repulsion. Hattori *et al.* (*8*) suggested that in deuterated phyco-

cyanin the hydrophobic forces were decreased, which would account for the smaller amount of higher aggregates they found.

In our study it seems logical to assume that the increase in aggregation observed in D_2O over that encountered in H_2O is the result of an increase in hydrophobic forces (entropic effect). The data in Table II and their analyses in Table III indicate little if any difference between the enhancement of this entropic effect in the protio or deuterio protein from H_2O to D_2O. [We have not discussed the increase in aggregation in D_2O as explicable in terms of hydrogen bonding *vs.* deuterium bonding since in all previous work reported for the phycocyanin system there is no evidence implicating hydrogen bonding as a major stabilizing influence in subunit interaction resulting in hexamer formation. The possible consequences of conventional secondary isotope effects in the deuterio protein have been discussed (*16*). They do not appear to be relevant to the interpretation of any of the current experimental data.]

These observations are difficult to explain if there were, as postulated by Hattori *et al.* (*8*), a smaller hydrophobic force contribution expected from the deuterated protein. Consequently, we suggest that the current results are consistent with our previous postulate that the entropic effect known as hydrophobic forces is sufficient to push the subunits together, and these aggregates are then stabilized by virtue of dispersion forces (*16*). Certainly, this postulate needs further experimental support; however, it is entirely consistent with currently accepted ideas concerning hydrophobic forces.

The only aggregate enhanced in D_2O is the *11S* species. This specific enhancement is additional support for our previous suggestion that the *11S* aggregate is favored under conditions that are associated with a hydrophobic force mechanism, and the *7S* is not. It appears then that comparative studies of aggregation phenomena in H_2O and D_2O are a convenient method for indicating aggregation processes favored by hydrophobic forces.

This study, therefore, presents a novel method for enhancement of hydrophobic forces and a sensitive method for detecting this effect. A properly constructed experiment using D_2O and H_2O solutions may also be used to measure the relative contribution of the several stabilizing forces in systems of biological interest.

Literature Cited

(1) Bartell, L. S., Roskos, R. R., *J. Chem. Phys.* **44**, 457 (1966).
(2) Berns, D. S., *J. Am. Chem. Soc.* **85**, 1676 (1963).
(3) Berns, D. S., Edwards, M. R., *Arch. Biochem. Biophys.* 110, 511 (1965).
(4) Berns, D. S., Morgenstern, A., *Biochemistry* **5**, 2985 (1966).
(5) Berns, D. S., Scott, E., *Biochemistry* **5**, 1528 (1966).

(6) Boucher, L. J., Crespi, H. L., Katz, J. J., *Biochemistry* **5**, 3796 (1966).
(7) Edelstein, S. J., Schachman, H. K., *J. Biol. Chem.* **242**, 306 (1967).
(8) Hattori, A. Crespi, H. L., Katz, J. J., *Biochemistry* **4**, 1225 (1965).
(9) Ho, C., Chen, A. H., *J. Biol. Chem.* **242**, 551 (1967).
(10) Ho, C., Waugh, D. F., *J. Am. Chem. Soc.* **87**, 110 (1965).
(11) Kresheck, G. C., Schneider, H., Scheraga, H. A., *J. Phys. Chem.* **69**, 3132 (1965).
(12) Northrop, J. H., Kunitz, M., Herriott, R. M., "Crystalline Enzymes," Columbia University Press, New York, 1948.
(13) Payens, T. A. J., Schmidt, D. G., *Biochem. Biophys. Acta* **109**, 214 (1965).
(14) Scheraga, H. A., *Proteins* 1, 477 (1963).
(15) Scott, E., Berns, D. S., *Biochemistry* **4**, 2597 (1965).
(16) *Ibid.*, **6**, 1327 (1967).
(17) Sheppard, E., McLaren, A. D., *J. Am. Chem. Soc.* **75**, 2587 (1953).
(18) Tanford, C., Lovrien, R., *J. Am. Chem. Soc.* **84**, 1892 (1962).

RECEIVED May 8, 1967. No. IV in the series "Fully Deuterated Proteins." No. III is (*16*). Work supported in part by a grant (GB 4460) from the National Science Foundation. J. J. Lee is postdoctoral fellow under U. S. Public Health Service Grant 1501 FR-5559-03.

Size and Structure of Bile Salt Micelles

Influence of Structure, Concentration, Counterion Concentration, pH, and Temperature

DONALD M. SMALL

Department of Medicine, Boston University School of Medicine, Boston, Mass. 02118

The aggregation numbers (Ag#) of free and conjugated di- and trihydroxy bile salts were studied by equilibrium ultracentrifugation and light scattering. The effect of concentration, counterion concentration, pH, temperature, and urea are shown. All trihydroxy bile salts form very small micelles (Ag# <10) which are resistant to change in counterion concentration, temperature, and urea. Dihydroxy bile salts form small micelles at low concentrations and large micelles at higher concentrations (Ag# 12 to 100). Temperature and urea markedly decrease their aggregation number. pH has little effect on the aggregation number of the trihydroxy bile salts, but enormous aggregates form in the deoxycholate series as pH decreases towards the pK_a. *The small micelles are probably bonded hydrophobically. Larger micelles are formed by the aggregation of small micelles through hydrogen bonding of hydroxyl groups.*

Although bile salts have been considered detergents, their structure is so markedly different from ordinary aliphatic anionic detergents that one might expect some differences in micelle formation and structure. Unlike the usual aliphatic detergents which possess a clear-cut polarity between hydrophobic and hydrophilic parts, bile salts possess a rigid ring structure, one side of which is spiked with hydroxyl groups, the other side with methyl groups. Further, one end possesses a short hydrocarbon chain ending in a carboxyl group which, for naturally occurring bile salts, is conjugated with glycine or taurine. Bile salts can be viewed as a rigid

ring structure with hydrophilic and hydrophobic sides to which is attached a mobile hydrophilic tail.

Monolayer studies on dilute HCl (*6*, *7*, *8*) have demonstrated that only cholanic acid (no hydroxyl groups) stands erect on the surface. All the other bile salts lie flat on the surface with both the hydrophilic part of the alkyl chain and the ring hydroxyl(s) in the aqueous phase. On the basis of these and other important studies Ekwall (*9*) suggested that bile salts aggregate at low concentrations to form ion pairs bonded through lipophilic regions and at higher concentrations form aggregates of these ion pairs bonded in some way hydrophilic part to hydrophilic part.

This paper reports the systematic study of the apparent anhydrous micellar weights of the three principal bile salts found in man and their glycine and taurine conjugates in respect to bile salt concentration, counterion concentration, temperature, pH, and urea concentration. On the basis of these studies, model structures of bile salt micelles are proposed. Sodium dehydrocholate, a triketo bile salt, was also studied but was not found to form micelles.

Materials and Methods

Bile Salts. The sodium salts of the following bile acids were studied: cholic acid (3α,7α,12α-trihydroxy-5β-cholanoic acid), deoxycholic acid (3α,12α-dihydroxy-5β-cholanoic acid), chenodeoxycholic acid (3α,7α-dihydroxy-5β-cholanoic acid), dehydrocholic acid (3α,7α,12α-triketocholanoic acid), glycocholic acid (3α,7α,12α-trihydroxy-5β-cholanoyl glycine), glycodeoxycholic acid (3α,12α-dihydroxy-5β-cholanoyl glycine), glycochenodeoxycholic acid (3α,7α-dihydroxy-5β-cholanoyl glycine), taurocholic acid (3α,7α,12α-trihydroxy-5β-cholanoyl taurine), taurodeoxycholic acid (3α,12α-dihydroxy-5β-cholanoyl taurine), and taurochenodeoxycholic acid (3α,7α-dihydroxy-5β-cholanoyl taurine). The trivial names of these bile acids or their sodium salts are used henceforth.

Free bile acids were obtained from the Cal Biochemical Co. Cholic acid, which contained a small amount of dihydroxy acid, was recrystallized several times from ethanol and petroleum ether. These crystals and the other free bile acids were pure as measured by thin-layer chromatography (TLC) (*14*) (100-μgram application) and gave the correct equivalent weight on titration. Conjugated bile acids were obtained from the Maybridge Co., Tintagel, England. Glycocholic acid, taurodeoxycholic acid, glycodeoxycholic acid, taurochenodeoxycholic acid, and glycochenodeoxycholic acid showed traces of impurity usually corresponding to the homologous free acid by TLC (200-μgram application) but gave correct equivalent curves by titration. Taurocholic acid, although pure by TLC, gave an erroneous curve by titration and was recrystallized by the method of Pope (*21*). All acids were titrated in doubly distilled water to pH 10, lyophilized, and stored under vacuum at $-10°$C.

Other chemicals used (NaCl, urea, and HCl) were reagent grade. The solutions for ultracentrifugation were made up in acid-washed 10-ml. volumetric flasks to contain the desired percentage of bile salt in water, NaCl solution, or a solution of NaCl and urea. These solutions were run in the Spinco model E analytical ultracentrifuge equipped with a temperature-control system and an electronic speed-control system within 3 days of preparation.

The method of equilibrium ultracentrifugation described by Yphantis (*28*) was used in these studies. A double-sector centerpiece with two 2 1/2° sectors 12 mm. in length was used with standard Schlieren optics. Apparent molecular weights, M, were determined from the equation:

$$M = \frac{1}{\bar{r}C_o} \frac{(dc)}{(dr)_{r=\bar{r}}} \frac{RT}{\omega^2(1 - \bar{V}p)}$$

where $\bar{r}$ is distance from center of the rotor to midpoint of the cell; (dc/dr) is the refractive index gradient at the midpoint of the cell $(\bar{r})$ given directly by the difference between the two solution traces; R is the gas constant; T is the absolute temperature; ω is the angular velocity. The partial specific volume, $\bar{V}$, of the bile salts was measured by picnometry in each solvent at 22°C. as a 3% solution. Values taken for 1.5 and 0.5% solutions were virtually the same as the 3% solutions. Values at 36°C. were slightly higher than at 22°C. The values found ranged from 0.74 to 0.78 ml. per gram, which agree well with the values found in the literature (*5*, *17*). The appropriate values were used in the calculations and are recorded in Table I. The density of the solutions, ρ, was obtained by picnometry and agreed well with solution densities calculated from either Svedberg and Pedersen (*27*) or the International Critical Tables (*16*).

The initial concentration, C_o, in square centimeters, was determined directly from the area under the curve of a synthetic boundary trace. Although usual practice is to place solvent in one cell and the solution in the other, the "solvent" used in this work was a solution of bile salt slightly above its critical micellar concentration, *CMC* (*15*), usually 0.5 gram per 100 ml. The "solution," which was placed in the other cell, was a more concentrated solution (1.5 to 5.0 grams per 100 ml.). Therefore, since both the solvent and the solution were saturated with monomers, C_o represents an initial concentration difference of bile salts in the micellar phase. The pertinent data for each equilibrium ultracentrifugation experiment are presented in Table I.

LIGHT-SCATTERING METHODS. A light-scattering photometer (Brice-Phoenix model 0M2000) was used with a No. T-104 (14-ml.) cell. A total of 15 solutions of sodium taurodeoxycholate varying in concentration from 0.08 to 2.5 grams per 100 ml. were made up in the following three salt concentrations: 0.1*M* NaCl, 0.3*M* NaCl, and 0.5*M* NaCl. The solutions were centrifuged in a Spinco model L ultracentrifuge at about 20,000 r.p.m. for about 2 hours before being transferred carefully to the cell. This was necessary to get rid of dust. Other techniques for removing dust, such as millipore filtration, gave erratic results.

Table I. Equilibrium

		Experimental Conditions	
Bile Salt[a]	*Temp., °C.*	*Solvent*	*pH*
NaC	20	H_2O	8–9
		0.01*M* NaCl	8–9
		0.05*M* NaCl	8–9
		0.15*M* NaCl	8–9
	36	0.15*M* NaCl	8–9
	20	0.3*M* NaCl	8–9
		1.0*M* NaCl	8–9
	36	1.0*M* NaCl	8–9
NaGC	20	H_2O	8–9
			8–9
			8–9
			8–9
			8–9
			8–9
			8–9
			8–9
			8–9
		0.05*M* NaCl	8–9
		0.15*M* NaCl	8–9
	36	0.15*M* NaCl	8–9
	20	0.3*M* NaCl	8–9
NaTC	20	0.05*M* NaCl	8–9
		0.15*M* NaCl	8–9
	36	0.15*M* NaCl	8–9
	20	0.3*M* NaCl	8–9
		0.01*M* NaCl	8–9
	4	0.15*M* NaCl	8–9
		0.3*M* NaCl	8–9
	20	1.0*M* NaCl	8–9
		4*M* urea + 0.15*M* NaCl	8–9
		6*M* urea + 0.15*M* NaCl	8–9
NaDC	20	0.01*M* NaCl	8–9
	36	0.01*M* NaCl	8–9
	20	0.05*M* NaCl	8–9
		0.15*M* NaCl	8–9
	36	0.15*M* NaCl	8–9
	20	0.3*M* NaCl	8–9
		6*M* urea + 0.15*M* NaCl	8–9
		0.15*M* NaCl	7.3
	36	0.15*M* NaCl	7.3
	20	0.15*M* NaCl	7.85
	36	0.15*M* NaCl	7.85

Untracentrafugation of Bile Salt Solutions

Data					*Results*	
$\bar{V}$	$\bar{r}$	C_0	$(dc/dr)_{r=\bar{r}}$	$\omega^2 \times 10^6$	*M*	*Ag#*
0.75	6.8784	0.10152	0.0690	11.2295	853	2.0
0.75	6.8401	0.08063	0.0586	8.40824	1227	2.8
0.75	6.8125	0.07991	0.0733	8.40824	1650	3.8
0.75	6.8206	0.07975	0.0954	8.40824	2061	4.8
0.76	6.8151	0.07977	0.0870	8.40824	2062	4.8
0.75	6.8605	0.07804	0.1120	8.40824	2519	5.8
0.75	6.9176	0.07753	0.0536	3.5452	3108	7.2
0.76	6.9132	0.07554	0.0632	4.5682	3137	7.3
0.75	6.9027	0.03621	0.0372	14.2123	1015	2.1
0.75	6.9042	0.07484	0.0346	7.4132	876	1.8
0.75	6.8810	0.11390	0.0554	7.4132	925	1.9
0.75	6.8892	0.15197	0.0710	7.4132	887	1.8
0.75	6.8624	0.1901	0.0774	6.3166	901	1.9
0.75	6.9179	0.22886	0.0668	4.3865	933	1.9
0.75	6.8626	0.26797	0.0752	4.3865	904	1.9
0.75	6.8796	0.30257	0.0860	4.3865	913	1.9
0.75	6.8880	0.34432	0.0778	3.5531	895	1.8
0.76	6.8560	0.07597	0.0652	5.1830	2455	5.0
0.76	6.9150	0.07041	0.0690	5.1830	2816	5.8
0.77	6.9094	0.06971	0.0620	5.1830	2750	5.6
0.76	6.9000	0.07838	0.0916	5.1830	3435	7.0
0.75	6.8475	0.06618	0.0770	7.4018	2243	4.2
0.75	6.86376	0.06587	0.0826	7.4018	2447	4.6
0.76	6.85902	0.06249	0.0716	7.4018	2395	4.5
0.75	6.8642	0.06534	0.1060	7.4018	3215	6.0
0.75	6.9235	0.07544	0.0764	7.4132	1916	3.6
0.75	6.8695	0.090547	0.1062	7.4132	2154	4.0
0.75	6.8578	0.077577	0.1158	7.4132	2788	5.2
0.74	6.8871	0.05492	0.1290	7.4132	4844	9.0
0.75	6.8961	0.10738	0.1178	8.5992	2282	4.2
0.76	6.8686	0.04699	0.0264	17.5461	943	1.8
0.76	6.8214	0.0826	0.0352	3.5452	1781	4.3
0.77	6.8144	0.0818	0.0540	6.6526	1582	3.8
0.76	6.8478	0.07940	0.0642	3.2632	3678	8.9
0.76	6.8994	0.08277	0.1138	3.2632	6290	15.2
0.77	6.8941	0.07811	0.0872	3.2632	5496	13.3
0.76	6.8712	0.07851	0.1080	1.7382	12107	29.2
0.78	6.8939	0.07562	0.0508	6.3166	2688	6.5
0.76	6.9086	0.07580	0.2124	0.18068	228809	551.9
0.77	6.90367	0.07798	0.0472	1.7382	5587	13.5
0.76	6.8866	0.08155	0.0530	1.3934	6975	16.8
0.77	6.8515	0.08254	0.0490	1.7382	5521	13.3

Table I.

	Experimental Conditions		
Bile Salt[a]	*Temp., °C.*	*Solvent*	*pH*
NaGDC	20	H_2O	8–9
			8–9
			8–9
			8–9
			8–9
			8–9
			8–9
			8–9
			8–9
		0.05*M* NaCl	8–9
		0.15*M* NaCl	8–9
	36	0.15*M* NaCl	8–9
	20	0.3*M* NaCl	8–9
		0.5*M* NaCl	8–9
	36	0.5*M* NaCl	8–9
	20	2*M* urea + 0.5*M* NaCl	8–9
	36	2*M* urea + 0.5*M* NaCl	8–9
	20	4*M* urea + 0.5*M* NaCl	8–9
		6*M* urea + 0.5*M* NaCl	8–9
		0.15*M* NaCl	4.9
		0.15*M* NaCl	6.2
		0.15*M* NaCl	7.2
NaTDC	20	0.01*M* NaCl	8–9
			8–9
			8–9
		0.05*M* NaCl	8–9
		0.15*M* NaCl	8–9
	36	0.15*M* NaCl	8–9
	20	0.3*M* NaCl	8–9
		0.5*M* NaCl	8–9
		2*M* urea + 0.5*M* NaCl	8–9
		4*M* urea + 0.15*M* NaCl	8–9
	36	4*M* urea + 0.15*M* NaCl	8–9
	20	4*M* urea + 0.5*M* NaCl	8–9
		6*M* urea + 0.15*M* NaCl	8.0
		6*M* urea + 0.5*M* NaCl	8–9
		0.15*M* NaCl	1.6
		0.15*M* NaCl	3.6
		0.15*M* NaCl	6.5
NaCDC	20	0.05*M* NaCl	8–9
		0.15*M* NaCl	8–9
	36	0.15*M* NaCl	8–9
	20	0.3*M* NaCl	8–9
		0.15*M* NaCl	7.00
		0.15*M* NaCl	7.05

Continued

Data					*Results*	
$\bar{V}$	$\bar{r}$	C_0	$(dc/dr)_{r=\bar{r}}$	$\omega^2 \times 10^6$	*M*	*Ag#*
0.77	6.8993	0.01785	0.0228	21.2307	919	2.0
0.77	6.8912	0.037867	0.0380	17.5461	876	1.9
0.77	6.8882	0.07835	0.0396	8.5976	901	1.9
0.77	6.8879	0.12014	0.0356	5.3077	855	1.8
0.77	6.8628	0.16236	0.0396	4.3865	855	1.8
0.77	6.8737	0.19937	0.0478	4.3865	839	1.8
0.77	6.8834	0.23814	0.0566	4.3865	831	1.8
0.77	6.8848	0.28608	0.0544	3.5531	821	1.7
0.77	6.8766	0.3545	0.536	2.8074	826	1.8
0.77	6.93447	0.079686	0.0644	2.2394	5520	11.7
0.77	6.8696	0.07747	0.0786	1.7382	9139	19.4
0.78	6.8631	0.07538	0.0592	1.7382	7618	16.2
0.77	6.8872	0.07903	0.1596	1.8533	17836	36.9
0.77	6.1972	0.07797	0.2666	1.8533	30143	63.9
0.78	6.9133	0.07859	0.1820	1.8533	21975	46.6
0.76	6.9379	0.07072	0.1054	1.8533	14059	29.8
0.77	6.8821	0.07271	0.0758	1.8533	10693	22.7
0.77	6.8813	0.05473	0.0474	1.8533	10018	21.2
0.78	6.9284	0.09567	0.0506	4.3865	3293	7.0
0.78	6.8561	0.08213	0.4088	0.079648	1030000	2184
0.76	6.8752	0.08963	0.1048	1.7382	10076	21.4
0.77	6.8960	0.086865	0.0832	1.7382	8644	18.3
0.76	6.8805	0.088905	0.0560	2.8074	3259	6.2
0.76	6.9185	0.17112	0.1000	2.8074	3044	5.8
0.76	6.8860	0.31068	0.1132	1.5791	3383	6.5
0.76	6.92958	0.08287	0.0572	1.7382	5885	11.3
0.76	6.78648	0.07352	0.0950	1.7382	11367	21.8
0.77	6.8801	0.0704	0.0712	1.7382	9367	18.0
0.76	6.87616	0.08002	0.1368	1.7382	15154	29.1
0.76	6.9121	0.06639	0.2230	2.1494	24402	46.8
0.76	6.9271	0.04336	0.0998	2.4674	16332	31.3
0.76	6.8480	0.065626	0.0652	3.2632	5798	11.1
0.77	6.8423	0.0664	0.0555	3.2632	5293	10.1
0.76	6.9162	0.05746	0.1000	3.1693	10991	21.1
0.78	6.8950	0.05581	0.0660	6.3166	4732	9.1
0.77	6.9071	0.05117	0.0600	3.5531	8321	16.0
0.76	6.8705	0.079534	0.1240	1.7382	13446	25.8
0.76	6.8704	0.08329	0.1104	1.7382	11431	21.9
0.76	6.8958	0.07298	0.0940	1.7382	11068	21.2
0.78	6.9092	0.07989	0.0478	3.5452	2709	6.5
0.78	6.9524	0.08938	0.0660	2.5403	4705	11.3
0.79	6.9465	0.08219	0.0752	3.5452	4502	10.9
0.78	8.8642	0.081263	0.0706	1.7382	8385	20.2
0.78	6.9327	0.08607	0.0720	1.7382	7812	18.8
0.78	6.8664	0.08094	0.0664	1.8533	7254	17.5

Table I.

		Experimental Conditions	
Bile Salt[a]	*Temp., °C.*	*Solvent*	*pH*
NaGCDC	20	0.05*M* NaCl	8.0
		0.15*M* NaCl	8.0
	36	0.15*M* NaCl	8–9
	20	0.3*M* NaCl	8–9
NaTCDC	20	0.15*M* NaCl	8–9
		0.15*M* NaCl	8–9
	36	0.15*M* NaCl	8–9
	4	0.15*M* NaCl	8–9
	20	0.3*M* NaCl	8–9
NaDHC[b]	20	0.15*M* NaCl	8–9
		0.15*M* NaCl	8–9
		1.0*M* NaCl	8–9

[a] Abbreviations as in Figures 5, 6, and 7.

The absolute turbidity, T, was calculated using a wavelength of 4360 A. from the equation:

$$T = 1.25\, n^2 aF(G_{90}/G_0)$$

where (G_{90}/G_0) is the scattering ratio at 90° and 0°; F is the filter factor; a is a constant relating the working glass standard to the opal glass reference standard; n is the refractive index of the solution measured in a standard four-place refractometer. The uncorrected micellar weights, M, were calculated by extrapolating HC/T values to zero concentration from the equation $1/M = HC/T$ where H is equal to $15.2 \times 10^{-5} \times n^2 (n - n_o)^2/C^2$, n is equal to the refractive index of the solution, and $(n - n_o)/C$ is the refractive increment for the given solvent-solute system determined with a Brice-Phoenix differential refractometer. Since the HC/T *vs.* concentration curve was erratic at concentrations below and around the *CMC*, only the linear part of the curve (approximately 1 to 2.5%) was used in extrapolating to zero concentration. The substitute "aggregation numbers" for "molecular weights" aggregation numbers shown in Figure 2 were not corrected for solvent turbidity or for *CMC*. The calculated corrected molecular weights were about 10% lower.

Results

Table I records the conditions of the experiment (temperature, pH, and solvent); the experimental data used to calculate the apparent micellar weights by equilibrium ultracentrifugation [$\bar{V}$, $\bar{r}$, C_o, $(dc)/(dr)_{r=\bar{r}}$, ω^2], and the results (apparent micellar weight, M, and apparent aggregation number, Ag#), for each bile salt studied. The results are illustrated in Figures 1 to 10.

Continued

Data					*Results*	
$\bar{V}$	$\bar{r}$	C_o	$(dc/dr)_{r=\bar{r}}$	$\omega^2 \times 10^6$	*M*	*Ag#*
0.77	6.9024	0.082629	0.0600	2.2394	4983	10.6
0.77	6.8751	0.07567	0.0816	1.7382	9706	20.6
0.78	6.8678	0.07459	0.0662	1.7382	8603	18.2
0.77	6.8563	0.07286	0.0750	1.2296	13417	28.4
0.76	6.8977	0.07938	0.0464	1.7382	4956	9.5
0.76	6.8522	0.07222	0.0600	1.2292	10155	19.5
0.77	6.8452	0.07334	0.0626	1.7382	7945	15.2
0.76	6.8442	0.07807	0.1054	1.5791	13313	25.5
0.76	6.9133	0.068163	0.0572	0.8427	15141	29.0
0.77	6.8393	1.11987	0.0514	13.8982	485	1.1
0.77	6.8716	0.03095	0.0250	2.5403	497	1.2
0.77	6.8918	0.2839	0.1218	6.3166	1199	2.8

[b] NaDHC = sodium dehydrocholate.

Effect of Concentration of Bile Salt. To study the effect of the concentration of bile salt on the apparent micellar weights, *M*, three different bile salts were studied at a series of different initial concentration differences, C_o, varying between 0.25 and 4.5 grams per 100 ml. A plot of the apparent micellar weights (M_Q *vs.* C_o (in grams per 100 ml.) appears in Figure 1. The two glycine conjugates were studied in water and the taurine conjugate in 0.01*N* NaCl. Sodium glycocholate (Na glycocholate), a trihydroxy bile salt, has a micellar weight extrapolated to zero concentration difference of 930. The dihydroxy bile salt sodium glycodeoxycholate (Na glycodeoxycholate) has a micellar weight of 900. Since the molecular weights of Na glychocholate and Na glycodeoxycholate are 487.6 and 471.6, respectively, the aggregation numbers for both are about 1.9. Dividing the micellar weights by the molecular weights of the bile salt anion gives aggregation numbers of almost exactly 2.0 in both cases. Hence, these two bile salts appear to form dimers in water and probably do not bind the sodium ion tightly.

Sodium taurodeoxycholate in 0.01*N* NaCl has an extrapolated micellar weight of about 3150, which gives an aggregation number of about 6. Since, in these three cases, the micellar weights obtained from extrapolation to zero concentration are not significantly different from the apparent micellar weights obtained at initial concentration differences ranging between 1.0 and 4.5 grams per 100 ml., the other bile salts were studied at only 1 or 2 initial concentration differences. The apparent micellar weights were divided by the molecular weight of the bile salt to obtain the apparent anhydrous aggregation numbers (number of molecules per micelle).

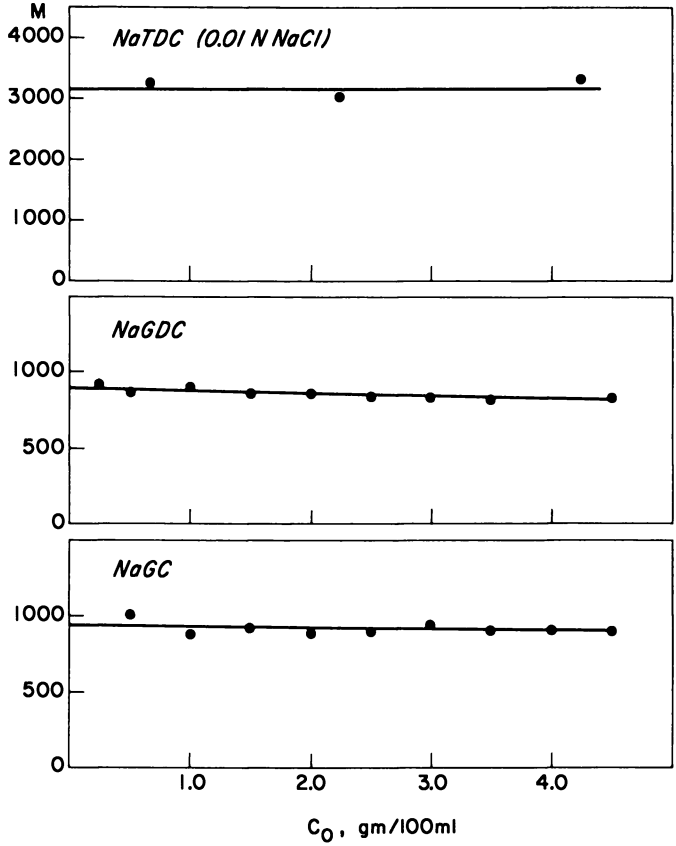

Figure 1. Apparent micellar weight by equilibrium ultracentrifugation vs. *initial concentration difference*

NaTDC. Sodium taurodeoxycholate
NaGDC. Sodium glycodeoxycholate
NaGC. Sodium glycocholate
Micellar weight extrapolated to zero initial concentration difference. NaTDC in 0.01 NaCl, 3150; NaGDC in H_2O, 900; NaGC in H_2O, 930

Comparison of Results Obtained by Equilibrium Ultracentrifugation and Light Scattering. Figure 2 represents comparison of the uncorrected micellar aggregation numbers found by light scattering and by equilibrium ultracentrifugation for sodium taurodeoxycholate in relation to the concentration of NaCl. The correlation is good. Figures 3 and 4 represent similar comparisons with light-scattering data reported from two other laboratories (*4*, *13*). The aggregation numbers of Na deoxycholate and Na cholate (*4*) and Na glycocholate (*13*) calculated from the light-scattering data show excellent correlation with the apparent

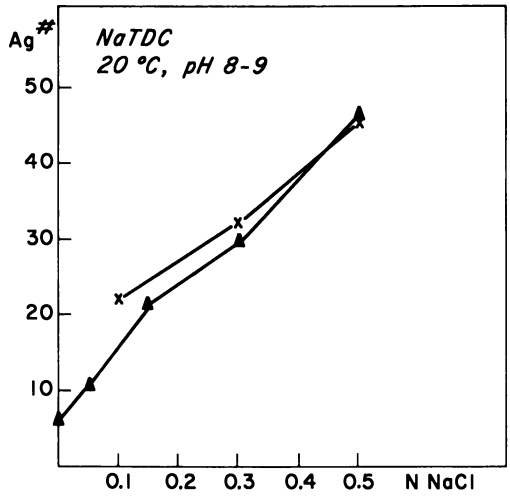

Figure 2. Apparent aggregation number vs. *counterion concentration*

× *Uncorrected, by light-scattering measurements*
▲ *Apparent, by equilibrium ultracentrifugation*

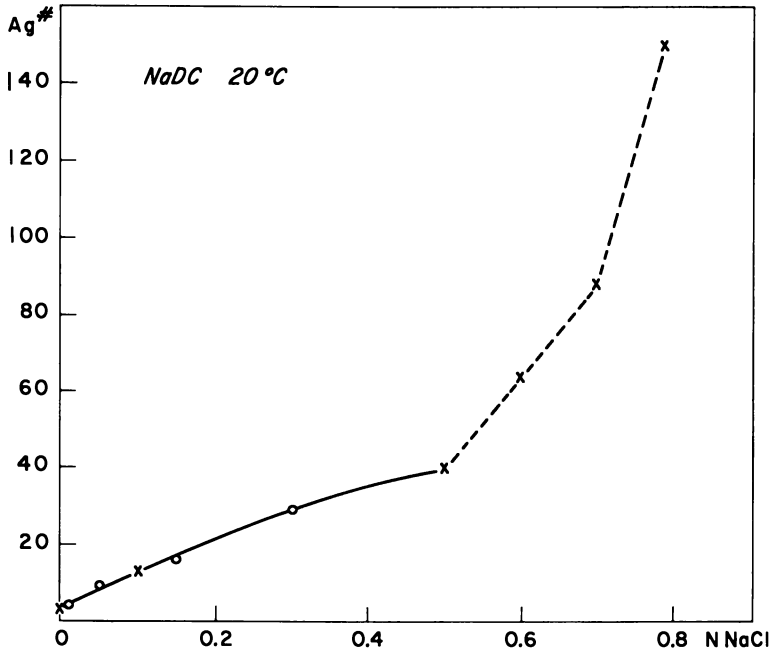

Figure 3. Apparent aggregation number vs. *counterion concentration*

× *By light scattering* (4)
○ *Apparent, by equilibrium centrifugation pH 8 to 9*

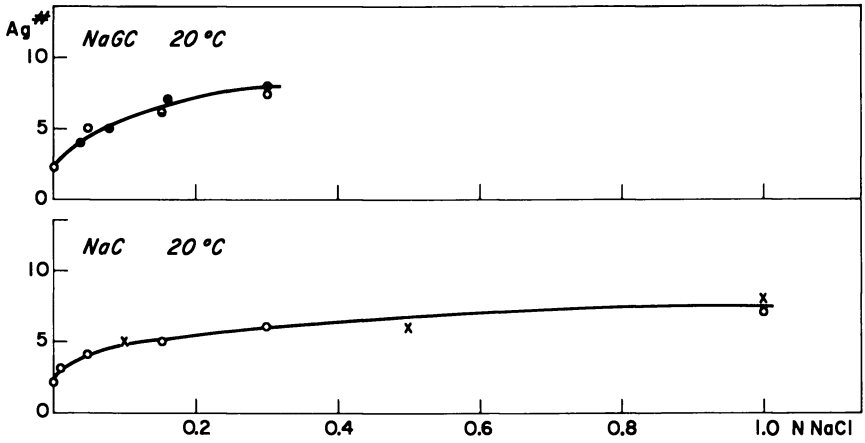

Figure 4. Apparent aggregation number vs. *counterion concentration*
Top. Sodium glycocholate
● *By light scattering* (13)
○ *Apparent, by equilibrium ultracentrifugation*
Lower. Na cholate
× *By light scattering* (4)
○ *Apparent, by equilibrium centrifugation pH 8 to 9*

aggregation numbers found in the present study by equilibrium ultracentrifugation.

Effect of Counterion Concentration. Figures, 5, 6, and 7 give the aggregation number of the micelle (number of molecules of bile salt per micelle) as the concentration of NaCl is increased for free bile salts (Figure 5), taurine conjugates (Figure 6), and glycine conjugates (Figure 7), respectively, at 20°C. and pH 8 to 9.

Free Bile Salts. Na dehydrocholate, a triketo bile salt, does not form micelles in salt concentrations up to 0.3*N* NaCl. Na cholate (Figure 5), the trihydroxy bile salt, forms small aggregates in low salt concentrations which become somewhat larger with increasing salt. However, even at 1.0*N* NaCl the micelle consists of only about seven monomers. Na chenodeoxycholate, a dihydroxy bile salt, forms similar very small aggregates at low salt concentrations. Increasing NaCl concentrations produce a marked increase in the aggregation number to 18 at 0.3*N* NaCl. Even more striking is the change in aggregation number of NaDC from four monomers at 0.01*N* NaCl to about 29 monomers at 0.3*N* NaCl.

Taurine and Glycine Conjugated Bile Salts. Figures 6 and 7 show that the conjugated bile salts behave in a way similar to their free homologs. The trihydroxy series (cholates) form small aggregates in the presence of low salt concentrations and increase only moderately in size with higher salt concentrations. The dihydroxy series (chenodeoxycholates and deoxycholates), like their free homologs, form small micelles at

low NaCl concentrations, but enlarge abruptly as the counterion concentration is increased.

Effect of pH. The effect of pH on the deoxycholate series of bile salts in 0.15*N* NaCl at 20° and 36°C. is summarized in Figure 8. Solutions of free and glycine conjugated bile salts were studied between pH 9.2 and their precipitation pH (NaDC = 6.95, NaGDC = 4.9). Taurine conjugates were studied between pH 10 and 1.6.

Sodium deoxycholate above pH 8 in 0.15*N* NaCl has an aggregation number of about 15. It increases moderately between pH 8 and 7.8. A marked increase occurs between pH 7.8 and 7.3: from 18 to over 500. This change corresponds to the formation of a thin gel. These gels have been reported and studied previously (*2*, *22*, *26*). Sodium glycodeoxycholate behaves in similar fashion, only the pH at which the marked increase in aggregation number occurs is much lower (about 5.0). In both cases the solutions were clear. The amount of free acid necessary to produce the gel state has been calculated from the titration curves of the bile salts and corresponds to less than 1 molecule of bile acid for 5 molecules of bile salt. These large aggregates are temperature sensitive. The large aggregation numbers of Na deoxycholate are reduced to small ones if temperature is raised from 20° to 36°C. (*see* Figure 8). The temperature dependence of the gels of Na deoxycholate has been pointed out by Sobotka (*26*). Trihydroxy bile salt aggregates remain small as the pH is lowered. They do not form gels.

Effect of Temperature. All of the bile salts in 0.15*N* NaCl at pH 8 to 9 were studied at 20°, 36°, and in some cases at 4°C. (Figure 9). Trihydroxy bile salts which form small micelles (Ag# 2 to 9) are unaffected between 4° and 36°C. Further, the small micelles formed by the dihydroxy bile salts in low salt concentrations are not affected by temperature. However, the sizes of the micelles of dihydroxy bile salts having aggregation numbers greater than 10 are decreased as the temperature is increased.

Effect of Added Urea. Several bile salts under conditions giving different aggregation numbers were studied with increasing concentrations of urea (Figure 10). The addition of 4*M* urea to the small aggregates (Ag# < 8) formed by trihydroxy bile salts has little or no effect. Urea (6*M*) reduces those small micelles to dimers. On the other hand, all of the dihydroxy aggregates under conditions giving aggregation numbers greater than 18 are markedly decreased in size by 2, 4, and 6*M* urea. Concentrations of 6*M* urea reduce the apparent aggregation number of NaGDC in 0.5*N* NaCl at 20°C. from 63 to 6. Therefore, in urea, small micelles do not behave like the large micelles. Small micelles resist change until concentrations of urea reach 6*M*, while large micelles are

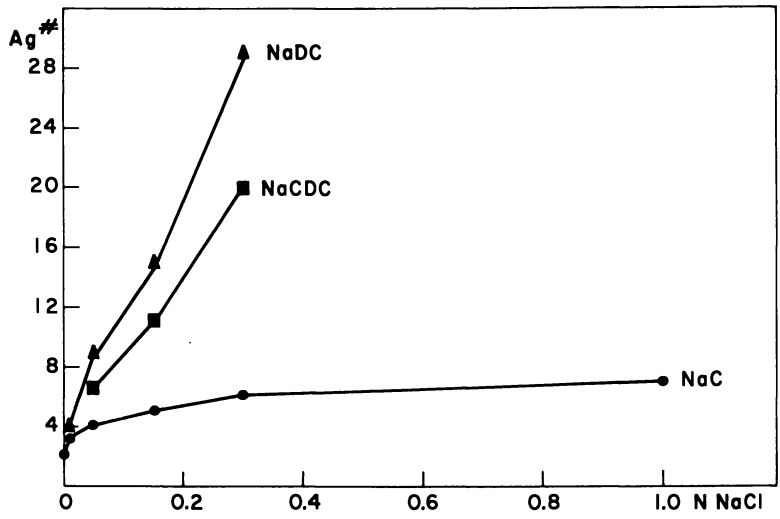

Figure 5. Apparent aggregation number vs. *counterion concentration of free bile salts at 20°C., pH 8–9*

● *Sodium cholate*
■ *Sodium chenodeoxycholate*
▲ *Sodium deoxycholate*

more sensitive to lower concentrations but are reduced in size by all concentrations of urea.

Discussion

Many studies have been carried out on the micellar size of bile salt micelles (*3, 4, 12, 13, 17, 20, 25*). The experimental conditions and results have been tabulated in a recent review (*15*). Because these studies were carried out with different bile salts in different laboratories using different techniques at different temperatures, pH, and salt concentrations, values have ranged from monomers (*4*) to aggregates having nearly 1000 associated molecules (*12*). This has tended to confuse investigators interested in biological and biochemical aspects of bile salts, who wanted to know the size of "the bile salt micelle." The emphasis here is that the type of bile salt, the pH, the temperature, and the counterion concentration all can affect the size and probably the structure of bile salt micelles.

In water at 20°C. the bile salts, free or conjugated, dihydroxy or trihydroxy bile salts, form very small aggregates, usually dimers. Unlike the dimers formed by some aliphatic detergent molecules which form at low concentrations below the *CMC* (*18, 19*), bile salts form dimers over a wide range of concentrations well above the *CMC*. As the counterion concentration is increased, a marked difference manifests itself between

the trihydroxy and dihydroxy bile salts. The trihydroxy bile salt micelles increase from dimers in water up to a maximum of about seven to nine molecules per micelle at 1.0*N* NaCl. On the other hand, the counterion concentration has a marked effect on the size of the dihydroxy bile salt micelles, even at relatively low salt concentrations—for instance, Na glycodeoxycholate, which forms dimers in water, forms large micelles with an aggregation number of about 63 in 0.5*N* NaCl (Figure 7). Since both deoxycholate and chenodeoxycholate show this marked increase in micelle size with an increase in counterion concentration, it does not appear to be the specific position of the OH group (7α or 12α) on the molecule, but rather the number of hydroxyl groups which is important. Further, higher counterion concentrations above about 0.8*N* NaCl cause precipitation of the dihydroxy bile salts at 20°C., while trihydroxy bile

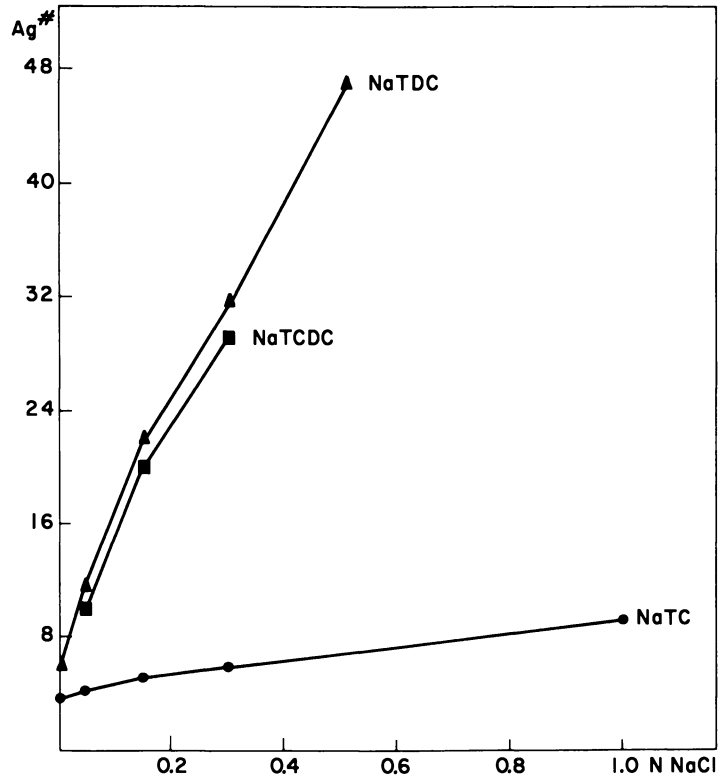

Figure 6. Apparent aggregation number vs. *counterion concentration of taurine conjugates at 20°C., pH 8–9*

● *Sodium taurocholate*
■ *Sodium taurochenodeoxycholate*
▲ *Sodium taurodeoxycholate*

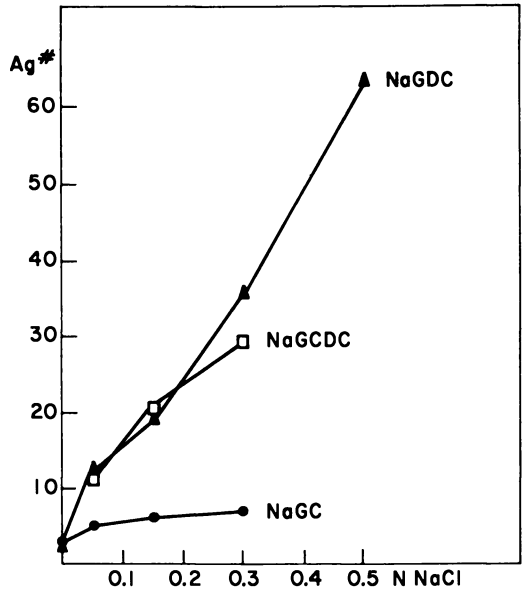

Figure 7. Apparent aggregation number vs. counterion concentration of glycine conjugates at 20°C., pH 8–9

● *Sodium glycocholate*
□ *Sodium glycochenodeoxycholate*
▲ *Sodium glycodeoxycholate*

salts remain in solution above 3*N* NaCl. It, therefore, appears that the number of hydroxyl groups are of importance not only in the type of micelles formed, but also in the solubility of bile salts. The dihydroxy bile salts "salt out" at a much lower NaCl concentration than trihydroxy bile salts.

The bile salts have a peculiar molecular structure compared with ordinary detergents, possessing both an ionic polar group and nonionic hydrophilic hydroxyl groups. These molecules might, therefore, have characteristics related to both anionic and nonionic detergents.

Since both the charged portion and the hydrophobic part of the molecule are identical for any given pair—*e.g.*, the taurine conjugates NaTC and NaTDC—the major difference in response to NaCl lies with the nonionic polar part of the molecule. Generally speaking, the increase in the aggregation number of nonionic detergents is related to the dehydration of the polar groups (*23*). Since there is a marked difference between dihydroxy and trihydroxy bile salts, it seems reasonable to conclude that the dihydroxy bile salts with only two hydroxyl groups are dehydrated much more readily than those with three groups.

Increasing temperature may bring about two opposite effects. It may favor hydrophobic bonding and thus promote micellar structure and stability or may increase the repulsive forces between the anionic polar heads and thus result in decreased micellar stability and structure breaking effects. Since temperature shows little or no effect on the small micelles formed by trihydroxy bile salts, it can be assumed that these two effects are roughly balanced. The large micelles formed by dihydroxy bile salts in NaCl solutions are markedly decreased in size by temperature. This behavior is opposite that observed for nonionic detergents, whose aggregation numbers increase with temperature (*23*, *24*). Therefore, it would appear that nonionic polar parts of the bile salt are hidden in these large micelles and that the anionic polar moiety predominates.

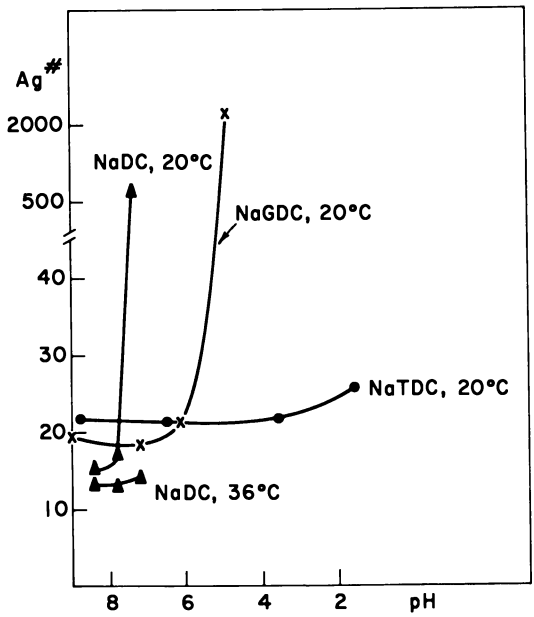

Figure 8. Apparent aggregation number vs. *pH of deoxycholate series (0.15*N *NaCl)*

▲ *Sodium deoxycholate*
× *Sodium glycodeoxycholate*
● *Sodium taurodeoxycholate*

The effect of low concentrations of urea (2*M*) on the large dihydroxy bile salt micelles is striking, while similar concentrations have no effect on the small trihydroxy or dihydroxy micelles. The effects of urea on micelle formation and aggregate size are undoubtedly complicated (*10*) and involve changes in solvent structure and thus hydrophobic bonding and hydration of polar groups. For large micelles of dihydroxy bile salt

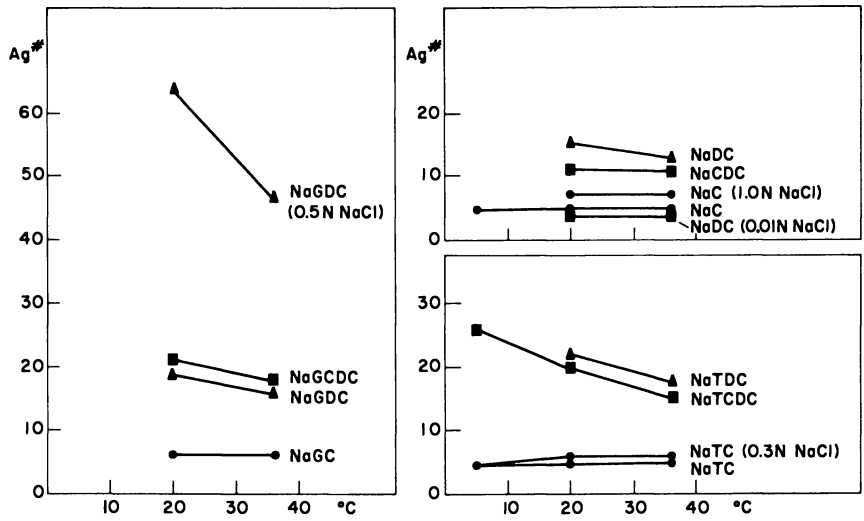

Figure 9. Apparent aggregation number vs. *temperature; pH 8–9, 0.15*N *NaCl*

*Left. Glycine conjugates, pH 8–9, 0.15*N *NaCl*
Upper right. Free bile salts
Lower right. Taurine conjugates

(formed in NaCl solutions) it is suggested that the urea competes effectively at relatively low concentrations (2*M*) with NaCl to re-establish hydration of the nonionic hydroxyl groups and thus reduce micelle size. If this is true, some of the hydroxyls in the large micelles are completely dehydrated. The most probable mechanism is by hydroxyl-hydroxyl hydrogen bonding between the bile salts, such as occurs with bile acid derivatives in organic solvents (*1*). These observations suggest that bile salts form two types of micelles, primary and secondary.

Primary Micelles. These micelles are formed by the trihydroxy series of bile salts, free or conjugated. They are also formed by the dihydroxy bile salts in water or at low salt concentrations ($< 0.03N$ NaCl) at 20°C. They are small, with aggregation numbers ranging from 2 (dimers) to 9. On the basis of the orientation of bile salts at air-water interfaces (*6*, *7*, *8*, *9*) and a consideration of their molecular structure, studied from Stuart-Breigleb models, the micellar structure shown in Figure 11a is proposed. In this model the hydrocarbon backs of the steroid nucleus (the only hydrophobic part of the bile salt molecule) associate hydrophobically. In water, even at concentrations many times greater than the *CMC*, dimers are present. Trimers, tetramers, pentamers, and hexamers are formed at low but increasing NaCl concentrations. As NaCl is increased further, in the case of trihydroxy bile salts, the aggregate increases to about seven to nine monomers. The increase in aggregation

number in the case of the small micelles with increasing counterion concentrations is probably caused by several factors, including decreased repulsion of the charged anionic polar groups, partial dehydration of the nonionic hydroxyl groups, and salting out of the hydrocarbon part of the molecule (*18*). A maximum aggregation number (< 10) was observed for the trihydroxy bile salts. The reason for this might be deduced from studies with space-filling molecular molecules. Working with Stuart-Breigleb models, it is possible to fit up to nine or 10 bile salts together so that the hydrophobic parts are in contact. Any number greater than 10 either leaves a space in the center, thus exposing the hydrophobic parts to water, which seems an unlikely structure, or necessitates contact with other molecules through the hydrophilic parts of the molecules. These primary micelles, though slightly asymmetric and of unfamiliar structure when compared with a representation of an aliphatic detergent micelle (Figure 11b), are probably analogous to detergent micelles, in that the proposed bonding is hydrophobic.

While the detergent molecule has a clear-cut polarity between its hydrophilic and lipophilic parts, the lipophilic part of the bile salt is confined to one side of the steroid nucleus, the other side being spiked with hydrophilic OH groups. In the small primary micelle, bile salt

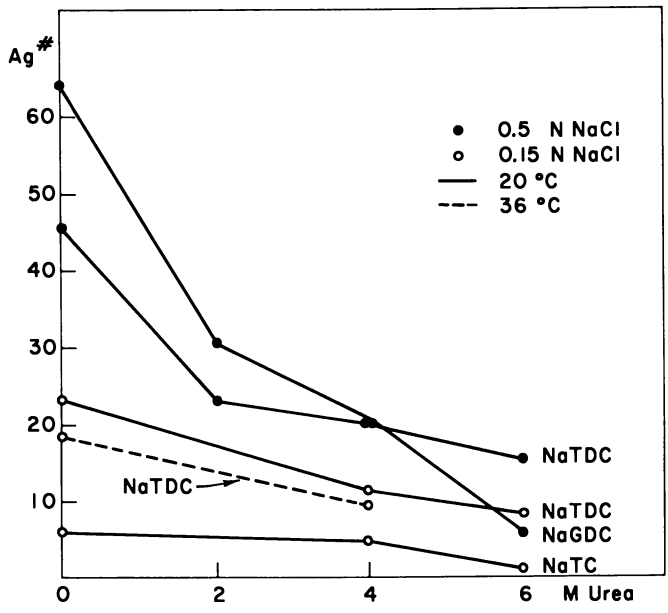

Figure 10. Apparent aggregation number vs. *urea concentration, pH 8–9*

molecules, like detergent molecules, probably associate by hydrophobic forces. The bonding of the bile salts, however, is back to back rather than chain to chain as with detergents. Secondary bile salt micelles are aggregates of primary micelles, probably associated by H-bonding of OH groups.

Secondary Micelles. These micelles are formed only by dihydroxy bile salts in the presence of increased counterions. Secondary micelles are probably formed by the aggregation of primary micelles. Since the surface available for hydrophobic interaction is expended in the formation of the primary micelles, the bonding that takes place is probably between some of the hydrophilic parts of the bile salts. It is suggested (Figure 11c) that in the presence of increased counterion concentrations

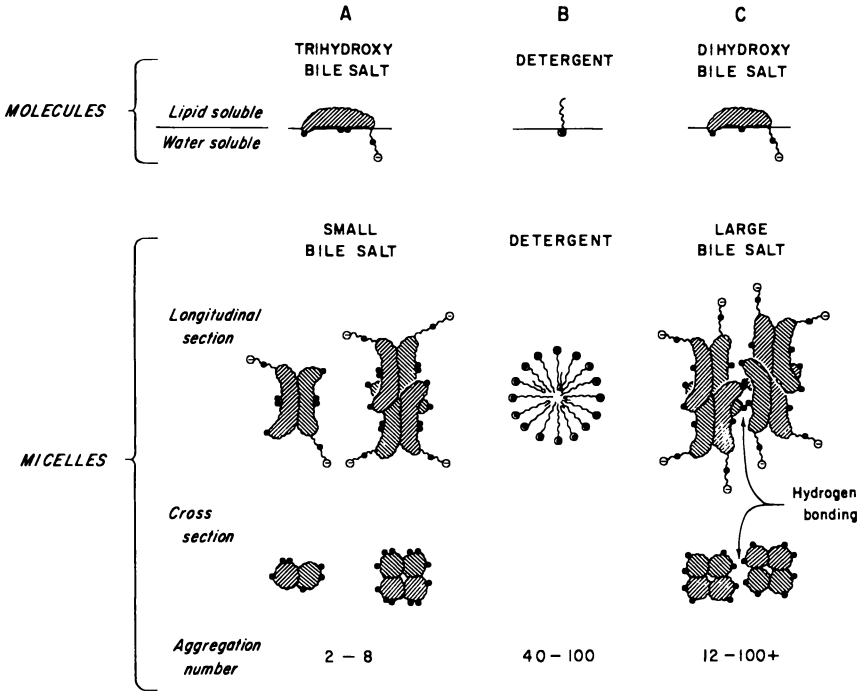

Figure 11. Comparison of proposed structure of primary and secondary bile salt micelles and a classical detergent micelle

A, C. Longitudinal and cross sections of primary and secondary bile salt micelles, respectively
B. Ordinary detergent micelle
Top. Orientation of molecules at oil-water interface
Wavy lines. Hydrocarbon chains of detergent molecules
Shaded area. Lipid-soluble cyclic hydrocarbon part of bile salt molecule
⊙ *Polar head of detergent molecule*
● *OH or ester groups*
⊖ *Negatively charged ionic group of bile salt*

dehydration of the weaker nonionic moiety of the dihydroxy bile salts occurs and hydrogen bonding between the nonionic polar parts (hydroxyls) of the bile salts takes place.

An alternative proposal might be that bile salts elongate in ribbon-like structures with increased counterion concentration. These micelles would be very asymmetric. However, in all previous studies where the shape of the bile salt micelles has been studied (*11*) it appeared to be almost spherical. This tends to rule out an elongated ribbon-like structure.

These results tend to support some of the original ideas of Ekwall (*9*). However, he suggested that transformation from small hydrophobically bonded micelles to larger micelles formed by aggregation of smaller micelles occurred with increasing concentration of both trihydroxy and dihydroxy bile salts. The present paper does not support the idea that the trihydroxy bile salts form large secondary micelles. Nor does it support, at least within the concentrations studied, the idea that the transformation from primary to secondary micelles occurs with increasing concentration of a given bile salt.

The fact that pH has a marked effect on dihydroxy bile salts and also on the monohydroxy bile salt Na lithocholate (*26*) when even a small amount of the free acid is present, suggests that gels are formed by H-bonding between the 3-α-hydroxyl of the bile salt and the carboxyl group of the free acid. These gels have been shown to be arranged in helices (*2*, *22*) and are probably not related structurally to the large micelles formed by dihydroxy bile salts at higher pH's in salt solutions. The extra hydroxyl group that the trihydroxy bile salts possess protects these bile salts from the formation of gels.

Acknowledgment

The author expresses his gratitude to Alise Polis and Elsie Stokes for their expert technical assistance.

Literature Cited

(1) Bennet, W. S., Eglinton, G., Kovac, S., *Nature* **214**, 776-780 (1967).
(2) Blow, D. M., Rich, A., *J. Am. Chem. Soc.* **82**, 3566 (1960).
(3) Borgstrom, B., *Biochim. Biophys. Acta* **106**, 171 (1965).
(4) DeMoerloose, P., Ruyssen, R. J., *Pharm. Belg.* **14**, 95 (1959).
(5) Ekwall, P., *J. Colloid Sci.*, Suppl. 1, 66-80 (1954).
(6) Ekwall, P., Ekholm, R., Proceedings of Second International Congress of Surface Activity, London, Vol. I, pp. 23-30, 1957.
(7) Ekwall, P., Ekholm, R., Norman, A., *Acta Chem. Scand.* **11**, 693-702 (1957).
(8) *Ibid.*, pp. 703-709.
(9) Ekwall, P., Fontell, K., Sten, A., Proceedings of Second International Congress of Surface Activity, London, Vol. I, pp. 357-373, 1957.
(10) Emerson, M. F., Holtzer, A., *J. Phys. Chem.* **71**, 3320-3330 (1967).

(11) Fontell, K., in "Surface Chemistry," P. Ekwall, K. Groth, v. Rünnström-Reio, eds., pp. 252-267, Academic Press, New York, 1965.
(12) Furusawa, T., *Fukuoka Acta Med.* **53**, 124 (1962).
(13) Herron, J., Olson, J. A., personal communication.
(14) Hofmann, A. F., in "New Biochemical Separations," A. T. James, L. S. Morris, eds., pp. 261-282, Van Nostrand, London, 1964.
(15) Hofmann, A., Small, D. M., *Ann. Rev. Med.* **18**, 333-376 (1967).
(16) International Critical Tables, McGraw-Hill, New York, 1927-1933.
(17) Laurent, T. C., Persson, H., *Biochim. Biophys. Acta* **106**, 616-624 (1965).
(18) Mukerjee, P., *Advan. Colloid Interface Sci.* 1, 241-275 (1967).
(19) Mukerjee, P., Mysels, K. J., Dulin, C. L., *J. Phys. Chem.* **62**, 1390 (1958).
(20) Olson, J. A., Herron, J. S., Proceedings of 6th International Congress on Biochemistry, New York, Vol. 7, p. 112, 1964 (Abstr.).
(21) Pope, J. L., *J. Lipid Res.* **8**, 146-147 (1967).
(22) Rich, A., Blow, D. M., *Nature* **182**, 423 (1958).
(23) Schick, M. J., *J. Am. Oil Chemists' Soc.* **40**, 680-687 (1963).
(24) Shinoda, K., Nakagawa, T., Tamamushi, B., Isemura, T., "Colloidal Surfactants," pp. 1-310, Academic Press, New York, 1963.
(25) Small, D. M., Bourges, M., Dervichian, D. G., *Nature* **211**, 816 (1966).
(26) Sobotka, H., Czeczowezka, N., *J. Colloid Sci.* **13**, 188 (1958).
(27) Svedberg, T., Pedersen, K. O., "The Ultracentrifuge," Appendix III, Clarendon Press, Oxford, 1940.
(28) Yphantis, D. A., *Ann. N.Y. Acad. Sci.* **88**, 586-601 (1960).

RECEIVED May 8, 1967. Investigation supported by Public Health Service Training Grant No. AM-05589 and Research Grant AM 11453.

Molecular Association in Fat Digestion

Interaction in Bulk of Monoolein, Oleic Acid, and Sodium Oleate with Dilute, Micellar Bile Salt Solutions

ALAN F. HOFMANN

Gastroenterology Unit, Mayo Clinic and Mayo Foundation, Rochester, Minn. 55901

Bile salts dispersed monoolein and oleic acid–sodium oleate mixtures into micellar solution far more effectively than an analogous detergent, lauryl taurate. Oleic acid and oleyl homologs which did not interact with water were poorly dispersed by bile salts, but monoolein and oleyl homologs, which spontaneously formed a liquid crystalline phase in water, were readily dispersed by bile salts. The bulk pH at which oleic acid was half ionized was 6.4 to 6.6 when the oleic acid was present in a bile salt micelle but above 7 in a lauryl taurate micelle, indicating that the bile salt micelle is relatively uncharged and that fatty acid readily ionizes when dispersed in micellar bile salt solution. Bile salts dispersed monoolein aggregates into micellar solution rapidly (< 1 millisecond) by stop-flow spectrophotometry. The hydroxylated steroid nucleus appears to be chiefly responsible for the distinctive dispersing properties of bile salts.

Ingested triglyceride is emulsified by bile and cleaved by pancreatic lipase to yield fatty acid and 2-monoglyceride as end products (*3*, *19*, *24*). These hydrolytic products are insoluble but disperse readily in bile salt solution to form mixed bile salt–fatty acid–monoglyceride micelles (*8*, *12*). The micellar phase of human intestinal content during fat digestion is readily isolated by ultracentrifugation; its major constituents are bile salt, fatty acid, and monoglyceride (*13*). If such a micellar dispersion is perfused into the human small intestine, its fatty acid and monoglyceride are rapidly absorbed (*25*). Thus, bile salts transport

insoluble lipids from the oil-water interface to the cell-lumen interface; bile salts are lipid carriers.

This paper considers the interaction of monoolein, oleic acid, and sodium oleate with bile salt solution in model systems whose compositions have been chosen to simulate those which may occur in small intestinal content. In addition, the behavior of several monoglyceride analogs has been examined to determine the influence of the type of polar head of the lipid on its dispersion by bile salts. Finally, titration experiments were performed to measure the extent of ionization of oleic acid in such systems.

Materials and Methods

Conjugated bile salts were prepared synthetically (*6*, *22*) and were chromatographically pure (*9*) and free of salt. (Systematic names of the bile acids of the bile salts and detergents referred to in the text by their trivial names only are: taurocholic acid, 3α, 7α, 12α-trihydroxy-5β-cholanoyl taurine; taurodeoxycholic acid, 3α, 12α-dihydroxy-5β-cholanoyl taurine; taurochenodeoxycholic acid, 3α, 7α-dihydroxy-5β-cholanoyl taurine; glycocholic acid, 3α, 7α, 12α-trihydroxy-5β-cholanoyl glycine; glycodeoxycholic acid, 3α, 12α-dhiydroxy-5β-cholanoyl glycine; glycochenodeoxycholic acid, 3α, 7α-dihydroxy-5β-cholanoyl glycine; deoxycholic acid, 3α-12α-dihydroxy-5β-cholanoic acid; allodeoxycholic acid, 3α, 12α-dihydroxy-5α-cholanoic acid; and lauryl taurate, *N*-lauroyl taurine.)

Sodium lauryl taurate was prepared synthetically (*22*) from lauric acid (12.0, 99%; 14.0, 1%, by gas-liquid chromatography) and crystallized twice from 95% ethanol; it was chromatographically pure by thin-layer chromatography (*9*). Sodium lauryl sulfate and sodium *p*-(*n*-octyl) benzene sulfonate were commercial samples of high purity (*8*). Hexadecylpyridinium chloride and cetyl trimethylammonium bromide were commercial samples; purity in the titration experiments in which they were employed was not essential. Glyceryl 1-monooleate was prepared by glycerolysis (*2*) from chromatographically pure oleic acid (Hormel Institute, Austin, Minn.). Sodium oleate was prepared from the same sample of oleic acid by neutralizing an ethanolic solution with an equivalent amount of sodium hydroxide; the solution was blown to a gum with a nitrogen stream, dried to a white solid *in vacuo* over phosphorus pentoxide, and dissolved in chloroform-methanol, 2 to 1, by volume. The oleyl alcohol, glyceryl 1-monooleyl ether, and propylene glycol 1-monooleate (propane 2-ol-1-yl oleate) were of class and homolog purity (*1*, *7*). Buffers (0.15*M* in Na^+) were prepared as described (*8*).

For phase equilibria experiments, either sodium taurodeoxycholate or an equimolar mixture of sodium taurocholate and sodium taurodeoxycholate was used, unless noted, as previous studies (*8*) had shown that the behavior of monoolein was similar in all of the bile salt conjugates. Previous studies (*7*) had also shown that the 1-monoolein and 2-monoolein behaved identically in bile salt solution. Therefore, 1-monoolein was used in all experiments because of its greater availability and stability (*7*). Lipids, dissolved in an appropriate solvent, were added to

sterile ampoules, and the solvent was removed by evaporation. In some experiments, a few micrograms of *trans*-azobenzene (*8*) were added to enhance the detection of small oil droplets. Bile salt or detergent and/or buffer or sodium chloride were added to give a volume of 5.0 ml. and a Na^+ concentration of 0.15*M*. Ampoules were fused and incubated at 37°C. for periods of 1 day to several weeks. Phase equilibria were determined by inspection and examination using a conventional and an inverted metallurgical microscope with polarizing filters. For experiments in which pH was a variable, the ampoules were opened at the completion of the experiment, and the pH was determined with a combination glass electrode.

Titration experiments were carried out as described previously (*11*). Detergent was present at a sufficient concentration (three to four times the critical micellar concentration) to disperse the sample in isotropic micellar solution irrespective of its state of ionization. The micellar solution, 0.15*M* in Na^+ concentration, was adjusted to pH 2 with 25 μliters of 1*N* HCl. The sample was then titrated to pH 9; 0.05*N* NaOH prepared in 0.1*M* NaCl was added from a micrometer buret, and the pH was recorded after each addition of base. The counterion concentration remained constant throughout the titration. A bulk pH corresponding to 50% ionization was read directly from the titration curve, after the titration curve obtained for detergent without micellar solute had been subtracted. The detergents used in these studies did not consume appreciable base between pH 4 and 8.

The rate at which liquid crystalline bile salt monoolein aggregates were dispersed by bile salt solutions was determined by Quentin Gibson (Cornell University, Ithaca, N. Y.) using a rapid mixing stop-flow spectrophotometer designed in his laboratory (*4*).

Results

Phase Equilibria of Monoolein, Oleic Acid, and Sodium Oleate. Bile Salts Compared with Lauryl Taurate. Figure 1 shows the phase equilibria for varying molar ratios of bile salt (left) or sodium lauryl taurate (right) and monoolein, oleic acid, or sodium oleate. In these experiments, the sum of the bile salt [an equimolar mixture of taurocholate and taurodeoxycholate, having a critical micellar concentration (*CMC*) less than 3 m*M*] and the oleyl compound was 20 m*M*. The counterion concentration was essentially constant (150 m*M* plus the Na^+ of the sodium oleate), and the water fraction (in terms of weight percentage of all components) was essentially constant at 99%. The composition of the samples falls in a line in the region of extremely high water concentration in the ternary phase diagram of detergent–oleyl additive–water (for a discussion of such systems *see* Ref. *16*); the line is parallel to the side opposite the aqueous corner. The edge of the clear area in Figure 1 indicates the molar ratio at which a phase change occurs; this molar ratio is determined by the slope of the edge of the micellar area in the ternary phase diagram.

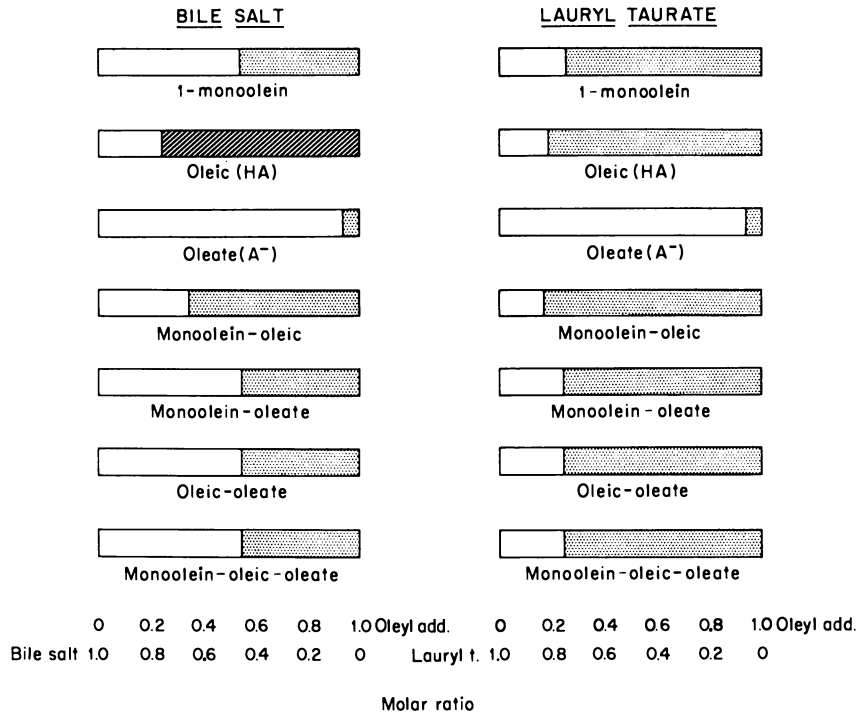

Figure 1. Phase equilibria for varying molar ratios of oleic acid, sodium oleate, and monoolein in bile salt and sodium lauryl taurate

Six molar ratios were examined and the vertical line is drawn mid-way between the highest molar ratio at which a micellar phase (clear) was present and the next molar ratio which was liquid crystalline (stipling) or an immiscible oil phase (hatching)

For this water concentration, the micellar region for the bile salt mixture is large for all oleyl compounds except oleic acid. Oleic acid is distinguished from the other compounds in that it does not form a lyotropic liquid crystalline phase spontaneously in water and, similarly, is present as oil droplets in bile salt solution when its micellar solubility is exceeded. Figure 1 shows also that the micellar area of an equimolar mixture of monoolein and sodium oleate is considerably greater than that of an equimolar mixture of monoolein and oleic acid, indicating that fatty acid ionization also enhances micellar solubility when monoolein is present. The equimolar mixture of sodium oleate and oleic acid has a micellar area similar in size to that of monoolein, as does the equimolar combination of all three compounds.

Sodium lauryl taurate was chosen as a prototypic anionic detergent to compare with the bile salt mixture. This detergent possesses a fatty acid chain rather than the hydroxylated cyclopentenophenanthrene

nucleus of the bile salt, but is similar to the bile salts employed since it is an *N*-acyl taurate. A comparison of interaction of these two compounds with the oleyl compounds should disclose the influence of the steroid nucleus. Figure 1 shows that the micellar region is considerably smaller with sodium lauryl taurate—*viz*, a liquid crystalline phase of oleyl additive, sodium lauryl taurate, and water occurs at a much lower ratio of oleyl additive to detergent. Oleic acid forms a liquid crystalline phase with sodium lauryl taurate, whereas it remains as poorly emulsified oil droplets in bile salt solution.

Effect of Bulk pH on Behavior and Solubility of Oleic Acid in Bile Salt Solution. Figure 2 shows the effect of bulk pH on the behavior and solubility of oleic acid in 0.15*M* buffer (above) and in 4 m*M* sodium glycodeoxycholate (below). In buffer, oleic acid has an extremely low solubility, and the excess, below pH 6.8, is present as an emulsion. In micellar bile salt solution, the oleic acid is solubilized to some extent. Above pH 6.5, its solubility rises markedly, and the excess now forms a dispersed phase which probably consists of droplets of fatty acid emul-

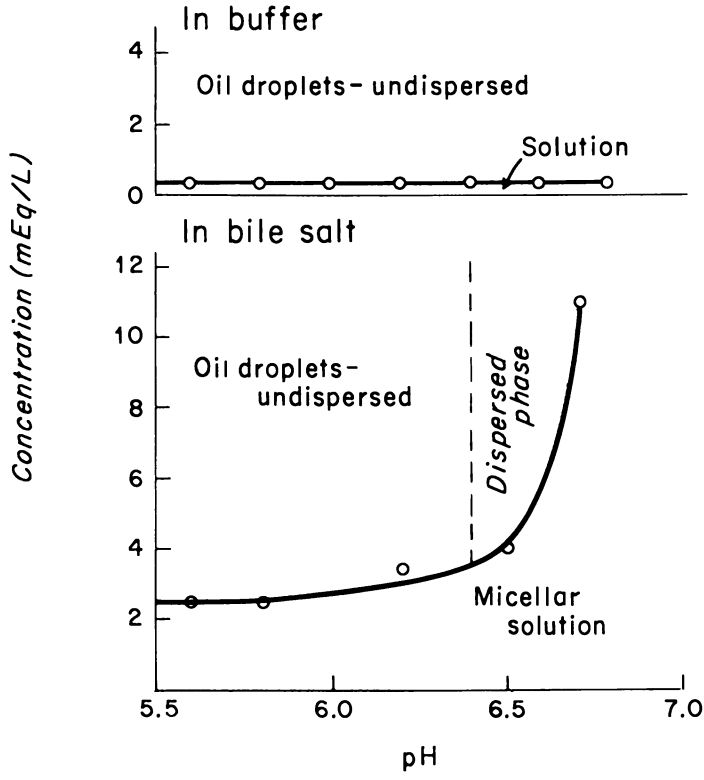

Figure 2. Effect of bulk pH on oleic acid solubility in buffer and bile salt

sified by acid soap. The increase in solubility and change in phase of the oleic acid when its micellar solubility is exceeded occur at a bulk pH corresponding to about half ionization. The increase in oleic acid solubility with ionization is also noted in Figure 1.

Complete System. BEHAVIOR OF MIXTURES OF OLEIC ACID, MONOOLEIN, AND SODIUM OLEATE IN SALINE AND BILE SALT SOLUTION. The experiments shown in Figures 1 and 2 did not give information about possible competitive or cooperative interactions between ionized and un-ionized oleic acid and monoolein in bile salt solution. Therefore, the phase equilibria for all possible molar ratios of these three substances were examined. Mixtures of the three compounds were composed, using triangular coordinates so that the sum of all three compounds was 5, 10, and 15 m*M;* the behavior of such mixtures when incubated in 150 m*M* sodium chloride solution or in 130 m*M* sodium chloride plus 20 m*M* bile salt (taurocholate-taurodeoxycholate, 1 to 1 molar ratio) was determined. These systems were extremely dilute ($> 99\%$ water) but had a relatively fixed counterion concentration, 150 m*M* sodium ion plus the sodium ion of the sodium oleate (from 5 to 15 m*M*). Such experiments, performed at 37°C., should describe the behavior of the products of pancreatic lipolysis in the absence and presence of bile salts, although the model system differs in two essential features from human small intestinal content in that 1-monoolein was employed, although the 2-isomer dominates physiologically (*13*), and in human small intestinal content, an oil phase composed of higher glycerides and un-ionized fatty acid coexists (and is presumably in equilibrium) with the aqueous micellar phase of bile salt, fatty acid, monoglyceride, and fatty acid soap (*13*). Thus, the polar lipids are partitioned between two immiscible phases.

The results of these experiments shown in Figure 3 confirm and extend the results presented in Figures 1 and 2 on simpler model systems. In the absence of bile salts (left) dispersion to micellar size aggregates is present, if at all, only with sodium oleate alone at 10 and 15 m*M*. These systems were opalescent and had considerable viscoelasticity; hence, the aggregates present were probably large. Adding 20 m*M* bile salt (Figure 3, right) results in the transition of the majority of phases to a micellar dispersion. Insoluble fatty acid is present in the fatty acid tip, consistent with the poor dispersability of oleic acid in bile salt solutions noted previously. The systems may be considered in more detail.

OLEIC ACID, SODIUM OLEATE, AND MONOOLEIN MIXTURES IN SALINE. Four major regions are distinguishable according to the degree and nature of the interaction of the component(s) with water.

No interaction with water, no dispersion. Oleic acid, and mixtures of components containing a predominance of oleic acid, do not interact with saline; oil droplets are present.

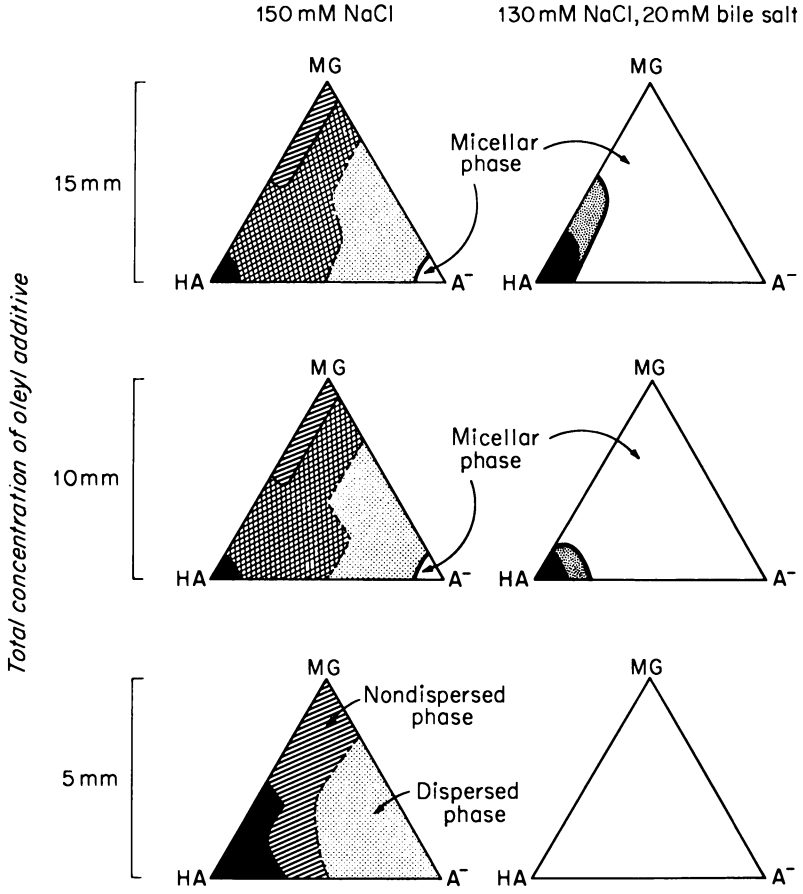

Figure 3. Solubility and behavior at 37°C. of mixtures of oleic acid (HA), sodium oleate (A^-), and monoolein (MG)

Solid black line separates dispersions of large aggregates from dispersions of micellar size—turbid dispersions from clear dispersions. In 150 mM sodium chloride, fatty acid is present as oil droplets (black with white stipling) and monoolein as a nondispersed smectic phase (horizontal hatching) or a viscous water-in-oil emulsion (cross hatching). Increased ratios of sodium oleate result in a dispersed phase (white with black stipling) and at 10 and 15 mM sodium oleate alone is present in micellar form. In bile salt, fatty acid is also present as oil droplets (black with white stipling) and at higher concentrations monoolein and fatty acid form a dispersed liquid crystalline phase (white with dots). In 20 mM bile salt most of the lipid mixtures are now present in micellar solution (clear)

Interaction with water, but no dispersion. Mixtures containing predominantly monoolein hydrate forming a birefringent mesomorphic (smectic phase) which remains adherent to the glass surface (*8*). At 10 and 15 m*M* the lipid in a number of samples containing predominantly monoolein aggregated into an opaque extremely viscous phase which appeared grossly to be crystalline. However, by light microscopy, this

phase contained a water-in-oil emulsion. Whether the appearance of such a phase reflected the homolog purity of the lipids used in these experiments is unknown.

Interaction with water, and dispersion into large aggregates. In samples containing appreciable sodium oleate, a turbid dispersion was present. Microscopically, this phase contained isotropic oil droplets, and the phase should represent emulsified fatty acid and monoglyceride droplets stabilized by acid soap. Unfortunately, x-ray diffraction facilities were not available to characterize this phase properly.

Interaction with water, and dispersion into micellar sized aggregates. As noted, dispersion into true micelle sized aggregates (aggregate weight less than 100,000) did not occur with any mixtures of these compounds in saline. Sodium oleate at 10 and 15 m*M* was viscoelastic, probably because of the high electrolyte concentration and/or hydrolysis. Although the aggregates present were not micellar in size, the slight turbidity indicated they were far smaller than systems in which monoolein and oleic acid were present.

Oleic Acid, Sodium Oleate, Monoolein Mixtures in Bile Salt Solution. Three of the four phases described were present, although most of the area of the triangle is now the fourth type—*i.e.*, present in a micellar dispersion. This dispersion was not opalescent, and its viscosity was grossly that of water. Oleic acid alone at 10 or 15 m*M* was neither hydrated nor dispersed. Oleic acid–monoolein mixtures containing predominantly oleic acid were faintly turbid and were probably large cylindrical aggregates (giant micelles), although a fine emulsion could not be excluded.

Ionization of Oleic Acid Present as a Micellar Solute. The preceding experiments had shown that increasing ionization of oleic acids strikingly altered its behavior in bile salt solution. Accordingly, titration experiments were carried out to determine the bulk pH at which the oleic acid ionized when present as a micellar solute. Table I summarizes the titration results which demonstrate the influence of detergent type on the ionization of micellar fatty acid. The bulk pH corresponding to 50% ionization varies over two p*K* units at a constant counterion concentration according to the charge on the detergent composing the micelle. Table I further indicates that oleic acid when present in a bile salt micelle is half ionized at a significantly lower bulk pH (6.4 to 6.6) than when present in a sodium lauryl taurate or sodium octyl benzene sulfonate micelle (7.2 to 7.4). The ionization of micellar oleic acid in bile salt solution is not significantly influenced by the fatty acid–bile salt ratio in the micelle. Table II indicates that adding monoolein either does not affect or may even increase the ionization of micellar oleic acid at a given bulk pH. Oleic acid ionization in bile salt solution was identical in sodium glycodeoxycholate, sodium taurodeoxycholate, and a mixture of all six bile salts (SIC) composed to resemble human small intestinal content (8).

Behavior of Oleyl Homologs in Bile Salt Solution. Figure 1 indicates that oleic acid had a low micellar solubility in bile salt solution and when present in excess formed an emulsion. In Figure 4, the solubility and behavior in bile salt solution of a number of oleyl compounds are examined by constructing phase diagrams as described in Figure 1. Oleic acid, propylene glycol 1-monooleate, and oleyl alcohol do not form a liquid crystalline phase in water and emulsify in bile salt solution. These compounds have appreciably lower solubilities in bile salt solution than the 1- and 2-monooleins as well as the glyceryl monoether.

Kinetics of Dispersion of Monoglycerides by Micellar Bile Salt Solutions. A dispersion containing 17.5 μmoles per ml. of monoolein and 9 μmoles per ml. of taurodeoxycholate was prepared. The solution was grossly turbid, indicative of large monoolein–bile salt aggregates. When the solution was mixed with 8 m*M* sodium taurodeoxycholate, the absorbance of the solution fell to zero in less than 1 msec., indicating a virtually instantaneous disruption of the large aggregates to smaller aggregates. Admixture with 0.15*M* sodium chloride did not alter the turbidity of the first solution.

Table I. The pK_a of Oleic Acid as a Micellar Solute[a]

	Concn., mM	*Oleic Acid, mM*	$pK_{micellar}$
Varying detergents			
CTAB (cationic)	16.0	4.8	5.2
HDPC (cationic)	16.0	5.0	5.4
Lauryl taurate (anionic)	20.0	4.0	7.4
ABS (anionic)	20.0	4.0	7.2
TDC (anionic)	16.0	5.0	6.6
Varying bile salts			
Taurodeoxycholate	16.0	5.0	6.6
TC-TDC (1 to 1)	20.0[b]	8.0	6.4
Glycodeoxycholate	16.0	5.0	6.6
SIC	16.0[b]	5.0	6.6
Varying ratios of bile salt to oleic acid			
TDC	12.0	5.0	6.65
	16.0	5.0	6.60
	20.0	5.0	6.50
	24.0	5.0	6.45

[a] Bulk pH corresponding to 50% ionization; all solutions were isotropic and 0.15*M* in total Na^+ concentration.
[b] For bile salt mixtures, total concentration of bile salts is given. CTAB = cetyltrimethylammonium bromide. HDPC = hexadecyl pyridinium chloride. Lauryl taurate = sodium lauryl taurate. TC-TDC: sodium taurocholate–sodium taurodeoxycholate. ABS = sodium *p*-(*n*-octyl) benzene sulfonate. SIC = a mixture of sodium taurocholate, sodium taurodeoxycholate, sodium taurochenodeoxycholate, sodium glycocholate, sodium glycodeoxycholate, and sodium glycochenodeoxycholate composed to resemble human small intestinal content during fat digestion and absorption (*8*).

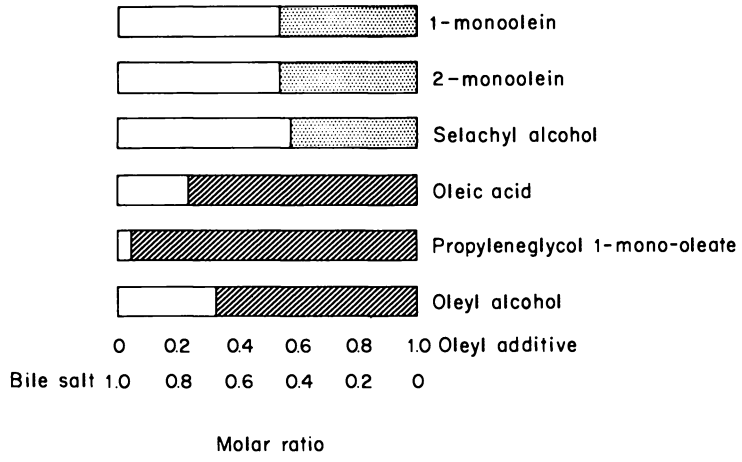

Figure 4. Phase equilibria for oleyl homologs varying in polar group in bile salt solution

Compounds possessing a small micellar area (clear) form an immiscible oil phase (diagonal hatching) when present in excess in bile salt solution or in buffer in absence of bile salt. Compounds with high micellar solubility form a liquid crystalline phase when present in excess in bile salt solutions and form liquid crystalline phases in buffer alone

Discussion

The experiments show clearly the ability of bile salts to disperse monoolein, sodium oleate, and oleic acid, alone and in mixture, to an isotropic micellar solution. The marked difference in the properties of bile salts when compared with lauryl taurate suggests that the hydroxylated 5β-cyclopentenophenanthrene nucleus must interact with polar lipids in a manner unlike that of the paraffin chain. The remarkable dispersing properties of bile salts for these polar lipids is shown by the large size of the micellar region in the phase diagram of bile salt–water–oleyl additive. The large size of the micellar region indicates the disinclination of bile salts to pack, together with monoglycerides, into a liquid crystalline phase, and correlates with the absence of a liquid crystalline state at high concentrations of bile salts in water (*8*, *28*), as well as the failure of bile salts to penetrate monolayers of monoglyceride (*1*). Conversely, the smaller micellar region in the lauryl taurate–water–oleyl additive ternary phase diagram derives from the readiness with which the lauryl taurate molecule packs into condensed films, as evidenced by monolayer penetration or the formation of a liquid crystalline phase at high concentrations in the binary system of lauryl taurate–water (*16*).

The appreciably lower micellar solubilities of oleic acid, oleyl alcohol, and propylene glycol monooleate are consistent with the view that the formation of a liquid crystalline aggregate—lamellar, cylindrical, or

viscous isotropic—is essential for a long-chain lipid to be dispersed effectively by bile salts. Formation of a mesomorphic phase in water by unsaturated monoglycerides is well established (*18*). Saturated long-chain monoglycerides such as monomyristin and monopalmitin also form a liquid crystalline phase in water. The transition from a solid to a liquid crystalline phase in water occurs only above a transition temperature, which for 1-monoglycerides is 15° to 30°C. below the melting point of the anhydrous crystalline form (*10, 17*). If crystals are dispersed in bile salt solution, rather than water, the transition temperature is a few degrees lower. At 37°C., monolaurin (anhydrous, melting point 63°C.) forms a liquid crystalline dispersion in bile salt solutions, but monomyristin (melting point 70°C.) and monopalmitin (melting point 77°C.) do not. Accordingly, at body temperature, only unsaturated lipids or mixtures of saturated lipids having a transition temperature (crystalline to liquid crystalline) in bile solutions near body temperature will be effectively dispersed by bile salts (*7*).

Two models for the bile salt–polar lipid aggregate have been proposed based on the observations that bile salts do not penetrate lipid monolayers yet effectively disperse smectic aggregates. The first, proposed by Small (*26*) for the bile salt–lecithin micelle, features a disk of lamellar (bimolecular) lecithin stabilized by adsorbed bile salts which are arranged in dimers, along the edge of the disk, much like the milling on a coin. The nonpolar side of the cyclopentenophenanthrene nucleus lies along the fatty acid chain of the lecithin; the hydroxylated side of the bile salt is toward the bulk water. The bile salt molecules are lying with their 3α-hydroxyl groups apposed; their sulfonate groups are away from each other. This model is compatible with x-ray diffraction data and nuclear magnetic resonance data (*27*), the latter indicating that the angular methyl groups of the bile salt molecules are present in a liquid

Table II. Effect of Added Monoolein on pK_a of Oleic Acid Present as a Micellar Solute (37°C.)[a]

Bile Salt	*Concn., mM*	*OA, mM*	*MO, mM*	*(OA + MO), mM*	$pK_{micellar}$
TDC	16.0	7.5	0	7.5	6.5
		3.75	3.75	7.5	6.4
		2.5	5.0	7.5	6.4
		5.0	5.0	10.0	6.6
TC-TDC	20.0[b]	4.0	4.0	8.0	6.4
		3.0	9.0	12.0	6.3
		9.0	3.0	12.0	6.3

[a] pK_a, defined as bulk pH corresponding to 50% ionization. All solutions were isotropic and 0.15*M* in total Na^+ concentration.
[b] For bile salt mixtures, total concentration of bile salts is given. TDC = sodium taurodeoxycholate. TC = sodium taurocholate. OA = oleic acid. MO = monoolein.

hydrocarbon environment when present in a monoglyceride–bile salt micelle. The second model, proposed by Dreher *et al.* (*1*), is in the form of a spherical aggregate of monoolein and fatty acid, to which the bile salt molecules are adsorbed by their hydroxyl groups, the sulfonate groups projecting into the aqueous phase. The proposed molecular arrangement of this model, however, does not appear to be compatible with the NMR data and seems less likely.

The kinetic studies indicated that the rate of equilibrium between large monoolein–bile salt aggregates and small monolein–bile salt aggregates was very fast. Information is needed on the rate of exchange of polar lipids between micelles since these aggregates have different structures than soap micelles, where the exchange rates are believed to be rapid (*15*, *21*).

The lower pK_a of fatty acid present in bile salt micelle (Tables I and II) probably also indicates that the bile salt–fatty acid aggregate has a different molecular arrangement than the lauryl taurate–fatty acid aggregate. In interpreting these experiments, it seems reasonable to assume that the fatty acid present is entirely in micellar form, and further that the intrinsic surface pK_a of fatty acid is not dissimilar in these two types of aggregates. The differences in fatty acid ionization should be caused by differences in the H^+ concentration at the micellar surface, this in turn being related to the charge density. In an extension of the early studies of Hartley and Roe (*5*), Mukerjee and Banerjee (*20*) have clearly shown that the pK_a of bromophenol blue present as a micellar solute may vary over three pK_a units according to the type of detergent. Mukerjee and Banerjee point out the difficulty in interpreting pK_a data even in such experiments when charge density may be estimated well, and no information exists on the charge density of bile salt–fatty acid aggregates.

The data clearly indicate that the surface pH of the bile salt micelle is higher than the surface pH of a lauryl taurate micelle for a given bulk pH—*i.e.*, the difference between bulk and surface pH is less with the bile salt micelle. The bile salt micelle should have a lower charge density and therefore a lower concentration of protons at the surface of the micelle. Therefore, the observed bulk pH at which micellar fatty acid ionizes is closer to the bulk pK_a of molecularly dispersed fatty acid (4.9) in bile salt solution than in lauryl taurate solution.

Long-chain fatty acids are insoluble in water, and their titration curves are concentration-dependent because of the formation of organized aggregates (acid soaps, soap micelles, fatty acid precipitates) which concentrate protons at the surface. At concentrations above the critical micellar concentration, solutions of long-chain fatty acid soaps manifest a diprotic curve when they are titrated from pH 10 to 4 (*23*). The first

region of proton consumption corresponds to the titration of fatty acid present in micelles; the system rapidly becomes heterogeneous, and acid soap precipitates from solution. The second portion of the titration curve corresponds to the fatty acid present in acid soap, which is probably liquid crystalline (*27*). Since these titration curves are concentration-dependent, any choice of a pK_a figure is arbitrary. However, values of 8.8 for the first region of the titration curve and 6.8 for the second appear representative. The mean of these figures, 7.8, could be regarded as the pK_a of a long-chain fatty acid soap in an aqueous system. In bile salt solutions, this fatty acid (soap) would have a pK_a of 6.4 to 6.6. Therefore, bile salt solutions lower the pK_a of fatty acid in aqueous systems and enhance fatty acid ionization.

The pK_a of the fatty acid present in a bile salt micelle is similar to the bulk pH reported to be present in small intestinal content during fat digestion and absorption; considerable fatty acid ionization must occur. The major buffer present in intestinal content is pancreatic bicarbonate, which should serve as the acceptor for the protons donated by fatty acid. Thus, by lowering the pK_a of fatty acid, bile salts appear to mediate proton transfer from fatty acid to pancreatic bicarbonate. The triangular phase diagram (Figure 4) clearly indicates that monoglycerides are dispersed better than fatty acids by bile salts. Thus, the positional specificity of pancreatic lipase, which generates 2-monoglyceride as an end product, is responsible for the formation of a product with a high micellar solubility, irrespective of intraluminal pH. If pancreatic lipase had no positional specificity and generated fatty acid as an end product, micellar solubilization would be strongly influenced by intraluminal pH. These factors may bear on the biochemical evolution of pancreatic lipase.

Acknowledgment

Kathleen Rydell gave skillful assistance. The titration curves and a number of the chemical syntheses were carried out when the author was a member of the laboratory of E. H. Ahrens, Jr., at the Rockefeller University, with the gracious help of Susan Stoeppler Saudek.

Literature Cited

(1) Dreher, K. D., Schulman, J. H., Hofmann, A. F., to be published.
(2) Franzke, C., Kretzschmann, F., *Fette Seifen Anstrichmittel* **65**, 276 (1963).
(3) Frazer, A. C., *Brit. Med. Bull.* **14**, 212 (1958).
(4) Gibson, Q. H., Milnes, L., *Biochem. J.* **91**, 161 (1964).
(5) Hartley, G. S., Roe, J. W., *Trans. Faraday Soc.* **36**, 101 (1940).
(6) Hofmann, A. F., *Acta Chem. Scand.* **17**, 173 (1963).

(7) Hofmann, A. F., *Biochim. Biophys. Acta* **70,** 306 (1963).
(8) Hofmann, A. F., *Biochem. J.* **89,** 57 (1963).
(9) Hofmann, A. F., "New Biochemical Separations," L. J. Morris and A. T. James, eds., p. 261, Van Nostrand, London, 1964.
(10) Hofmann, A. F., Ph.D. Thesis, University of Lund, 1964.
(11) Hofmann, A. F., Borgstrom, B., *Biochim. Biophys. Acta* **70,** 317 (1963).
(12) Hofmann, A. F., Borgstrom, B., *Federation Proc.* **21,** 43 (1962).
(13) Hofmann, A. F., Borgstrom, B., *J. Clin. Invest.* **43,** 247 (1964).
(14) Hofmann, A. F., Mosbach, E. H., *J. Biol. Chem.* **239,** 2813 (1964).
(15) Kresheck, G. C., Hamori, E., Davenport, G., Scheraga, H. A., *J. Am. Chem. Soc.* **88,** 246 (1965).
(16) Lawrence, A. S. C., "Surface Activity and Detergency," K. Durham, ed., p. 158, Macmillan, London, 1961.
(17) Lawrence, A. S. C., Hume, K., Capper, C. B., Bingham, A., *J. Phys. Chem.* **68,** 3470 (1964).
(18) Lutton, E. S., *J. Am. Oil Chemists' Soc.* **42,** 1068 (1965).
(19) Mattson, F. H., Beck, L. W., *J. Biol. Chem.* **219,** 735 (1956).
(20) Mukerjee, P., Banerjee, K., *J. Phys. Chem.* **68,** 3567 (1964).
(21) Nakagawa, T., Tori, K., *Kolloid-Z.* **194,** 143 (1964).
(22) Norman, A., *Arkiv. Kemi* **8,** 331 (1955).
(23) Rosano, H. L., Breindel, K., Schulman, J. H., Eydt, A. J., *J. Colloid Interface Sci.* **22,** 58 (1966).
(24) Senior, J. R., *J. Lipid Res.* **5,** 495 (1964).
(25) Simmonds, W. J., Hofmann, A. F., Theodor, E., *J. Clin. Invest.* **46,** 874 (1967).
(26) Small, D. M., *Gastroenterology* **52,** 607 (1967).
(27) Small, D. M., personal communication.
(28) Small, D. M., Bourges, M. C., Dervichian, D. G., *Biochim. Biophys. Acta* **125,** 563 (1966).

RECEIVED June 12, 1967. Work supported in part by U. S. Public Health Service Grant AM-06908 to the Mayo Clinic from the National Institutes of Health. Support for work at Rockefeller University received in part from U. S. Public Health Service Grant HE-06222.

Molecular Association in Fatty Acid–Potassium Soap Systems

E. D. GODDARD, S. GOLDWASSER, G. GOLIKERI, and H. C. KUNG

Lever Brothers Co., Edgewater, N. J.

The association of fatty acids with their potassium salts has been studied for the even-carbon number acids C_4 to C_{18} and valeric acid. The investigation used differential thermal, infrared, x-ray, and analytical titration techniques, and the mixed species were prepared by two methods which used the solvents ethanol and petroleum ether. All the acids associated with their corresponding potassium salts at the 1 to 1 molar ratio to form well-defined "acid-soap" complexes which exist in different phases, the particular phase being determined chiefly by chain length. Three distinct phases were established. On heating, the acid-soaps generally pass through a phase transition temperature before melting with decomposition at a higher temperature into the constituent acid and soap. Energies of association are reported.

In previous communications (*7*, *9*, *10*, *11*, *12*) from this laboratory results have been presented on association reactions between long-chain ionic and long-chain polar compounds. The results have implications regarding the properties of interfaces, including those present in certain biological systems. The latter aspects have been emphasized by Schulman and Rideal (*22*).

One association of the above type—*viz.*, "acid-soap" formation between a fatty acid and its neutral salt or soap—was postulated a century and a half ago by Chevreul (*2*). However, this concept was not generally accepted until much later, when studies of such workers as McBain (*15*, *16*, *17*), Ekwall (*6*), Malkin (*18*), Piper (*19*), and Levi (*13*) provided convincing evidence of its correctness. The most recently published data on sodium acid-soaps are those of Ryer (*20*) who, for the stearate system,

reported the existence of acid-soaps of 1 to 1, 3 to 2, and 2 to 1 stoichiometry; no evidence of the 1 to 2 species was obtained. For the potassium acid-soaps, there now seems to be general agreement that the only association complexes formed are those of 1 to 1 stoichiometry.

Several preparative methods have been used for the acid-soaps, including cooling of an anhydrous melt, formation in an aqueous environment and, most generally, crystallization from ethanol. In the present studies, acid-soaps have been made both by the ethanol route and by a novel method, using petroleum ether as a solvent for the fatty acid. It was the purpose of the work to prepare a series of potassium acid-soaps of a wide range of chain length and to subject them to the investigative techniques—differential thermal analysis (DTA), x-ray, and infrared methods—employed by us to characterize other long-chain complexes. A further purpose was to obtain information on the energetics of the association reactions.

Experimental

The caprylic, capric, lauric, myristic, palmitic, and stearic acids purchased from the Hormel Institute were of high purity (~99%) as determined by gas chromatographic analysis (GLC). Eastman caprylic, lauric, myristic, palmitic, and stearic acids of equivalent purity (GLC) were also used. The butyric, valeric, and caproic acids were obtained from J. T. Baker Chemical Co.; analysis (GLC) showed them to be of 99, 97.4, and 99.3% purity, respectively.

The potassium soaps were prepared from hot ethanol solutions of fatty acids by adding an equivalent quantity of alcoholic KOH, and the solutions were cooled to promote crystallization.

The potassium acid-soaps were made by two methods.

Ethanol Solution. Early workers frequently prepared their acid-soaps from ethanol solutions containing acid and soap in a ratio corresponding to the composition of the anticipated acid-soap. Levi (*13*), however, found that ratios of acid to potassium soap of 2 to 1, 1 to 1, and 1 to 2 in ethanol solution all gave rise to a 1 to 1 acid-soap. The noncriticality of the acid-soap ratio in ethanol solution was confirmed by Ryer (*21*), who found that as little as 0.04% stearic acid incorporated in a hot 0.6% solution of potassium stearate resulted in a crop of 1 to 1 potassium acid-stearate crystals on cooling. The amount of stearic acid could be raised to 1.8%—*i.e.*, 45-fold—without altering the composition of the deposited crystals. Outside of this concentration range mixed crystals were obtained: neutral soap and acid-soap at lower fatty acid concentrations, acid-soap and fatty acid at higher concentrations. To prepare potassium acid-stearate 1.4 grams of stearic acid and 1.0 gram of potassium stearate were dissolved in 150 ml. of hot 95% ethanol. The solution was cooled to 21°C. for crystallization. For shorter-chain systems, not only the amounts of acid and soap but also the weight ratio of acid to soap had to be increased because of increased solubility. For example, for the caprylic system 6.0 grams of acid and 3.0 grams of

potassium soap were used, and refrigeration (4°C.) was necessary for crystallization. The crystals were in all cases washed with small amounts of cold ethanol.

Petroleum Ether. Although fatty acids are readily soluble in petroleum ether, the soaps are poorly soluble. While experimenting with extractive techniques for "superfatted" soaps, it was discovered that a soap exposed to a petroleum ether solution of a fatty acid could react, forming an acid-soap. This constitutes the basis of an extremely simple method for forming these mixed species. The acid-soaps were prepared by dispersing a small amount of finely powdered potassium soap in heated petroleum ether containing an appropriate quantity of a dissolved fatty acid. The suspension was allowed to cool to separate the acid-soap complex. For example, 1.0 gram of palmitic acid was first dissolved in 70 ml. of warm petroleum ether, and 0.9 gram of potassium palmitate was added. The mixture was then heated and agitated by a magnetic stirrer for 30 minutes. After cooling to room temperature, the acid-soap crystals were filtered off and dried in a vacuum desiccator. For shorter-chain acid-soaps, the amounts of both acid and soap were increased.

The acid content of the acid-soaps was determined as follows: About 0.5 gram of acid-soap was dissolved in 100 ml. of hot ethanol and titrated against standardized 0.1*N* NaOH, using phenolphthalein as indicator.

Differential thermal analysis was performed with the DuPont 900 differential thermal analyzer; the heating rate was usually 10°C. per minute. To determine heats of reaction, the calorimeter attachment to the Du Pont instrument was employed. Planimeter determinations of peak areas were converted to heat values by using standard calibration curves. For the infrared spectra either a Beckman IR5A instrument or a Perkin Elmer 521 spectrophotometer with a Barnes Engineering temperature-controlled chamber, maintained dry, was used. Specimens for infrared were examined, respectively, as Nujol mulls on a NaCl prism or as finely divided powders, sandwiched between two AgCl plates. For x-ray diffraction studies, the acid-soap samples were enclosed in a fine capillary. Exposures were 1.5 hours in standard Norelco equipment with Cu Kα radiation. For powder patterns the specimen-to-film distance was 57.3 mm. and, for long-spacing determinations, 156 mm.

Results

Composition. Crystals deposited from ethanol solution as well-formed thin plates. The fatty acid content of the crystals is given in Table I. For all chain lengths the acid content approximates closely that required for 1 to 1 stoichiometry. This is also the case for most of the acid-soaps prepared by the petroleum ether route; the low values of titratable acid in some instances are ascribable to the presence of free soap.

Differential Thermal Analysis. Results obtained from thermal analysis are shown in Figure 1. Except for the C_6, C_5, and C_4 members, the potassium soaps themselves undergo an endothermic phase transition

between 50° and 80°C. These transition temperatures are indicated by arrows labeled S in Figure 1.

Table I. Per Cent Acid in Potassium Acid-Soaps

		Acid-Soap Prepared from		
		Ethanol	*Petroleum Ether*	*Theoretical*
K acid-stearate	(H)[a]	45.7	45.4	46.9
	(E)[b]	46.9	47.1	46.9
K acid-palmitate	(H)	47.1	39.5	46.5
	(E)	46.1	46.2	46.5
K acid-myristate	(H)	45.7	44.7	46.2
	(E)	45.8	45.7	46.2
K acid-laurate	(H)	45.5	40.4	45.7
	(E)	45.3	41.3	45.7
K acid-caprate	(H)	44.6	44.0	45.0
K acid-caprylate	(H)	43.8	39.9	44.2
K acid-caproate	(B)	43.5	44.9	43.0
K acid-butyrate	(B)	40.0	38.9	41.1

[a] Hormel acid.
[b] Eastman acid.

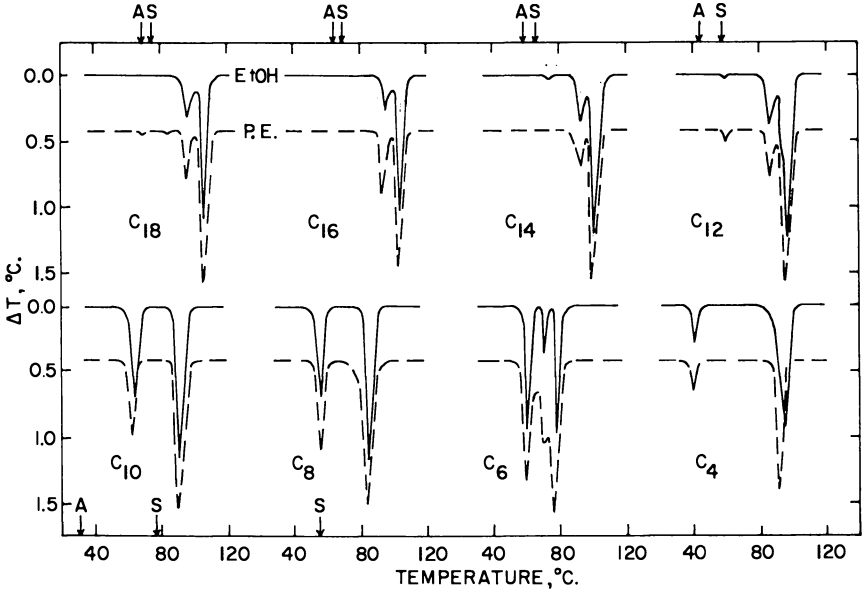

Figure 1. Differential thermograms of potassium acid-soaps (Hormel and Baker fatty acids) prepared from ethanol and petroleum ether

A and S. Transition temperatures of pure acid and soap, respectively

If we consider the main peaks of the thermograms, the patterns of the acid-soaps divide the even-carbon number acid-soaps into two categories: For carbon numbers C_{12} to C_{18}, there is a major peak at a temperature from 95° to 106°C. and a subsidiary peak appearing as a shoulder to the major peak 8° to 10° lower. To obtain further information about the latter, the following experiment was carried out. After the acid-soap (C_{12} and C_{18}) had been heated to a temperature just beyond the first transition, the temperature was kept constant for 15 minutes. On resuming heating, the major peak was observed. Upon cooling the specimen two exothermic peaks appeared at exactly the same temperatures as those of the endothermic peaks obtained on heating. This indicates complete reversibility of the transitions. The sharpness of the peaks on cooling weighs against the existence of solid solution phenomena, and this test confirms the presence of two independent transitions.

In the second group of acid-soaps of carbon numbers C_4 to C_{10} the thermograms also possess a high temperature major peak (in the temperature range 78° to 95°C.) but have in addition a relatively large subsidiary peak lying 16° to 53° below the major peak. The temperature of the subsidiary peak in C_8 acid-soap coincides with a phase transition in the C_8 soap. This is not caused by the presence of uncombined soap since a correspondingly large amount of free acid would be required, and no free acid is indicated by the thermogram. In the C_6 acid-soap, there is an additional minor endothermic transition at a temperature (71°C.) between that of the major and subsidiary peaks. The thermogram of the C_5 acid-soap, not included in Figure 1, shows only one transition (major) in the temperature range 0° to 200°C. This occurs at 62°C.

Other peaks present in the thermograms are generally attributable to small amounts of unchanged soap or fatty acid and are found more in the acid-soaps of longer chain length than the shorter chain.

X-Ray Diffraction. Each of the prepared acid-soaps gave rise to an x-ray diffraction pattern which showed it to be structurally different from both its constituents, acid and soap. The side-spacing patterns indicated that at least three different phases can be ascribed to the potassium acid-soaps: phases 1, 2, and 3 (Table II). A plot of the long spacing, d, in Figure 2 shows that d increases linearly with chain length. Values of d for the petroleum ether–derived acid-soaps tend to be slightly higher than for those prepared from ethanol solution.

Infrared. The C=O absorption region of the infrared spectrum is of interest so far as the acid-soaps are concerned. Un-ionized fatty acids have a C=O absorption band at 5.9 microns (~1700 $cm.^{-1}$). For soaps there is a strong absorption band at 6.4 microns (~1560 $cm.^{-1}$) (*1*).

Table II lists the absorption peaks observed in the 6-micron region for the acid-soaps. With the exception of potassium acid-butyrate all members up to C_{12} have their major absorption peak (underlined in Table II) at 5.82 to 5.9 microns. On the other hand, the acid-soaps of chain length C_{14} or greater have their major C=O absorption band at 6.1 microns. A sole exception in Table II is the potassium acid-stearate prepared from Eastman fatty acid, whose major absorption peak falls in the range 5.82 to 5.9 microns again.

Table II. X-Ray and Infrared Results for Potassium Acid-Soaps

	Petroleum Ether				*Ethanol*			
Acid-Soap[a]	*Phase*[b]	*I-R (6 microns)*			*Phase*[b]	*I-R (6 microns)*		
C_4 (B)	1	6.1	5.9	6.4	1	6.2	5.9	6.4
C_5 (B)	1	5.85	6.1	6.4	1	5.9	6.1	6.4
C_6 (B)	1	5.85	6.1	6.4	1	5.9	6.1	
C_8 (H)	1	5.93		6.4	1	5.83	6.1	6.4
C_{10} (H)	1	5.87	6.1	6.4	1	5.83	6.1	6.4
C_{12} (H)	1	5.9	6.1	6.4	1	5.83	6.1	
C_{12} (E)	1	5.9	6.1	6.4	1	5.82	6.1	6.4
C_{14} (H)	2	6.1	5.8		2	6.1	5.9	
C_{14} (E)	2	6.1	5.9	6.4	2	6.1	5.9	
C_{16} (H)	2[c]	6.1	5.9	6.4	2	6.1	5.9	
C_{16} (E)	2	6.1	5.8	6.4	2	6.1	5.9	
C_{18} (H)	2[c]	6.1	5.8	6.4	2	6.1	5.9	
C_{18} (E)	2	6.1	5.8		3	5.83	6.1	6.4

[a] B = Baker, H = Hormel, E = Eastman acid
[b] By x-ray diffraction.
[c] Pattern shows presence of free soap.

The influence of temperature on the infrared characteristics of acid-soaps was investigated for two members—*viz.*, potassium acid-laurate (Eastman, prepared from ethanol) and a melt-prepared potassium acid-caprylate. On heating the acid-laurate, no change in the 6-micron region was detectable up to 80°C.; at 90°C., however, which lies between the two peaks characterizing the thermogram of this complex (Figure 1), the absorption peak was observed to have shifted from 5.82 to 6.1 microns. Because of the lower transition temperatures, and a wider temperature separation, the C_8 acid-soap could be more conveniently studied by this method. At 49°C., which is below the first transition temperature, the C=O absorption characteristics were virtually the same as at room temperature. At 61°C., which is between the two transition temperatures shown in DTA, the absorption peak had shifted to 6.1 microns. On further heating there was no change until the major transition temperature was reached or exceeded: Thus, at 88°C. two major peaks were

present at 5.88 and 6.41 microns (very large). These peaks are characteristic of fatty acid and soap—*i.e.*, the two components in the uncombined state—and were of intensity greater than those corresponding to the acid-soap.

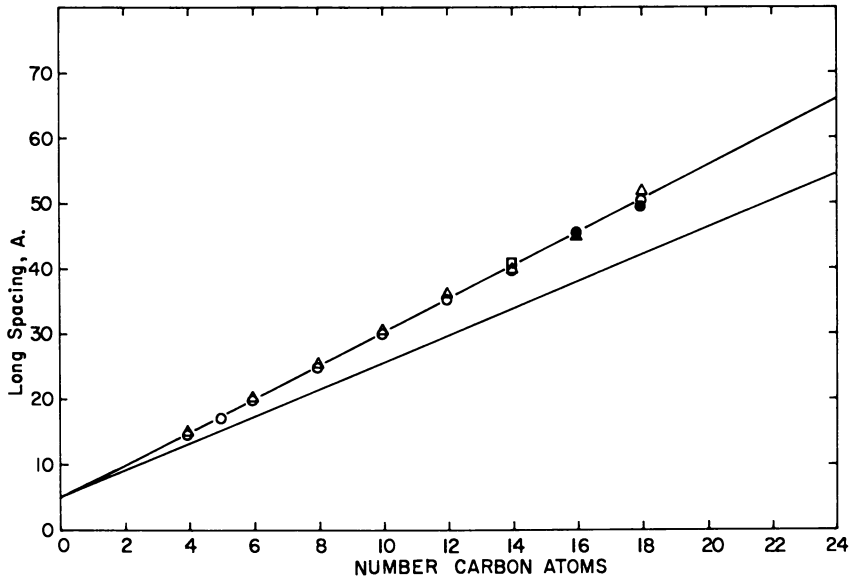

Figure 2. Long spacing (d) results

Upper and lower lines. Those of Piper (18) for potassium acid-soaps and potassium soaps, respectively
○ △ *Results for acid-soaps from ethanol and petroleum ether, respectively (Hormel and Baker acids)*
● ▲ *Results for Eastman fatty acids*
□ *Result of Dumbleton (3)*

Discussion

The composition data obtained for the series of mixed fatty acid–potassium soap systems, prepared by both the ethanol and petroleum ether routes, lend strong support to the formation of 1 to 1 acid-soap complexes. It is of interest to inquire into the phase relationships in these two-component systems. A phase diagram presented by McBain and Field (*15*) for the lauric acid–potassium laurate system shows that compound formation takes place between the two components at the 1 to 1 molar ratio, but the compound undergoes melting with decomposition at 91.3°C. [A similar type of phase behavior has been reported by us for the sodium alkyl sulfate–alkyl alcohol (*9*) and sodium alkyl sulfonate–alkyl alcohol (*12*) systems, but in these cases the stoichiometry is 2 to 1].

The thermal data presented here provide general support for the above phase diagrams and interpretation, the major endothermic transition of the thermograms corresponding in all cases to the incongruent melting point of the acid-soap complex. However, it is now clear that the McBain diagram is incomplete, in that it does not make provision below the incongruent melting point (95°C.) for a transition in the soap (57°C.) and what appears to be a transition in the acid-soap itself (87°C.). As seen in the results of Figure 1, similar transitions occur in most of the other potassium soaps and in their acid-soaps. The incongruent melting points (Table III) decrease regularly with decreasing chain length. An exception is the potassium acid-butyrate; this suggests a different structure for this system which is supported by the x-ray and infrared data discussed below. The infrared data obtained as a function of temperature for the C_8 system provide strong over-all support for the correctness of the above interpretation since above the incongruent melting or meritectic point (85°C.), infrared characteristics of the uncombined components are obtained, but below it, the evidence is that the components are not in the free state. Furthermore, the change in infrared absorption behavior in passing through the temperature of the subsidiary thermal peak (57°C.) is consistent with the latter's being a transition of the acid-soap itself.

Table III. Thermal Data for Fatty Acids and Potassium Acid-Soaps[a]

Heats expressed in kcal./mole

Fatty Acid[b]		*Potassium Acid-Soap*[b]		
Chain Length	*Heat of Fusion,*[c] ΔH_f	*Heat of Decomp.,* ΔH_1	ΔH_2 $(\Delta H_1 - \Delta H_f)$	*Decomp. Temp., °C.*
C_4	2.7	4.2	1.5	95
C_5		6.1		62
C_6	3.9	6.0	2.1	78
C_8	5.1	9.1	4.0	85
C_{10}	6.7	11.2	4.5	91
C_{12}	8.8	14.2	5.4	95
C_{14}	10.6	14.1	3.5	100
C_{16}	12.8	15.9	3.1	104
C_{18}	14.0	18.1	4.1	106

[a] Prepared by crystallization from ethanol.
[b] Hormel acids.
[c] Heats of fusion of C_4-C_{12} acids taken from International Critical Tables (8).

The x-ray side-spacing results allow us tentatively to classify the acid-soaps into three phases, determined chiefly by chain length but to some extent by source of fatty acid. Since the fatty acids were all of high

purity, the crystalline structure must be sensitive to the presence of minor impurities, presumably fatty acids of different chain length. Despite the fact that side-spacing data indicate that at least two phases are present for the acid-soaps (Hormel) whose long spacings are presented in Figure 2, all points lie on a straight line, which is in reasonably good agreement with that of Piper (*19*) and with one point of Dumbleton (3). The *d* spacing for the C_{18} acid-soap (Eastman) in the 3 phase is also close to this line. This indicates that although chain packing may vary, the tilt angle of the chains to the plane of the polar sheets is the same. This angle is close to vertical as compared with an angle of *ca.* 55° for the neutral potassium soaps (*19*).

With the exception of the C_4 system, the infrared results show a general conformity with the x-ray data in that, if the phase by x-ray is 1, the predominant infrared band in the 6-micron region is at 5.82 to 5.9 microns; when the phase is 2, the predominant infrared band is at 6.1 microns. Occasionally, however, with acid-soaps in the C_{14} to C_{18} range prepared by the petroleum ether route, specimens with 6.1-micron absorption were found to contain both phases 1 and 2. The emergence of yet a third phase (3) at the 18-carbon chain length is accompanied by a shift in infrared absorption back to the 5.82- to 5.9-micron region.

Infrared evidence for the formation of an acid-soap complex is, of course, most cogent for the species existing in phase 2, where the main absorption band of the C=O group centers at a frequency different from that of either of the two constituents. Similar absorption at 6.1 microns for the 1 to 1 sodium stearate–stearic acid complex had been observed by one of us (S. G.). Some of the acid-soaps show a complete absence of the 6.4-micron absorption band (Table II). It is therefore likely that this band in the spectra of the other acid-soaps results from the presence of a small amount of unreacted soap which has very strong absorption at this frequency. On the other hand, acid-soaps in the 1 (or 3) phase are seldom completely free of 6.1-micron absorbing material—*i.e.*, phase 2. Nor are those in phase 2 free of 5.8- to 5.9-micron absorbing material. The latter peak is characteristic of both free fatty acid and phase 1 acid-soap. Hence, this does not allow a definitive statement of the second species present. It is, however, likely to be phase 1 (or 3) material since the DTA results point to the absence of free fatty acid in most cases. Furthermore, acid-soap in one phase can transform to another phase as has been clearly demonstrated.

Dunken and Winter (*5*) have recently postulated the existence of two phases of the potassium acid-stearates characterized by infrared peaks at 6.06 microns (form 2) and 6.41, 6.02, and 5.82 microns (form 1). It is likely that their form 2 corresponds to our phase 2 and their form 1

to our phase 3, which we believe contains a small quantity of free soap (absorbing at 6.4 microns).

We turn now to consideration of the energetics of acid-soap associations. The heats of decomposition, ΔH_1, listed in Table III, refer to the reaction signified by the major decomposition peak of each acid-soap system (Figure 1).

$$KA \cdot HA(s) \rightarrow KA(s) + HA(l) \qquad \Delta H_1$$

Values for the C_{12} to C_{18} acid-soaps are less reliable than for the others because of overlap of the transition and decomposition peaks. The heat values are appreciable and are a measure of the energy which would be liberated if liquid acid and solid soap were allowed to react just below the decomposition temperature.

Decomposition of the acid-soap complex in a sense includes the melting of the acid since the latter is removed from a solid matrix and transformed into a liquid in a process akin to formal melting. To evaluate the energy data it is, therefore, convenient to compute a heat of dissociation (or association) involving the solid fatty acid and the soap—*i.e.*, the measured heats should be corrected for the heat of fusion of the fatty acid. Two courses are open for this purpose:

Course A. To calculate the heat of dissociation, ΔH_2, at the decomposition temperature of the individual acid-soaps,

$$KA \cdot HA(s) \rightarrow KA(s) + HA(s) \qquad \Delta H_2$$

This has the advantage that all the released soap will presumably be in the same form [high temperature form C (*14*)], but the disadvantage that heats for the acid-soaps of different chain length have to be compared at different temperatures (a 30°C. range, from 80° to 110°C.).

Course B. To correct the heats of dissociation to correspond to dissociation (or association) at room temperature. This has the disadvantages that heat capacity effect corrections (at present unknown and unmeasured) would have to be made to embrace a considerable temperature range, heats of transition of the soaps and acid-soaps to the phases stable at room temperature would have to be measured, and the heats of interaction would in certain cases involve soaps in different forms [form A for C_8, C_{10}; B for C_{12} to C_{18} (*14*)]. It would, on the other hand, allow heats to be compared at one standard temperature.

In the absence of the required heat capacity data we have chosen course A. The calculated heats of decomposition involving solid fatty acid, ΔH_s, are given in Table III.

The molar heats, ΔH_2, are reasonably close for all potassium acid-soaps investigated and appear to be independent of chain length. This is not surprising since the device of subtracting the heat of fusion of the fatty acid will, to a first approximation, have accounted for the effect of the chain interactions. The amount of heat—about 4 kcal. per mole—is in the hydrogen bonding range and indicates that hydrogen bonding may

play an important role in forming these acid-soaps; on the other hand, we believe that a substantial rearrangement of the head group structure takes place in a soap on forming an acid-soap complex, so that the effect of these changes will also be embodied in the ΔH_2 values. From single crystal data recently presented by Dumbleton and Lomer (*4*) for potassium palmitate it can be seen that the positive and negative ions in the polar sheet are nearly coplanar. In other words, the ionic head groups tend to dominate the crystalline packing arrangement, and this results in a somewhat weak, "open" crystal structure. For this reason we feel that soaps react avidly with fatty acids and in this way achieve a more stable state of packing in the mixed crystals. Similar reasoning seems applicable to reactions involving other pairs of long-chain ionic and long-chain polar materials (*7*).

Acknowledgment

We thank R. E. Eichenlaub, J. Jip, and J. J. Joyce for their assistance with the measurements, and the Lever Brothers Co. for permission to publish this paper.

Literature Cited

(1) Chapman, D., "Structure of Lipids," Wiley, New York, 1965.
(2) Chevreul, M. E., "Recherches Chimique sur les Corps Gras d'Origine Animal," pp. 34, 53, 408, Paris, 1823.
(3) Dumbleton, J. H., *Acta Cryst.* **19**, 279 (1965).
(4) Dumbleton, J. H., Lomer, T. R., *Acta Cryst.* **19**, 301 (1965).
(5) Dunken, H., Winter, H., *Z. Chem.* **4**, 438 (1964).
(6) Ekwall, P., Mylius, W., *Ber.* **62**, 1080 (1929).
(7) Goddard, E. D., Kung, H. C., *Soap Chem. Specialties* **42**, 60 (1966).
(8) International Critical Tables, Vol. 5, Table C, p. 134, McGraw-Hill, New York, 1929
(9) Kung, H. C., Goddard, E. D., *J. Phys. Chem.* **67**, 1965 (1963).
(10) *Ibid.*, **68**, 3465 (1964).
(11) Kung, H. C., Goddard, E. D., *J. Colloid Sci.* **20**, 766 (1965).
(12) Kung, H. C., Goddard, E. D., Proceedings of 4th International Congress on Surface Activity, Brussels, Vol. 2, p. 751, 1964.
(13) Levi, T. G., *Gazz. chim. ital.* **62**, 709 (1932).
(14) Lomer, T. R., *Acta Cryst.* **5**, 11 (1952).
(15) McBain, J. W., Field, M. C., *J. Chem. Soc.* **1933**, 920.
(16) McBain, J. W., Field, M. C., *J. Phys. Chem.* **37**, 675 (1933).
(17) McBain, J. W., Stewart, A., *J. Chem. Soc.* **1933**, 924.
(18) Malkin, T., *Ber.* **63**, 1807 (1930).
(19) Piper, S. H., *J. Chem. Soc.* **1929**, 234.
(20) Ryer, F. V., *Oil Soap* **23**, 310 (1946).
(21) Ryer, F. V., unpublished results.
(22) Schulman, J. H., Rideal, E. K., *Proc. Roy. Soc. (London)* **B122**, 29 (1937).

RECEIVED July 3, 1967.

7

Molecular Associations Considered from the Point of View of the Lipophilic-Hydrophilic Balance

D. G. DERVICHIAN

Department of Biophysics, Institut Pasteur, Paris, France

Substances having amphiphilic molecules may give molecular associations in the presence of either water or organic solvents. The principal governing factor for the formation of molecular compounds in the case of these substances is the realization of the best hydrophilic-lipophilic balance permitting the formation of lyotropic mesomorphous phases or dispersion into micelles. The realization of such conditions is illustrated by the association of lecithin and bile salt in the presence of water or organic solvents and the association between lecithin and cholesterol. The molecular association appears as a consequence of the orientation of the molecules by the solvent, one species of molecules being dissolved in the other, and the whole being dispersed in the solvent.

The formation of molecular or addition compounds by organic substances is well known, and many handbooks cite as an example the mixture of benzophenone and diphenylamine to produce a stable equimolecular addition compound. Another example is the molecular compound formed by benzene and picric acid. This is stable only in the presence of an excess of picric acid.

Different factors govern the formation of these molecular compounds. Where lipids and related substances are concerned the governing factor is the realization of the best hydrophilic-lipophilic balance producing hydration or dispersion. The case of lecithin and sodium cholate associated in the presence of water may be used to illustrate the conditions of association and formation of different types of structure and of micelles.

Sodium cholate is insoluble in chloroform and in nonpolar solvents in general, but it is very soluble in alcohol and in water. Lecithin, on the contrary, is soluble in chloroform and only swells in water without dissolving in it. These differences in solubility are evidently related to the molecular structure and to the position of the hydrophilic groups in each of these molecules. The lecithin molecule has two important paraffinic chains and a group of hydrophilic functions (choline phosphate) localized at one end. In the presence of water, the lecithin molecules are oriented with their hydrophilic groups toward the water, and they hide their paraffinic chains inside a structure formed of two superposed layers of molecules. Conversely, in a nonpolar solvent the paraffinic chains are turned toward the solvent, while the polar groups are hidden inside the micelle.

In addition to its carboxylic function at the end of the molecule, sodium cholate has three OH groups located on the steroid ring. This structure explains the great solubility of the cholate in water and its insolubility in the nonpolar solvents, but the three OH groups are distributed on the same side of the steroid ring, so that it is possible to talk of a lipophilic face and a hydrophilic face in the molecule.

Thus, if two of these cholate molecules are fastened together by their hydrophilic face and held by three hydrogen bonds, only their lipophilic faces will appear laterally. Such a pair of molecules can therefore behave as an amphiphilic unit and be oriented with the carboxylic end groups toward water. The paraffinic portion of the pair can also be embedded between the paraffinic chains of other lipid molecules.

Two complementary experiments show that the orientation and hiding of one or the other face of the steroid ring of cholate can occur when mixtures of lecithin and bile salt are considered. One of these experiments was performed by Etienne (*4*), who observed the following facts incidentally while extracting lipids from the serum lipoproteins by Delsal's method. This method utilizes a mixture of methanol and methylal (1 to 4) in the cold. The proteins are precipitated, while the lipids are dissolved in the methanol-methylal solvent mixture. If this solution of the lipids is evaporated, the residue is soluble in nonpolar solvents, such as chloroform. However, if sodium cholate is added to the lipoproteins before their extraction, the residue obtained after the methylal-methanol solvent evaporates is insoluble in chloroform. More precisely, while cholesterol and the triglycerides of the lipidic residue are extracted by chloroform, all of the lecithin remains insoluble, associated to the bile salt. The explanation is probably as follows. During evaporation, methylal with its low boiling point (44°C.), evaporates first, and the solvent becomes more and more concentrated with methanol and the residual water from the lipoprotein aqueous solution. Therefore, in the lecithin plus

bile salt residue, it is the bile salt, because of its greater affinity for the polar groups of methanol and water, which forms the outer portion of the residue particles. These particles thus structured are insoluble in chloroform, as is sodium cholate.

The other experiment was performed by Isaksson (5) earlier. He extracted desiccated bile, using different solvents in succession. With chloroform, all of the lecithin was extracted but was accompanied by a large part of the bile salts. While bile salts by themselves are insoluble in chloroform, the extract thus obtained contains a proportion by weight of 2 parts of bile salt to 1 of lecithin—about one molecule of lecithin for three molecules of bile salt. Here, it is the lecithin, soluble in chloroform because of its paraffinic chains, which by association solubilizes the bile salt. It is interesting to inquire how these associations are achieved in both cases—*i.e.*, how the molecules of bile salt are arranged and oriented in relation to the molecules of lecithin and to the polar or non-polar solvent. Let us examine first the state of the bile salt molecules in an aqueous phase.

Study of solutions of bile salt in water and in particular of sodium cholate by light scattering (7) has shown that the dissolved molecules form associations of few molecules: two, three, or four.

With amphiphilic substances the structure of the micelles corresponds to a state of minimum free energy because the paraffinic parts of the molecules are hidden inside the micelles and the soluble groups directed toward the water. As suggested by Small (7), the sodium cholate molecules will have the same tendency to associate in water, sticking the lipophilic face of the steroid ring back to back and turning the OH groups outside, toward water (Figure 1). When bile salt is associated with lecithin in aqueous phases the most favorable arrangement would still be to have the lipophilic face of the cholate molecule in contact with the paraffinic chains of the lecithin, so that the mixed micelles are partially covered by all the OH groups of the bile salt and partially by the ionized groups of the lecithin (Figure 2).

The phenomenon observed by Etienne can therefore be interpreted as follows. In the methanol + methylal + water solvent the mixture of lecithin and bile salt is dissolved in the form of mixed micelles with the OH groups of the cholate oriented outward, as in the case of the aqueous solution (Figure 2). This structure is maintained throughout the evaporation and after it, so that the aggregates cannot dissolve in chloroform. Inversely, in the case of Isaksson's experiment, the bile salt is solubilized in chloroform because of the formation of mixed micelles in which the bile salt is hidden by being dissolved between the paraffinic chains of the lecithin. This requires that the cholate molecules are already bound, probably in pairs, forming hydrogen bonds between their OH groups,

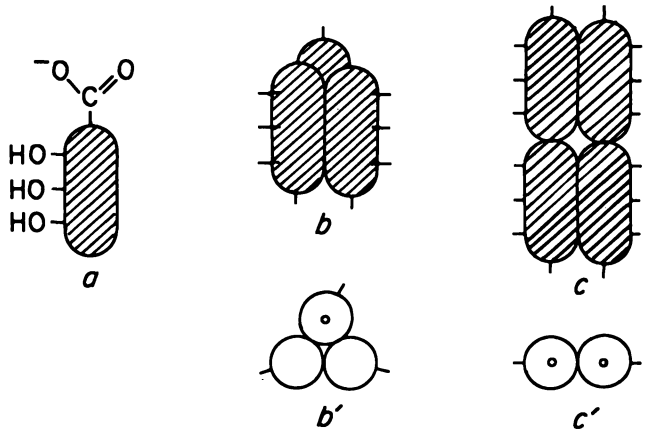

Figure 1. Possible association of cholate molecules into micelles

a. Schematic view of single molecule
b. First alternative of association of two or three molecules in single layer
c. Second alternative of association of four molecules into two oriented layers
b', c'. Cross sections of b and c

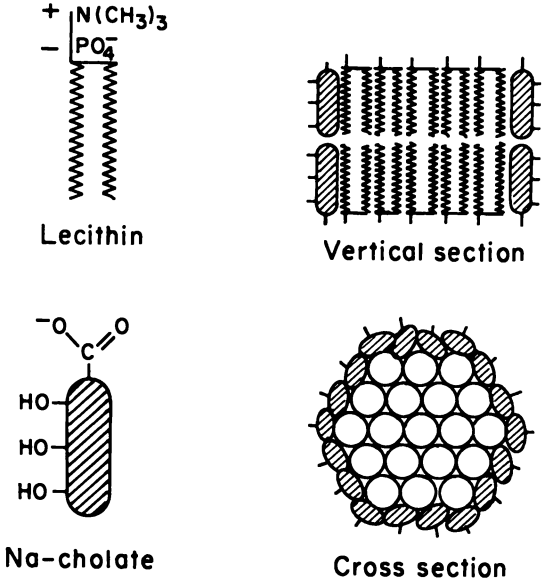

Figure 2. Schematic view of proposed model for association of lecithin and Na cholate into mixed micelles

and showing the lipophilic face of their steroid ring. Thus, the outside of the micelle is itself formed by an assembly of the paraffinic chains of the lecithin.

This situation can be deduced systematically by starting from the lamellar phase which is obtained with the more concentrated water-lecithin–sodium cholate systems recently investigated in this laboratory (*8*) (region I in the ternary diagram of Figure 3). Taking into account the quantity of water, the measurements of the long spacing of the mixed lamellar phase (I) tend to demonstrate that the molecules of bile salt stand elongated between the elongated molecules of the lecithin.

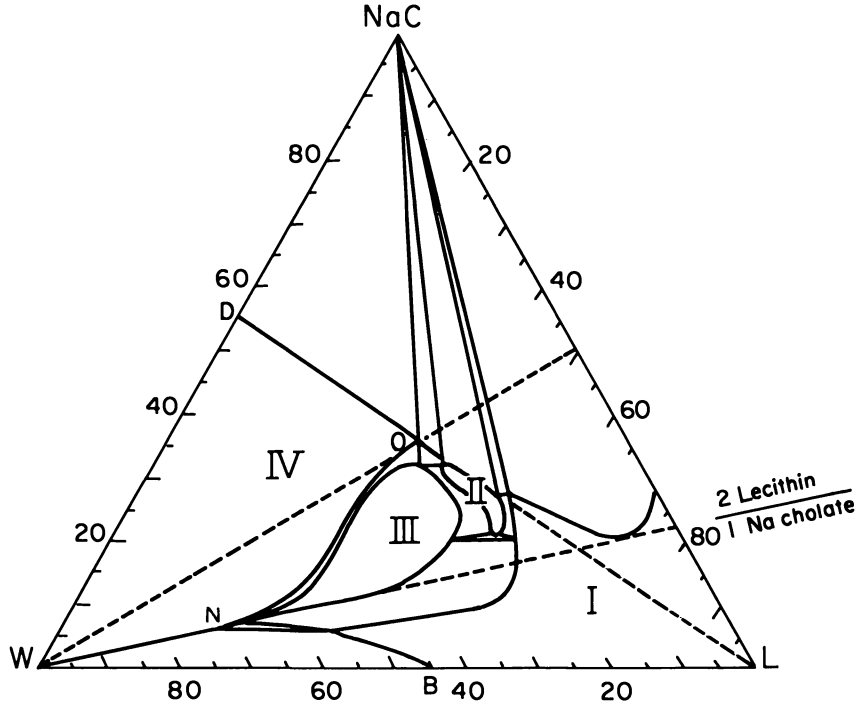

Figure 3. Ternary phase diagram for system lecithin (L), Na cholate (NaC), and water (W). Scales in weight per cent

Region I. Relative to lamellar liquid crystalline phase
Region III. Relative to hexagonal liquid crystalline phase
Region IV. Relative to isotropic micellar solution

This solution of the cholate molecules between the chains of the lecithin is conceivable only if the cholate molecules are associated by their OH groups, showing their lipophilic sides outward. Thus, where the cholate molecules are associated in pairs, the maximum quantity incorporated in the lamellar phase corresponds at the most to one pair of cholate mole-

cules for two molecules of lecithin (region *F*, Figure 3). The hexagonal phase (III) may contain up to three molecules of bile salt for two of lecithin. Generally speaking, this hexagonal phase appears with larger quantities of water.

For still larger quantities of water, one obtains the isotropic phase (IV), formed of mixed micelles. By extending the frontier line, *WN*, up to its intersection with side *L-NaC* of the triangle of the Figure 3, it can be seen that in order to get this micellar dispersion, at least one molecule of Na cholate is needed for two molecules of lecithin.

Let us assume that the solubilization of lecithin is caused by the presence of a ring, one molecule thick, of cholate molecules around a core of lecithin molecules (Figure 2). Because of the amphiphilic structure of the lecithin molecules, these form an oriented double layer as in the lamellar phase. Consequently, to cover the outer chains of the lecithin core, two rings of cholate molecules are needed. These molecules have their lipophilic face in contact with the hydrocarbon chains of the lecithin, their OH groups oriented toward the water, and their carboxyl groups level with the ionic heads of the lecithin. In a sense sodium cholate plays, at least in part, the role of an emulsifying agent for lecithin, although the ionic groups of the lecithin also contribute largely to the solubilization of the whole of the micelle.

We can now raise the question as to what must be the size of the particle in order to have a certain weight ratio, or molecular ratio, of cholate to lecithin. It is evident, as in the case of emulsion, that the higher the relative quantity of cholate to lecithin, the smaller are the particles. We can assume a reasonable molecular area for the lecithin molecule deduced from measurements in monolayers (*1*) or from an x-ray study of lecithin swollen in water (*6*)—*i.e.*, 70 sq. A. We can also assume an area of about 50 sq. A. for the cross section of the cholate molecule, this being larger than the value we know for cholesterol (39 sq. A.). It would correspond to an average width of 7 to 8 A. for the surrounding steroidal ring, including the OH groups. The problem then becomes a matter of geometry.

Consider first the weight proportion of 77% of Na cholate for 33% lecithin which has to be reached in order to solubilize all the lecithin in water. This corresponds nearly to one molecule of Na cholate for two of lecithin. Taking as a model the one proposed in Figure 2, we can calculate the size which the mixed micelles should have so that the proportion of one molecule of Na cholate for two of lecithin will be obeyed. In other words, we want to know the number of lecithin molecules packed side by side which, surrounded by a ring of adjacent Na cholate molecules, can give the desired proportion. The calculation gives for each

of the two superposed layers forming the model, 84 lecithin molecules having their paraffinic chains packed side by side and surrounded by 42 molecules of Na cholate. The whole micelle with its two layers would therefore contain about 170 molecules of lecithin for 85 of Na cholate and would have a molecular weight of about 170,000.

For the proportion of one molecule of Na cholate to one of lecithin —*i.e.*, 37% Na cholate and 63% lecithin—the same calculation gives 24 molecules of lecithin for 24 of Na cholate in each layer—*i.e.*, 48 molecules of each species for the whole of the mixed micelles and a molecular weight of about 60,000. Finally, for the weight proportion of 1 to 1 (about five molecules of Na cholate for three of lecithin), we find per layer 10 molecules of lecithin for 17 of Na cholate. This leads to 20 molecules of lecithin for 34 of Na cholate for the whole mixed micelle and a molecular weight of about 30,000.

This final proportion also corresponds to the largest quantity of lecithin solubilized in water as an isotropic phase. This system contains only 30% water and 35% lecithin and is represented by point *O* on Figure 3. All systems with their representative point situated at any place on line *WO* have the same relative proportion of lecithin and bile salt; the relative quantity of water alone increases when moving from *O* toward *W*.

Preliminary determinations by light scattering of the size of the mixed micelles on mixtures containing increasing proportions of Na cholate show that the molecular weight is on the order of 150,000 for the maximum proportion of lecithin, but only on the order of 20,000 to 30,000 for equal weights of lecithin and Na cholate. Thus, despite their lack of precision, the experimental measurements are in conformity with the results of the calculation. The molecular weight starting at a high value, superior to 150,000 for the ratio of 1 molecule of Na cholate for 2 of lecithin, decreases rapidly with the increase of Na cholate and reaches a value of 20,000 or 30,000 when the ratio is five molecules of Na cholate to three of lecithin.

Other properties—*e.g.*, viscosity and conductivity—show a definite change when the relative quantity of Na cholate is larger than that indicated by line *WO* on Figure 3. Different facts lead to the conclusion that beyond the weight proportion of Na cholate to lecithin of 1 to 1, the excess of Na cholate in the solution remains in the form of micelles of pure Na cholate in equilibrium with the mixed micelles having the fixed weight composition of 1 to 1 lecithin–Na cholate. Among other things, this explains the fact that frontier *DO* when extrapolated passes through apex *L* (Figure 3). Indeed, all along the *OD* frontier the concentration of free Na cholate in water is constant, being independent of the quantity of lecithin present, and equal to the saturation concentra-

tion, 55%. This is expected if in all systems situated along line *OD* the mixed micelles, with their composition indicated by point *O*, were in equilibrium with a saturated micellar solution of Na cholate having the saturation concentration indicated by point *D*.

It is also reasonable to admit that the size of the mixed micelle could be the same in all systems situated along line *OW* since in all these cases the mixed micelles would always be in equilibrium with a micellar solution of pure Na cholate. Indeed, the chemical potential of the Na cholate in solution remains practically constant whatever the concentration, as long as micelles are present. Consequently, the chemical potential of the Na cholate attached to lecithin on the mixed micelles must also be constant since there is equilibrium.

Although the values of the calculated dimensions of the mixed micelles agree with the order of magnitude of the measured values, it cannot be asserted that the molecules of Na cholate forming the ring around the mixed micelles necessarily touch each other. All that can be said is that as the free Na cholate in solution is at its maximum chemical potential (since the solution is micellar), the surface of the mixed micelles must be saturated by Na cholate, in the sense of a saturated solution of one component in or on the other. As this is an equilibrium, it seems obvious that there is a permanent exchange between the Na cholate molecules fixed on the surface of the mixed micelles and those free in solution.

These statements lead to the conclusion that the limiting proportion of 1 gram of Na cholate associated to 1 gram of lecithin is simply imposed by the size of a certain form of mixed micelle which can remain in equilibrium with an excess of Na cholate in micellar solution. Thus, it clearly appears that association is governed by the necessity of securing the proper hydrophilic-lipophilic balance of the mixture of two components. Here, as in the case of other amphiphilic substances, by the progressive increase in proportion of the more hydrophilic amphiphile, the association can reach complete micellar dispersion in water.

For mixtures of lecithin plus Na cholate it appears possible to infer the molecular arrangement in the dispersed micelles from the most likely structure of the liquid crystalline phase suggested by x-ray analysis. However, there are cases where dispersion is not possible because neither component is sufficiently hydrophilic to be dispersed even when alone in water. This is shown by the association of cholesterol and lecithin in the presence of water. The ternary diagram of Figure 4 is relative to these systems. Here only the lamellar liquid crystalline phase is obtained (region 1ϕ in Figure 4). This phase is already given by lecithin alone, which can absorb up to 55% water. Cholesterol can be incorporated within this lamellar phase up to the proportion of one molecule of choles-

terol per molecule of lecithin. Such a mixture can swell to incorporate up to 43% water.

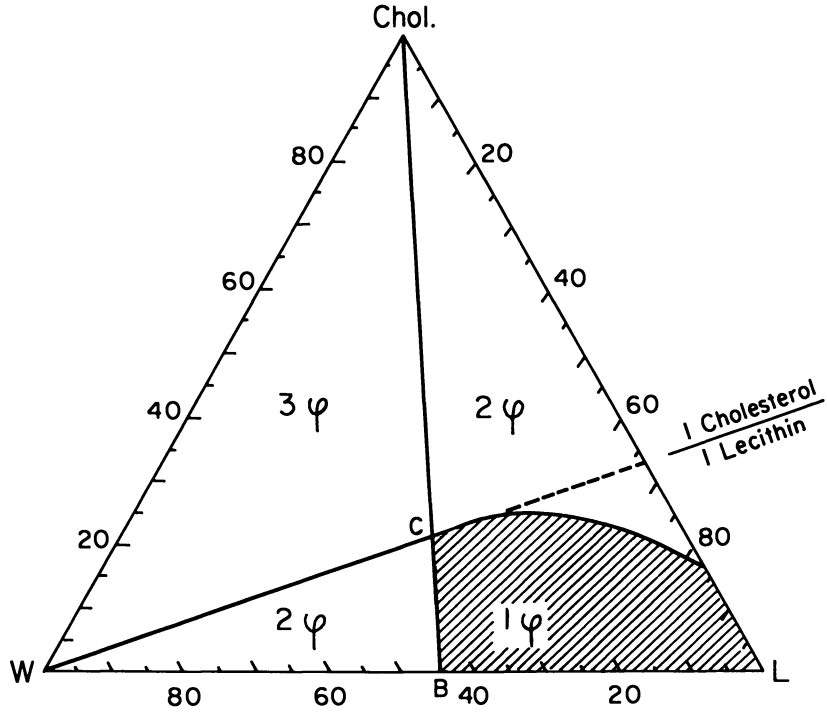

Figure 4. Ternary phase diagram for system lecithin (L), cholesterol (Chol), and water (W)

1 φ is the only region where a single phase is obtained. This is a lamellar liquid crystalline phase. Scales in weight %

This lamellar phase is formed of alternate sheets of lipid and water. The lipidic sheets containing the lecithin and the cholesterol are made of two superposed layers of oriented molecules. Each of these two monolayers is mixed and consists of lecithin and cholesterol molecules arranged side by side with their paraffinic ends turned toward the inside of the sheet and their polar groups (phosphatidyl choline group for lecithin and hydroxyl group for the cholesterol) outward—*i.e.*, toward the adjacent sheet of water. This constitution of each of the two monolayers forming the lipidic sheet is in conformity with the conclusion arising from the study of mixed monolayers of cholesterol and lecithin spread on the free surface of water (*1*).

In general, the two components in the anhydrous state do not necessarily build up in a common network to give a mixed crystal and cannot

be said to associate. The association of the two components in a liquid crystal to give a common network is the consequence of the orientation of their molecules by water. This type of association of cholesterol and lecithin is caused simply by the solution of the paraffinic parts of the cholesterol molecule between the paraffinic chains of lecithin. Such is also the case, in a sense, with the mixtures of Na cholate plus lecithin. Orientation and swelling by water are cooperative actions which can lead to the solubilization of the less soluble component and to the dispersion into micelles whenever the over-all lipophilic-hydrophilic balance largely favors the hydrophilic character (*3*). Another condition is necessary for this mutual solution of the hydrocarbon ends of the molecules to occur. The chains must be in the fluid state at the temperature considered (*2*)—for instance, with a lecithin having saturated chains, association with cholesterol or with Na cholate can occur only much above room temperature.

Literature Cited

(1) De Bernard, L., *Bull. Soc. Chim. Biol.* **40,** 161 (1958).
(2) Dervichian, D. G., *Progr. Biophys. Mol. Biol.* **14,** 329 (1964).
(3) Dervichian, D. G., *Trans. Faraday Soc.* **42 B,** 180 (1946).
(4) Etienne, J., *Rev. Pathol. Biol.* **16,** 409 (1968).
(5) Isaksson, B., *Acta Soc. Med. Upsalien.* **59,** 296 (1953-1954).
(6) Lécuyer, H., Dervichian, D. G., unpublished manuscript.
(7) Small, D. M., ADVAN. CHEM. SER. **84,** 31 (1968).
(8) Small, D. M., Bourgès, M. C., Dervichian, D. G., *Biochim. Biophys. Acta* **125,** 563 (1966).

RECEIVED September 27, 1967.

8

Association of Membrane Constituents Using Nuclear Resonance Spectroscopy

D. CHAPMAN

Unilever Research Laboratory, The Frythe, Welwyn, Herts, England

At a certain transition temperature anhydrous phospholipids exhibit an abrupt fall in their PMR line width, owing to the occurrence of a mesomorphic phase in which considerable molecular motion of the hydrocarbon chains occurs. Phospholipids in this mesomorphic phase can be dispersed in D_2O by ultrasonication and show high resolution PMR spectra. This enables studies to be made of the interaction with lipid and cholesterol. Erythrocyte ghost fragments dispersed in D_2O also show high resolution PMR spectra. The spectra show separate peaks assigned to choline, sugar, and sialic acid protons. Signals from the protons of the lipid chains and from the amino acids of the protein are either absent or considerably diminished in intensity. This may be caused by hydrophobic interactions between the lipid chains and the membrane protein.

At present there is considerable interest in the way in which the constituents of membranes are associated to form the dynamic complex entity of the cell membrane. Speculations range from the Danielli-type structure, first advanced in 1935, to structures which now place greater emphasis on the so-called "hydrophobic bonding" of the lipid polymethylene chains and amino acids of the membrane protein (*10*). Various other speculations about the associations of the membrane components are built around these two main themes. In a field of research where there are such a considerable speculation and divergence of opinion, this usually indicates a shortage of experimental information rather than variations in perspicacity. This seems to be true of our present knowledge of membrane structure.

Because of the shortage of experimental information we have been exploring the technique of nuclear magnetic resonance (NMR) spectroscopy. The basic equation underlying this branch of spectroscopy is $h\nu = 2\mu H_o$, where h is Planck's constant, ν is the frequency of the radiation (radio-frequency in this case), μ is the magnetic moment of the nucleus, and H_o is the magnetic field in which the nucleus is placed. To satisfy the condition for resonance to occur, either the frequency or the magnetic field can be varied. The features of NMR spectroscopy are such that we are able to look at the behavior of a particular nucleus while the other nuclei are "transparent." Thus, we can look at the hydrogen, phosphorus, or nitrogen nucleus and obtain information about its degree of molecular freedom. If molecular motion occurs at a frequency equal to or greater than the line width expressed in frequency units, a narrowing of the line width will occur. In this study reorientation frequencies greater than 60 Kc. per second will cause narrowing. If there is less molecular motion, broader lines are observed. Thus, if we look at the NMR spectrum of a solid, lines as broad as 10 or 15 gauss are observed because magnetic dipole-dipole interactions cause the nuclear resonance to occur over a wide range of magnetic field. The field experienced by any nucleus is produced by the magnetic fields of the other nuclei of the same type as well as by the main experimental field H_o. If we look at a liquid, extremely narrow lines of the order of milligauss are seen because the magnetic interactions, caused by the various nuclei, average out because of the random motion of the nuclei. With liquids observed under conditions of high resolution fine structure is seen. Separate signals occur which are associated with the different proton groups present.

The association, or interaction, of one molecule with a second type of molecule may be expected to affect their relative molecular motion. In particular cases the motion of a segment, or part of a molecule, may be more affected by the mutual interaction than other parts of that molecule. If this is the case, differential broadening of lines in the high resolution NMR spectra can occur, and information about the mode of interaction can sometimes be obtained (*11*).

Experimental

High resolution proton magnetic resonance (PMR) spectra were recorded on a Perkin-Elmer R-10, 60-megacycle per second spectrometer fitted with a decoupling unit, a temperature probe, and a computer averaging attachment. Unless specified otherwise, spectra were obtained at 33.5°C. Chemical shifts in the high resolution NMR spectra are expressed as usual in parts per million relative to the protons of tetramethylsilane at 10 p.p.m. (τ scale).

Results and Discussion

The PMR spectroscopy of solid phospholipids (9) shows that, at liquid nitrogen temperatures in the solid state, broad lines occur some 15 gauss wide. As the temperature increases, the line narrows gradually until, at a particular transition temperature, there is a considerable fall in the line width (Figure 1). This sudden drop to about 0.1 gauss occurs because of the onset of a mesomorphic condition. In this mesomorphic state considerable molecular motion of the polymethylene chains of the lipid occurs, and this motion averages out the magnetic dipole-dipole interactions. This averaging process involves translational modes as well as rotational oscillation of the methylene groups. These movements are particularly marked at the ends of the chains and also involve a marked departure from the all-trans character of the hydrocarbon chains. This is shown by the infrared spectra of the lipids in this mesomorphic phase (2). Spin-lattice relaxation measurements (9) indicate how the motion of the polymethylene chains approaches, but is not as great as, that of a liquid hydrocarbon of a similar chain length.

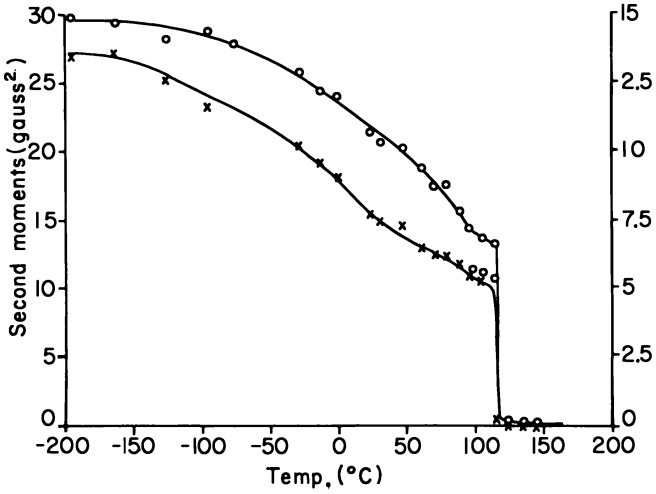

Figure 1. Proton magnetic resonance spectra of dimyristoyl-DL-phosphatidylethanolamine at different temperatures, showing onset of mesomorphic phase (9)

● *Line width*
× *Second moment*

The transition temperature at which this change from a crystalline to a mesomorphic phase occurs varies with the chain length and with the unsaturation. The effect of water is to lower this transition tempera-

ture. As the amount of water increases, the transition temperature reaches a lower limiting value, so that with phospholipids containing higher unsaturated chains of the type frequently found in biological membranes, the transition temperature can be below 0°C. Thus, NMR studies show that there is considerable motion of the polymethylene chains of pure phospholipids at biological temperatures. We can expect at least as much motion of the lipid chains when the lipid is present in a membrane, unless this motion is inhibited somehow by association with other membrane components.

When unsaturated phospholipids are examined in water, they show an absorption line width of about 0.1 gauss. Fine structure and high resolution PMR spectra are not observed until the large liquid crystalline aggregates are broken up by ultrasonication. After ultrasonication for a few minutes the phospholipid disperses in the water, and now a high resolution NMR spectrum is observed (*8*), as shown in Figure 2A. Previous studies (*6*) using phospholipids dissolved in various solvents have led to the assignment of various peaks in the spectra to particular functional groups. On the basis of these assignments we have been able to assign the peaks in the spectra of the phospholipid dispersed in water. Individual peaks assignable to the protons of the choline group, $N(CH_3)_3$, the CH_2OP group, the polymethylene chain, $[CH_2]_n$, and the methyl group at the end of the hydrocarbon chain, are clearly delineated.

The fact that one observes a high resolution PMR spectrum with this phospholipid only after ultrasonication raises the important question as to whether some phase change has occurred. Most authors (*15*), however, suggest that ultrasonication merely breaks up the large lamellar aggregates into smaller fragments, but that these fragments consist of a bilayer organization. The fact that we observe a high resolution NMR spectrum suggests that there is considerable molecular freedom, including translational freedom, of the phospholipid molecules in this state. This is needed to average out the magnet dipole-dipole interactions. The line width of the peak corresponding to the $[CH_2]_n$ groups of the polymethylene chain is slightly broader than is observed when the phospholipid is dissolved in a solvent such as chloroform. The association of cholesterol with phospholipid has been studied by many techniques, notably monolayer techniques at the air–water interphase (*7*, *12*). There are many difficulties, however, in interpreting the monolayer studies, and discussions and debates over many years have resulted in various interpretations of the interactions (*16*). If the phospholipid is indeed in a bilayer arrangement, we have the possibility of studying (by NMR spectroscopy) the interaction of cholesterol with phospholipid.

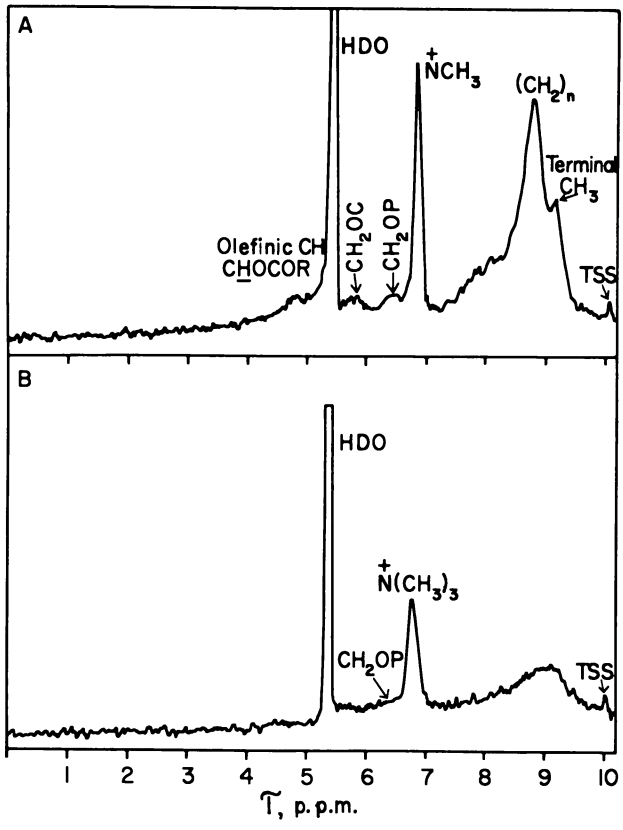

Figure 2. High resolution proton magnetic resonance spectra

A. Egg yolk lecithin dispersed by ultrasonics in D_2O
B. Egg yolk lecithin and cholesterol dispersed in 1 to 1 molar ratio in D_2O (8)

With NMR spectroscopic technique it is possible to study the interaction of cholesterol with phospholipid in a situation which should be nearer the real biological situation—*i.e.*, not at the air–water interphase. Further, by studying the broadening of each of the peaks in the spectrum, it is possible to study the effect of interaction with cholesterol with the various parts of the phospholipid molecule. If we look at Figure 2B, the high resolution NMR spectroscopy of phospholipid and cholesterol dispersed in water, we see that the hydrocarbon chain signal has now disappeared, and only a broad absorption is left in this region. The choline peak, on the other hand, still remains clear in the spectrum. Thus, a differential broadening of the peaks in the spectrum has occurred. One interpretation of this effect is that the presence of cholesterol in the

mixture affects the molecular motion of the polymethylene chain of the lipid, but there is less effect on the molecular motion of the choline group. Perhaps the cholesterol, owing to its flat bulky shape, inhibits some of the molecular motion of methylene groups within a polymethylene chain. This then increases the magnetic dipole-dipole interaction between the protons of the CH_2 groups, causing a broadening of the line associated with those protons.

The unsaturated phospholipid from soybean lecithin also shows a similar effect, while the unsaturated phospholipids from red blood cell membranes, although showing a slight effect of cholesterol interaction, still show a prominent polymethylene peak in the high resolution spectrum.

This phospholipid-cholesterol interaction is being explored further using the NMR spectroscopic technique, studying the influence of temperature and of other sterols, and with phospholipids containing various amounts of unsaturation. Other interpretations of the results are also being considered. Because of the encouraging results obtained from this work, biological membranes themselves have also been studied. It was thought that there might be sufficient molecular motion in these complex structures to show NMR peaks. Recently the NMR spectra of red blood cell membranes have been studied (*3*). With erythrocyte membranes dispersed in D_2O a high resolution PMR spectrum is observed. This spectrum is weak, but a stronger spectrum is observed when the membrane material is homogenized, or after ultrasonication for a few minutes. There is a danger associated with the use of ultrasonics for dispersing the membrane. One may disturb, or break up, the association of the membrane components by this process. Recent studies (*14*) have shown that a soluble lipoprotein can be isolated from human erythrocytes by ultrasonication. However, a 10% butanol solution was used during the ultrasonication process to produce this soluble lipoprotein. To elucidate this possibility, the effect of ultrasonication on the erythrocyte membrane with and without the presence of butanol is being studied to ensure that what we are examining are "membrane fragments." Accepting these reservations let us discuss the spectra which have been observed recently in our laboratory.

The PMR spectrum of the erythrocyte membrane fragments dispersed in D_2O is shown in Figure 3A. We have assigned the peaks in the spectrum on the basis of correlation tables (*5*) and by comparison with model substances. Peaks occur which we assign to protons of the choline group 6.7τ (present in the lecithin and spingomyelin lipids), sugar 6.3τ, and sialic acid groups 7.8τ. It is noticeable that there is no peak in the spectrum which we can associate with the HC=CH group of the lipid

polymethylene chain, nor is there a strong signal associated with the large number of protons in the polymethylene chain $[CH_2]_n$.

We consider that the peaks present in the spectrum of the erythrocyte membrane are caused by the rapid segmental motion of these proton groupings. An analogous situation occurs with large polymers such as polystyrene (*1*). Here in the PMR spectrum of the polymer narrow peaks occur, which are associated with segments of the polymer. The peak widths are independent of the molecular weight of the polymer and of the microscopic viscosity of the solution. The local viscosity in the immediate neighborhood of the segment appears to be the determining factor for observation of a narrow PMR peak.

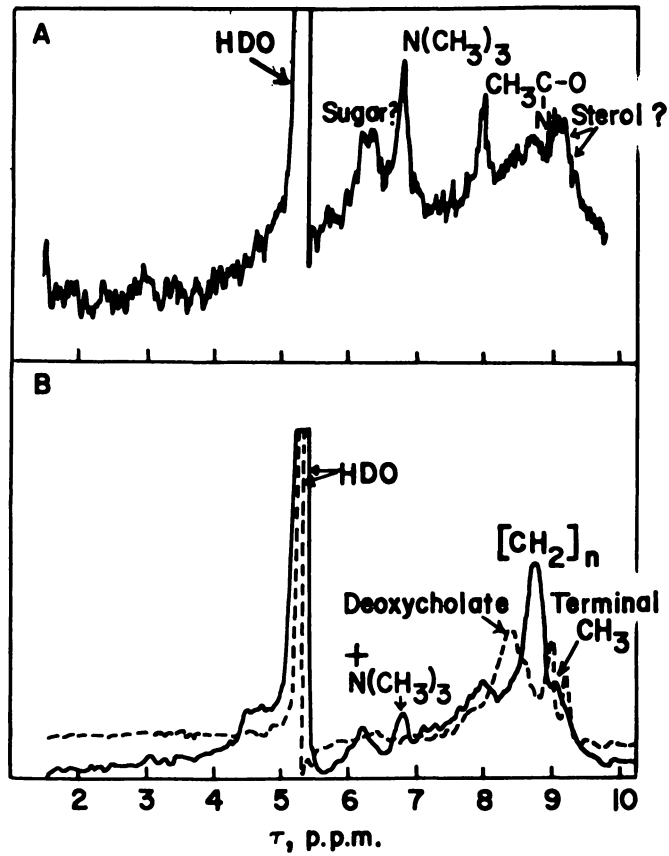

Figure 3. Proton magnetic resonance spectra

A. High resolution spectrum of erythrocyte membrane fragments dispersed in D_2O
B. Spectrum of membrane fragments treated with sodium deoxycholate (3) dispersed in D_2O

Previous studies of erythrocyte ghosts by other workers have suggested that their outer surfaces contain mucopolysaccharide and sialic acid groups; hence, it is not inconsistent that the segmental motion of these groups should be sufficient to give rise to the observed narrow PMR signals. The appearance of a peak associated with the choline protons is perhaps at first surprising if we think in terms of the Danielli bilayer model since we might have expected the motion of these protons to be somewhat inhibited by the amino acids of the protein sandwich. The presence of this narrow peak in the spectrum suggests that the local viscosity around the choline group is low. The complete absence of the HC═CH signal, and the absence of a sharp polymethylene chain strong $[CH_2]_n$ signal from the spectrum of the membrane, can be considered to reflect the inhibition of the segmental motion of these groups owing to a higher local viscosity.

We have examined the effect of temperature and enzymes and other materials on the spectrum of the membrane fragment (*4*). As the temperature increases up to 120°C. the lipid chain $[CH_2]_n$ signal becomes more prominent, suggesting that, at lower temperatures, the polymethylene chain is somehow inhibited in its molecular freedom. Treatment with phospholipase *C* removes the peak at 6.7τ which we associate with the choline protons. Urea, which is known to have an unfolding effect on proteins, produces new peaks in the spectrum of the membrane which can be assigned to some of the constituent amino acids of the protein. There is, however, no marked increase in the polymethylene chain signal. The effect of trifluoroacetic acid on the membrane is to increase the intensity of the peak associated with the constituent amino acids of the protein, and now the polymethylene chain of the lipid is also clearly visible.

The appearance in the spectrum of the membrane of peaks assigned to amino acids of the protein, only after the membrane has been placed in urea or trifluoroacetic acid, shows that the segmental motion of these amino acid groups is inhibited by high local viscosity when the membrane is present in normal D_2O. The spectroscopic evidence suggests that the polymethylene chains of the lipid and some of the amino acids of the protein may be mutually interlocked. However, both lipid-lipid and amino acid-amino acid interactions could also be occurring.

When the membrane is washed with ether to remove all of the cholesterol, the resultant PMR spectrum shows little change in the intensity of the polymethylene chain signal compared with that of the original membrane spectrum. This appears to rule out lipid-cholesterol interaction in this membrane as having a dominant effect upon the polymethylene chain freedom. In the membrane fragments either lipid chain-chain interactions have increased as a result of the protein interaction

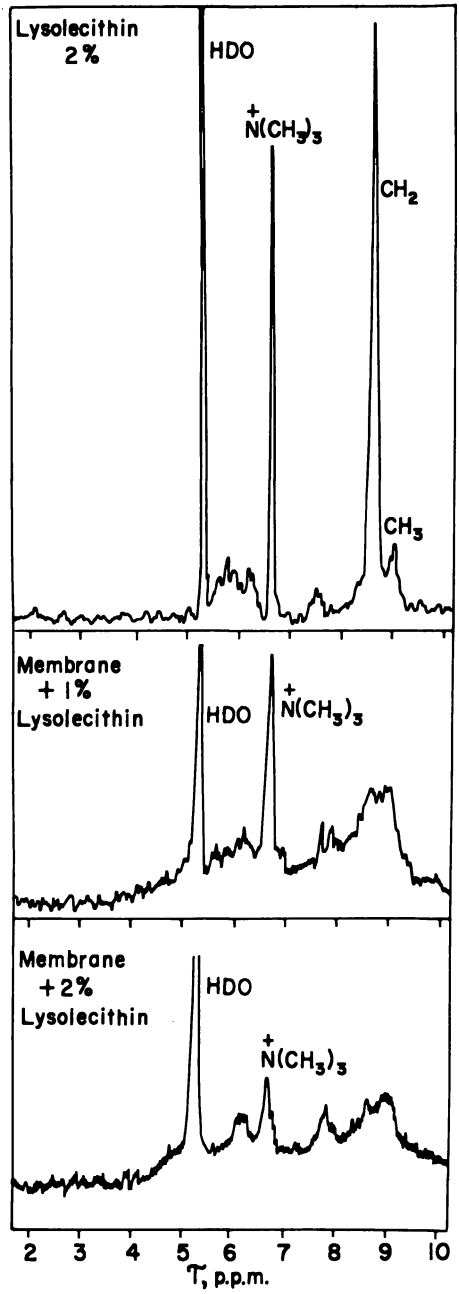

Figure 4. High resolution proton magnetic resonance spectra of lysolecithin and membrane fragments dispersed with lysolecithin in D_2O (4)

with the lipid, or amino acid–polymethylene chain interaction is occurring, of the type expected if hydrophobic bonding is taking place. Taken together with the studies of Lenard and Singer (*13*) on erythrocyte membranes, using ORD techniques, the possibility of hydrophobic lipid-protein interactions being involved in the structure of these membranes receives additional support from our spectroscopic studies.

The interaction of bile salts and solvents such as sodium deoxycholate and saponin and lysolecithin with the erythrocyte membrane fragments has also been studied. The effect of sodium deoxycholate is shown in Figure 3B, where the whole spectrum of the lipid can be seen, including strong peaks caused by the $[CH_2]_n$ chain signal. Also a peak caused by the HC=CH group appears at 4.7τ. The remarkable effect on the spectrum of lysolecithin can be seen in Figure 4. The PMR spectra of lysolecithin with and without the erythrocyte membrane material are shown. The strong $[CH_2]_n$ signal of lysolecithin is markedly suppressed in the presence of the membrane fragments. An additional contribution to the membrane choline signal arises from the lysolecithin protons.

Our studies of the interaction effects have already shown that valuable information can be obtained about the mode of interaction of these molecules within these membrane fragments. NMR spectroscopy appears sufficiently promising as a technique for us to expand our studies to other nuclei, such as phosphorus and nitrogen, and also to other biological membranes and lipid-protein systems. In this way we hope to provide increased understanding of the way in which the constituents of membranes are associated. A more complete account of our NMR studies of membranes will be published (*4*).

Literature Cited

(1) Bovey, F. A., Tiers, G. V. D., Filipovich, G., *J. Polymer Sci.* **38**, 73 (1959).
(2) Chapman, D., Byrne, P., Shipley, G. G., *Proc. Roy. Soc.* **A290**, 115 (1966).
(3) Chapman, D., Kamat, V. B., de Gier, J., Penkett, S. A., *Nature* **213**, 74 (1967).
(4) Chapman, D., Kamat, V. B., de Gier, J., Penkett, S. A., unpublished manuscript.
(5) Chapman, D., Magnus, P. D., "Introduction to Practical High Resolution Nuclear Magnetic Resonance Spectroscopy," Academic Press, London, 1966.
(6) Chapman, D., Morrison, A., *J. Biol. Chem.* **241**, 5044 (1966).
(7) Chapman, D., Owens, N. F., Walker, D. A., *Biochim. Biophys. Acta* **120**, 148 (1966).
(8) Chapman, D., Penkett, S. A., *Nature* **211**, 1304 (1966).
(9) Chapman, D., Salsbury, N. J., *Trans. Faraday Soc.* **62**, 2607 (1966).
(10) Green, D. E., Fleischer, S., "Metabolism and Physiological Significance of Lipids," p. 581, Wiley, New York, 1964.

(11) Jardetzky, O., *Advan. Chem. Phys.* **7,** 499 (1964).
(12) Leathes, J. B., *Lancet* **208,** 853 (1925).
(13) Lenard, J., Singer, S. J., *Proc. Natl. Acad. Sci.* **56,** 1828 (1966).
(14) Morgan, T. E., Hanahan, D. J., *Biochemistry* **5,** 1050 (1966).
(15) Saunders, L., *Biochim. Biophys. Acta* **125,** 70 (1966).
(16) Shah, D. O., Schulman, J. H., *J. Lipid Res.*, in press.

RECEIVED May 8, 1967.

Interaction of Bimolecular Phospholipid Leaflets with Polyelectrolytes

H. J. van den BERG

Philips Research Laboratories, N.V. Philips Gloeilampenfabrieken, Eindhoven, Netherlands

The influence of adsorption of polyelectrolytes on bimolecular phospholipid leaflets was studied. All polyelectrolytes studied were adsorbed on the surface of the film, as demonstrated by greatly increased drainage times. Only some of the polyelectrolytes investigated are able to decrease the d.c. resistance, notably a protein derived from ox erythrocyte ghosts and a Na-K polyphosphate. The combination of these latter substances proved particularly effective. It is concluded that the decrease of d.c. resistance is caused by adsorption and penetration of the polyelectrolytes into the membrane, resulting in the formation of pores or water channels, and not by the possibility of transport of charged macromolecules through the membrane.

Since the introduction by Mueller *et al.* (*11*) of a method for producing black lipid films, the study of black lipid films has expanded rapidly. Numerous publications have appeared in which these films are used to study physicochemical properties, others in which they are used as a model for biological membranes. Survey articles have been published by Mueller *et al.* (*12*), by Thompson (*18*), and more recently by Tien and Dawidowicz (*19*). As a model for a cellular membrane the black lipid film is bound to be a poor model since it lacks an essential part of even the simplest membrane conception, the polyelectrolyte coating. One of the few properties of black lipid membranes within biological ranges is its water permeability (*4*, *5*, *6*, *20*).

Little is known about the influence of a surface layer of polyelectrolyte on this membrane, though Mueller *et al.* (*9*, *11*) have described the influence of certain polyelectrolytes, especially a protein which they called "excitability inducing material" (EIM). Black lipid films with a

polyelectrolyte coating may serve as a more realistic model for cellular membranes, though in view of the complexity of many active natural membranes, their significance must not be overestimated.

Experimental Methods

The experimental methods have been described (*1*). Films are drawn by passing a hole in a Teflon screen through the oil-water interphase. The oil is a 0.5% solution of purified egg lecithin in a 3:1 vol./vol. heptane-chloroform mixture. By varying the heptane-chloroform ratio the specific density may be varied and thereby the drainage time of the film. The temperature is 23°C. throughout.

Calomel electrodes are used, connected to the water phase on both sides of the black lipid film by KCl-containing capillaries. The water phase is generally 0.25*M* KCl, which precludes interface contamination by spontaneous emulsification. Carbon tetrachloride is used as the undermost oil layer, which serves exclusively as an electric seal.

D.c. resistance is measured by a high impedance electrometer (Vibron Electrometer 33B).

Chromatographically pure egg lecithin was prepared from a commercially available pure egg lecithin by column chromatography (*16*). Ox erythrocyte ghost protein was prepared starting from hemoglobin-free ox erythrocyte ghosts, using the method of Dodge *et al.* (*2*). Protein was extracted from them by the method reported by Maddy (*7*). K-Na polyphosphate was prepared by the method of Pfanstiel and Iler (*13*).

Results

The addition of proteins to the aqueous phase has some marked effects. Even at concentrations of 0.1% the time necessary for the formation of black lipid film increases drastically—*i.e.*, from some 5 minutes to several hours. There is, moreover, generally a marked loss of stability. During the prolonged drainage time the probability of rupture of the film is enhanced. Once the film has become black, it is stable. To avoid this difficulty the polyelectrolyte was introduced by injection from a syringe after complete drainage. With polyphosphate similar effects are observed.

Several polyelectrolytes were studied—gelatin, bovine serum albumin, structural protein from beef heart mitochondria (*14*), ox erythrocyte ghost protein, and polyphosphate. Apart from an increase in drainage time, gelatin and bovine serum albumin did not give rise to changes in membrane properties. Studies with the structural protein of beef heart mitochondria were seriously hampered by the sensitivity of black films to cholate and deoxycholate, which are necessary to solubilize the protein. Detergents have a great influence on black lipid films (*15*).

On adding bovine erythrocyte ghost protein d.c. resistance suddenly decreases. Similar experiments were reported by Maddy *et al.* (8), though no change in electrical properties of the membrane was mentioned. The amount of this decrease is not very reproducible and may vary from a factor of 50 to 500. Generally it is about 100. An analogous result can be obtained upon adding polyphosphate, though the decrease is less spectacular (20 to 50×).

The amount of decrease of d.c. resistance is not or only insignificantly dependent upon polyelectrolyte concentration, as long as this is over 0.05%. The most drastic decrease in d.c. resistance may be obtained by combining polyphosphate and bovine erythrocyte ghost protein. Resistances as low as 5×10^3 ohms per sq. cm. have been obtained at pH 6.8.

To obtain more insight into the mechanism underlying the permeability changes, the electrophoretic behavior of the protein was investigated. Its isoelectric point was 2.9. Maddy (7) suggested that this protein would be rather acidic by virtue of its sialic acid residues. Subsequently, the d.c. resistance of black lipid films was investigated as a function of the pH of the water phase. The d.c. resistance turns out to be only slightly dependent on pH, with a decreased resistance at lower pH. No indication of a maximum in resistance was found at the isoelectric point of the protein, as should be expected if the decrease in d.c. resistance were to be ascribed to the transport of charged macromolecules through the membrane.

Discussion

From the experiments it is clear that polyelectrolyte is adsorbed on the surface of the black lipid film. This applies both to the experiments with gelatin and bovine serum albumin, which gave no decrease of film resistance, and to the experiments with bovine erythrocyte ghost protein and polyphosphate. The adsorption of protein on the phospholipid-water interface may be controlled independently by investigating the electrophoretic behavior of emulsion droplets, stabilized by phospholipid, in a protein solution, as a function of pH. In this way Haydon (3) established protein adsorption on the phospholipid-water interface. If the high resistance (10^7 ohms per sq. cm.) of black lipid films is to be ascribed to the continuous layer of hydrocarbon chains in the interior of the film, as is generally done, an increase in film conductivity is not expected from adsorption without penetration.

For the increase of conductivity by a protein which physiologically has a strong interaction with phospholipid, two mechanisms may be envisaged—notably a partial solubility of the protein in the hydrocarbon phase, presumably accompanied by a conformational change and electro-

phoretic transport of the protein through the membrane, or adsorption and penetration of the protein onto and into the film, and consequently the formation of pores or water channels, either permanent or temporary, through the film, conductivity being caused by the possibility of ionic transport. By working at its isoelectric point and thereby reducing the electrophoretic mobility, the former possibility was ruled out for the protein, though not for the polyphosphate. No detailed investigations were made into the cause of the slight increase of membrane conductivity at low pH.

Polyphosphate was chosen as a polyelectrolyte in addition to the erythrocyte ghost protein, because van Steveninck demonstrated (*17*) that polyphosphate plays an important role in membrane transport in yeast cells. The results obtained with polyphosphate, especially on protein-covered membranes, indicate that the possibility of ionic transport is strongly enhanced.

In all experiments the aqueous phases on both sides of the black lipid film were identical. Therefore, no membrane potential can be expected. The protein-covered membrane showed no membrane potential, which indicates that once the protein has penetrated through the film, the surface of the black lipid film is covered identically on both sides. Therefore, no action potential phenomena as demonstrated in other membranes by Mueller and Rudin (*10*) are to be expected in this kind of film.

Literature Cited

(1) Berg, H. J. van den, *J. Mol. Biol.* **12**, 290 (1965).
(2) Dodge, J. T., Mitchell, C., Hanahan, D. J., *Arch. Biochem. Biophys.* **100**, 119 (1963).
(3) Haydon, D. A., private communication.
(4) Huang, C., Ph.D. thesis, Johns Hopkins University, Baltimore, Md. 1965.
(5) Huang, C., Thompson, T. E., *J. Mol. Biol.* **13**, 183 (1965); **15**, 539 (1966).
(6) Huang, C., Wheeldon, L., Thompson, T. E., *J. Mol. Biol.* **8**, 148 (1964).
(7) Maddy, A. H., *Biochem. Biophys. Acta* **88**, 448 (1964).
(8) Maddy, A. H., Huang, C., Thompson, T. E., *Federation Proc.* **25**, 933 (1966).
(9) Mueller, P., Rudin, D. O., *J. Theoret. Biol.* **4**, 268 (1963).
(10) Mueller, P., Rudin, D. O., *Nature* **203**, 603 (1967).
(11) Mueller, P., Rudin, D. O., Tien, H. T., Westcott, W. C., *Nature* **194**, 979 (1962).
(12) Mueller, P., Rudin, D. O., Tien, H. T., Westcott, W. C., "Progress in Surface Science," J. F. Danielli, K. G. A. Pankhurst, A. C. Riddiford, eds., Vol. 1, p. 379, Academic Press, New York, 1964.
(13) Pfanstiel, A., Iler, R. V., *J. Am. Chem. Soc.* **74**, 6059 (1952).
(14) Richardson, S. H., Hultin, H. O., Fleischer, S., *Arch. Biochem. Biophys.* **105**, 288, 454 (1964).
(15) Seufert, W. D., *Nature* **207**, 174 (1965).

(16) Singleton, W. S., Gray, M. S., Brown, M. L., White, J. L., *J. Am. Oil Chemists' Soc.* **41**, 16 (1964).
(17) Steveninck, J. van, thesis, Leiden, 1962.
(18) Thompson, T. E., "Cellular Membranes in Development," Academic Press, New York, 1964.
(19) Tien, H. T., Dawidowicz, E. A., *J. Colloid Interface Sci.* **22**, 438 (1966).
(20) Vreeman, H. J., thesis, Utrecht, 1966.

RECEIVED May 8, 1967.

10

Bifacial Tension of Black Lipid Membranes

H. TI TIEN

Department of Biophysics, Michigan State University, East Lansing, Mich. 48823

The phenomena of association colloids in which the limiting structure of a lamellar micelle may be pictured as composed of a bimolecular leaflet are well known. The isolated existence of such a limiting structure as black lipid membranes (BLM) of about two molecules in thickness has been established. The bifacial tension (γ_b) on several BLM has been measured. Typical values lie slightly above zero to about 6 dynes per cm. The growth of the concept of the bimolecular leaflet membrane model with adsorbed protein monolayers is traceable to the initial experiments at the cell–solution interface. The results of interfacial tension measurements which were essential to the development of the paucimolecular membrane model are discussed in the light of the present bifacial tension data on BLM.

The idea of the bimolecular lipid leaflet as a basis of natural membranes was first suggested in the classical work of Gorter and Grendel in the 1920's (*7*). A detailed model of the natural membrane consisting of a bilayer leaflet with adsorbed protein monolayers was subsequently proposed in the 1930's (*3*). The lipid bilayer model has been generally accepted (*5*, *14*). The experimental evidence supporting this model comes from various sources, such as permeability studies, electrical impedance and capacitance measurements, electron microscopic investigations, x-ray work, and chemical analyses on natural membranes which in some cells constitute anywhere from 40 to more than 80% of the total dry weight (*5*, *12*).

This widespread recognition of the membranous nature of cellular organization suggests that a detailed physical and chemical characterization is of some importance to our understanding of biological processes. However, owing to the complexity of natural membranes, many investigators interested in cellular properties and function were compelled to

study model systems. Until recently these have consisted largely of precipitated copper ferrocyanide, gelatine, thick "oil" layers, collodin, cellophane, ion exchange materials of various kinds, and filter papers. In addition, monolayers at the air–water and oil–water interfaces have also been used as model systems. Obviously these models either lack the required thickness of cell membranes (generally believed to be less than 100 A.) or approximate poorly the known properties of natural membranes and their environment. Recently, a more "realistic" model system for cell membranes has become available. In 1961 we reported the formation of membranous structures by the following technique:

A solution of brain lipids was brushed across a small hole in a 5-ml. polyethylene pH cup immersed in an electrolyte solution. As observed under low power magnification, the thick lipid film initially formed exhibited intense interference colors. Finally, after thinning, black spots of poor reflectivity suddenly appeared in the film. The black spots grew rapidly and evenutally extended to the limit of the opening (*5*, *10*). The black membranes have a thickness ranging from 60–90 A. under the electron microscope. Optical and electrical capacitance measurements have also demonstrated that the membrane, when in the final black state, corresponds closely to a bimolecular leaflet structure. Hence, these membranous structures are known as bimolecular, black, or bilayer lipid membranes (abbreviated as BLM). The transverse electrical and transport properties of BLM have been studied usually by forming such a structure interposed between two aqueous phases (*10*, *17*).

Hitherto, property measurements of BLM have been confined mainly to thickness, water permeability, electrical characteristics, and current-voltage. The bifacial tension (γ_b) of BLM is believed to be very small, and a value of about 1 dyne per cm. has been estimated (*10*). Since no detailed investigations of the bifacial tension of BLM have been reported, the immediate purpose of this work was to develop suitable techniques for γ_b measurements. The results of measurements on BLM formed from various lipid solutions are given. The general applicability of the apparatus and method described here to studying other interfacial and bifacial phenomena is briefly discussed.

Definition and Abbreviation of Terms

To describe the system under study more precisely and to avoid ambiguity in the discussion, the following terms are defined:

Biface: the two co-existing water–oil or solution–membrane interfaces (W/O/W).

Bifacial Tension: the tension of the biface. The Helmholtz free energy per unit of biface. In the absence of surface-active materials the term simply refers to twice the oil–water interfacial tension ($\gamma_{O/W}$).

BLM: bimolecular, bilayer, or black lipid membrane (or film). Not all BLM are bimolecular in thickness, however.

γ_{BLM} or γ_b: the bifacial tension of BLM measured in dynes per cm. (or ergs per sq. cm.).

Interfacial pressure: π_i, the change in interfacial tension as a result of sorption (usually positive adsorption) of the surface-active material. It may be regarded as a measure of the tendency of adsorbed species at the interface (or biface) to enlarge the area occupied by the BLM.

Lipid membrane (or film): thin membrane other than BLM at the biface. Thickness in the range of 1 micron to 1000 A.

Plateau-Gibbs border: P-G border, the edge where the lipid film (or BLM) is terminated.

Bifacial Tension of Ultrathin Films at the Biface

Since the technique developed during this investigation differs from the classical methods for studying films at interfaces, a brief consideration of traditional techniques seems desirable. In general, the interfacial tension of films (*e.g.*, insoluble monolayers) at interfaces is not measured as such. Instead, the so-called interfacial pressure is determined, which is given by:

$$\pi_i = \gamma_o - \gamma_i \qquad (1)$$

where γ_o and γ_i are the interfacial (or surface) tensions in the absence and presence of the film, respectively. The two classical methods generally used are the Wilhelmy plate and the Langmuir film balance. In both cases, π_i is measured directly (*6*).

Owing to the small area ($<<$ 1 sq. cm.) and fragility of BLM, neither of the above-mentioned methods was successfully adapted. Further, the BLM differs from the interfacial films at air–water and oil–water interfaces in that a BLM has two "oil–water" interfaces (Figure 1). There is one further difficulty with the BLM since its bifacial tension (γ_b) is believed to be low (a few dynes per cm. at the most). Hence, any apparatus should be also capable of measuring small γ_i.

After surveying classical methods for the measurements of interfacial tension, the so-called "bubble pressure" method (or the bulging method), although used much less today, seemed most suitable for measuring γ_i of ultrathin films at the biface.

Elementary Theory. The theory of the bulging method assumes that the maximum pressure is reached when it is just hemispherical (*1*). Implicit in the theory, an interfacial tension (γ_i) exists in every thin film separating two phases (liquid, solid, or gaseous). Further, the interfacial

tension is assumed to be the same at every point in a given film. It can be shown that at equilibrium the work done in changing the radius of a BLM bubble, R, to $(R + dR)$ is equal to $P \times 4\pi R^2 dR$. Thus

$$16\pi\, \gamma_b\, RdR = 4\pi PR^2 dR \tag{2}$$

or

$$P = \frac{8\gamma_b}{d} \tag{3}$$

where $d = 2R$, the diameter of the BLM bubble or the diameter of the opening used in the membrane support, and P is the pressure difference across the BLM.

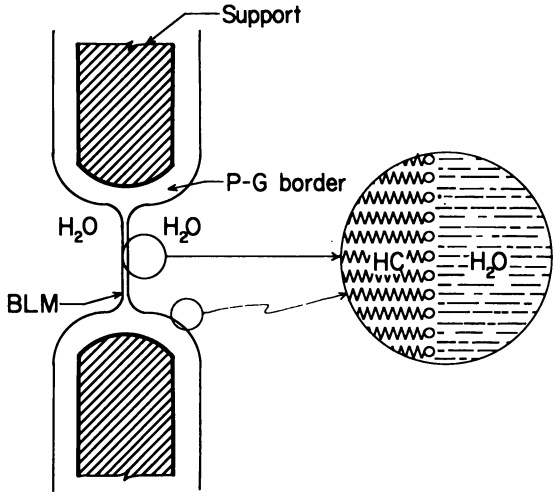

Figure 1. Possible structural arrangement of a bimolecular lipid membrane (BLM) separating two aqueous solutions. Open circles and zig-zag lines denote polar groups and hydrocarbon chains, respectively. The structure of BLM is akin to a neat or smectic mesophase found in liquid crystals

Although we shall limit our consideration to the bifacial tension of BLM, it is useful to comment briefly its relationship with the Plateau-Gibbs border. At equilibrium, the BLM separates two aqueous phases which are also in equilibrium with the P-G border (Phase III). Thus, three interfaces intersect along a line of contact at N (*see* Figure 2). According to the theorem of Neumann's triangle (*4*), an element of the line of length dl through N is subjected to the three forces. At equilibrium the vectorial sum of the three forces must be zero. For a stable BLM, the following relationship must be satisfied:

$$\gamma_{BLM} = 2\gamma_i \cos \theta \quad (4)$$

where γ_i is the interfacial tension between the two bulk phases (for a BLM interposed between two solutions of the same composition, $\gamma_i = \gamma' = \gamma''$, *see* Figure 2). It is evident that Equation 4 suggests an alternate method for determining the bifacial tension of BLM. The method entails measuring γ_i in the usual way and the angle θ (Refs. *11* and *13* discuss this point).

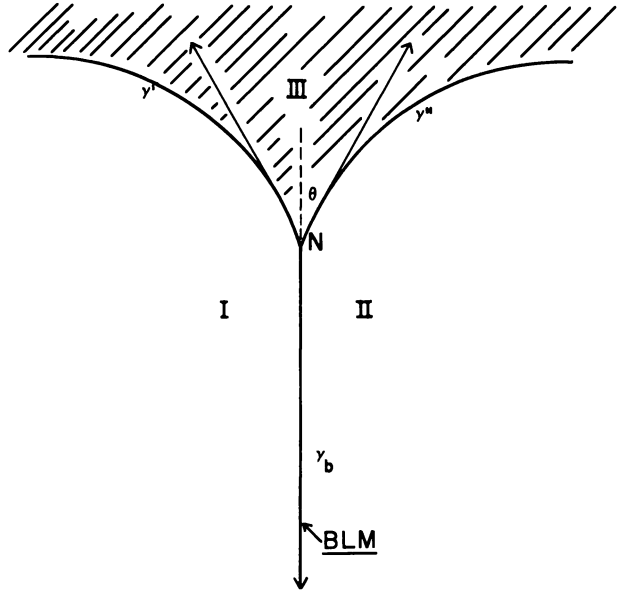

Figure 2. Plateau-Gibbs (P-G) border and bimolecular lipid membrane (BLM). N is the line of intersection of three interfaces, I, II, and III

Experimental Methods

Lipid Solutions. One of the difficulties in studying BLM is to find a lipid solution from which stable BLM can be formed. Using a simple apparatus described previously (*15*), several lipid solutions have been established. Cholesterol obtained from Eastman (Rochester, N. Y.) was twice recrystallized from nitrogenated absolute ethyl alcohol before use. Chromatographically pure egg lecithin was obtained from General Biochemicals (Chagrin, Ohio). Glycerol dioleate was supplied by K and K Chemicals Co. (N. Y.). Both practical and reagent grade octane, and dodecane (99 mole%, Phillips Petroleum Co.) were used as solvent for

the lipids. All were used as received without further purification. Reagent grade NaCl and doubly distilled water from an all-glass still were used. The procedure established in preparing the lipid solutions used in this work is given below.

"OXIDIZED" CHOLESTEROL. A 4% solution of chloesterol in octane was heated at the reflux temperature for 6.5 hours in a three-necked flask. The flask was fitted with a thermometer, a condenser, and a gas dispersing tube (fritted glass, medium porosity) through which molecular oxygen was introduced. The rate of oxygen flow was about 90 ml. per min. (A shorter duration worked equally well if the solvent had a higher boiling point and a faster rate of oxygen flow was used). The resulting solution was colorless with white precipitates upon cooling. The supernatant was used to form BLM. This solution has given very stable membranes, and it is by far the easiest to work with.

LECITHIN. This solution was prepared by dissolving 1 gram (white waxy solid) of lecithin in 100 ml. dodecane. To facilitate dissolution of lecithin, the mixture was warmed gently to about 40°C. under nitrogen. Since the amount used for each run was very small, the solution was divided into 2-ml. aliquots for storage in a freezer. This solution is not one of the best to use since egg lecithin deteriorates rapidly on standing.

GLYCEROL DIOLEATE. This solution was prepared by mixing 1 ml. of glycerol dioleate with 100 ml. of dodecane. The solution may be stored at room temperature without any apparent deterioration. However, trace impurities associated with the lipid have not been established, which could be important in producing stable BLM.

Apparatus. The apparatus used to measure the bifacial tension of BLM consisted of a chamber for membrane formation (*see* below and Figure 1 in Ref. *16*); an infusion-withdrawal pump for generating the hydrostatic head; a sensitive pressure transducer together with an amplifier (model 270, Sanborn Co.); and a strip chart recorder. The temperature of the membrane chamber was maintained by flowing water from a constant temperature bath through a glass coil placed in the membrane chamber. The temperature could be controlled to within ±0.1°C. The inner chamber of the membrane cell for BLM support was made of a Teflon sleeve held in place by ground-glass joints. The small hole in the Teflon sleeve was punched as follows. A simple device was made of two pieces of steel plate welded together with a small clearance. A smooth hole that fitted a carefully machined rod of hardened steel was first drilled through the plates. The hole in the Teflon sleeve was punched by ramming the rod through the holes in the plates while the sleeve was placed in the clearance. A smooth hole without frilled edges could be made in this way.

Procedure. To form a BLM, a small amount ($\sim$ 0.005 ml.) of lipid solution was applied *via* a Teflon capillary attached to a micrometer syringe. The formation characteristics leading to the black state were observed under reflected light at 20–40× magnification. Other precautions that should be exercised are essentially those described previously (*10*). The bifacial tension of BLM was measured as follows. After the membrane had become completely black (except at the Plateau-Gibbs border), the infusion-withdrawal pump was started. The pressure difference across the BLM was continuously monitored and reached a maximum when the membrane was hemispherical. The interfacial tension was calculated from this point using Equation 3.

Results and Discussion

The results of interfacial tension measurements on BLM formed from five different lipid solutions are given in Table I. One of the immediate questions is whether the measured values represent the true bifacial tension of BLM. It is implicitly assumed in order to apply equation 3 that γ_b is a characteristic property of BLM and should be independent of the extension of the BLM area. It is generally recognized that if the BLM also possessed elastic properties, the measured γ_b would be different when it is stretched. To answer this question, γ_b was measured during both expansion and contraction of the membrane. A typical trace of pressure difference *vs.* time in which the membrane was being expanded and contracted is shown in Figure 3. The symmetric nature of the curve indicates that little hysteresis was present during inflation and deflation of the BLM. Therefore, it seems safe to conclude that for BLM formed from lipid materials alone the membrane does not appear to possess appreciable elastic properties.

Table I. Bifacial Tension[a] of Some Bimolecular Membranes at 25°C.

BLM Generated From:	γ_b, *dynes/cm.*
Lecithin (egg) in dodecane, 1% (w/v)	0.9 ± 0.1
Cholesterol (oxidized) in octane, 4% (w/v)	1.9 ± 0.5[b]
Glycerol dioleate in dodecane, 1% (v/v)	1.5 ± 0.2
Dioctadecyl phosphite (DODP) and cholesterol	5.7 ± 0.2[c]
Hexadecyltrimethylammonium bromide (HDTAB) and cholesterol	0.15 ± 0.5[d]

[a] Aqueous phase used was 0.1*N* NaCl, unless otherwise noted.
[b] Variable depending upon the extent of oxidation.
[c] In distilled water.
[d] HDTAB (0.008%) in 0.1*N* NaCl.

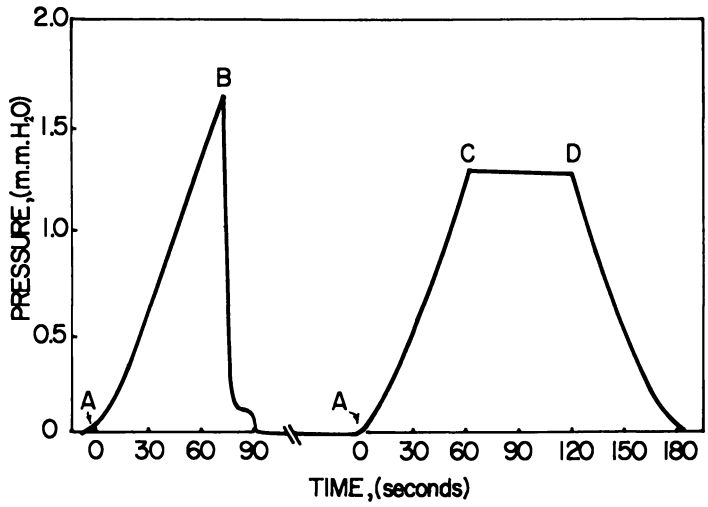

Figure 3. Typical trace during inflation and deflation of a BLM by hydrostatic pressure as a function of time. A, beginning of infusion; B, at maximum pressure difference; C, infusion stopped; D, withdrawal started. The shoulder after point B was caused by the formation of a bubble

In addition to the results of γ_{lb} values presented in Table I, measurements have also been made on a number of BLM formed from cholesterol-surfactant systems. Some of the surface-active compounds used include hexadecyltrimethylammonium bromide (HDTAB), dodecyl acid phosphate (DAP), and dioctadecyl phosphite (DODP). It is interesting to note that in the case studied a BLM could be formed only when the measured γ_{lb} was below 6 dynes. The quantitative results obtained fully substantiate the belief that BLM possesses low γ values. If we assume that Equation 1 is also valid for the BLM, certain inferences may be made concerning the molecular packing of the lipid molecules at the membrane–solution interfaces. Since γ_l for most aliphatic hydrocarbons is of the order of 50 dynes per cm., $\pi_l \simeq \gamma_o \simeq 50$ according to Equation 1. Therefore, at the observed interfacial pressure, one would expect the lipid molecules in the BLM to occupy their limiting areas (*i.e.*, about 50–55 sq. A. for lecithin and 35–37 sq. A. for cholesterol). A more detailed consideration of the relationship between γ_{lb} and BLM formation and stability will be given elsewhere (*16*). However, BLM exhibited considerable "kinetic" stability—*i.e.*, the average lifetime of BLM could be appreciably increased during the bulging process. One obvious explanation is that during the generating of additional "black" areas, the weaker

spots of BLM, presumably located at the Plateau-Gibbs border, were being continuously removed.

The apparatus developed for γ_b measurements of BLM deserves brief comment since it can be used not only to examine the effects of various substances on BLM but is readily adaptable for studying other types of interfacial films and related adsorption phenomena at either air–water or oil–water interfaces (and bifaces). Unlike both the Wilhelmy plate and film balance methods, the present technique measures γ_i directly. From the description of the apparatus and procedure that the present method relies on the ability to measure the very small pressure difference across an interface (or biface). For certain BLM's, the pressure heads measured are only fractions of a millimeter of water. Therefore, the method described here has been possible only as a result of developing pressure transducers of high sensitivity.

The relevance of γ_b of BLM and cell membranes may be considered in terms of the proposed plasma membrane model. Briefly, the model consists of a bimolecular leaflet of lipid sandwiched between two monolayers of adsorbed protein. This simple picture of the membrane has greatly influenced thinking concerning the molecular organization of cell membranes (5). The deduction of the bilayer leaflet model was based largely upon the consideration of the interfacial forces at the cell surfaces. Pioneer studies of Cole (2), Harvey and Shapiro (9) showed that the interfacial tension at the cell surface was of the order of 0.1–1 dynes per cm. These earlier workers found that cell membranes also possessed elastic properties. That is, in terms of interfacial tension, a dependence of γ_i was found with the state of stretching of the cell. However, the methods used by Cole, Harvey, and co-workers were incapable of distinguishing between elastic forces at the surface and those of the internal structures. The limitation of these methods was fully recognized by these earlier workers. To determine the physical basis for the observed low γ_i of the cell surface, Harvey and co-workers (8, 9) measured γ_i at the interface between the aqueous egg material and the egg oil. γ_i was found to be 0.8 dynes per cm., in contrast to values of about 7 dynes per cm. found at the interface between sea water and egg oil. Harvey *et al.* also showed that the difference between sea water and the aqueous egg material was caused by the presence of a highly surface-active agent (*i.e.*, a protein) in the latter. In view of the results quoted above and the fact that no lipid was known to these earlier workers which had an interfacial tension of less than about 9 dynes at the normal environment of the cell, a picture in which the molecular conditions at the oil–aqueous egg content interface were believed to exist was proposed. This has since been developed to the present-day bilayer model for the cell membrane (3).

Although the present finding that BLM formed from simple lipids alone can possess intrinsic low γ_b without the presence of protein layers, it in no sense invalidates the bimolecular leaflet model. Our study does suggest, however, that natural lipids such as lecithin when in a "bilayer" configuration could exist in natural membranes to give the results of low γ_i observed by earlier workers, which has been thought essential in the development of the concept of the bimolecular lipo-protein model based upon interfacial tension measurements.

Table II. Known Physical Properties of Unmodified BLM[a]

Property	*Experimental Method*
Thickness, A.	
60–90	Electron microscopy
40–80	Optical methods
40–130	Electrical capacity
Resistance, ohm-sq. cm. $\times 10^6$	
0.01–100	D.c. and a.c.
Capacitance, μF/sq. cm.	
0.2–1.3	D.c. and a.c.
Dielectric strength, volts/cm. $\times 10^6$	
0.3–1.2	Applied voltage
Refractive index	
1.56–1.66	Brewster's angle
Water permeability, μ/sec.	
2–24	Osmotic
Bifacial tension, dynes/cm.	
0.2–6.0	Bulging

[a] Data from Tien and Diana (*17*).

Conclusions

The bimolecular lipid membrane (BLM) produced in aqueous solution described in this paper is of considerable interest for two main reasons. First, the BLM is a new type of interfacial film of ultrathinness. The limiting thickness of BLM is 40–130 A. as estimated from various measurements. The values obtained by optical methods are probably most reliable, indicating that the thickness of the BLM is equal to about twice the length of the lipid molecules. The environment in which the BLM is formed and the molecular orientation at the biface lends itself as a promising tool in understanding some outstanding problems in colloid and interfacial chemistry such as Van der Waals attraction and

the stability of emulsions. The second reason for the interest in BLM is attributed to the close semblance of these membranes to the postulated model of the biological membrane. The formation of BLM in aqueous solution has allowed for the first time detailed investigations of the properties of the fundamental structure. For example, when BLM is formed, separating two aqueous solutions, the electrical properties and transport phenomena can be investigated readily. Although the data so far gathered on the BLM corresponds in varying degree to the properties of natural membranes (*17*), the BLM is by no means an "exact" model (*e.g.*, BLM possesses no elastic properties contrary to cell surface). Nevertheless, the fact that BLM can be generated *in vitro* provides a strong experimental support for the lipid bilayer concept as the structural foundation of cell membranes as has been repeatedly revealed by electron microscopy and other studies (*5*). Finally, for the convenience of those who may wish to initiate work in the area of BLM, a summary of the known physical properties is presented in Table II.

Literature Cited

(1) Adamson, A. W., "Physical Chemistry of Surfaces," 2nd ed., Chap. 1, Interscience, New York, 1967.
(2) Cole, K. S., *J. Cell. Comp. Physiol.* 1, 1 (1932).
(3) Davson, H., *Circulation* **26,** 1022 (1962).
(4) Defay, R., Prigogine, I., Bellemans, A., "Surface Tension and Adsorption," p. 9, Wiley, New York, 1966.
(5) Fishman, A. P., ed., *Symp. Plasma Membrane* **1961,** 1167 (1962).
(6) Gaines, G. L., "Insoluble Monolayers at Liquid-Gas Interfaces," p. 126, Interscience, 1965.
(7) Gorter, E., Grendel, F., *J. Exp. Med.* **41,** 439 (1925).
(8) Harvey, E. N., Danielli, J. F., *J. Cell. Comp. Physiol.* **5,** 483 (1935).
(9) Harvey, E. N., Shapiro, H., *J. Cell. Comp. Physiol.* **5,** 255 (1934).
(10) Mueller, P., Rudin, D. O., Tien, H. T., Westcott, W. C., *Recent Progr. Surface Sci.* 1, Chap. 11 (1964).
(11) Mysels, K. J., Huisman, H. F., Razouk, R. I., *J. Phys. Chem.* **70,** 1339 (1966).
(12) O'Brien, J. S., *J. Theoret. Biol.* **15,** 307 (1967).
(13) Princen, H. M., Mason, S. G., *J. Colloid Sci.* **20,** 156 (1965).
(14) Sjostrand, F. S., *Rad. Res. Suppl.* **2,** 349 (1960).
(15) Tien, H. T., *J. Theoret. Biol.* **16,** 97 (1967).
(16) Tien, H. T., *J. Phys. Chem.* 71, 3395 (1967); **72** (8) (1968).
(17) Tien, H. T., Diana, A. L., *Chem. Phys. Lipids* **2,** 55 (1968).

RECEIVED June 12, 1967. Work supported by National Institute of Health Grant (GM-14971).

Cohesive Forces in Monomolecular Films at an Air–Water Interface

NORMAN L. GERSHFELD

Laboratory of Physical Biology, National Institute of Arthritis and Metabolic Diseases, National Institutes of Health, U. S. Department of Health, Education, and Welfare, Bethesda, Md. 20014

Free energies of cohesion per —CH_2— group in condensed monomolecular films were determined by comparing k_s, *the rate constant of desorption, at a given pH and film area for* C_{16} *and* C_{18} *sulfate, for* C_{16} *and* C_{18} *phosphonate and for stearic and palmitic acids. The London–van der Waals interactions among the hydrocarbon chains of these films were found to be between —100 and —400 cal. per mole of —CH_2—. Polar group interactions for sulfate, phosphonate, and carboxyl films were observed by studying* k_s *as a function of pH. Cohesive forces were found among these groups which increase with pH, and the energies are of the order of 1 kcal. per mole. These interactions are believed to be between ionized and nonionized species in the polar region of the monolayer.*

In principle, it is possible to obtain the cohesive forces in monomolecular lipid films from the surface pressure (π)–area (A) isotherms by integrating the relation $\int_{\pi_i}^{\pi} A d\pi$ between the limits of the surface pressures in the "ideal-gas" and condensed states, π_i and π, respectively (*31*). However, despite the large body of experimental data which exists for monolayers, there have been few measurements which permit assigning cohesive forces to either the polar group or the hydrocarbon region of the monolayer. This arises from both theoretical and experimental difficulties (*17, 31*).

For many condensed lipoidal systems interpretation of the cohesive forces in terms of the polar and hydrocarbon group interactions is conceptually feasible because the molecular orientations are reasonably well

established. However, measurement of the cohesive forces is not practicable because it is extremely difficult to measure the very low surface pressures at which the films exhibit ideal-gas behavior. This is particularly true for the compounds which form liquid-condensed films like stearic acid since these films have been shown to form molecular aggregates at very low surface concentrations and very low surface pressures (*1, 14*).

This study presents an experimental approach for measuring the cohesive energies in condensed lipid monolayers which avoids the difficulty of measuring extremely low values of π. The approach depends on evaluating the free energy of desorption (or adsorption) of condensed films and comparing this value with the free energy of desorption of the film in the ideal-gas state.

For this study, compounds were selected which formed condensed films when spread as a monolayer on water, yet whose solubility in water was sufficiently high to allow measurements of the rate of film desorption from the surface to the bulk solution. For these compounds the free energies of desorption may be obtained from monolayer desorption studies (*6*).

Cohesive Energies from Monolayer Desorption Studies

For an adsorbed film in equilibrium with a solution of surface-active molecules, the standard free energy of desorption may be written as

$$\lambda = RT \ln \frac{\Gamma}{\delta} \gamma^*/C\gamma \qquad (1)$$

where Γ is the surface concentration, in moles per square centimeter, C is the bulk concentration of the surface active compounds, in moles per cubic centimeter, γ^* is the monolayer activity coefficient, γ is the activity coefficient in bulk solution, and δ is the film thickness (*1, 31*). Further, $\lim \gamma^*_{\Gamma \to 0} = 1$, and $\lim_{C \to 0} \gamma = 1$. Values of λ may be calculated from measurements of Γ/C for very dilute solutions of surface-active compounds, where γ^* and γ equal 1. It is assumed that deviation of λ from ideality is reflected by changes in γ^*, the term introduced in Equation 1 to correct for interactions in the monolayer, and that the activity coefficient in solution, γ, is unity. For compounds with long hydrocarbon "tails" which are only slightly soluble in water, Γ/C may be obtained from the kinetics of monolayer desorption.

If the slightly soluble, surface-active compound is spread as a monolayer, the film is unstable and desorbs from the surface. Analysis of the kinetics of desorption follows the treatment given by Ter Minassian-Saraga (*29*). Immediately upon spreading the monolayer, film molecules

dissolve (film dissolution), and an equilibrium is established between the film and a very thin region directly beneath the surface. Film desorption is limited by solute diffusion across the "unstirred layer" of thickness ϵ to the bulk of the solution where the solute concentration is essentially zero. After a short while a steady state is established in which the rate of film loss equals the rate of diffusion.

The rate constant for desorption at constant surface pressure, π, in the steady state, k_s, is given by

$$k_s = \frac{-d \ln A_T}{dt} \tag{2}$$

where A_T is the total film area at surface pressure, π, and time t. Ter Minassian-Saraga shows that at constant π, in the steady-state k_s becomes

$$k_s = \frac{D}{\epsilon} \frac{C}{\Gamma} \tag{3}$$

where D is the solute diffusion coefficient; for small C, D should be constant. Hence, from Equation 3 values of Γ/C may be obtained for slightly soluble surface-active compounds.

From Equations 1 and 3, assuming that $\gamma = 1$, and eliminating Γ/C from both equations,

$$k_s = \frac{D\gamma^*}{\epsilon\delta} e^{-\lambda/RT} \tag{4}$$

Alternatively, γ^*, which accounts for the interactions in the film, may be written in the form

$$\gamma^* = e^{(\mu^s - \mu^s{}_{id})/RT} \tag{5}$$

where $\mu^s{}_{id}$ is the chemical potential of the monolayer in the ideal-gas state—*i.e.*, when $\gamma^* = 1$. Setting $\phi = \mu^s - \mu^s{}_{id}$, Equation 5 becomes

$$k_s = \frac{D}{\epsilon\delta} e^{(\phi-\lambda)/RT} \tag{6}$$

Thus, the rate constant for desorption can be expressed as a function of the standard free energy of desorption, λ, and the change in free energy of the monolayer resulting from interactions within the film, ϕ, when the film is compressed. It is noteworthy that Equation 6 is similar to one developed by Davies (*6*).

Equation 6 assumes that the film is in equilibrium with a thin region immediately beneath the monolayer, and that film desorption is limited by diffusion. Before Equation 6 can be used, its validity must be established for each system studied. A theoretical relation developed previously (*11*) allows one to test whether these conditions hold, and thus whether Equation 6 is applicable. It has been shown, for the conditions

of Equation 6 using the Gibbs adsorption isotherm in the form $\Gamma d\mu = d\pi$, that the rate constant for desorption, k_s, will depend on the surface pressure, π, in the following way

$$\frac{d \ln k_s}{d\pi} = \frac{1}{\Gamma RT} - C_s \tag{7}$$

where C_s is the surface compressibility (*14*). For surface-active molecules which are completely ionized in solution, and in the presence of simple electrolytes (concentration C_i), the Gibbs equation takes the form $d\pi = x\Gamma d\mu$ (*5, 22*), and Equation 7 becomes

$$\frac{d \ln k_s}{d\pi} = \frac{1}{x\Gamma RT} - C_s \tag{8}$$

where $x = 1 + \left(\frac{C}{C + C_i}\right)$. When $C >> C_i$, $x = 2$, and when $C_i >> C$, $x = 1$. For the compounds in this study, Equation 8 is used with $x = 1$ because their solubility is so low that the concentration is negligible compared with the total electrolyte concentration. Moreover, it is assumed that, at the pH's used in this study, the weak acids are completely ionized in solution.

In order to relate changes in free energy of desorption as determined by Equation 6 to molecular parameters, it is assumed that λ and ϕ may be expressed as the sum of independent contributions from the polar and hydrocarbon moieties of the monolayer. Thus for ionized lipid films, λ is defined by $(mW_o - ZF\Psi_o + \lambda_p)$, where mW_o is the work necessary to desorb m(—CH_2—) groups from films in which the hydrocarbon chains do not interact; $ZF\Psi_o$ is the electrical potential energy which facilitates the desorption of the ionized molecule from the surface, where F is the Faraday constant, Ψ_o the electrical potential, and Z the charge of the ionized groups in the film; λ_p is the contribution to the free energy of desorption arising from the van der Waals interactions between the polar group and water; and ϕ is defined as mW_c, the contribution to the free energy of the film arising from the cohesive forces among the hydrocarbon chains, with each chain containing m(—CH_2—) groups. W_o is positive, and W_c is negative for forces of attraction. Combining the definitions of ϕ and λ yields

$$(\phi - \lambda) = ZF\Psi_o - m(W_o - W_c) + \lambda_p \tag{9}$$

Various theoretical expressions have been developed to evaluate Ψ_o. However, when Ψ_o is sufficiently high (> 50 mv.) all the expressions for Ψ_o take the same form (*3, 7*),

$$-\Psi_o = 2.3 \frac{RT}{F} \log (H^+) + \text{constant} \tag{10}$$

For the films in this study Ψ_o is greater than 50 mv., and Equation 10 will be used to examine the polar group interactions. From Equations 6, 9, and 10,

$$\log k_s = \log D/\epsilon\delta - m\frac{(W_o - W_c)}{2.3\,RT} + \text{pH} + \lambda_p + \text{constant} \qquad (11)$$

The cohesive energies in the monolayers will be obtained with Equation 11. For the cohesive energy in the hydrocarbon region of the monolayer, W_c, the rates of desorption of homologous compounds will be compared at constant pH. For the forces in the polar region of the film, the variation of k_s with pH, for a given compound (constant m), will be examined.

Experimental

Material. The compounds whose film properties were investigated are listed in Table I. Benzene, methanol, 2-propanol, and hexane (Fisher certified reagent) were percolated through a combined Florisil–silica gel column to remove surface-active contaminants; benzene was also tested for acidic contamination.

Table II. Free Energies of Desorption (W_o-W_c) and Cohesion (W_c)

	A, Sq. A. per Molecule	$-(W_o{}^a\text{-}W_c)$, *Cal./Mole—CH_2—*	$-W_c$, *Cal./Mole—CH_2—*
Carboxyl film pH 9.2 (Figure 4)	20–24	1010 ± 25	385
Phosphonate film pH 5.8 (Figure 3)	23–26	930 ± 25	305
Sulfate film pH 2.1 (Figure 2)	50–90	735 ± 15	110

[a] W_o = 625 cal. per mole —CH_2— (*16, 28*).

A mixture of benzene and methanol (19 to 1) was used for spreading the alkyl phosphonates. To minimize the influence of benzene on the film properties, the concentrations of the spreading solutions were $> 1.5 \times 10^{-3}$ gram per ml., and the experiments were performed at $\pi > 4$ dynes per cm. (25). Moreover, higher proportions of methanol in the spreading solution did not alter the film properties under study for selected monolayers. For the sulfates, a mixed solvent containing water-benzene–2-propanol (1:10:10) was used because with the benzene–methanol solutions the properties of the films depended on the age of solution from which the films were prepared. Stearic and palmitic acids were spread from either hexane or the benzene–methanol solvent used for the phosphonates. Identical desorption results were obtained with the two solvents.

Aqueous solutions were prepared from water distilled twice from quartz glass. To maintain pH's < 6, HCl was used; for pH 7 to 8, NaH_2PO_4–NaOH, total phosphate $2 \times 10^{-3}M$; for pH 9.2, $10^{-3}M$

$Na_2B_4O_7 \cdot 10\ H_2O$. These solutions maintained the indicated pH and gave a minimum of heavy-metal ion contamination (*18*). It was not possible to buffer the solutions adequately at pH > 9.2 without appreciably increasing the concentration of buffer. To do so would have introduced additional complications whose treatment is beyond the scope of this paper. Hence pH 9.2 was the highest studied.

Method. In the steady state the first-order rate law $-d \ln A_T/dt = k_s$ is obeyed (*8*, *29*). Experimentally one follows the change in total film area (A_T) as desorption proceeds while maintaining a constant π. The apparatus (Figure 1) is essentially the same as previously used (*8*) but modified to maintain automatically a constant π, while recording changes in A_T owing to desorption.

Surface pressures were measured by the conventional horizontal float–torsion wire assembly. A strain gage bridge, F (Statham G10 B), senses the surface pressure in the film balance from one arm of the torsion

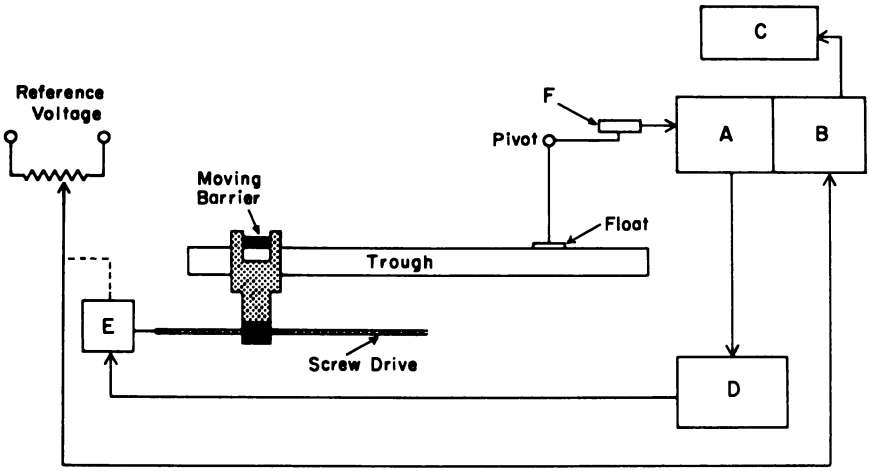

Figure 1. Schematic of apparatus for measuring rates of monolayer desorption at constant surface pressure

wire float assembly. The gage is excited by the carrier section, A, of a Brush amplifier which also amplifies and demodulates the gage output. The control unit, D, further amplifies the signal, introduces an adjustable offset for the signal, and provides an output to drive a d.c. motor, E. The motor drives a lead-screw which repositions the movable barrier to adjust the surface pressure in the film to a value such that the signal to the motor is reduced to zero. The position of the barrier is indicated by a voltage obtained from a ten-turn potentiometer geared to the lead-screw. This voltage is amplified by the d.c. section, B, of the same Brush amplifier and then recorded, C.

The apparatus is sensitive to changes in π of 0.05 dynes per cm.; for a trough 12 cm. wide changes in area as small as 0.25 sq. cm. could be recorded. The trough was fabricated from borosilicate glass and was 60

$\times$ 12 cm.; total volume $\sim$ 500 ml. Constant solution depth is necessary and was ensured by using the same volume of solution in each experiment.

Barrier leak must always be suspected, and the film balance was periodically checked for "leakiness" either by maintaining an insoluble film of stearyl alcohol at constant π for several hours (barrier leaks deduced if π decreases) or by spreading talc on the water surface where barrier leak is most likely to occur. Careful preparation of the rim of the trough ensured a leakproof system. The mean deviation for k_s was $< 2\%$ for the more rapidly desorbing sulfate films, and $\sim 5\%$ for the phosphonate and carboxyl films. Experimental conditions were limited to systems in which the rates of desorption are neither too rapid nor too slow for the most precise measurements of k_s.

To determine the π-A isotherms of dissolving films, two extrapolation methods were employed (*29*): either log π at constant A_T, or log A_T at constant π was plotted as a function of $\sqrt{t}$, where t is elapsed time. Extrapolation to $t = 0$ yields values of A or π to within $\pm$ 5% for rapidly desorbing films. Palmitic acid at pH 9.2 was an exception; its desorption rate was so rapid that the error in A was $\pm$ 10%. All the experiments were performed at 23° $\pm$ 0.5°C.; the maximum temperature variation during a single run was < 0.2°C. The surface potential, ΔV, was monitored and found not to drift by more than 10 mv. during a single run. Reproducibility was $\pm$ 10 mv.

Results

To test whether Equation 6 is valid for alkyl sulfate, phosphonate, and carboxyl films, Equation 8 was applied to the desorption data of these compounds. If the logarithm of k_s is plotted against π, the slope of the resultant curve should be equal to $\left(\frac{1}{\Gamma RT} - C_s\right)$, where $\Gamma = 1/A$ (*11*). To calculate these slopes, the corresponding π-A isotherms of the desorption systems were used (shown in the insets of Figures 2, 3, and 4). Each point in the isotherms was obtained by extrapolating a single desorption run (*see* Methods section). The solid line in each of these figure insets represents the isotherms obtained by the technique used for insoluble films. The films to which these curves refer desorb slowly enough so that the complete isotherm may be obtained from a single film without introducing significant error from desorption. In all cases but one the maximum variation obtained by changing experimental conditions is about 5%, which is within the limits of experimental error. The exception is palmitic acid at pH 9.2 (Figure 4), which desorbs so rapidly that the error in A is $\pm$ 10%. Hence, for the compounds studied, in all cases the π-A isotherms are independent of pH and length of hydrocarbon chain.

Figures 2, 3, and 4 are semilogarithmic plots of k_s *vs.* π for alkyl sulfate, phosphonate, and carboxyl monolayers, respectively, at various pH's and for two different hydrocarbon chain lengths. The points are the

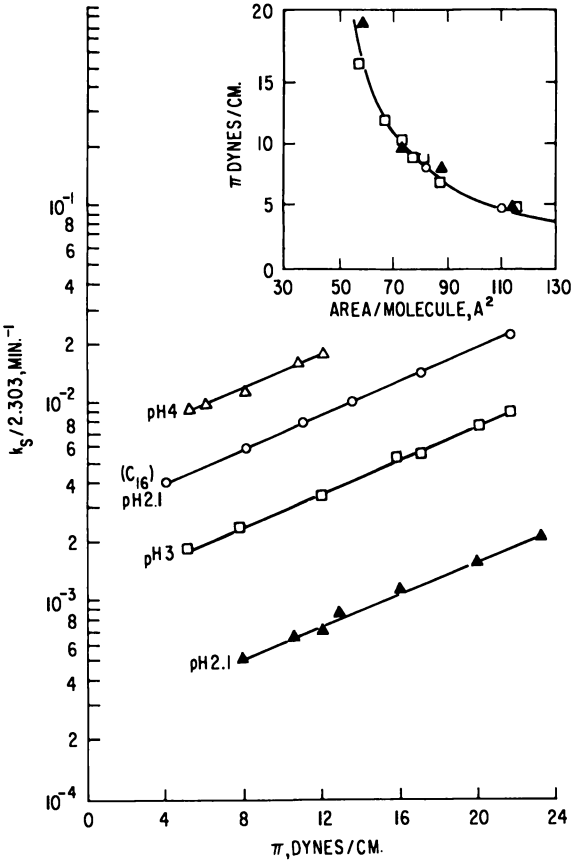

Figure 2. Influence of surface pressure on steady-state rate constant of desorption

n-*Octadecyl sulfate monolayers,* T = 23°C.
▲ *pH 2.1*
□ *pH 3*
△ *pH 4*
n-*Hexadecyl sulfate*
○ *pH 2.1*
Inset: π–A isotherms. Each point determined by extrapolating log A *at constant* π *to* t = 0

ctual experimental values of k_s, and the lines were drawn according to the theoretical slope, $\left(\frac{1}{\Gamma RT} - C_s\right)$. Desorption rate data and the π-A isotherm results agree well, and thus Equation 6 may be applied to the alkyl sulfate, phosphonate, and carboxyl systems to determine free energies of desorption.

The free energy of desorption for a —CH_2— group, $(W_o - W_c)$, was obtained by comparing, at the same pH and film area, the desorption rate constants for two films differing only in the length of the hydrocarbon chain. From Equation 11, assuming $D/\epsilon\delta$ and W_c are constant for $\Delta m = 2$, when m is large, it follows that

$$2.3\,RT \log \frac{k_{s,m}}{k_{s,m+2}} = \Delta m(W_o - W_c) \qquad (12)$$

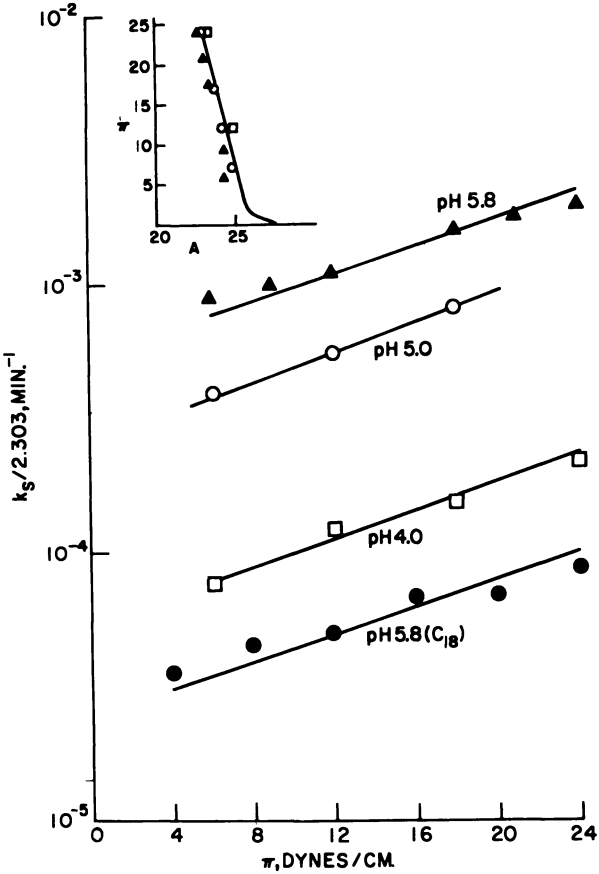

Figure 3. Influence of π on k_s

T = 23°C.
n-*Hexadecyl phosphonate*
□ *pH 4*
○ *pH 5*
▲ *pH 5.8*
n-*Octadecyl phosphonate*
● *pH 5.8*
Inset: π–A isotherms. Each point determined by extrapolating log A at constant π to t = 0
—— n-*Octadecyl phosphonate, pH 5.8*

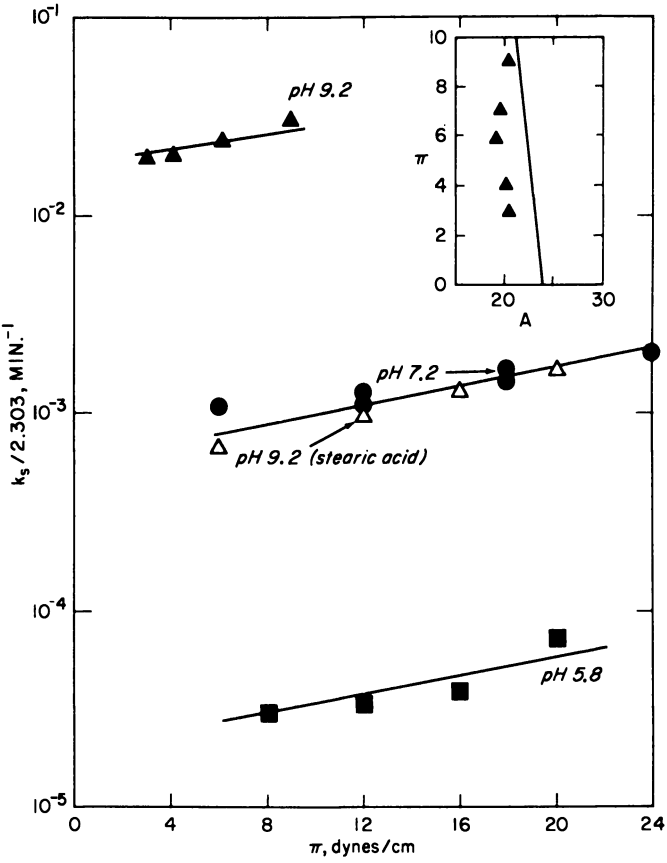

Figure 4. Influence of π on k_s

T = 23°C.
Palmitic acid
■ *pH 5.8, 2 × 10⁻³M NaCl*
● *pH 7.2, 2 × 10⁻³M phosphate buffer*
▲ *pH 9.2, 10⁻³M borate buffer*
Stearic acid
△ *pH 9.2, 10⁻³M borate buffer*
Inset: π–A isotherms
Palmitic acid
▲ *pH 9.2, determined by extrapolating to t = 0*
—— *Stearic acid, pH 9.2; palmitic acid, pH 5.8 and 7.2. No points shown*

The calculations for $(W_o - W_c)$ obtained by comparing the desorption rate constants of C_{16} and C_{18} sulfates and phosphonates and palmitic and stearic acids are summarized in Table II.

To evaluate the free energy of cohesion in the hydrocarbon region of the monolayer, W_c, it is necessary only to obtain the value of W_o, the free energy of desorption of the hydrocarbon in the absence of interac-

Table I. Compounds Investigated

Compound	*M.P., °C.*	*Source*
Sodium *n*-octadecyl sulfate	190–192	V. Lamberti
Sodium *n*-hexadecyl sulfate	202–204	V. Lamberti
n-Octadecyl phosphonic acid[a]	96.5–97.5	H. E. Ries, Jr.
n-Hexadecyl phosphonic acid[a]	94.5–95.5	R. B. Fox
Stearic acid	69.5	Mann Research
Palmitic acid	63.6	Mann Research

[a] Samples recrystallized from cyclohexane.

tions among the hydrocarbon chains. Various investigators have obtained the value of 625 cal. per mole of $—CH_2—$ for W_o (*16*, *28*). This value has been obtained from studies of the effect of hydrocarbon chain length on the lowering of the surface tension of dilute aqueous solutions where the films exhibit ideal-gas behavior. By using this value of W_o, W_c was calculated for three systems (Table II).

The interactions in the ionized region of the monolayer were obtained from the variation of k_s with pH. For a given film (constant m) at a fixed value of π, and assuming $\frac{D}{\epsilon\delta}$ is constant (*29*), differentiation of of Equation 11 with respect to pH yields

$$\frac{d \log k_s}{d\,\mathrm{pH}} = 1 \tag{13}$$

The results of plotting log k_s at constant π as a function of pH for sulfate, phosphonate, and carboxylate films are shown in Figure 5, and the values of Δ log k_s/ΔpH are given in Table III. Except for palmitic acid between pH 5.8 and 7.2, Δ log k_s/ΔpH values for the films were significantly less than predicted by Equation 13. Moreover, the values increasingly deviate from Equation 13 with increase in pH.

Discussion

Measurement of the free energies of monolayer desorption from the rates of desorption depends on whether equilibrium exists between the monolayer and a thin region of solution immediately beneath the film. The relation which tests this condition (Equation 8) must correctly predict the dependence of the rate constant for desorption, k_s, on π. For the sulfate, phosphonate, and carboxyl films in this study Equation 8 is obeyed within the range of experimental error (2 to 5%). Therefore, it is reasonable to assume that the necessary equilibrium condition does exist. The cohesive forces in the monolayer follow directly from the evaluation of the free energies of desorption.

Implicit in the determination of W_c, the cohesive energy in the hydrocarbon region of the long-chain monolayer, is the assumption that W_o, the free energy of desorption for one —CH_2— group, obtained with relatively short hydrocarbon chains, is independent of the length of the hydrocarbon moiety. The validity of this assumption can be checked for sulfate films where W_c may be obtained from desorption studies as

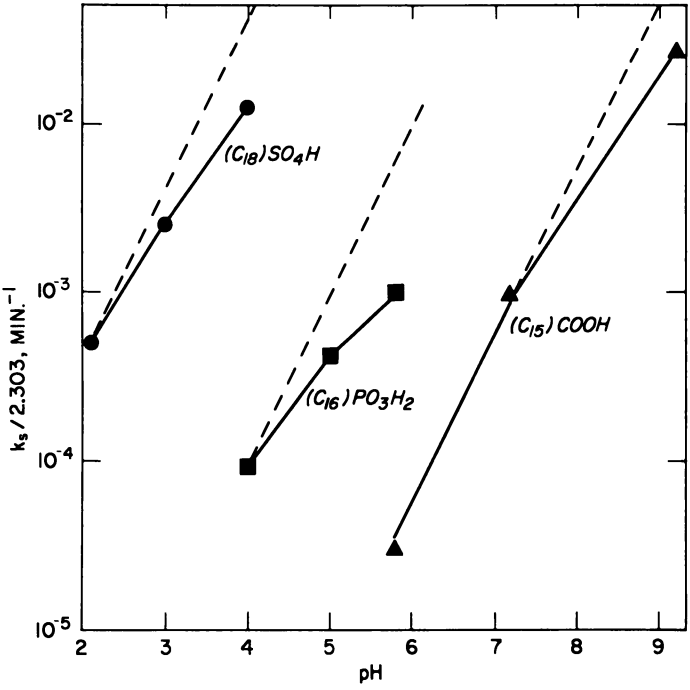

Figure 5. *log* k_s vs. *pH*

T = *23°C.*
π = *8 dynes per cm.*

well as from the π-*A* isotherms. The desorption method yields a value of −110 cal. per mole of —CH_2— (Table II) while from π-*A* isotherms, Davies obtained −100 cal. per mole of —CH_2— (*4, 6*). This agreement is sufficiently close to warrant using the value for W_o of 625 cal. per mole of —CH_2— to obtain W_c. The relative magnitudes of W_c obtained in this way are of the order one would expect—*i.e.*, the cohesive energies in the liquid-condensed phosphonate and carboxyl films are greater than in the "gaseous," sulfate films (Table II).

The polar group interactions were examined through the dependence of k_s on pH as described by Equation 13. For the most part this equation

is not obeyed, as mentioned in the results. In Figure 5, the theoretical relation given by Equation 13 is shown by the dashed lines. These deviations may reflect a weakness in one or more assumptions upon which Equation 13 is based. This equation assumes that Ψ_0 is > 50 mv. for the monolayers, and, as determined by surface potential studies, this appears to be true for sulfate (*23*), phosphonate (*10*) [The ΔV–pH curves are similar to those reported for alkyl phosphate monolayers (*20*).] and carboxylate (*12*) films in the intervals used in this study. Equation 13 also assumes that the π-A isotherm does not undergo a change in the experimental pH range, so that W_c remains unchanged; within the experimental variability for these films there appears to be no change in the isotherms as seen in Figures 2 to 4. Moreover, the discrepancy between theory and experiment is beyond any experimental errors in the determination of k_s. The error in k_s is about 2 to 5%, while deviations from Equation 13 are of the order of 20 to 50% (Table III).

Table III. Influence of pH on k_s

Monolayer	*pH Range*	$\Delta \log k_s/\Delta pH$[a]
n-Octadecyl sulfate	2–3	0.8
	3–4	0.7
n-Hexadecyl phosphonate	4–5	0.65
	5–5.8	0.45
Palmitic acid	5.8–7.2	1.0
	7.2–9.2	0.7

[a] Theoretical value $\Delta \log k_s/\Delta \text{ pH} = 1.0$.

It seems most plausible to explain this discrepancy by assuming that cohesive forces exist in the plane of the polar groups which act to reduce the electrostatic potential arising from the ionized groups of the monolayer. These may be interactions among the polar groups of the monolayer and/or the binding of counterions by the film charges, either of which will reduce k_s.

The presence of cohesive forces in the ionized region of monolayers has also been suggested by studies of the influence of pH on π-A isotherms of compounds similar to those used in this study. Various investigators have reported that sulfate (*24*), phosphonate (*21*), and carboxylate (*27*) films contract in the pH range where the films are ionized and where increasing pH would be expected to expand these monolayers (*12*, *21*). The film contraction usually has been attributed to attractive forces among the ionized "head groups" of the monolayer. However, most of the films which were investigated are soluble to varying degrees in water; hence these results have been criticized on the basis

that enhanced film solubility at the higher pH's may lead to anomolous smaller apparent film areas. This criticism is, of course, mitigated in the desorption studies. Thus, the presence of attractive forces in the ionized region of the monolayer is now supported by independent studies.

Unfortunately, the k_s results cannot distinguish between head-group interactions and the interaction of the head group with the counterions since both effects will influence Ψ_o and correspondingly, k_s. However, the evidence suggests that for weakly acidic films—*e.g.*, phosphonate and carboxylate—both interactions occur simultaneously. For example, the dissociation constant of the acid radical in the surface, K, for carboxylate (*2*), phosphonate (*21*), and phosphate (*19*) films is about 1 pK unit higher than in bulk solution, even after correcting for the potential field with the Gouy equation (*13*). The increase in pK suggests that H^+ is bound to the monolayer by about 1 kcal. per mole in excess of the free energy of dissociation of the acid radical.

It is significant that the magnitude of these interactions obtained from desorption studies is also about 1 kcal. per mole for the phosphonate, sulfate, and carboxyl films in Figure 5, in agreement with the results obtained from the change in pK values. These values were obtained by comparing k_s at the pH where the maximum deviations from Equation 13 was observed. The relation which was used is

$$2.3\,RT \log \frac{k_s\,(\text{measured})}{k_s\,(\text{theoretical})} = \Delta(\phi - \lambda) \qquad (14)$$

Thus, the increase in surface pK supports the argument that the counterion is bound to the film, while the film contraction with increasing pH is in keeping with the existence of a cohesive force among the ionized groups of the film.

The nature of the head-group interactions for phosphonate and carboxyl films is suggested by the fact that the maximum film contraction generally occurs in the pH region where the monolayers are partially dissociated (*21*, *27*). This has been confirmed recently for monooctadecyl phosphate films (which are very similar in behavior to the phosphonate analog) from equilibrium spreading pressure measurements, where film spreading is accompanied by a decrease in entropy. The entropy of spreading decreases with increasing pH, with a maximum entropy decrease occurring at the pH of 50% dissociation (*9*). Moreover, the deviations from Equation 13 appear to increase as the pH approaches the point where the molecules are 50% ionized—*e.g.*, pH 7 for phosphonate and pH 9 to 10 for carboxyl. On the basis of these results it is suggested that head-group interactions are between ionized and nonionized moieties forming acid-soap complexes (*12*) of the type which have been reported to exist in solution (*15*, *26*).

The sulfate film behavior with pH is difficult to explain. It has been suggested that the film is incompletely dissociated (*23, 30*), in which case the films may be treated like the carboxyl and phosphonate films. However, other models suggest that H-bonding with water is important (*30*). Further discussion of this phenomenon is beyond the scope of this paper.

The results emphasize that in addition to the London–van der Waals interactions in the hydrocarbon region of the monolayer, cohesive forces also exist in the ionized region of acidic films. The question of how general the attractive forces in the ionic region of the monolayer are remains to be answered, but the fact that they exist over a wide range of p*K* values suggests that they may be present in all ionized monolayers. Though a reasonable model for the interactions in partially dissociated films has been presented, the nature of the interactions in strong acid films is not clear. In the latter case, these interactions may be favored in the surface because of the constraints imposed on the system by the interactions among the hydrocarbon chains of the film.

Literature Cited

(1) Adam, N. K., "Physics and Chemistry of Surfaces," 3rd ed., Oxford University Press, London, 1941.
(2) Betts, J., Pethica, B. A., *Trans. Faraday Soc.* **52,** 1581 (1956).
(3) Crisp, D. J., "Surface Chemistry," p. 65, Butterworths, London, 1949.
(4) Davies, J. T., *J. Colloid Sci.* 11, 377 (1956).
(5) Davies, J. T., as quoted in E. Matijevic and B. A. Pethica, *Trans. Faraday Soc.* **54,** 1383 (1958).
(6) *Ibid.*, **48,** 1052 (1952).
(7) Davies, J. T., Rideal, E. K., "Interfacial Phenomena," Academic Press, New York, 1961.
(8) Gershfeld, N. L., *J. Phys. Chem.* **66,** 1923 (1962).
(9) Gershfeld, N. L., Pak, C. Y. C., *J. Colloid Interface Sci.* **23,** 215 (1967).
(10) Gershfeld, N. L., Pak, C. Y. C., unpublished results.
(11) Gershfeld, N. L., Patlak, C. S., *J. Phys. Chem.* **70,** 286 (1966).
(12) Goddard, E. D., Ackilli, J. A., *J. Colloid Sci.* **18,** 585 (1963).
(13) Gouy, J., *J. Phys. Radium* **9,** 457 (1910).
(14) Harkins, W. D., "Physical Chemistry of Surface Films," Reinhold, New York, 1952.
(15) John, L. M., McBain, J. W., *J. Am. Oil Chemists' Soc.* **25,** 141 (1948).
(16) Langmuir, I., *J. Am. Chem. Soc.* **39,** 1848 (1917).
(17) Mitchell, J. S., *Trans. Faraday Soc.* 31, 980 (1935).
(18) Pak, C. Y. C., Gershfeld, N. L., *J. Colloid Sci.* 19, 831 (1964).
(19) Parreira, H. C., *J. Colloid Sci.* **20,** 742 (1965).
(20) Parreira, H. C., Pethica, B. A., "Proceedings of 2nd International Congress on Surface Activity," Vol. 1, p. 44, Butterworth & Co., London, 1957.
(21) Payens, Th. A. J., *Phillips Res. Rept.* **10,** 425 (1955).
(22) Pethica, B. A., *Trans. Faraday Soc.* **50,** 413 (1954).
(23) Pethica, B. A., Few, A. V., *Discussions Faraday Soc.* **18,** 258 (1954).
(24) Phillips, J. N., Rideal, E. K., *Proc. Roy. Soc. (London)* **A232,** 159 (1955).
(25) Robbins, M. L., LaMer, V. K., *J. Colloid Sci.* **15,** 123 (1960).

(26) Ryer, F. V., *Oil and Soap* **23,** 310 (1946).
(27) Spink, J. A., *J. Colloid Sci.* **18,** 512 (1963.
(28) Stauff, J., *Z. Physik. Chem.* **10,** 24 (1957).
(29) Ter Minassian-Saraga, L., *J. chim. phys.* **52,** 181 (1955).
(30) Thomas, J. G. N., Schulman, J. H., *Trans. Faraday Soc.* **50,** 1131 (1954).
(31) Ward, A. F. H., Tordai, L., *Trans. Faraday Soc.* **42,** 408 (1946).

RECEIVED July 19, 1967.

12

Molecular Interactions in Mixed Monolayers

D. A. CADENHEAD and M. C. PHILLIPS

Department of Chemistry, Acheson Hall, State University of New York at Buffalo, Buffalo, N. Y. 14214

Using an automated film balance the behavior of mixed monomolecular films exhibiting deviations from ideality was studied. Particular attention was paid to condensation effects obtained when cholesterol is mixed with a more expanded component. The deviations at various film pressures are discussed in terms of the partial molecular areas of the film components. Slope changes in these plots are caused by phase transitions of the expanded monolayer component and do not indicate the formation of surface complexes. In addition, the excess free energies, entropies, and enthalpies of mixing were evaluated, but these parameters could be interpreted only for systems involving pure expanded components, for which it is clear that the observed condensation effects must involve molecular interactions.

Many studies of the behavior of mixed monomolecular films have been reported (*12*), often with systems having components found in biological membranes. Clearly, information pertaining to molecular packing and interactions of biologically significant amphipathic molecules at the air-water interface would be relevant in understanding membrane physics. Unfortunately, most of the early work was carried out with poorly defined materials extracted from natural sources, precluding a precise molecular interpretation of the results. For this reason, we felt it necessary to survey this area extensively while restricting ourselves to the use of chromatographically pure, synthetic materials.

Experimental and Results

The surface pressure, π, and surface potential, ΔV, were determined as a function of molecular area, A, for the various single- and mixed-

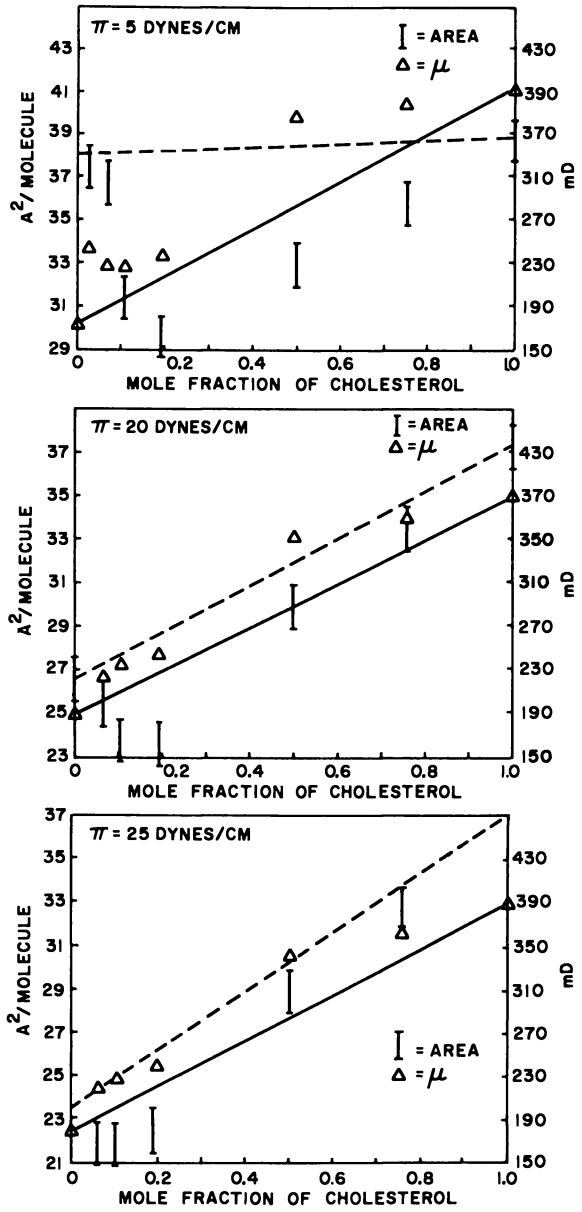

Figure 1. Mixed monolayers of cholesterol–myristic acid system at 23.5°C. and pH 2

Left ordinate: Mean molecular area, sq. A. per molecule
Right ordinate: Mean surface dipole moment, millidebyes

component systems examined, using a fully automated Langmuir–Wilhelmy trough. This apparatus and the techniques used to handle single-component films have been described (*6*). For mixed films the separate components were dissolved in an appropriate solvent (either pure hexane or a 10 to 1 by volume hexane–ethanol mixture), then premixed in the

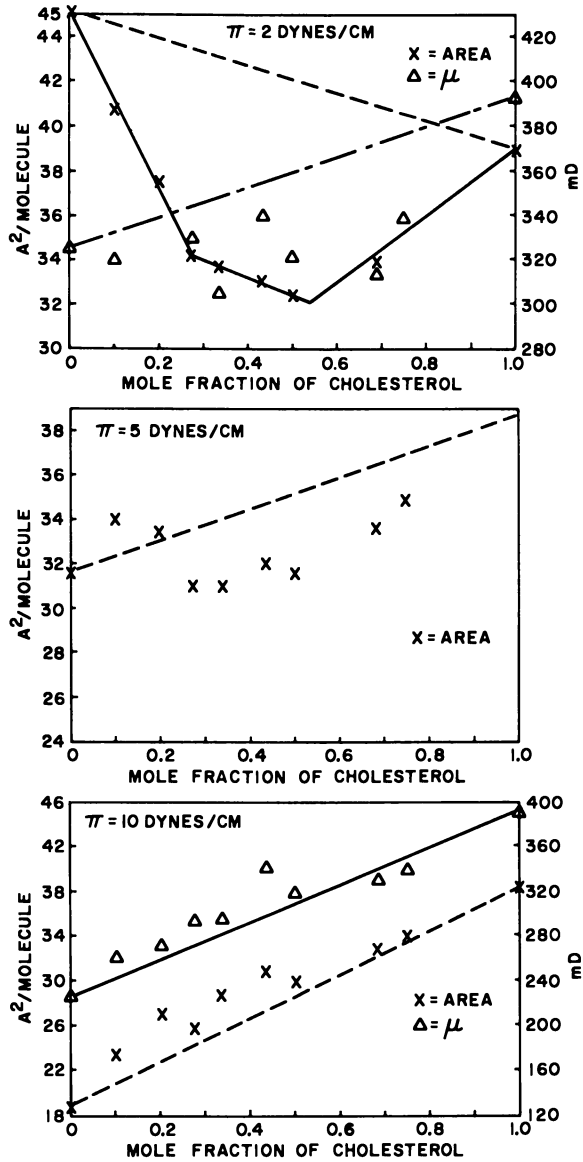

Figure 2. Mixed monolayers of cholesterol–methyl palmitate system at 27° C. and pH 6

required ratio and spread at the air–water interface. Pressure-area curves were reproducible to within ± 2 sq. A. per molecule and ± 1 dyne

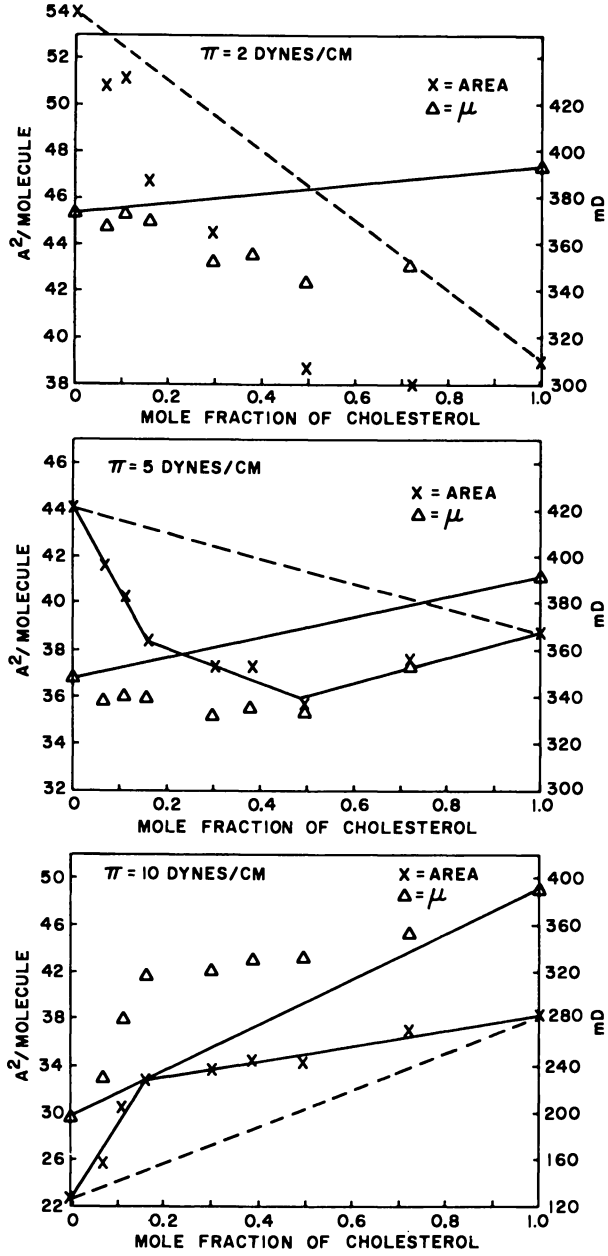

Figure 3. Mixed monolayers of cholesterol–ethyl palmitate system at 23.5°C. and pH 6

per cm., while the reproducibility of the surface potentials was within ± 15 mv.

Materials. The samples of 1,2-dimyristoyl-3-lecithin (L-configuration) and 1,2-didecanoyl-3 lecithin (L-configuration) were respectively donated by Erich Baer, Banting and Best Institute, Toronto, Canada, and D. Chapman, Unilever Research Laboratories, Welwyn Garden City, England. All other materials were obtained from the Applied Science Laboratories, State College, Pa. All materials examined were synthesized and purified chromatographically.

Eight binary systems are reported. Six include cholesterol as one component of the mixed film. The second components in these six films were myristic acid, methyl palmitate, ethyl palmitate, 1,2-dimyristin, 1,2-dimyristoyl-3-lecithin, and 1,2-didecanoyl-3-lecithin. In addition, the systems trilaurin–dimyristoyl lecithin and triolein–dimyristoyl lecithin

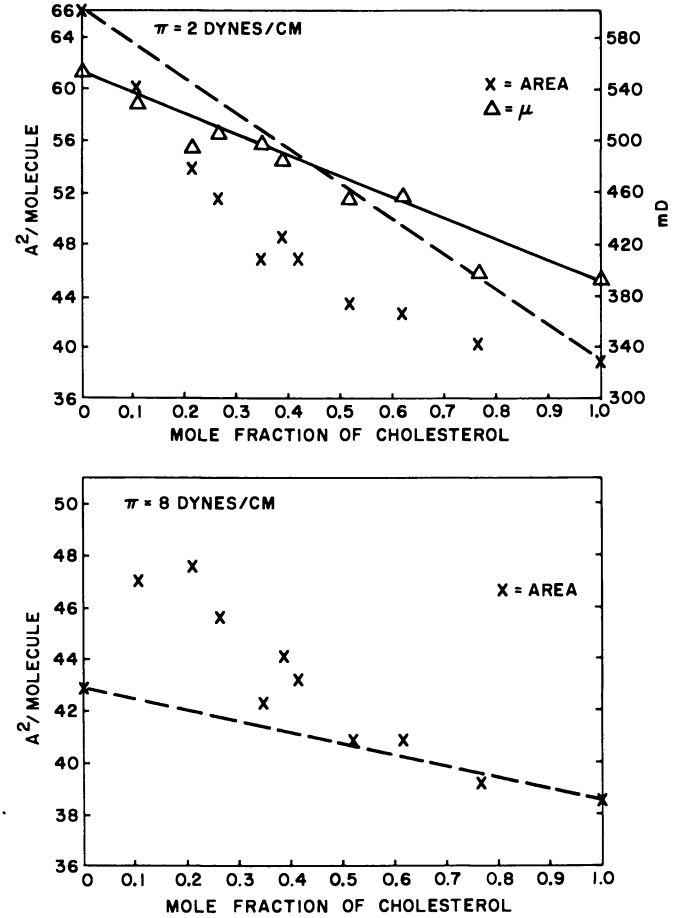

Figure 4. Mixed monolayers of cholesterol–1,2-dimyristin system at 27°C. and pH 6

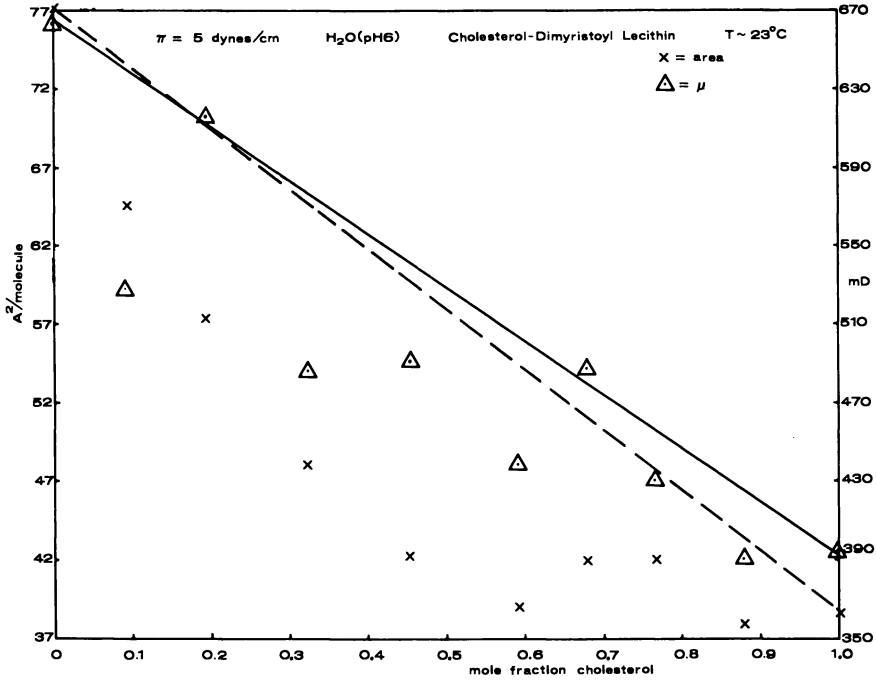

Figure 5. Mixed monolayers of cholesterol–1,2-dimyristoyl-3-lecithin system at 23°C., pH 6, and 5 dynes per cm.

were studied. Data were obtained over the temperature range 22°–27°C., for the complete compositional range of each system. Each individual temperature was controlled to within ± 0.2°C. Such data are presented here by illustrating the mean molecular area (area of film divided by the total number of molecules in the film) as a function of composition at constant temperature and surface pressure.

Figures 1 through 9 illustrate such plots, as well as the corresponding mean surface dipole plots, μ, for the systems listed above. [In Figures 1 and 6 through 9 the broken line (molecular areas) and the solid line (surface dipole moments) represent the path followed when either ideal mixing or nonmixing occurs. In Figures 2 through 5 the straight lines between the ordinates (×, molecular areas, and △, surface dipole moments) represent this path.] Features of the isotherms of the pure expanded components which are necessary for understanding the following discussion are listed in Table I.

The surface pressure–area and surface dipole moment–area data for both components and a 1 to 1 molar ratio of all but the last mixture were obtained for at least two temperatures in the range 0° to 40°C. From such data excess thermodynamic quantities were calculated. For reasons

Table I. Mean Molecular Area Characteristics of Various Mixed Films

Film Composition	*Expanded Noncholesterol Component Phase Change Exhibited*	*Temp., °C.*	*Transition Pressure, Dynes/Cm.*	*Expected Behavior Type*
Cholesterol–myristic acid	Yes	22	19	I
Cholesterol–methyl palmitate	Yes	27	3	I
Cholesterol–ethyl palmitate	Yes	23	8	I
Cholesterol–dimyristin	Yes	27	4	I
Cholesterol–dimyristoyl lecithin	No	23	–	II or III
Cholesterol–didecanoyl lecithin	No	23	–	II or III
Trilaurin–dimyristoyl lecithin	No	24.5	–	III
Triolein–dimyristoyl lecithin	No	23.5	–	III

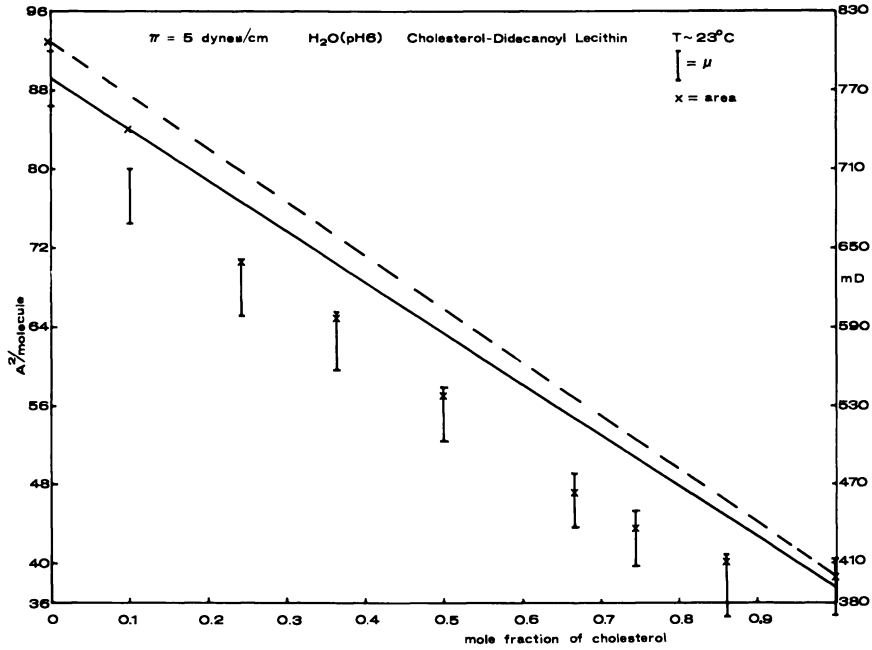

Figure 6. Mixed monolayers of cholesterol–1,2-didecanoyl-3-lecithin system at 23°C. and pH 6

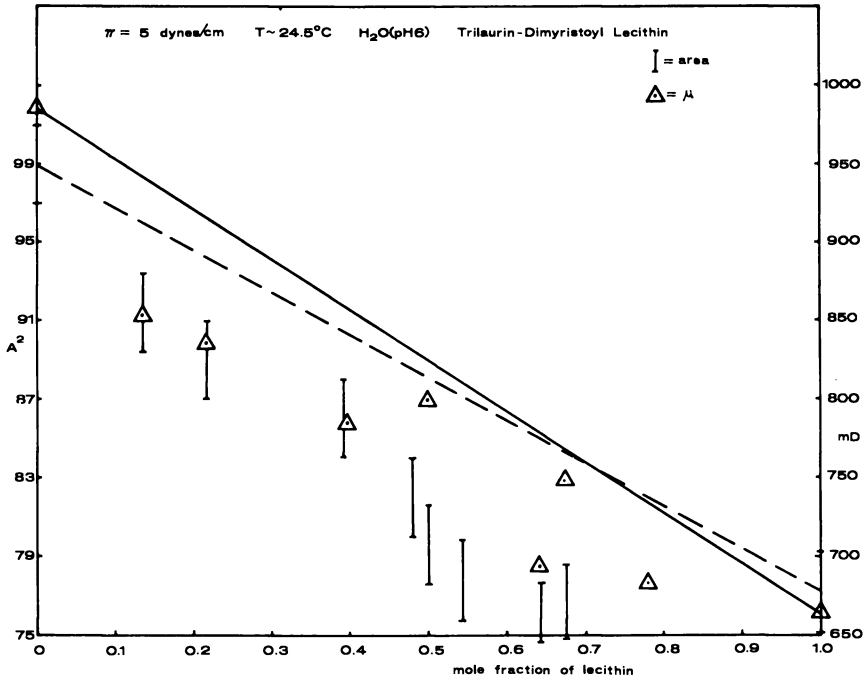

Figure 7. Mixed monolayers of trilaurin–1,2-dimyristoyl-3-lecithin system at 24.5°C., pH 6, and 5 dynes per cm.

Table II. Thermodynamic Excess Functions for an Equimolar Mixed Monolayer of Trilaurin–Dimyristoyl Lecithin

π, Dynes/Cm.	T, °C.	ΔG_{xs}, ±20 Cal./Mole	ΔH_{xs}, ±0.5 Kcal./Mole	ΔS_{xs}, ±2 Cal./Deg./Mole
3	23	−35	−3.1	−10.5
5	23	−51	−3.9	−13.1
10	23	−92	−5.0	−16.5

explained later, we report these quantities for the system trilaurin–dimyristoyl lecithin only (Table II). Figures 10 and 11 illustrate the isotherms and potentials of this system at 5° and 22°C., respectively.

Discussion

Since most of the data presented here are in the form of plots of mean molecular area (or corresponding surface dipole moment) *vs.* composition, it is clearly important to understand the implications of such a representation and to explain the range of behavior found for different mixtures in terms of the characteristics of the individual components.

In Figure 12, a generalized diagram of this type is illustrated for a series of mixtures of cholesterol and a more expanded component. The broken line, LM, represents the behavior when the following molecular area additivity rule is obeyed:

$$(1 - n)A_1 + nA_2 = A_{12}$$

where

A_1 = area per molecule of the pure expanded component

A_2 = area per molecule of pure cholesterol

A_{12} = area per mixed molecule in the mixed film

and

n = mole fraction of cholesterol in the mixed film

Such behavior occurs when the two components either form an ideal mixture or are immiscible. Before drawing conclusions concerning molecular interactions (*12*, *13*), it is clearly important to establish that homogeneous mixed films have been formed. Any deviation from line LM is, of course, indicative of both mixing and nonideality. In discussing such effects, we define any negative deviation from LM as a "condensation" and any positive deviation as an "expansion." Our results fall into three distinct categories.

Type I is represented by lines LONM in Figure 12, with two well-defined changes of slope occurring at O and N; the precise form depends on the surface pressure. This behavior is found when the π-A curve of the pure expanded component exhibits a two-dimensional condensation (Table I and Figures 2, 3, and 4).

Type II is represented by line LOM in Figure 12, with a sharp change in slope at point O. Either this behavior or Type III behavior can be found when the pure expanded component exhibits a fully expanded π-A curve. The cholesterol–dimyristoyl lecithin system, illustrated in Figure 5, is an example of Type II behavior.

Type III is adequately represented by the systems illustrated in Figures 6, 7, 8, and 9. This behavior is characterized by condensations where there is no sharp change of slope in line LM.

With a condensed monolayer, such as cholesterol, it may safely be assumed that each molecule occupies essentially the same area in both pure and mixed films (*4*). This value is approximately 38 sq. A. per cholesterol molecule. By making this assumption it is possible to obtain, by the method of intercepts (*16*), the partial molecular areas, $(\partial A/\partial n)_{\pi,T}$, at constant π and temperature, of the expanded component in a cholesterol-mixed film. An extrapolation (*10*) through MN (Type I, Figure 12), or MO if linear (Type II, Figure 12) to the A_1 ordinate, yields the area per molecule of the expanded component in the mixed films, where the cholesterol content is either equal to or in excess of the compositions denoted by point N (Type I) or point O (Type II). Such

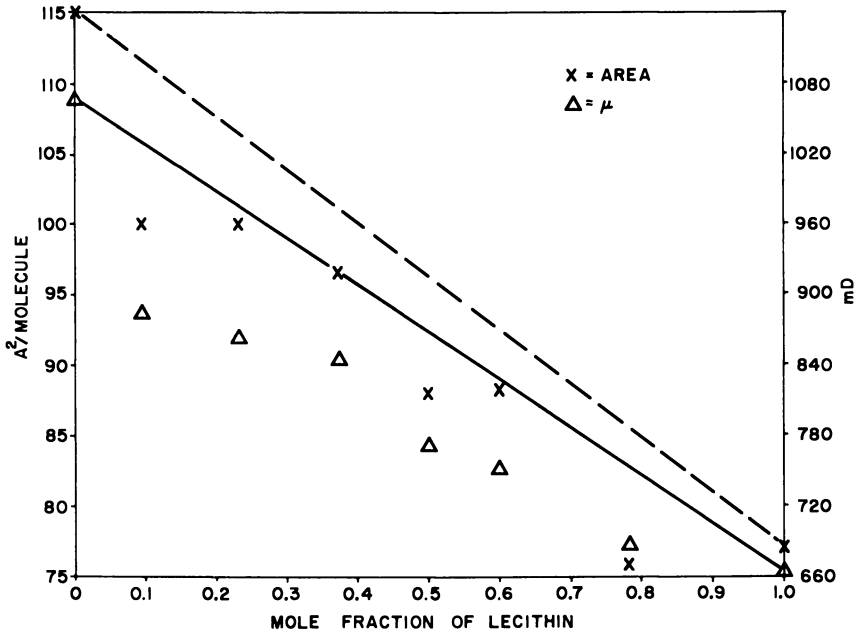

Figure 8. Mixed monolayers of triolein–1,2-dimyristoyl-3-lecithin system at 23.5°C., pH 6, and 5 dynes per cm.

calculations are not feasible when both pure components form expanded films.

Type I. Figure 13 illustrates the corresponding plots of π *vs.* the area per molecule of the more expanded component (*4*), for the compositional regions "low," "high," and "maximum effect" cholesterol content, designated by LO, ON, and MN in Figure 12. The solid line, ABCD, in Figure 13 represents the π-*A* curve of a pure expanded component undergoing a liquid expanded (DC)–liquid condensed (AB) transition, with the film in a transitional state in the section designated by BC and a fully condensed state at A (*1*). Line AL indicates the limiting area per molecule for the more expanded component (approximately 20 sq. A. per *n*-alkane chain). The broken lines denote the area per molecule occupied by the expanded component in the mixed films, after subtracting the cholesterol area, with M_1, M_2 - - - - - - M_F designating increasing cholesterol content. We may better understand the effects of adding cholesterol by considering the various mixtures at three increasing surface pressures:

π_1 below the transition pressure for the pure expanded component (liquid-expanded region of mixed film).

π_2 above the transition pressure for the pure expanded component (liquid condensed region of mixed film).

π_3 in the condensed region of the pure expanded component.

LOW-PRESSURE REGION (π_1). At low cholesterol content (Figure 13a) the effects of cholesterol addition are relatively large since the film is in a liquid expanded state. The lift-off area per expanded molecule is sharply reduced, and a significant condensation effect can be observed. When the cholesterol content has been increased to the extent that the isotherm of the mixed film no longer exhibits a phase transition (Figure 13b), further condensing effect is markedly reduced in magnitude. The film is now in a liquid-condensed state and is much less condensable. In Figure 12, this would be indicated by the change in slope of the mean molecular area plot (pressure π_1) at point O. This change in behavior will be determined by the length of the intermediate region of the pure expanded component, and the molecular ratio of the mixed film at point O will vary in a corresponding manner. Thus, a small intermediate region will reduce the length of line LO in Figure 12, with the behavior illustrated in Figure 13a, existing only for mixed films of very low cholesterol content. Ultimately increasing the cholesterol content will produce no further condensation, and the mixed-film isotherm will lie along the broken line designated by M_F (Figure 13c). The system will now obey the additivity rule:

$$(1 - n)A_1^{\pi_1} + nA_2 = A_{12}$$

where $A_1^{\pi_1}$ is the area per molecule of expanded component corresponding to maximum condensation by cholesterol at pressure π_1 and temperature T.

The actual value of $A_1^{\pi_1}$ in square Angstroms per molecule may be obtained by extrapolating MN to the left-hand ordinate of Figure 12. Clearly, the effects on the expanded component of increasing the cholesterol content, and of increasing the pressure, are similar but not identical. At low pressures, $A_1^{\pi_1}$ is greater than the true limiting area per molecule of the expanded component. As the pressure is increased, this difference will decrease, eventually becoming negligible. The precise behavior exhibited by a given system would again depend on the nature of the expanded component.

INTERMEDIATE PRESSURE REGION (π_2). Initially (Figure 13, 13a) the presence of the cholesterol delays the onset of the liquid expanded–liquid condensed phase transition until lower areas per molecule of expanded component and higher surface pressures are attained, the extent of the delay increasing with increasing cholesterol content. This delay changes the condensation caused by the cholesterol to expansion. Thus, while the mixed films are still increasingly condensed with increasing cholesterol

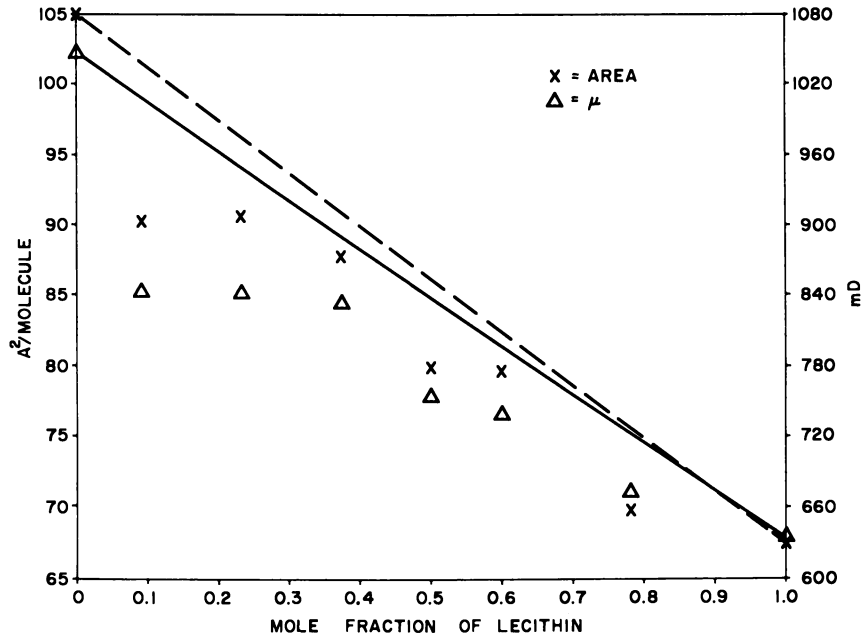

Figure 9. Mixed monolayers of triolein–1,2-dimyristoyl-3-lecithin system at 23.5°C., pH 6, and 10 dynes per cm.

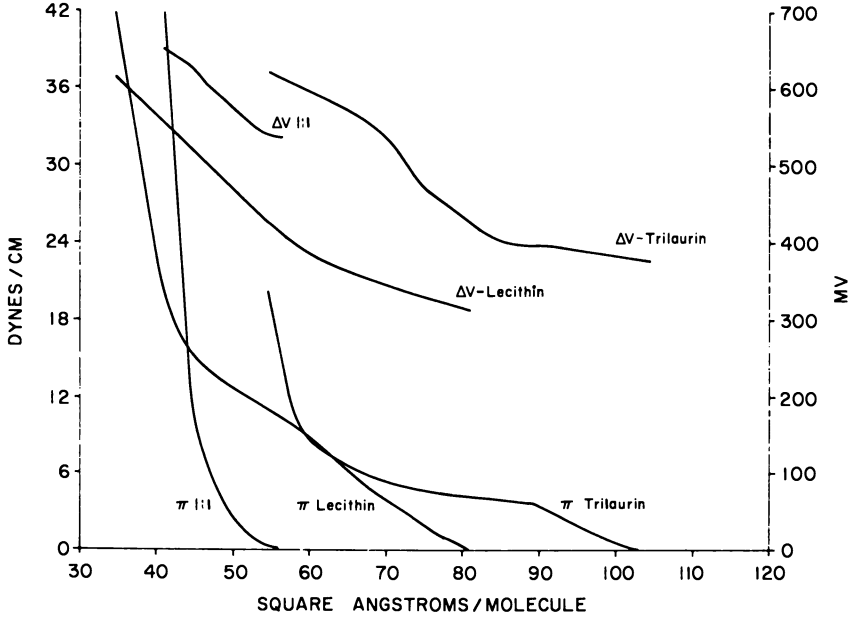

Figure 10. Surface pressure–area and surface potential–area plots for 1,2-dimyristol-3-lecithin, trilaurin, and a 1 to 1 molar mixture at 5°C.

content, the pure expanded component has undergone an even greater condensation because of its phase change. The resultant behavior, as indicated by the mean molecular area plot, will depend on the relative magnitude of these two effects. When the cholesterol content is sufficiently high, the mixed films also become liquid-condensed (Figure 13b) and the area per molecule of the expanded component will decrease with increasing cholesterol until (Figure 13c) a limiting value is attained ($A_1^{\pi_2}$) and an additivity rule is once again obeyed.

HIGH PRESSURE REGION (π_3). In this region a reduced expansion may still be observable with low cholesterol content (Figure 13a), but this will be small, decreasing with increasing cholesterol, to give additivity of molecular areas ($A_1^{\pi_3}$) and near ideal behavior (Figure 13b and c).

Throughout this discussion, we have ignored consideration of the behavior of the surface potentials. In general, the surface dipole moments have provided qualitative support for the findings obtained from molecular area data. At this stage, however, we are not able to account quantitatively for the surface dipole moments.

We are now in a position to examine the various systems listed in Table I which follow Type I behavior. Experimentally (Figure 2) the behavior of the cholesterol–methyl palmitate system shows excellent agreement with the generalized system depicted in Figures 12 and 13,

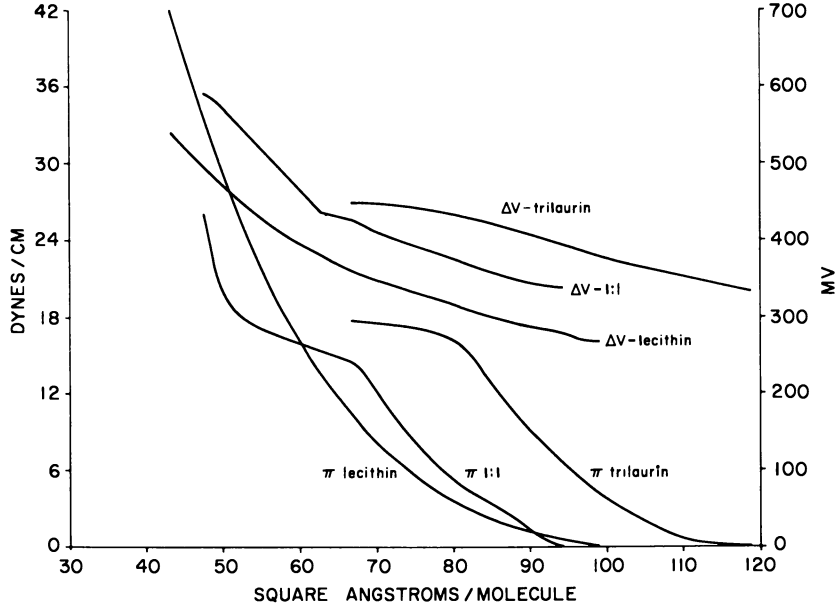

Figure 11. Surface pressure–area and surface potential–area plots for 1,2-dimyristoyl-3-lecithin, trilaurin, and a 1 to 1 molar mixture at 22°C.

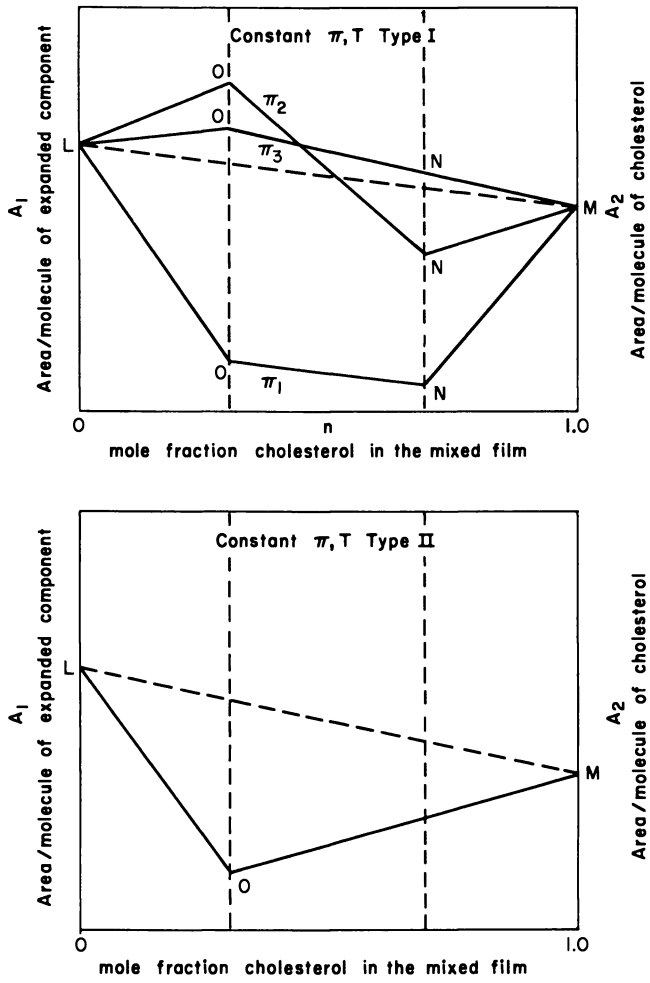

Figure 12. Generalized mean molecular area plot for systems containing cholesterol

taking π_1, π_2, and π_3 at 2, 5, and 10 dynes per cm., respectively. At different pressures and differing values for molar ratios at points O and N the cholesterol–ethyl palmitate system also shows good agreement (Figure 3) as does that of cholesterol–dimyristin (Figure 4). The small intermediate region of myristic acid at room temperature (2) resulted in such a small region of high condensability (Figure 1) that the behavior of the cholesterol–myristic acid system approximated Type II behavior at all pressures. Such behavior is to be expected when the intermediate region is small or a phase change is absent in the isotherm of the pure expanded component.

Type II. Since 1,2-dimyristoyl-3-lecithin (L-configuration) does not exhibit any phase change at 22°C. (Figure 11), the dimyristoyl lecithin–cholesterol system should follow Type II behavior (Figure 5). Van Deenen *et al.* (*9*) have reported such results for a dimyristoyl lecithin, as has Shah (*18*) for a dipalmitoyl lecithin. Especially with mean molecular area plots obtained at higher surface pressures, extrapolating lines corresponding to MN (Type I) or MO (Type II) of Figure 12 gives limiting areas per molecule of close to 20 sq. A. per *n*-alkane chain.

Type III. The cholesterol–didecanoyl lecithin system (Figure 6) exhibits Type III behavior at 5 dynes per cm. Since the limiting area of this molecule is about 50 sq. A. (*7*), it is clear that a Type II classification would require a well-defined linear portion in Figure 6 at cholesterol-rich concentrations extrapolating to this value at the A_1 ordinate, and no such linear portion is evident. The suggestion here is that we are just beyond the ability of cholesterol to condense this molecule fully. If this is the case, it may be possible to move to Type II behavior by repeating this particular study at a lower temperature. Since we find these components to be miscible, comparison with dimyristoyl lecithin would indicate that the shorter chains interact less with the cholesterol, as van Deenen *et al.* (*9*) have suggested. In finding any condensation we disagree with these workers who found either ideal mixing or nonmiscibility. Moreover, for both the dimyristoyl (*6*) and didecanoyl (*7*) lecithins our isotherms were somewhat less expanded than either their original (*20*) or revised isotherms (*9*).

We also report here mean molecular area plots for two further systems which exhibited Type III behavior: trilaurin–dimyristoyl lecithin

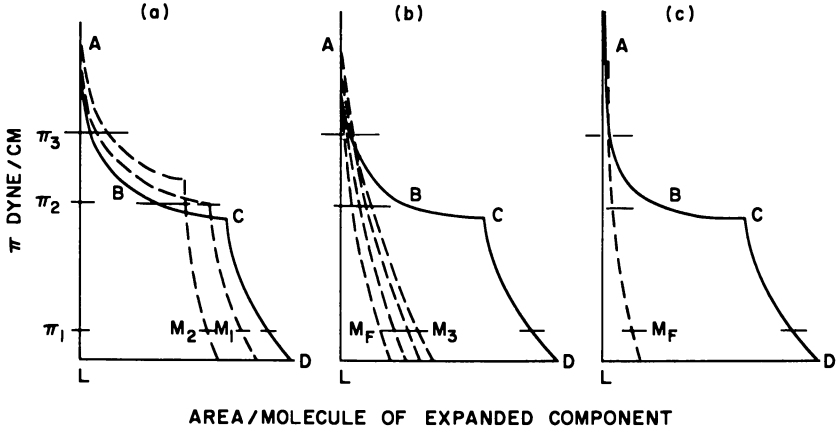

Figure 13. Effects of cholesterol addition on isotherm of originally expanded component

and triolein–dimyristoyl lecithin (Figures 7, 8, and 9). Since both components can undergo condensation, no quantitative conclusions can be reached with regard to area per molecule of either component in the mixed films. Nevertheless, several valuable qualitative observations can be made. The extent of the condensations (*see* Figures 10 and 11) reflects the number of paraffinic chains involved, and the systems appear particularly sensitive to cholesterol addition at temperatures within the range where a liquid expanded to liquid-condensed phase transition may be observed (Figure 10). Also the similarity between the behavior of the trilaurin-lecithin and triolein-lecithin systems further suggests that while molecular interactions involving unsaturated bonds may be involved, such interactions do not appear to play any special role, as has been suggested (*17*). Dervichian *et al.* (*11*) have also observed condensation effects between triglycerides and lecithins, and finding what we would describe as Type I behavior, they attributed the two sharp breaks in the mean molecular area plot to the formation of 1 to 3 and 3 to 1 "complexes." This latter work was carried out with triglyceride and lecithin mixtures (materials extracted from natural sources) and not with single molecular species.

Besides indicating that the molecular ratios at which such breaks are found have no special significance, our results suggest an alternative interpretation for the Dervichian results. Thus, for the three linear portions observed, the first and third portions could be caused by the condensation of the more condensable components (highly unsaturated or short-chain materials exhibiting expanded isotherms), and the intermediate portion to somewhat less-condensable components of a further condensation of the first group of molecules (equivalent to our liquid-condensed regions). The cholesterol–mixed lecithin system reported by De Bernard (*8*) could be similarly interpreted except that the third portion (cholesterol-rich) would follow an additivity rule for mixed condensed molecules. Such explanations could be checked by studying the effects of changing the known composition of a mixed film using purified synthetic materials.

Mechanism. The molecular mechanism by which these various effects occur still must be elucidated. Two limiting models have been proposed, in which the deviations from ideality are accredited either to entropy changes with enthalpy changes zero, or the reverse, with molecular interactions playing a primary role. An athermal model was suggested by Adam (*3*, *4*) and, in a more elaborate form, by Shah and Schulman (*19*). A regular solution model has been favored by Dervichian (*10*, *11*). It seems to us, however, that the correct version will lie somewhere between these two limiting models, and that it would be worthwhile to obtain the excess free energies, enthalpies, and entropies according to

the methods outlined by Goodrich (*15*) and amplified by Gaines (*12, 14*). These were calculated using isotherms for the pure components and 1 to 1 molar ratio mixtures as discussed above.

While the thermodynamic treatment is applicable to the mixed cholesterol systems we listed, we are not reporting the excess thermodynamic quantities for these systems at this time because of difficulties in allowing for differences in the initial physical states of the pure component monolayers. The conclusions drawn by van Deenen *et al.* (*9*) for the dimyristoyl lecithin–cholesterol system must be regarded as invalid since they did not take this factor into account.

However, interpretation of the quantitative values obtained for the system trilaurin–dimyristoyl lecithin at $\pi = 3$ dynes per cm. should be valid since both pure components are initially liquid-expanded. The results obtained at this pressure indicate significant exothermic molecular interactions (Table II), accompanied by a large decrease in the excess entropy, a picture consistent with the observed condensation effects. The entropy loss is approximately three times greater than that observed by Goodrich (*15*) for mixtures of single *n*-alkane chain compounds and presumably reflects the increased number of chains per molecule. The heat of mixing probably arises from an improved packing of molecules in the mixed trilaurin-lecithin system. At comparable surface pressure, Gaines (*13*) obtained excess free energies for another fully expanded system: chlorophyll α and vitamin K_1. The observation that molecular interactions play a role in the trilaurin-lecithin system suggests that this will also be the case for the mixed systems containing cholesterol, contrary to the views of Shah and Schulman (*19*).

The results obtained at surface pressures of 5 and 10 dynes per cm. are complicated by the fact that the trilaurin has undergone a two-dimensional condensation at 5°C., and we will not attempt interpretation at this time. A complete understanding of the molecular interactions involved in such mixed films must await a deeper insight into the interactions involved in films of pure components. We are presently attempting to evaluate such interactions by a thermodynamic study of compression of single-component films (*5*), with the ultimate objective of obtaining a fuller understanding of mixed films on a molecular basis.

Acknowledgment

We acknowledge the financial assistance in the completion of this work of the Theoretical Biology Center, State University of New York at Buffalo, also N.I.H. program grant GM-11603 and N.A.S.A. grants NSG-501 and NGR-33-015-016.

Literature Cited

(1) Adam, N. K., "Physics and Chemistry of Surfaces," 3rd ed., Chap. II, p. 17, Oxford University Press, London, 1941.
(2) *Ibid.*, p. 59.
(3) *Ibid.*, p. 70.
(4) Adam, N. K., Jessop, G., *Proc. Roy Soc.* **A120,** 473 (1928).
(5) Cadenhead, D. A., Demchak, R. J., Phillips, M. C., to be published.
(6) Cadenhead, D. A., Demchak, R. J., Phillips, M. C., *Kolloid Z. Z. Polymer* **220,** 59 (1967).
(7) Cadenhead, D. A., Phillips, M. C., unpublished work.
(8) De Bernard, L., *Bull. Soc. Chim. Biol.* **40,** 161 (1958).
(9) Demel, R. A., van Deenen, L. L. M., Pethica, B. A., *Biochim. Biophys. Acta* **135,** 11 (1967).
(10) Dervichian, D. G., "Surface Science in Chemistry and Biology," J. F. Danielli, K. G. A. Panhurst, A. C. Riddiford, eds., p. 70, Pergamon Press, London, 1958.
(11) Desnuelle, P., Molines, J., Dervichian, D., *Bull. Soc. Chim. France* **18,** 197 (1951).
(12) Gaines, G. L., "Insoluble Monolayers at Liquid-Gas Interfaces," Chap. 6, pp. 281-300, Interscience, New York, 1966.
(13) Gaines, G. L., *J. Chem. Phys.* **42,** 2193 (1965).
(14) Gaines, G. L., *J. Colloid Interface Sci.* **21,** 315 (1966).
(15) Goodrich, F. C., "Proceedings of 2nd International Congress on Surface Activity," Vol. I, p. 85, Butterworths, London, 1957.
(16) Guggenheim, E. A., "Thermodynamics," 4th ed., p. 214, North Holland, Amsterdam, 1959.
(17) Pethica, B. A., "Surface Activity and the Microbial Cell," p. 85, Society of Chemical Industry Symposium, London, 1965.
(18) Shah, D. O., Ph.D. thesis, Columbia University, 1965.
(19) Shah, D. O., Schulman, J. H., ADVAN. CHEM. SER. **84,** 189 (1968).
(20) van Deenen, L. L. M., Houtsmuller, U. M. T., de Haas, G. H., Mulder, E., *J. Pharm. Pharmacol.* **14,** 429 (1962).

RECEIVED July 18, 1967.

Some Properties of Interfacial Films of Colloidal Electrolyte–Protein Complexes

IRA BLEI[1]

Lever Brothers Research and Development Center, 45 River Rd., Edgewater, N. J.

Protein (bovine serum albumin) monomolecular films spread at the air–water interface were complexed with anionic or cationic detergents injected into the support phase. Changes in the surface pressure of the complex, maintained at constant area, were determined as a function of support phase pH. Surface pressures paralleled the general features of the pure protein monolayers' titration curve. Notable exceptions were a shift in ammonium group pK from 11.5 (pure protein monolayer) to 8.5 (protein–sodium dodecyl sulfate complex monolayer), and retention by the protein monolayer of significant quantities of cetyl trimethyl ammonium bromide at pH values corresponding to virtually no negative charge on the protein. The large difference between pure protein and complex monomolecular film ammonium group pK was similar to the difference in pK between organic amines in a surface film and in bulk.

The stoichiometric characterization of detergent-protein complexes has been the object of many studies over the past 30 years (*6*). Recent studies have placed more emphasis upon developing a molecular-kinetic description of the complex (*2*, *8*). The importance of such descriptions lies in the fact that detergent-protein complexes can be considered as lipoprotein model systems. Indeed, virtually all conceptions of the microscopic nature of lipid-protein interactions are based on the properties of detergent-protein complexes (*3*).

[1] Present address: Richmond College, C.U.N.Y., 130 Stuyvesant Pl., Staten Island, N. Y. 10314

This report describes the titration of monomolecular films of bovine serum albumin spread on supporting phases containing soluble detergents. The object was to compare the results of this study with those from titration studies of the pure protein, hoping that this comparison would permit a more detailed description of the nature of the binding sites of the complex.

Experimental Procedures

The experimental procedure consisted first of generating a detergent-protein complex monolayer of fixed area at the air–water interface, followed by varying the substrate pH. The experimental parameters were film surface pressure and the subphase pH.

The surface trough was made of Lucite, 45 × 15 × 1.5 cm. and was divided into two compartments of equal size by a septum of Lucite, 1.5 cm. high. Cooling channels for temperature control were milled into the bottom of the trough. The monolayer was spread inside a paraffined mica frame which floated on the water and was firmly positioned by external mounts. The surface tension was measured with a double-hook torsion balance and a sand-blasted platinum Wilhemy plate. A Beckman model G pH meter with standard glass and KCl electrodes was used to measure pH.

The protein used was crystalline bovine serum albumin (BSA) obtained from Armour Laboratories. Sodium dodecyl sulfate (SDS) was synthesized from pure dodecyl alcohol and chlorosulfonic acid, recrystallized, and washed with ethyl ether. Sulfuric acid was reagent grade purchased from the J. T. Baker Chemical Co. and used directly. Reagent grade potassium hydroxide purchased from the Mallinkrodt Co. was purified by foaming a concentrated solution, removing the foam, and using the solution directly.

The detergent-protein interfacial complex was generated by the monolayer penetration technique (7) as follows. BSA crystals were deposited on water in a Lucite trough consisting of two compartments separated by a wall parallel to the ends, and equal in height to the side walls of the trough. The top of this septum was sanded to make it wettable, and sufficient water covered it to permit the unhindered movement of the monolayer. The protein was allowed to spread at zero pressure over the entire trough area, and could then be compressed to a liquid-condensed state so that it covered only one of the compartments of the trough. In this way, the volume of solution in contact with the monolayer was fixed. Detergent was injected into the subphase with a 20-ml. hypodermic syringe, and mixing was effected by drawing solution into and extruding from the syringe for about one minute. Final concentration of SDS was 1.25×10^{-5} mole per liter; Cetab, 5×10^{-6} mole per liter. The effectiveness of this method of mixing was established by using dyes instead of detergents, and checking concentrations at various points in the trough. Detergent concentrations were chosen so that maximum film pressures would not exceed the collapse pressures of the protein monolayers.

After sufficient time for the surface pressure to reach a constant value, the pH of the subphase was brought to *ca.* 2.0 by injecting sulfuric acid. Potassium hydroxide was then added by injection in small increments, and the surface tension and pH were measured after each addition. The pH was measured by placing glass and KCl electrodes directly in the trough. Neutralization of the sulfuric acid resulted in the formation of salt at a final concentration of *ca.* 0.01*N*. Therefore, the effects of added salt on the extent of the penetration reaction were determined. NaCl and $CaCl_2$ were added incrementally to unbuffered solutions supporting SDS-BSA monolayers. The final concentration of NaCl was 1×10^{-3} mole per liter; $CaCl_2$, 3.3×10^{-2} mole per liter.

Although added electrolyte increased the extent of reaction somewhat (*ca.* 5 to 10%), surface pressures remained constant through the range of salt concentrations encountered in the titration experiments—*viz.*, above $5 \times 10^{-3}M$ for both salts. In addition, surface pressure changes of the pure protein monolayer in response to changes in salt concentration and pH were negligible compared with the pressure changes observed when detergent was in the subphase.

The data are presented as:

$$\Delta P = P_o - (P_P + P_D)$$

where P_o is the observed or experimental surface pressure, P_P is the initial surface pressure of the pure protein monolayer, and P_D is the surface pressure of the pure detergent at the experimental concentration. P_P was 5 dynes per cm. in all the experiments. P_D was less than 0.1 dyne per cm., the sensitivity of the apparatus. The surface pressure was calculated as the difference between the surface tension of the pure liquid interface, and the film-covered interface.

The contact angle of film-covered solution on the Wilhelmy plate increased with time. One could observe a nonzero contact angle after *ca.* 5 minutes' exposure of film to plate. This was handled in two ways. First, the plate was maintained below the surface except for the time required to measure the surface tension, *ca.* 5 to 10 seconds. Secondly, the plate was cleaned by placing it in a Bunsen flame every 3 to 4 minutes. These precautions prevented any observable dewetting of the Wilhemy plate. Finally, when measured, the magnitude of the maximum error in surface tension owing to dewetting was of the order of 1 to 2 dynes/cm. in the worst case.

Results

The reaction between insoluble protein monolayer and injected soluble surface-active agent was time-dependent. Injection of SDS under an unbuffered (*ca.* pH 6.0) liquid condensed BSA monolayer increased

P_o, which equilibrated in approximately 2 minutes. Injection of Cetab also increased P_o, which required 10 to 15 minutes for equilibration.

For SDS, the reaction proceeded to a reproducible end point rapidly —*viz.*, 1 to 2 minutes—when nonionic surface active impurities such as parent dodecyl alcohol, DOH, were removed by ethyl ether extractions. This "impurity effect" was verified by adding traces of alkyl alcohol—*viz.*, 1×10^{-9} mole per liter—to purified SDS, whereupon the penetration reaction rate was halved. A possible explanation for this behavior is that formation of an SDS-DOH interfacial complex reduced the SDS activity in the interface and consequently its rate of reaction with the protein monolayer. The reasons for the somewhat slower rate of reaction of Cetab with the protein film are more obscure. The reaction rate did not increase after extracting the detergent repeatedly. Two possible reasons for the time dependence in this case may have been that (1) the ether extraction method was not effective in removing surface active impurities, or (2) because of the greater bulk of the Cetab hydrocarbon chain, C_{16} *vs.* C_{12} for SDS, more time was required for diffusion and appropriate orientation before complex formation.

The reaction of interest—response of the monomolecular complex film to changes of pH—occurred more rapidly than the measurement technique could follow—*i.e.*, in less than *ca.* 10 seconds. Such rapid response implied that the dissociation equilibrium was mobile and depended principally upon the electrostatic state of the film.

SDS increased P_o to a maximum of 22 dynes per cm. (some 6 dynes per cm. greater than the collapse pressure of the BSA monolayer). This maximum (*see* Figure 1) occurred below pH 3.0. P_o then decreased with increase in pH. P_o was constant between pH 6.0 and 7.5 and between pH 2.7 and 3.3. There were two inflection points: at pH 4.7 and at pH 8.5. ΔP vanished at pH 10—*i.e.*, $P_o = P_P$ at pH 10.0.

Cetab increased P_o to a maximum of *ca.* 23 to 25 dynes per cm. (7 to 9 dynes per cm. in excess of the collapse pressure of the BSA monolayer) at about pH 12.0 (*see* Figure 2). P_o decreased with decrease in pH, and at pH 8.0 it became constant and remained constant between pH 8.0 and 5.0. P_o decreased rapidly between pH 5.0 and 4.0. At pH 4.0, the rate of change of P_o with pH slowed markedly and approached linearity.

Discussion

Glazer and Dogan (*4*) studied BSA spread as a monomolecular film on water. In general, the surface titration curve resembled that of BSA in solution, with two inflections in the pH ranges 3.5 to 6.5 and 10.0 to 13.0. They ascribed these two inflections to the ionization of carboxyl groups and neutralization of amino groups, respectively.

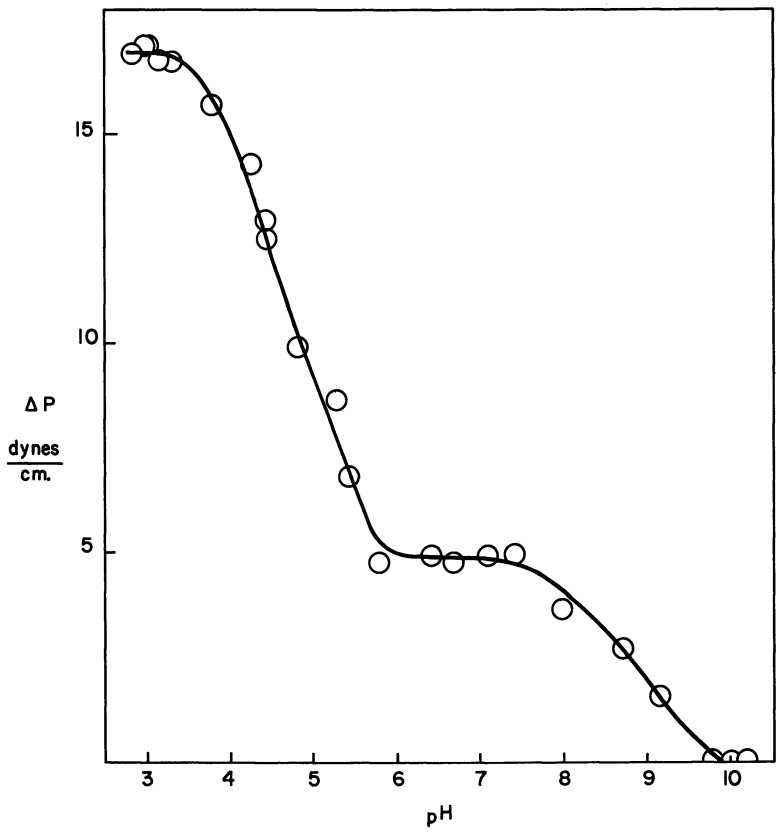

Figure 1. Effect of pH on surface pressure of a BSA monolayer spread on distilled water subsequently injected with SDS

SDS concentration: 1.25 × 10^{-5} mole per liter
Initial surface pressure of BSA monolayer: 5 dynes per cm.

There were two significant differences between the titration curve of BSA in aqueous solution and as a monomolecular film at the air–water interface. The first was that although the shapes of the curves were similar, the entire titration curve of the surface film was shifted to slightly more alkaline pH values, thereby yielding somewhat higher apparent pK values for the dissociating groups. Secondly, the neutralization of imidazolium groups could not be detected by the surface titration technique.

If it is assumed that the magnitude of the change in complex film surface pressure reflects the extent of protein-detergent interaction, it is possible to identify and characterize the binding groups.

The data indicate that the binding of detergent depended strongly on the presence of ionizing groups, SDS probably being bound to am-

monium groups, and Cetab to carboxyl groups. The decrease in P_o of the SDS-BSA monolayer with increase in pH was coincident with the titration curve of the pure protein monolayer in the carboxyl ionization pH range. Since SDS was probably bound at cationic ammonium groups, the decrease in SDS binding in this region was probably caused by electrostatic repulsion of the anionic detergent by the ionized carboxyl groups. This implies that either the protein carboxyl groups were close to the ammonium-binding sites or that SDS binding depended on the magnitude of the net positive charge of the protein.

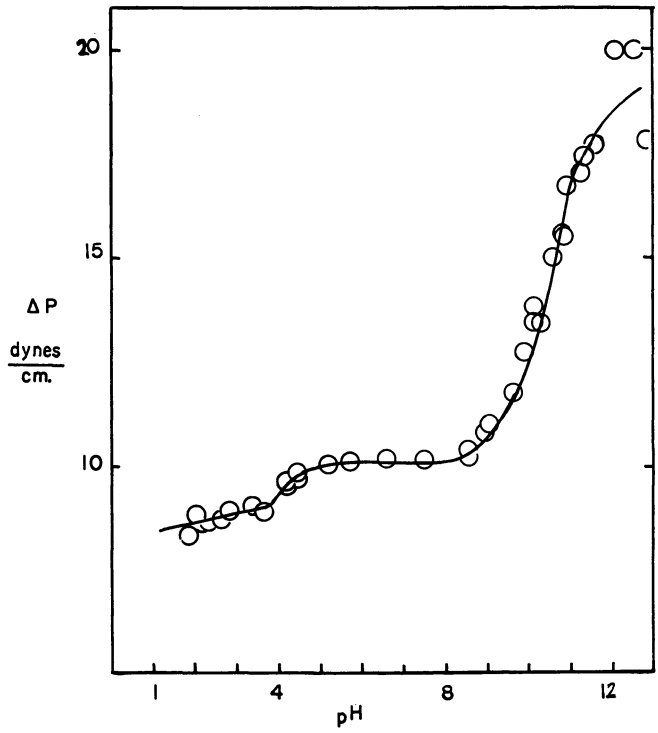

Figure 2. Effect of pH on surface pressure of a BSA monolayer spread on distilled water subsequently injected with Cetab

Cetab concentration: 5 × 10^{-6} mole per liter
Initial surface pressure of BSA monolayer: 5 dynes per cm.

According to Glazer and Dogan's data, the ammonium groups' p*K* should have been *ca.* 11.5. However, the p*K* of the SDS-BSA surface complex had a value of *ca.* 8.5. Shifts in p*K* of this order of magnitude—*i.e.*, 3 pH units—have been observed in titrations of monomolecular films of long-chain amines (5). The explanation offered for the shift in apparent

p*K* of these materials was that the proximity of charged amino groups led to the repulsion of protons (neutralization) at lower pH than would be required for neutralization in solution.

The shift in apparent p*K* of the SDC-BSA film may result from the formation of a surface film with structural characteristics strongly analogous to a monolayer of a long chain amine. The required characteristics would be formation of a surface structure which would lead to a high density of charged groups immersed in the aqueous phase, and formation of a bond which permits the bonding partners to retain their identities—*e.g.*, an ion pair.

These requirements would be fulfilled if SDS were bound to the BSA monolayer in the form of small aggregates or "pseudo-micelles." Such aggregates have been demonstrated to be formed as the result of the interaction of SDS and BSA in solution (2). Further, the electrostatic nature of the interaction was demonstrated by the fact that the complex was completely dissociated by adjusting pH to values above 10.0. Therefore, it is suggested that the cause of the marked shift in pK of the ammonium groups of the SDS-BSA surface complex was the presence of aggregates of SDS bound at cationic sites of the protein monolayer. It may be inferred from this hypothesis that the natural result of the interaction of anionic lipids with an interfacial protein film is the formation of a "mosaic" structure—one of the proposed characteristics of biological membranes.

The binding of Cetab by the BSA monolayer was coincident with the protein's titration curve through the alkaline pH region in which ammonium groups are neutralized. Although Cetab was probably bound at anionic carboxyl groups, the extent of the binding appeared to depend, as in the SDS-BSA system, on either the characteristics of the binding sites—*i.e.*, close proximity of anionic and cationic groups—or more generally, on the over-all electrostatic state of the protein monolayer.

Because Cetab was presumed to be bound to the protein carboxyl groups, the extent of interaction was expected to decrease rapidly at pH values below pH 4.0, approaching zero at *ca.* pH 2.0. The data indicate a trend in that direction between pH 5.0 and 4.0. However, at a pH slightly lower than 4.0, the downward concave curve became a straight line of shallow slope down to a pH of 1.5 to 2.0. This indicated substantial binding of Cetab at pH values where the carboxyl group binding sites should have been completely neutralized.

This behavior indicates that there may be two mechanisms for Cetab-BSA interaction:

$$\text{Cetab}^+ + \text{BSA—COO}^- \rightleftarrows \text{BSA—COO—Cetab} \quad (1)$$

$$\text{Cetab}^+ + \text{BSA—COOH} \rightleftarrows \text{BSA—COO—Cetab} + \text{H}^+ \quad (2)$$

Reaction 1 should predominate above pH 5.0 (carboxyl groups largely ionized) and Reaction 2 below pH 4.0 (carboxyl groups largely un-ionized). Reaction 1 represents an electrostatic association in which Cetab replaces H^+. The shape of the curve might therefore be expected to follow the acid-base titration curve. Reaction 2 is a displacement in which H^+ and $Cetab^+$ compete for the carboxylate binding site, the extent of the reaction depending upon the $[Cetab]/[H^+]$ ratio. Reaction 2 implies a measure of chemical specificity in the Cetab-BSA reaction. This is particularly relevant to the comparative effects of Cetab and SDS as germicidal agents as illustrated by the following facts (*1*). Cationic detergents penetrate bacterial cells at low concentrations, and are toxic at concentrations as low as 1×10^{-5} mole per liter. Anionic surface active agents are poor germicides even at high concentrations and penetrate bacterial cells to a far lesser extent than cationic agents. Washing bacterial cells after exposure to anionic surface active agents reverses the inhibition of growth caused by these materials. The growth-inhibition effect caused by exposure to cationic detergents cannot be reversed by washing.

Literature Cited

(1) Alexander, A. E., McMullen, A. I., *Research (London) Suppl.*, Surface Chemistry, **1949**, 309.
(2) Blei, J., *J. Colloid Sci.* **15**, 370 (1960).
(3) Engstrom, A., Finean, J. B., "Biological Ultrastructure," Academic Press, New York, 1958.
(4) Glazer, J., Dogan, M. Z., *Nature* **170**, 417 (1952).
(5) Glazer, J., Dogan, M. Z., *Trans. Faraday Soc.* **49**, 448 (1953).
(6) Putnam, F. W., *Advances Prot. Chem.* **4**, 80 (1948).
(7) Schulman, J. H., Hughes, A. H., *Biochem. J.* **29**, 1236, 1243 (1935).
(8) Strauss, U. P., Breuer, M., *J. Phys. Chem.* **64**, 228, (1960).

RECEIVED May 8, 1967.

Lipid Monolayers

Effect of Phosphatidyl Choline and Cholesterol on the Interaction of Dihydroceramide Lactoside with Rabbit γ-Globulin

GIUSEPPE COLACICCO and MAURICE M. RAPPORT[1]

Department of Biochemistry, Albert Einstein College of Medicine, Yeshiva University, Bronx, N. Y. 10461

Discontinuities are seen in the relationship between increase in film pressure, ΔΠ, and lipid composition following the injection of globulin under monolayers of lecithin–dihydroceramide lactoside and lecithin–cholesterol mixtures. The breaks occur at 80 mole % C_{16}-dihydrocaramide lactoside and 50 mole % cholesterol. Between 0 and 80 mole % lactoside and between 0 and 50 mole % cholesterol the mixed films behave as pure lecithin. Two possible explanations are: the formation of complexes, having molar ratios of lecithin-lactoside 1 to 4 and lecithin-cholesterol 1 to 1; and/or the effect of monolayer configurations (surface micelles). In this model, lecithin is at the periphery of the surface micelle and shields the other lipid from interaction with globulin.

The participation of ceramide lactosides in immunological reactions (*15*) prompted interest in the surface properties of these lipids. Previous work (*7*) on the nonspecific interaction of monolayers of synthetic dihydrocaramide lactosides with rabbit γ-globulin showed the dependence of the magnitude of the interaction, ΔΠ, on the initial film pressure of the lipid, the length of the fatty acid chain of the sphingolipid, the temperature, and protein concentration. The data were in accord with earlier experience in lipid–protein interaction (*10, 11, 12*) in show-

[1] Present address: New York State Psychiatric Institute, New York, N. Y.

ing that $\Delta\Pi$ decreased as the initial film pressure increased, $\Delta\Pi$ increased with increasing length of the fatty acid chain, and the curve relating $\Delta\Pi$ to protein concentration had marked discontinuities. A relationship between lipid structure and interaction with protein was seen. The magnitude of $\Delta\Pi$ decreased in the order cholesterol > C_{16}-dihydroceramide lactoside > phosphatidyl ethanolamine > phosphatidyl choline >> sphingomyelin.

Although glycosphingolipids are the specific lipid components in the antigen–antibody complex, their activity is markedly enhanced by other (auxiliary) lipids such as lecithin and lecithin–cholesterol mixtures (*15*). The present study deals with the effect of lipid composition on the penetration of lactoside–cholesterol and lactoside–lecithin monolayers by rabbit γ-globulin. We also investigated the lecithin–cholesterol system. Furthemore, since criteria for the existence of lipid-lipid complexes in monolayers are still few (*8*, *17*), we have used infrared spectroscopy to examine lipid mixtures for the presence of complexes.

Experimental

Materials. LIPIDS AND PROTEIN. The sources of synthetic *N*-palmitoyl and *N*-stearoyldihydrosphingosyl lactosides, phosphatidyl choline (egg), cholesterol, and rabbit γ-globulin have been described (*7*).

WATER AND SALT SOLUTIONS. Distilled water was redistilled over alkaline permanganate from all-glass apparatus. Water of low conductivity (1 μmho per cm.) was collected in polyethylene bottles and stored at room temperature (25°C.) for not longer than 2 days before use. Phosphate buffer (pH 7.0) containing 0.04*M* potassium phosphate and 0.10*M* NaCl was used for the aqueous subphase. It was prepared with low conductivity water and reagent grade salts and stored in polyethylene bottles at room temperature for not longer than 5 days. Protein solutions (1 mg. per ml.) were prepared with this buffer and stored in borosilicate glass flasks for not longer than 5 days at 5°C.

ORGANIC SOLVENTS AND LIPID SOLUTIONS. Reagent grade solvents were distilled before use. The lipids were dissolved in chloroform–methanol (85 to 15 v./v.) at a concentration of about 0.5 mg. per ml. and stored in glass-stoppered borosilicate glass tubes for not longer than 5 days at 5°C. Lipid mixtures were freshly prepared from the stock solutions of the individual components.

Apparatus and Procedure. SURFACE ISOTHERMS. The technique for determining the Π–*A* and ΔV–*A* curves of the lipid films has been described (*6*). Briefly, the Wilhelmy plate method was used to measure surface tension, from which the surface pressure was calculated ($\Pi = \gamma_{H_2O} - \gamma_{film}$). The surface potential was measured by means of a radioactive (^{226}Ra) air electrode and a saturated calomel electrode connected to a high impedance model 610 B Keithley electrometer (Keithley Instruments, Cleveland, Ohio).

LIPID–PROTEIN INTERACTION. The technique of Doty and Schulman was used to bring lipid monolayer and protein into contact (*7*). A rec-

tangular Lucite trough (25 × 7.6 cm. and 1.9 cm. deep) was filled to the rim with the aqueous subphase at 25°C. The surface was cleaned, and the lipid was spread. The film was then compressed until the pressure was 2 dynes per cm., the total area being about 80 sq. cm. Stirring of the subphase was started, and after 1 minute the protein was injected deep into the subphase. The fall in surface tension (increase in surface pressure) was recorded at 1-minute intervals for 40 minutes.

The subphase under the monolayer was stirred by a Teflon-covered magnetic bar that was moved back and forth over the length of the trough by a motor-driven mechanism. The fastest rate which did not cause disruption of the monolayer was about 4 strokes per minute.

INFRARED SPECTRA. A Perkin-Elmer model 237 spectrometer was used. Solutions of 5 to 10 mg. per ml. of lipid in spectral grade chloroform were placed in a NaCl microcell of 1.0-mm. path length for study in the region from 2.5 to 6.0 microns. The film technique was used for observations between 5 and 15 microns, with a beam condenser and attenuator (Perkin-Elmer, Norwalk, Conn.). The lipid, 75 to 100 μgrams in either chloroform or chloroform–methanol 85 to 15, was deposited on 1 sq. cm. of the NaCl plate, and the solvent was removed by evaporation under an infrared lamp for 10 minutes.

Results

Lipid-Protein Interaction. Although measurements were made over a 40-minute period, for convenience in the presentation of the results (7), only the rise in pressure at 15 minutes is given. A linear relationship was found between film penetration, $\Delta\Pi$, and lipid composition for mixtures of cholesterol and either *N*-palmitoyl or *N*-stearoyldihydrosphingosyl lactoside (Figure 1).

In contrast, marked discontinuities were observed with mixtures containing phosphatidyl choline (Figure 2). A 20 mole % concentration of lecithin in C_{16}-dihydroceramide lactoside or 25 mole % in C_{18}-dihydroceramide lactoside lowered the value of $\Delta\Pi$ to that for pure lecithin.

Similarly, a marked discontinuity was found at 50 mole % in the curve relating $\Delta\Pi$ to the composition of cholesterol–lecithin films (Figure 3). Up to 50 mole % cholesterol the magnitude of $\Delta\Pi$ was the same as with lecithin alone; above this, $\Delta\Pi$ increased linearly with cholesterol concentration.

Infrared Spectra. The effect of composition on infrared absorption of cholesterol–lecithin mixtures was striking in two regions of the spectrum—near 2.8 and 9.2 microns—which are associated with O-H and P-O-C stretching frequencies, respectively (Figure 4).

Pure cholesterol in $CHCl_3$ solution has a sharp peak at 2.8 microns, owing to the free O-H group. Lecithin has a broad absorption between 2.9 and 3.2 microns, attributed to bound water (2). The peak at 2.8 microns disappeared in mixtures containing 50 mole % or more of

lecithin. This indicates that in these mixtures the cholesterol is probably bound to lecithin in an equimolar complex. The absorption at 2.8 microns was shifted to 2.9 microns, producing a shoulder on the broad "water peak" of lecithin. The intensity of the absorption at 2.8 microns of pure cholesterol solutions increased with concentration but without any shift. This indicates that neither OH-OH interactions of cholesterol nor possible traces of water in the chloroform could account for the shift observed with lecithin–cholesterol mixtures.

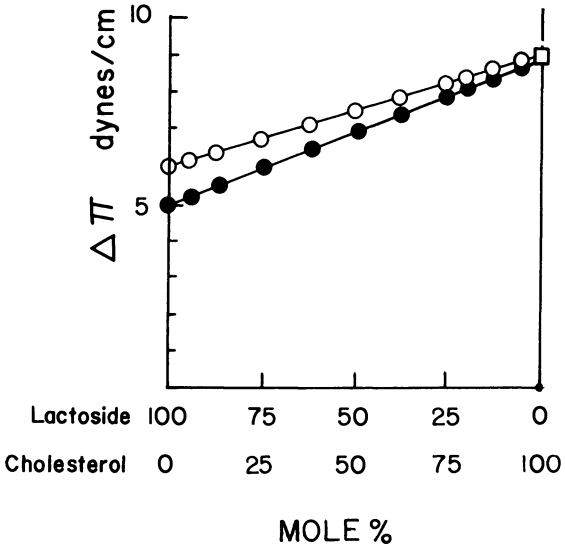

Figure 1. Effect of lipid composition on surface pressure of films in interaction with rabbit γ-globulin at 1 μgram/ml.

○ *Cholesterol–C_{16}-dihydroceramide lactoside*
● *Cholesterol–C_{18}-dihydroceramide lactoside*
Measurement at 15 minutes
Initial film pressure, 2 dynes/cm.
0.04M phosphate buffer, 0.1M NaCl, pH 7.0, 25°C.

The infrared spectrum of lecithin was affected markedly in the region of the P-O-C absorption. The peaks between 9.1 and 9.4 microns showed a continuous shift from the higher frequency to the lower frequency component as the concentration of cholesterol increased from 0 to 75 mole %. The two peaks were equal at a composition of 50 mole % (Figure 4).

The infrared spectra of systems containing lactoside could not be analyzed in a similar way because the absorption of the hydroxyl groups of the sugar masked the absorptions of cholesterol at 2.8 microns and of the P-O-C group of lecithin between 8 and 10 microns.

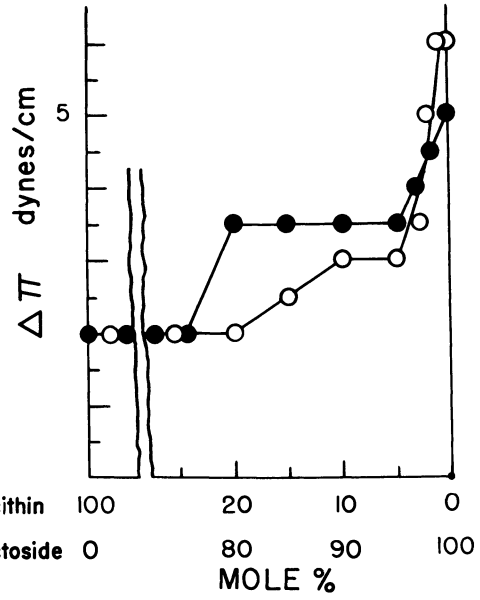

Figure 2. Effect of lipid composition on surface pressure of films in interaction with rabbit γ-globulin at 1 μgram/ml.

○ *Egg lecithin–C_{16}-dihydroceramide lactoside*
● *Egg lecithin–C_{18}-dihydroceramide lactoside*
Measurement at 15 minutes
Initial film pressure, 2 dynes/cm.
0.04M phosphate buffer, 0.1M NaCl, pH 7.0, 25°C.

Discussion

A remarkable effect of lecithin is seen in the discontinuities of the ΔΠ curves for both the lecithin–lactoside and the lecithin–cholesterol systems (Figures 2 and 3) when these are compared with the linear increase of ΔΠ in the cholesterol–lactoside system (Figure 1).

Since these effects probably result from the organization of lipids in the monolayer, we must first consider criteria for ascertaining the nature of lipid-lipid associations. Moreover, since the discontinuities in the ΔΠ–composition curves probably reflect transitions in monolayer configurations, we discuss these from the standpoint of penetration of protein into the lipid film and its relation to specific lactoside-antibody interaction.

Lipid-Lipid Associations

Three criteria for lipid-lipid interactions in lipid mixtures are the mean area of the lipids in the mixed film, the surface potential of the mixed monolayer, and the infrared spectra of the lipid mixtures.

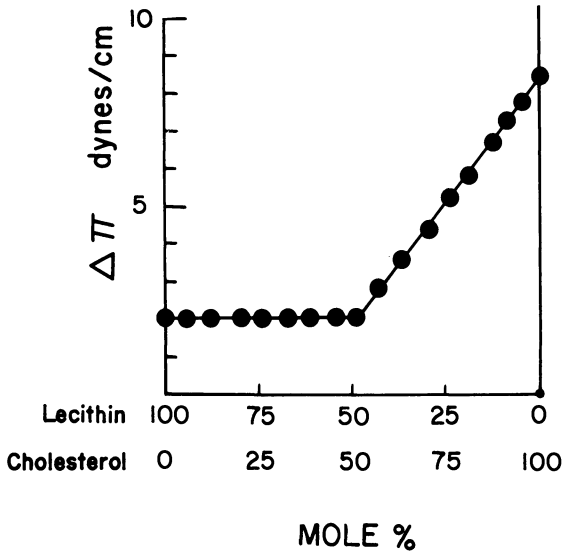

Figure 3. Effect of lipid composition on surface pressure of films of egg lecithin–cholesterol in interaction with rabbit γ-globulin at 1 μgram/ ml.

Measurement at 15 minutes
Initial film pressure, 2 dynes/cm.
0.04M phosphate buffer, 0.1M NaCl, pH 7.0, 25°C.

Mean Area. If the association of two lipids in the monolayer is accompanied by a reduction in the average molecular area (film contraction), the curve relating mean area to composition will show a deviation from molecular additivity (ideal miscibility). The significance of such contractions is still not clear (*8*, *17*), and contraction in itself is not a sufficient criterion for detecting interaction.

On the one hand, the cholesterol–lactoside system did not show film contraction (unpublished data). This was expected since the monolayers of dihydroceramide lactosides (*7*) and of cholesterol are not compressible. On the other hand, lecithin–lactoside and lecithin–cholesterol systems did show contraction, which could have been predicted since the lecithin monolayer is of the expanded type and is very compressible. (The area per molecule of lecithin at 2 dynes per cm. is large, 110 sq. A., as opposed to 52 sq. A. for C_{16}-dihydroceramide lactoside and 40 sq. A. for cholesterol.)

However, no direct correlation exists between contraction of the mixed film and discontinuities in the ΔΠ–composition curve. The sharp breaks at 80 mole % C_{16}-dihydroceramide lactoside (Figure 2) and at 50 mole % cholesterol (Figure 3) are not seen in the mean area–composition curves (unpublished data). Since the ΔΠ value is constant between

20 and 100 mole % lecithin with lactoside (Figure 2) and between 50 and 100 mole % lecithin with cholesterol (Figure 3), lecithin probably forms a complex with the other lipid.

Surface Potential. Shah and Schulman have proposed that interaction between dipoles of uncharged lipids in mixed monolayers should result in a change in surface potential, ΔV. Linearity of the relation of ΔV to composition of the lecithin-cholesterol monolayer was taken to indicate absence of interaction (*17*). We do not agree with Shah and Schulman, since surface potential does not appear to be a valid criterion for assaying interaction between dipoles of uncharged lipids. Except for the speculations of Shah and Schulman (*17, 18*), there is neither theoretical nor experimental evidence that dipole-dipole interactions have

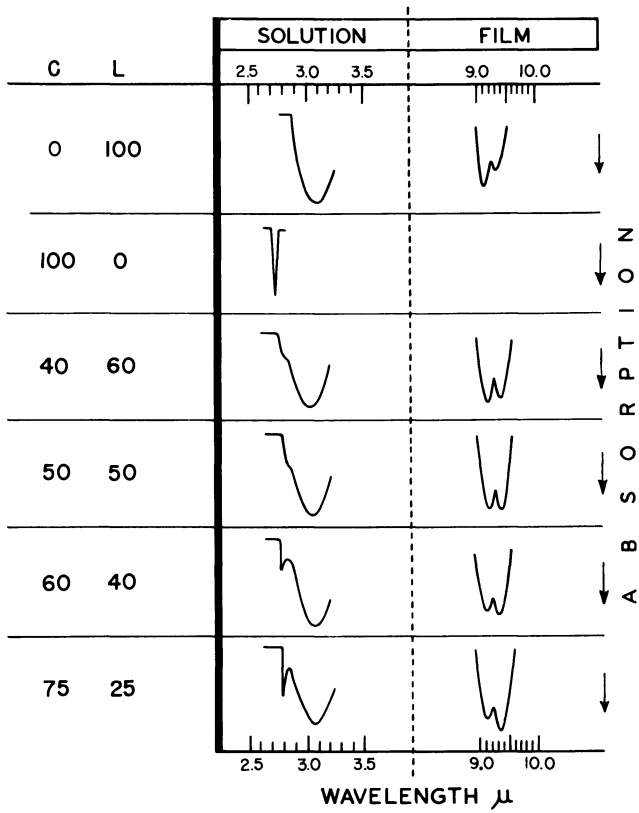

Figure 4. Infrared absorption spectra of cholesterol (C)–lecithin(L) mixtures

Solution in chloroform, 5 to 10 mg./ml., 25°C.; path length, 1 mm.
Film, 75 to 100 μgrams lipid on 1 sq. cm. of NaCl plate 2 mm. thick

any direct effect on the surface potential. These interactions should not be confused with charge-charge interactions.

Therefore, neither mean area nor surface potential changes are a valid criterion for lipid-lipid interaction. Although large deviations from ideality were seen in the mean area–composition curves and little or no deviations were seen in the ΔV-composition curves, these curves did not show the sharp discontinuities present in the $\Delta\Pi$-composition curves. However, the absence of such discontinuities indicates neither the presence nor the absence of molecular interactions.

Infrared Spectra. The shift of the absorption of the OH group of cholesterol to lower frequency (from 2.8 to 2.9 microns) in the presence of 50 mole % or more of lecithin indicates that cholesterol is involved in an equimolar complex with lecithin, probably through hydrogen bonding. However, the H acceptor is still not known. Although three-dimensional models support the view that the oxygen of the P-O-C group of phosphatidylcholine is a possible H bond acceptor from the OH group of cholesterol, the interpretation of the infrared absorption data is complicated by the fact that the P-O-C peak (9.1 to 9.4 microns) changes continuously from 0 to 75 mole % cholesterol, whereas the shift of the OH peak is no longer discernible above 50 mole % cholesterol (Figure 4).

The infrared evidence for hydrogen bonding between cholesterol and lecithin in chloroform solution is no evidence of a similar complex in the monolayer but suggests such a possibility. It does not exclude the hydrophobic bonding suggested by Chapman from NMR studies of the aqueous suspensions of equimolar mixtures of cholesterol and lecithin (*3*).

Monolayer Configurations

Film penetration studies show unequivocally that lecithin–cholesterol mixtures containing from 0 to 50 mole % cholesterol and lecithin–lactoside mixtures containing from 0 to 80 mole % C_{16}-dihydroceramide lactoside have the same effect as pure lecithin. This suggests the presence of a lipid complex in which lecithin prevents the interaction of the cholesterol or ceramide lactoside with globulin. Over these ranges of composition the lipid film would consist of a mixture of the lecithin-cholesterol or the lecithin-lactoside complex with excess lecithin. One may picture two models in which the protein contact is restricted to molecules of lecithin. In one, individual polar groups of the protein interact with the excess lecithin molecules as well as with the lecithin portions of the complex. In the other model, the protein as a whole interacts with the lecithin sites of polymeric lipid structures. The latter, which could be referred to as surface micelles (*1*), are visualized also through the term "mono-

layer configurations." The two terms are not interchangeable. Whereas the surface micelle is a physical entity, monolayer configurations are meant to convey the concepts of orientation of molecules and topography of the monolayer.

Intermolecular Area and Film Compressibility. Since the observations on film penetration, $\Delta\Pi$, serve to define discontinuities in film structure, the relation of $\Delta\Pi$ to intermolecular areas and film compressibility (*13, 16*) requires some analysis. Does protein penetrate the interface simply because the lipid monolayer is compressible and has available intermolecular areas, or does the protein interact with the lipid?

Schulman (*16*) and Eley and Miller (*12*) pointed out that, with monolayers which are incompressible and thus contain little free area, a small quantity of protein is sufficient to cause a large rise in pressure (such as that obtained with cholesterol).

The phenomena of intermolecular area and film compressibility do not take into account the mechanism of lipid-protein interaction, nor do they offer a satisfactory explanation for the most recent observations. When applied to the interaction of lipid mixtures with globulin, they lead to an absurdity. To have the same value of $\Delta\Pi$ at 80 mole % lactoside, 50 mole % cholesterol, and 100 mole % lecithin would require the same intermolecular area for films having these compositions. This is not true. Moreover, on the basis of intermolecular area and compressibility one would have expected the magnitude of $\Delta\Pi$ values to be in the order: cholesterol $>$ spingomyelin $=$ hydrogenated egg lecithin $=$ egg lecithin. However, in the interaction of these lipids with rabbit γ-globulin the values of $\Delta\Pi$ were in the order: cholesterol $>$ hydrogenated egg lecithin $=$ egg lecithin $>>$ sphingomyelin.

An alternative explanation for these data may be found by considering monolayer configurations. In a suitable model, the protein as a whole would penetrate between the surface micelles. Two new parameters should thus become important in studying film penetration: intermicellar area, and structure and orientation of lipid molecules at the periphery of the surface micelles.

State of Protein in Lipid-Protein Monolayer. According to Doty and Schulman (*9*), Matalon and Schulman (*14*), and Eley and Hedge (*10, 11, 13*), protein coming into contact with the lipid film unfolds, and its hydrophobic residues penetrate between the hydrophobic chains of the lipid; the polar groups of the lipid interact with the peptide groups of the protein. The salient feature of this model is the uniform distribution (interpenetration) of the side chains of the protein between the hydrophobic chains of the lipid.

This representation is not supported by two observations. One is that when either trypsin or pronase was injected into the subphase con-

taining protein at equilibrium with the lipid monolayer, no fall in surface pressure was observed although hydrolysis of the protein in the subphase was extensive. If the protein, after penetration in the monolayer, were in the form of extended polypeptide chains, the peptide bonds would be more susceptible to attack by proteolytic enzymes. The release of soluble peptides from the film into the subphase should have caused a decrease in surface pressure, but this was not the case. The absence of appreciable hydrolysis of the protein in the film could suggest that, in entering regions of low dielectric constant at the air-water interface, the protein changes to a more compact structure and is not accessible to the enzyme (*4, 5*).

The second observation which does not support the unfolded protein model is that when phospholipase A (*N. naja* venom) was injected into the subphase under the lipid monolayer at equilibrium with globulin, lecithin was readily attacked, as indicated by the rapid fall of surface potential (*4, 5, 6*). If the penetrated protein were to cover entirely the polar groups of the lipid facing the aqueous subphase (as postulated in the unfolded protein model), the lipid molecules should not be accessible to the lipolytic enzyme.

A model that is consistent with these observations of the action of trypsin and phospholipase A and with the discontinuities in the $\Delta\Pi$-composition curves (Figures 2 and 3) is one in which the lipid monolayer is not a continuous palisade of uniformly oriented lipid molecules but rather an assembly of surface micelles. In this model, proposed by Colacicco (*4, 5*), the protein first comes into contact with the lipid molecules at the periphery of the surface micelles and then inserts itself as a unit between them. This is the basis for the generalized nonspecific interaction between lipids and proteins which results in increase of surface pressure. One may thus explain the identical $\Delta\Pi$ values obtained with films of lecithin and 80 mole % lactoside by picturing the lecithin molecules outside and the lactoside molecules inside the surface micelles. In this model lecithin prevents the bound lactoside from interacting nonspecifically with globulin and produces the same increase in pressure as with a film of pure lecithin. In the mixed micelle the lactose moiety of the lactoside protrudes into the aqueous subphase. Contact of the protein with these or other nonperipheral regions of the surface micelle would not increase the surface pressure.

With this model one might predict that when the lactose moiety is responsible for a specific interaction with protein (as in interaction with antibody directed against lactose), binding of the specific protein to the lactose would block its further penetration into the intermicellar (interlecithin) spaces. Experiments in which a specific antilactoside antibody was used in place of globulin (unpublished data) showed that this was indeed the case. The $\Delta\Pi$ value was much smaller than with nonspecific

globulin. The large value of $\Delta\Pi$ characteristic of the nonspecific interaction was restored when the specific interaction was inhibited by the presence of 0.1*M* lactose.

Conclusions

The role of lecithin as an auxiliary lipid in the specific interaction of lactosides with globulin in monolayers is related to two processes: complex formation between 3 or 4 molecules of lactoside and each lecithin molecule, and the protection of the lactoside molecules in surface micelles from nonspecific interaction. The location of lecithin at the periphery of the surface micelle would explain why the mixed micelle behaves as lecithin in nonspecific interaction. Lactoside molecules, located in the center of the surface micelle, would be in a position to interact specifically with antibody in the aqueous subphase (5).

The nature of the lecithin-cholesterol association is probably also that of a complex (1 to 1), in which the OH group of cholesterol is involved through hydrogen bonding. It is not known, however, whether the monolayer consists of a uniform population of bimolecular complexes or of configurations (surface micelles) in which cholesterol molecules are surrounded by an equal number of lecithin molecules.

The concept of monolayer configurations is particularly useful in explaining penetration of the protein as a unit, in a form in which it has more structure than in solution. Studies of interactions between protein and monolayers of mixed lipids are very useful for examining the nature of lipid-lipid associations.

Literature Cited

(1) Abood, L. G., Rushmer, D. S., ADVAN. CHEM. SER. **84**, 169 (1968).
(2) Chapman, D., "The Structure of Lipids," Wiley, New York, 1965.
(3) Chapman, D., Penkett, S. A., *Nature* **211**, 1304 (1966).
(4) Colacicco, G., *J. Am. Oil Chemists' Soc.*, in press.
(5) Colacicco, G., *J. Colloid Interface Sci.*, in press.
(6) Colacicco, G., Rapport, M. M., *J. Lipid Res.* **7**, 258 (1966).
(7) Colacicco, G., Rapport, M. M., Shapiro, D., *J. Colloid Interface Sci.* **25**, 5 (1967).
(8) Demel, R. A., Van Deenen, L. L. M., Pethica, B. A., *Biochim. Biophys. Acta* **135**, 11 (1967).
(9) Doty, P., Schulman, J. H., *Discussions Faraday Soc.* **6**, 21 (1949).
(10) Eley, D. D., Hedge, D. G., *Discussions Faraday Soc.* **21**, 221 (1956).
(11) Eley, D. D., Hedge, D. G., *J. Colloid Sci.* 11, 445 (1956).
(12) Eley, D. D., Miller, G., *Proc. Intern. Congr. Surface Activity, 3rd, Cologne 1960*, **II**, B157.
(13) Eley, D. D., Hedge, D. G., *J. Colloid Sci.* **12**, 419 (1957).
(14) Matalon, R., Schulman, J. H., *Discussions Faraday Soc.* **6**, 27 (1949).
(15) Rapport, M. M., *Res. Publ. Assoc. Nervous Mental Diseases* **40**, 159 (1962).

(16) Schulman, J. H., *Discussions Faraday Soc.* 21, 272 (1956).
(17) Shah, D., Schulman, J. H., *J. Lipid Res.* 8, 215 (1967).
(18) *Ibid.*, 6, 341 (1965).

RECEIVED July 17, 1967. Work supported by research grants from the American Cancer Society (P-410) and the National Science Foundation (GB-5984).

15

Surface Interaction of Calcium and ATP with Phospholipids and Other Surfactants

L. G. ABOOD and D. S. RUSHMER

Center for Brain Research and Department of Biochemistry, University of Rochester, Rochester, N. Y.

Surface pressure, potential, and adsorption studies were carried out on lipid surface films to elucidate the nature of interaction occurring between the lipids, calcium, psychotomimetic agents, and ATP. Results demonstrate that (a) a strong interaction is occurring between lipids and the drugs, resembling that occurring between Ca^{2+} and the lipids; (b) an interaction occurs between the drugs, ATP, and lipids; (c) the drugs do not interfere with the interaction of Ca^{2+} with lipids, but Ca^{2+} can influence the interaction of the drugs with lipids. Evidence, including electron microscopy, shows that phospholipid–calcium–ATP surface complexes can occur. The results suggest that calcium and ATP may regulate membrane permeability.

In recent years the role of calcium in the regulation of membrane permeability, particularly in excitatory tissues, has received considerable attention (*see* Ref. *11* for review). Calcium is evidently required for the "coupling" phenomenon between excitation and contraction in muscle contraction, while its removal from neural tissue is associated first with lowered excitatory threshold and eventual inexcitability. Among the many problems concerning the role of calcium in regulating membrane permeability, the most pressing are those regarding the localization of calcium and the nature of its interaction with the macromolecular and other components of the membrane. It has been suggested that the excitatory membrane is comprised of complexes of phospholipid, adenosine triphosphate (ATP), and calcium which undergo dissociation during excitation (*1*). [The following abbreviations were used: PMCG = 1-methyl-3-piperidyl cyclopentylphenyl glycolate, BQ = 3-quinuclidyl ben-

zilate, ATP = adenosinetriphosphate, EDTA = ethylenediaminetetraacetate.]

To demonstrate the involvement of such a mechanism in bioelectric phenomena of nerve membranes, various experimental approaches have been used. It has been observed that a group of substituted glycolic acid esters of heterocyclic imino alcohols, which are potent psychotomimetic agents (*2*), can modify the bioelectric and structural characteristics of excitatory membranes. It can be shown, for example, that the lowered intracellular resting potential following the removal of Ca^{2+} from frog sartorius muscle can be restored by adding the glycolate esters to the bathing solution (*3*). Evidently, the drugs can substitute for Ca^{2+} in maintaining the resting potential and are able to interact with those components of the membrane normally occupied by Ca^{2+}. As discussed elsewhere (*1, 11*), there is good evidence for believing that the Ca^{2+} is associated largely with phospholipids and other anionic lipids present in the membrane. The use of lipid films may, thus, help clarify the similarity in the action of Ca^{2+} and the drugs.

Another significant finding is that ATP, which readily complexes with Ca^{2+} and other divalent cations, can also interact with the drugs. Among the observations suggesting an interaction of glycolate esters with ATP were the following: (a) ATP (and other chelates) interfered with the uptake of the drug by isolated sartorius muscle (*1*); (b) certain enzymatic reactions in sartorius muscle requiring ATP, particularly fructose-6-phosphate + ATP → fructose-1,6-diphosphate + ADP catalyzed by phosphofructokinase, are inhibited by the drugs; (c) the drugs formed associations with Ca^{2+} and phosphate ions (*1*); (d) the partition coefficient of the glycolate esters between an aqueous phase (pH 8.0) and various organic solvents was modified significantly by the presence of ATP. More recently evidence from surface pressure and viscosity studies with various lipid surface films have suggested that an interaction occurred between ATP and the glycolate esters (*13, 14*).

In the present study various surface measurements were made on interfacial lipid films to analyze in more detail the nature of interactions of lipids, Ca^{2+}, ATP, and the glycolate esters. Surface pressure-area and surface potential-area diagrams were obtained on surface films of stearic acid, lecithin, and a mixture of brain lipids with Ca^{2+}, ATP, and the drugs present in the subsolution, individually or in combination. Using radioactive Ca^{2+}, ATP, and drug, quantitative measurements were made on the surface adsorption of these substances to lipid films. In addition, electron microscopy was performed on brain lipid films formed in the presence or absence of Ca^{2+} and ATP. Our objective was to establish the existence of surface complexes involving these substances with the hope

of better understanding the role of Ca^{2+} and ATP in membrane phenomena and the mechanism of action of the glycolate esters.

Experimental

Radioactivity Measurements. The surface adsorption of radioactively labeled compounds was measured by the technique of Aniasson (*5*). ^{45}Ca was measured using a Geiger-Müller tube with a mica end window (thickness = 150 μgram/sq. cm.) housed in a lead shield and mounted 0.5 cm. from the surface to be counted. ^{14}C and tritium-labeled compounds were measured by the windowless gas flow technique employing a Nuclear-Chicago G-M detector (model D-47K2). To prevent contamination and damage to the detector by moisture the "Q" gas flow pressure was maintained at 15 p.s.i.g. The measurements were carried out in Teflon planchets 0.6 cm. high, diameter 2 cm., and having a final fluid volume of 1.2 ml. All measurements were done in a solution of $10^{-2}M$ NaCl, which was adjusted to a given pH with tris(hydroxymethylaminomethane) in the alkaline range and acetic acid or HCl in the acid range. The amount of ^{45}Ca or ATP-^{14}C in each planchet was about 10^{-3} μcuries and of PMCG-^{3}H, 10^{-2} μcuries. Nonradioactive carrier was added to adjust to the final concentration required. Stearic acid was dissolved in petroleum ether and beef brain lipid in ethanol–ethyl ether (2:1 v./v.), both at a concentration of 0.2 mg./ml. After the sample was counted in the absence of lipid, 0.01 ml. of the lipid was applied to the surface and counted at various intervals up to periods of 8 hours.

The amount of the radioisotope adsorbed to the surface film was calculated according to the expression (*12*):

$$\Gamma = \frac{I_m - I}{SA}$$

where I is the radioactivity (c.p.m.) of the solution without the surface film, I_m the radioactivity with the film, S the specific activity (c.p.m./mole) of the isotope, and A the surface area (sq. cm.) exposed to the G-M detector.

Surface Potential. The apparatus used to measure surface potentials was the vibrating electrode type after the design of Yamins and Zisman (*19*). The stainless steel vibrating electrode had a surface area of approximately 4 sq. cm. and was attached with a plastic rod to the center of a small loud speaker, connected to an audiooscillator with an output of 400 c.p.s. The Langmuir trough, machined from Teflon, had a capacity of approximately 50 ml. and dimensions of 12 cm. × 7 cm. × 0.5 cm. The indifferent electrodes were two Beckman fiber junction calomel reference electrodes wired in parallel, a configuration which tended to increase the signal-to-noise ratio of the apparatus. A Tektronix type 122 preamplifier employing differential inputs was used for signal amplification at a gain of 1000. The output of the preamplifier was displayed on a Tektronix type 502 oscilloscope, and the sensitivity of the system as displayed was 20 μvolts/cm. The concentration of the lipid solution used for spreading on the troughs was 0.2 to 0.3 mg./ml., the solvent being

petroleum ether for stearic acid and ethanol–ethyl ether (2:1) for lecithin and brain lipid. A microsyringe was used to apply the lipid uniformly on the surface, and 3 minutes were allowed to lapse before the first potential or pressure reading was taken. The film was compressed slowly in increments of 1 cm. Surface potential measurements were made with the drugs dissolved in $10^{-2}M$ NaCl (pH adjusted as described above); since film compression did not alter ΔV of the drug alone, the measurement was made in the expanded state. Surface pressure was measured by the Wilhemy plate method (*8*), and the details are described elsewhere (*13*).

Materials. The water used for all purposes was double-distilled (once with glassware) and deionized (final conductance was less than 1×10^{-6} ohm^{-1} $cm.^{-1}$). Stearic acid (obtained from Sigma Chemical Co.) was at least 99% pure as determined by silica gel thin-layer chromatography (*4*), and the synthetic L-α(β,γ-dipalmitoyl)lecithin was about 90% pure (*see* Ref. *13* for analysis). The ATP-^{14}C and its derivatives were obtained from Nuclear-Chicago or New England Nuclear Corp. and were found to be 95–98% pure as determined by cellulose thin-layer chromatography (*16*).

The beef brain lipid was prepared by homogenizing the cerebral gray matter of fresh beef brain in 20 volumes of chloroform–methanol (2:1), filtering, and then drying and storing *in vacuo*. A sample of the dried lipid was added to ethanol–ethyl ether (2:1), heated at 50°C. for 10 minutes, and filtered. A portion of the brain lipid was extracted with twice its volume of $10^{-4}M$ EDTA (pH 7) to remove Ca^{2+} and other metals bound to the lipid. The extracted lipid, which was dried *in vacuo*, then taken up in the original volume of ethyl ether, was designated the EDTA-extracted lipid. The beef brain lipid (in its final form) was shown by thin-layer chromatography (*4*) to be comprised of the following (% total weight): cholesterol 8%, cholesterol esters 4%, cerebroside 15%, sphingomyelin 7%, phosphatidyl ethanolamine 26%, phosphatidyl serine 7%, phosphatidyl choline 15%, plasmalogen 5%, gangliosides 3%, phosphatidyl peptide 5%, phosphoinositides 1.5%, cardiolipin 2%, unidentified 3%. Since surface films comprised of cholesterol, cholesterol oleate, or cerebrosides alone or in combination adsorbed neither ^{45}Ca nor ATP-^{14}C, while pure phosphatides are known to adsorb Ca^{2+}, it can be assumed that the adsorption occurred with phospholipids.

Preparation of Tritium Labeled PMCG. Tritiated PMCG was prepared by reaction of tritiated 1-methyl-3-hydroxypiperidine with the acid chloride of cyclopentylphenyl glycolic acid according to the method of Biel *et al.* (*7*) (the authors are indebted to him for preparing this compound). Tritiated 1-methyl-3-hydroxypiperidine was prepared by reduction of 3-hydroxypyridine methyl bromide by tritium gas (*2*). A total of 40 grams of 3-hydroxypyridine methyl bromide were dissolved in 400 ml. of methanol containing 4 grams of rhodium on alumina catalyst and exposed to an atmosphere of 3 curies of tritium gas at 40 p.s.i.g. for 2 hours at 27°C. After the catalyst was filtered off, the methanol was removed *in vacuo* until the solid began to separate. To the methanol concentrate was added with stirring 12 grams of sodium methoxide, followed by 250 ml. of anhydrous ethyl ether to precipitate the NaBr. After filtrating the precipitated NaBr, the filtrate was desiccated over

anhydrous K_2CO_3 and concentrated by distilling off methanol and ethyl ether through a Vigreaux column. The remaining residue was subjected to vacuum distillation, and the major fraction of the residue distilled at 80°–85°C. (12-15 mm.). The n^{25}_D was 1.4755 (identical to known material), and the yield was 15.2 grams. The radioactive specific activity of the final material was 1.2 curies/mmole.

Electron Microscopy. The electron microscopic studies (done by Manuel P. del Cerro) were carried out with surface films where the amount of brain lipid added was over five times more than needed to form a monomolecular film [total phospholipid (as orthophosphate) = 5×10^{-9} moles/sq. cm. surface]. To the surface of a solution containing $10^{-4}M$ ATP, $10^{-4}M$ $CaCl_2$, $10^{-2}M$ NaCl (adjusted to pH 7.5) in a final volume of 40 ml. in a 10 cm. Petri dish was applied 0.2 ml. (0.2 mg.) of beef brain lipid (in 0.02 ml. drops throughout the surface from a microsyringe) dissolved in ethanol–ethyl ether. A second Petri dish contained no ATP. After the dishes stood exposed to the atmosphere for 6 hours (28°C.), a saturated solution of gelatin was added through a syringe to make a final concentration of 5%. After the solution gelled (1 hour at 5°C.), it was exposed to osmium tetroxide vapors overnight. The gel was then successively exposed for 30 minutes each to 50%, 75%, and 100% ethanol at 0°C. The material was then embedded in Epon and sectioned for electron microscopy.

Results

The surface adsorption of tritiated PMCG and the surface potential of PMCG and BQ(3-quinuclidyl benzilate) were examined as a function of pH (Figure 1). Both ΔV and the surface adsorption of the PMCG solution increased sharply as the pH exceeded 6.3 and attained a maximum at about pH 8.0. With BQ a similar ΔV-pH curve was obtained except that the change occurred at pH 7 while the increase was slightly greater. The slight decrease in potential at higher pH is probably caused by vaporization of the drugs in the form of free bases.

The concentration-adsorption isotherm of a PMCG could be determined readily by measuring ΔV at pH 9.5 (Figure 2). A potential change was first measurable at $10^{-6}M$ PMCG and reached a maximum of about 450 mv. at $10^{-4}M$. When ΔV was plotted against the pH at which ΔV was one-half the maximum for a given bulk concentration of PMCG (*i.e.*, the pK), a straight line was obtained (Figure 1) according to the expression (*6, 8*):

$$pH_s = pH_b + \epsilon\psi/kT$$

where pH_s = surface pH, pH_b = bulk pH, ϵ = electronic charge, ψ = surface electrical potential, k = Boltzmann constant, T = temperature, a potential of +200 mv. can be expected to elevate the surface pH almost three units above that of the bulk phase. A potential change of about 200 mv. accounted for an increase in pH_s of about two units,

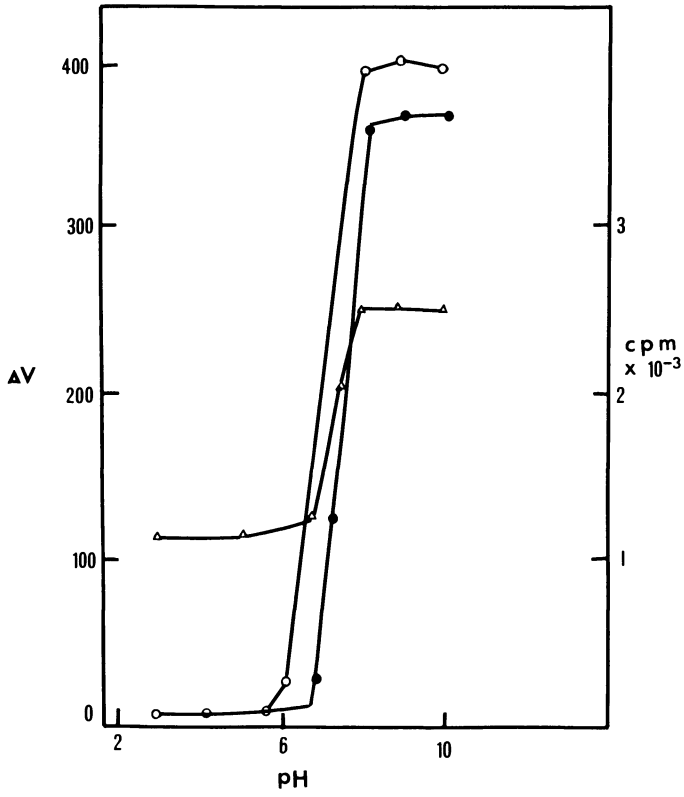

Figure 1. Effect of pH on ΔV and surface adsorption of PMCG and BQ. (○), PMCG at 10^{-4}M and (●), BQ at 10^{-4}M refer to ΔV (mvolts); (△) refers to surface adsorption of tritiated PMCG (c.p.m. × 10^{-3})

assuming ΔV to be equivalent to ψ. Since the pK of the drug in solution is 7.5, the Gouy potential (diffuse ionic double layer) would be virtually zero at pH > 8.

P-A and ΔV-*A* studies were carried out with stearic acid films in the presence of Ca^{2+} and ATP (Figure 3). The *P-A* curve in the absence of Ca^{2+} exhibits the typical linear liquid-condensed and solid-condensed regions; however, in the presence of $10^{-4}M$ Ca^{2+} the liquid-condensed region vanishes. When an equimolar concentration of ATP is present with Ca^{2+}, the *P-A* curve is almost identical to that obtained without Ca^{2+}. The surface potential for stearic acid in the absence of ATP and added Ca^{2+} increased gradually with film compression, attaining a maximal value of 230 mv. At a concentration of $5 \times 10^{-5}M$ Ca^{2+}, ΔV increased to a value of 150 mv. and decreased to the original value with film compression. A similar curve was obtained with $10^{-4}M$ Ca^{2+}

except that the initial value for ΔV was somewhat greater. When the concentration of both ATP and Ca^{2+} was $10^{-4}M$, the ΔV-A curve closely resembled that obtained with stearic acid alone; whereas, when the concentration for both ATP and Ca^{2+} was $5 \times 10^{-5}M$, the initial value for ΔV was considerably greater. The results with Ca^{2+} are essentially in agreement with those of Goddard and Ackilli (9), who observed (at pH 10) that Ca^{2+} lowered the ΔV values. They further observed that the normally fluid condition at collapse of the monolayers is changed to a very viscous state at $10^{-6}M$ Ca^{2+} and to a solid state at $10^{-5}M$. They also demonstrated that sequestrants, such as pyrophosphate and tripolyphosphate, completely eliminated the effects of Ca^{2+} and Mg^{2+}.

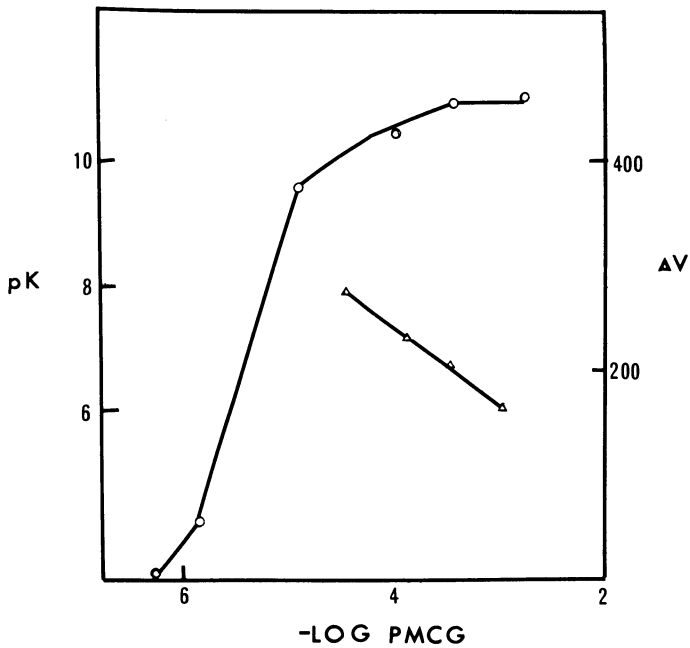

Figure 2. Relationship of concentration of PMCG to surface pH and potential. (○) refers to ΔV *and (△) to pK.* $\Delta V =$ *mvolts, pH 7.6. pK refers to pH at one-half maximal* ΔV

The *P-A* and ΔV-*A* curves were determined for stearic acid films in the presence of PMCG alone and in combination with Ca^{2+} or Ca^{2+} + ATP (Figure 4). When Ca^{2+} and PMCG were present together, there was an initial spreading pressure of about 4 dynes. The *P-A* curve differs from that without Ca^{2+} in that there is an initial rise in pressure at 24 sq. A., a leveling off again at 22 sq. A., and a limiting area which is slightly less than that with Ca^{2+} or PMCG alone. In the presence of $2 \times 10^{-5}M$

PMCG alone or with $2 \times 10^{-5}M$ Ca^{2+}, the surface potential did not vary with film compression from the initial value of about 20 mv. At a concentration of $10^{-4}M$ Ca^{2+} and $2 \times 10^{-5}M$ PMCG ΔV remained at first constant with compression, then decreased to −100 mv., and finally returned almost to the initial value. At intermediate concentrations of Ca^{2+} and the same concentration of PMCG, ΔV was initially −100 mv., remaining either constant ($5 \times 10^{-5}M$ Ca^{2+}) or increasing ($10^{-4}M$ Ca^{2+}) with film compression.

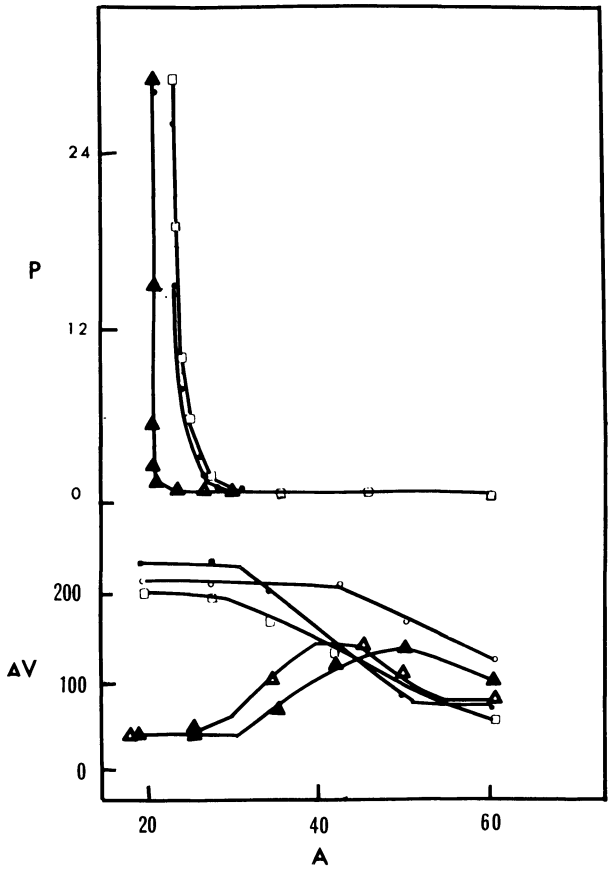

Figure 3. P-A *and* ΔV-A *curves for stearic acid monolayers at pH 7.8. (□), buffer alone; (●), [Ca^{2+}] = [ATP] = 10^{-4}M; (○), [Ca^{2+}] = [ATP] = 5×10^{-5}M; (△), [Ca^{2+}] = 5×10^{-4}M; (▲), [Ca^{2+}] = 10^{-4}M. ΔV = mvolts, A = sq. A./molecule*

The surface potential of the brain lipid film increased linearly with film compression attaining a potential of 375 mvolts at the limiting area

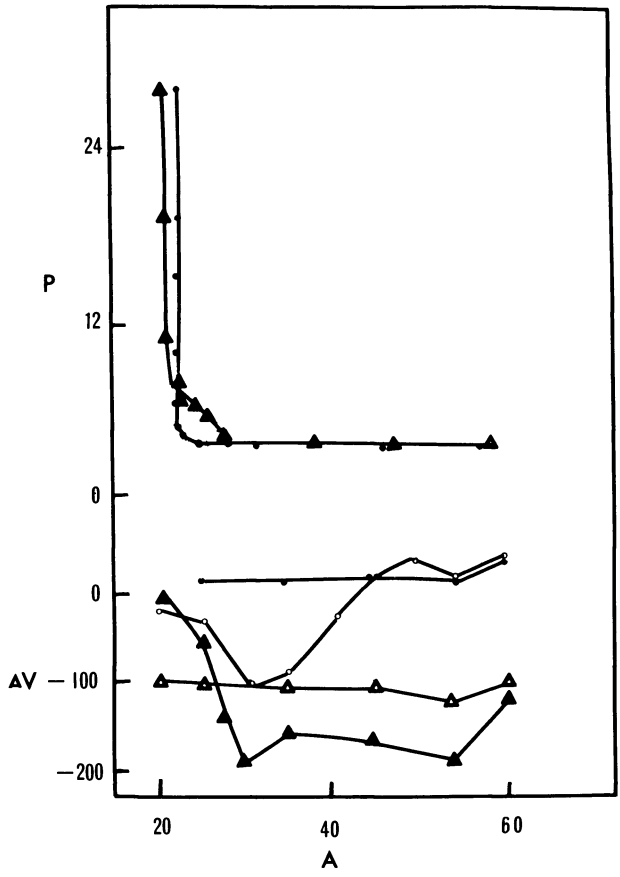

Figure 4. P-A *and* ΔV-A *curves for stearic acid monolayers at pH 7.8. (●),* $[Ca^{2+}] = 0$, *(*$[Ca^{2+}] = 0$, $[PMCG]) = 2 \times 10^{-5}$M *PMCG; (○),* $[Ca^{2+}] = 10^{-3}$M, $[PMCG] = 2 \times 10^{-5}$M; *(▲),* $[Ca^{2+}] = 10^{-4}$M, $[PMCG] = 2 \times 10^{-5}$M; *(△),* $[Ca^{2+}] = [ATP] = 5 \times 10^{-5}$M, $[PMCG] = 2 \times 10^{-5}$M. ΔV = *mvolts,* P = *dynes/cm.,* A = *sq. A./molecule*

of 52 sq. A. (Figure 5). Ca^{2+} was without effect on the ΔV-*A* curve. Shah and Schulman (*15*) have demonstrated that Ca^{2+} has no effect on the ΔV of lecithins containing a large degree of unsaturation in the hydrocarbon chains. In the presence of PMCG ΔV was lowered 100 mv., while the increase with compression was somewhat less. In the presence of $10^{-4}M$ ATP and $2 \times 10^{-5}M$ PMCG the initial value of ΔV was still lower (60 mvolts) and with compression to the limiting area attained the ΔV value of PMCG alone. Since the value of the interfacial potential with the lipid film (*i.e.*, V_f, where $\Delta V = V_f - V_o$ where V_o = the potential

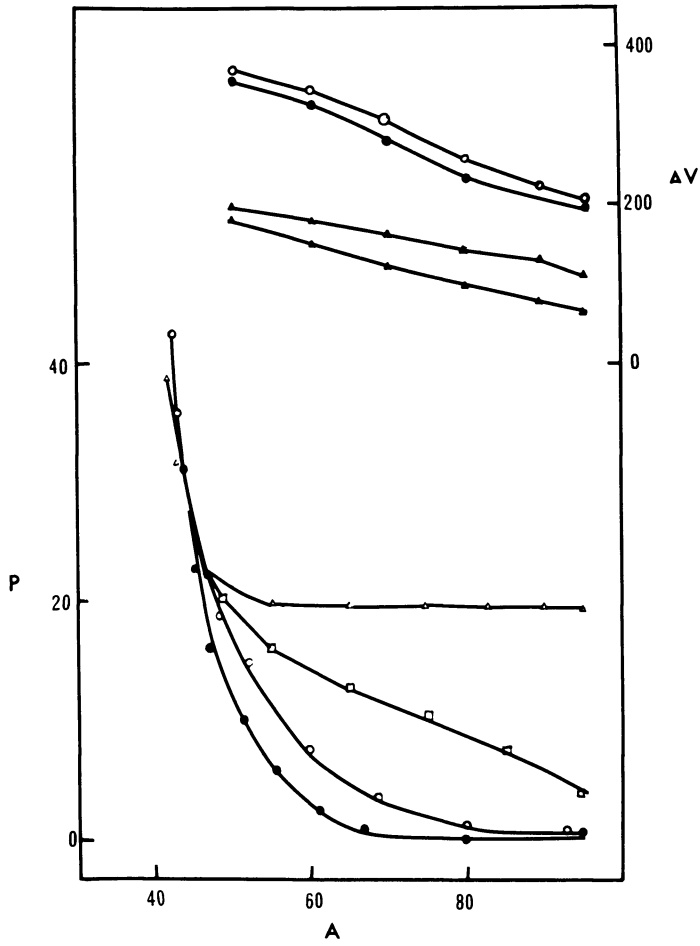

Figure 5. P-A *curves for synthetic lecithin monolayer and* ΔV-A *curve for beef brain lipid at pH 7.8.* (○), $[Ca^{2+}] = [PMCG] = [ATP] = 0$; (●), $[Ca^{2+}] = 10^{-4}$M, $[ATP] = [PMCG] = 0$; (△), $[PMCG] = [Ca^{2+}] = 2 \times 10^{-5}$M, $[ATP] = 0$; (▲), $[PMCG] = 2 \times 10^{-5}$M, $[ATP] = 2 \times 10^{-4}$M, $[Ca^{2+}] = 0$; (□), $[Ca^{2+}] = 10^{-4}$M, $[ATP] = [PMCG] = 0$. ΔV = *mvolts*, P = *dynes/cm.*, A = *molecule*

without the film) at full compression was the same with or without PMCG, the drug would appear to be completely expelled at the limiting area for the lipid. Furthermore, there would not appear to be any significant head group interaction at this stage, a factor which would contribute to ψ_o, the potential of the diffuse ionic double layer. The *P-A* curves for lecithin (which, on the basis of preliminary studies, were found

roughly to approximate those for the brain lipid material) are presented for comparative purposes (Figure 5). Two linear phases are apparent in the *P-A* curve, and Ca^{2+} causes condensation in the first linear phase by apparently combining with the phosphate groups of lecithin (*14*). In the presence of PMCG there is a large initial drop in surface tension before the spreading of the monolayer which is added onto the *P-A* curves. In the absence of Ca^{2+} the *P-A* curve is relatively flat until the limiting area is reached, an effect which occurs as the PMCG molecules are displaced from the surface. In combination with Ca^{2+} PMCG contributes to the stability of the lecithin monolayer; however, Rogeness *et al.* (*14*) showed that this stability disappears as the concentration of PMCG decreases.

The adsorption of ATP-^{14}C to surface films of stearic acid and brain lipid was examined over an extended period of time under various conditions (Table I and Figure 6B). Table I shows the short-term results, where adsorption was studied during the first 30 minutes, and evaporation was not a factor. Upon adding stearic acid or brain lipid the measurable radioactivity decreased, probably as a result of displacement of ATP-^{14}C from the surface layer and self-absorption of the beta particles by the lipid film. When PMCG was present, there was a slight but significant increase in the surface adsorption of ATP. The amount of ATP adsorbed was 4×10^{-10} moles/sq. cm. for stearic acid and 2.5×10^{-10} moles/sq. cm. for brain lipid. If the lipid concentration in the surface is assumed to be about $8 \times 10^{-10} M$ (as phospholipid in the case of brain lipid), the molar ratio of ATP to lipid would be about 0.5 for stearic acid and 0.3 for brain lipid.

Table I. Surface Adsorption of ATP-^{14}C to Films of Stearic Acid and Brain Lipid[a]

	Radioactivity, counts/3 min.	*% Change*	*Moles ATP Adsorbed/sq. cm. surface*
No added lipid	2810 ± 62	—	—
Stearic acid	2870 ± 64	2	0
Stearic acid + PMCG	3065 ± 59	9	1×10^{-10}
Brain lipid	2650 ± 55	−6	(-0.5×10^{-10})
Brain lipid + PMCG	2970 ± 70	6	0.6×10^{-10}

[a] Radioactivity was measured 10 minutes after adding lipid. Concentration of ATP-^{14}C and PMCG was $5 \times 10^{-5} M$; pH, 8.0. The results are expressed as mean ± standard deviation.

If the surface adsorption of ATP-^{14}C to brain lipid films is examined over extended time intervals where evaporation is allowed to occur, it is possible to demonstrate a considerable adsorption of ATP to lipid, par-

ticularly in the presence of $10^{-5}M$ Ca^{2+} (Figure 6A). The rate of adsorption was constant during the first 2.5 hours and then doubled thereafter. When the EDTA-extracted lipid was used, the rate of surface adsorption of ATP was reduced over 50%. Apparently the absence of Ca^{2+} or other divalent ions markedly restricts the adsorption of ATP. Similar results (not shown) were obtained with stearic acid monolayers, except that in the absence of Ca^{2+} the rate of adsorption was only one-third that obtained in its presence. All of the derivatives of adenine were found to be adsorbed to lipid films; although immediate adsorption occurred only with those derivatives not containing phosphate (Table II). Evidently, the immediate interaction with the lipid involves van der Waal's forces while the presence of phosphate groups retards adsorption, possibly because of the electrostatic repulsion of phosphate groups. ATP-C^{14} was not adsorbed to monolayers of tripalmitin, cholesterol, or cholesterol oleate; however, preliminary findings show that adsorption of adenine-C^{14} to such lipid monolayers readily occurs (data not given).

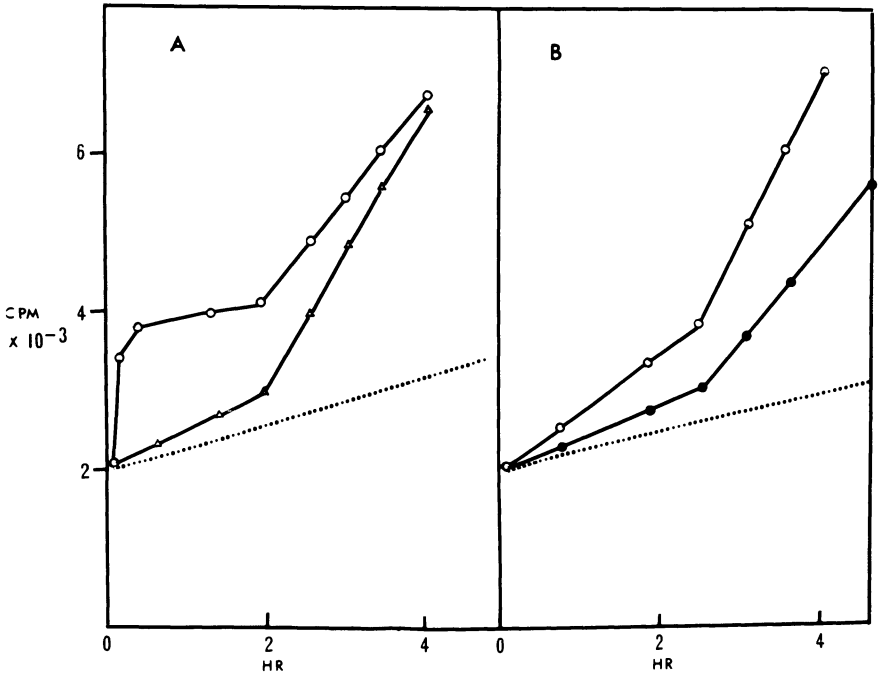

Figure 6. (A): ^{45}Ca adsorption to monolayer of beef brain lipid. (●), 10^{-5}M $^{45}CaCl_2$; (○), 10^{-5}M $^{45}CaCl_2$ + 5 × 10^{-4}M ATP; . . . ., 10^{-5}M $^{45}CaCl_2$, no lipid. (B): ATP-^{14}C adsorption to brain lipid. (●), 10^{-5}M ATP-^{14}C + 10^{-5}M $CaCl_2$; (○), same except EDTA-treated lipid; . . . ., same—no lipid; ordinate, radioactive counts/min.; abscissa, time in hours

The surface adsorption of tritiated PMCG was studied as a function of its bulk concentration (Figure 7). In the absence of brain lipid the surface adsorption increased sharply as the concentration approached $10^{-4}M$, reaching a maximum at $5 \times 10^{-3}M$. When brain lipid (5×10^{-9} moles, as phospholipid) was added, the surface adsorption of PMCG was significantly reduced. If the solutions were allowed to dry, the concentration-radioactivity curve was essentially parallel to that obtained for PMCG in solution. When brain lipid was present as the samples were dried, the radioactivity increased twofold. Since the residue could not be dried as a uniform layer, it is not possible to make any reasonable estimation of the amount of PMCG adsorbed to the dried lipid film.

Table II. Surface Adsorption of Various ^{14}C-Labeled Adenine Derivatives to Beef Brain Lipid[a]

	Surface Adsorption to Lipid, moles $\times 10^{10}$		
	10 min.	*2 hr.*	*6 hr.*
Adenine	0.5	1.0	3.0
Adenosine	0.3	0.8	2.8
AMP	0.0	0.5	2.6
ADP	0.0	0.5	2.8
ATP	0.0	0.6	3.0

[a] Planchet contained $2 \times 10^{-5}M$ of derivative, $10^{-4}M$ $CaCl_2$, in 1.2 ml. $10^{-2}M$ NaCl adjusted to pH 7.8 with tris buffer. 10^{-7} moles of lipid (as phospholipid) were added. Radioactive measurements made at various times (indicated) after adding lipid.

The sequestering action of ATP on the Ca^{2+} adsorption to stearic acid monolayers was studied at varying concentrations of both ATP and Ca^{2+} (Figure 8). At a concentration of $10^{-5}M$ ATP and $5 \times 10^{-5}M$ Ca^{2+}, 50% of the Ca^{2+} adsorption to the monolayer was suppressed. At a concentration of $10^{-3}M$ Ca^{2+} the concentration of ATP needed to suppress Ca^{2+} adsorption 50% was $10^{-3}M$.

Electron microscopy revealed the surface films formed in the presence of either Ca^{2+} alone or in combination with ATP to consist of continuous filamentous membranes containing electron-dense aggregates (Figures 9–11). The membranous structure appeared somewhat less amorphous in the presence of ATP although the electron-dense granules were present in both preparations. The ribbon-like unit membrane was about 50 A. thick and the granules which were associated exclusively with the membrane varied in diameter from about 20 to 100 A. Occasionally laminar structures resembling myelin could be seen. In the absence of Ca^{2+} and presence of ATP the structures were largely amorphous with no distinct membranous character or electron-dense granules (Figure 12).

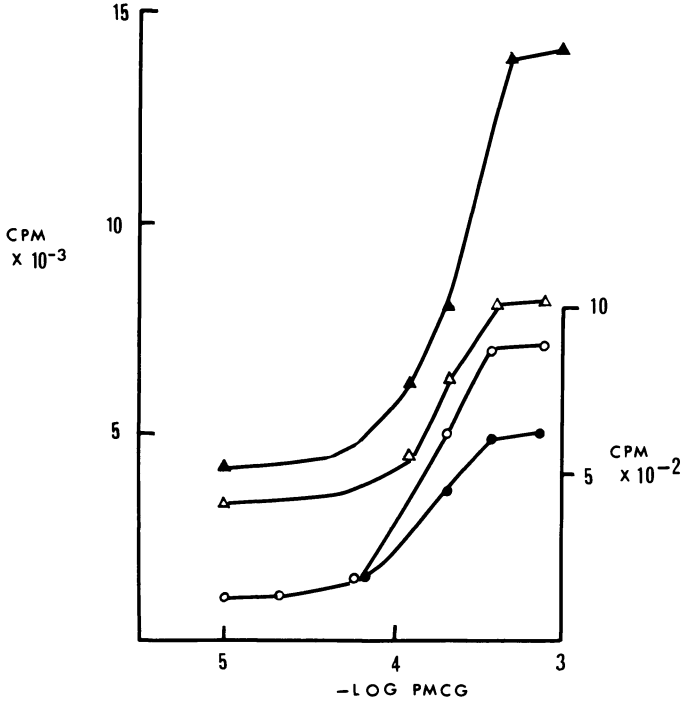

Figure 7. Surface adsorption of tritium-labeled PMCG at pH 7.8. (○), in solution with no lipid added; (●), in solution with brain lipid added; (△), dried sample, no lipid; (▲), dried sample, with brain lipid. Ordinates, radioactive c.p.m. × 10^{-2} for two lower curves (circles) and c.p.m. × 10^{-3} for two upper curves (triangles); abscissa, −log molar concentration of PMCG

Discussion

The present findings clearly demonstrate that ATP and its derivatives are able to form surface complexes with phospholipids and other lipophilic substances. The nature of this association is complex and involves not only a van der Waal interaction between the adenine moiety and the hydrocarbon residues of the lipids but also a link between the phosphate groups of ATP and the Ca^{2+} associated with phospholipids. As in the case of the interaction between adenine and PMCG, the presence of the ribose and phosphate moieties in ATP actually diminishes the strength of interaction (*14*).

Both the surface adsorption and potential studies support and extend the conclusion derived from surface pressure and viscosity measurements that (a) a strong interaction is occurring between lipids and the drugs; (b) the nature of the interaction bears some resemblance to that occur-

ring between Ca^{2+} and lipids; (c) an interaction occurs between the drugs and ATP alone or in combination with phospholipids; (d) although the drugs do not interfere with the interaction of Ca^{2+} with phospholipids, Ca^{2+} can influence the interaction of the drugs with lipids. Such observations on surface films support the hypothesis that the drugs affect excitatory membranes by substituting for Ca^{2+} (*1*) or by interfering with the action of ATP on the membranes (*1, 14*).

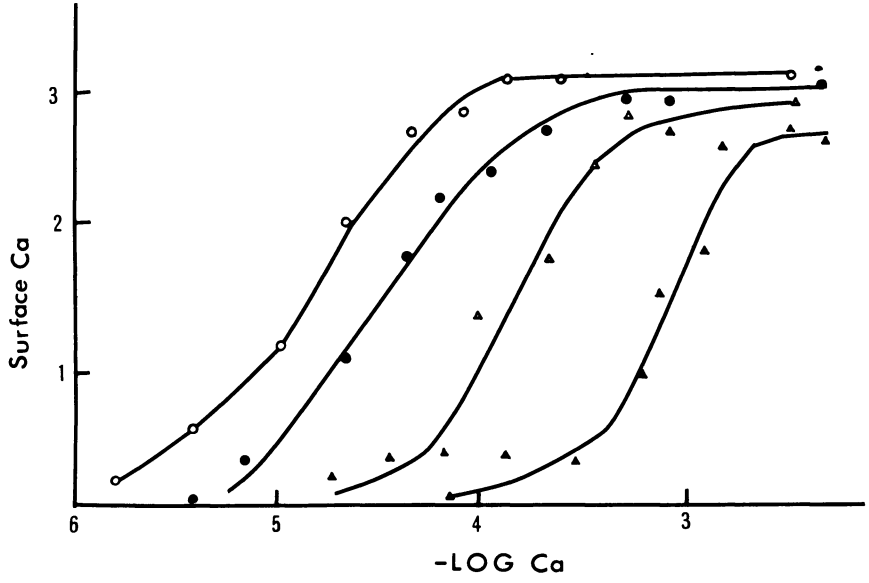

Figure 8. Effect of varying concentrations of ATP on adsorption of calcium to stearic acid monolayer. (○), no ATP; (●), 10^{-5}M ATP; (△), 10^{-4}M ATP; (▲), 10^{-3}M ATP; ordinate, surface concentration of Ca^{2+} in moles/sq. cm.; abscissa, −log molar concentration of Ca^{2+} at pH 7.6

Although most of the results with stearic acid monolayers conform to Gibbsian adsorption, it is difficult to determine to what extent Gibbsian equations are applicable to mixed monolayers as in the case of brain lipids. Some components in the lipid mixture may be displaced with film compression, while surface micelles, bimolecular leaflets, and other complex molecular arrangements may also occur. In a general way the present results suggest certain similarities in the surface phenomena of stearic acid, which form distinct monolayers, and brain lipid, so that meaningful, quantitative measurements can be carried out with biological materials. One important characteristic of biological lipids is the presence of many unsaturated fatty acids groups which significantly influence surface measurements. Shah and Schulman (*15*) have recently demonstrated that the limiting area of various lecithins increases with the degree of unsaturation

in the fatty acid residues, while the presence of a vinyl ether linkage in phosphatidal choline (a significant component of nerve membranes) accounts for a lower ΔV than is obtained with dipalmitoyl lecithin. The difference is attributable to the presence of an additional induced dipole in the double bond of the vinyl ether.

From the Equation

$$\Gamma = \frac{I_m - I}{SA}$$

the surface concentration of Ca^{2+} or Ca^{2+} + ATP could be calculated. At the end of about 4 hours the relative ratio of Ca^{2+}, ATP, and phospholipid approached unity; however, because of the formation of surface aggregates and the fact that surface accumulation was still proceeding rapidly, it is difficult to determine the ratio accurately. Since surface aggregates were microscopically visible after this period, the surface film could no longer be regarded as a monolayer or homogeneous multilayered system. Similar behavior was observed with monolayers of stearic acid and synthetic cephalin.

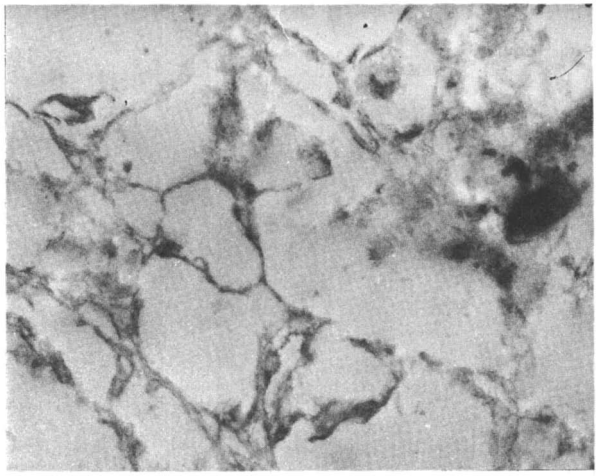

Figure 9. Electron micrograph of brain lipid surface film formed in presence of ATP alone, × 22,500

The time required for saturation of a surface monolayer by an adsorbable substance in the subsolution where no allowance is made for desorption, can be calculated from the following equation (*18*):

$$n = (D/\pi)^{1/2} ct^{1/2} N/500$$

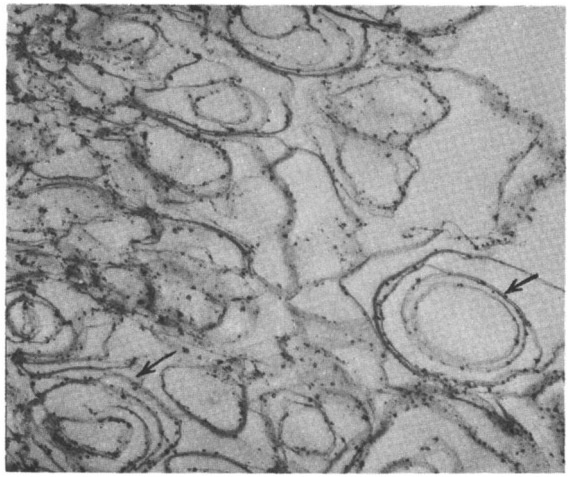

Figure 10. Electron micrograph of brain lipid surface film formed in presence of Ca^{2+} and ATP. Presence of myelin-like laminar structure indicated by arrow, × 22,500

where D is the bulk phase diffusion coefficient (6×10^{-6} sq. cm./sec.), c the bulk concentration of the isotope in moles/liter, n the number of adsorbed molecules/sq. cm. after a time t following application of the lipid ($\sim 2 \times 10^{14}$ at saturation), N is Avogadro's number, and t is the time in seconds for saturation. For a Ca^{2+} concentration of $10^{-5}M$, t should be about 2 minutes and for a concentration of $10^{-6}M$, t is about 230 minutes. Although the rate of surface adsorption for Ca^{2+} and adenine during the initial period conformed to the equation, the second phase in the adsorption of Ca^{2+} and the ATP derivatives did not. Evidently, the rate of formation of the surface aggregates or micelles involving Ca^{2+} and the ATP derivatives was not limited by their diffusion coefficients. Evaporation was an important factor in the long-term surface adsorption of both Ca^{2+} and ATP. If the planchets were kept in an atmosphere saturated with water vapor, surface adsorption of ATP did not occur nor did the long-term adsorption of Ca^{2+}. Evaporation was apparently required for the mobile ions to reach the surface; and once the surface complex occurred, a net desorption of the mobile ions could not occur without disruption (stirring the solution in the planchet) of the surface film. In the absence of a surface film the concentrations of ions in the vicinity of the surface is prevented by convection; however, in the presence of a surface-active agent the surface compressional modulus and viscosity will restrict convection currents (*8*). As a result, evaporation will preferentially concentrate the surface region. Conformity to the above equation

is restricted to a monolayer, and Lawrence (*10*) has suggested that lipids may form ternary liquid crystalline or smectic structures at interfaces where back diffusion of the mobile ions cannot readily occur.

On the basis of the present findings and other data, some attempt can be made to construct a model for the surface complex of ATP, Ca^{2+}, and phospholipid, assuming equimolar concentrations of each component. Ca^{2+} would be bound to both the phosphate group of the phospholipid and the terminal phosphate of ATP, while the adenine group interacts with the hydrocarbon residues of the lipid. Although from the data on surface adsorption the ratio of Ca^{2+} to ATP is probably 1, the actual number of Ca^{2+}-ATP molecules per lipid molecule cannot be determined. The electron-dense particles seen in the electron micrographs would appear to be crystalline aggregates of Ca^{2+} formed in conjunction with phospholipids and, when present, ATP. The existence of polymeric complexes involving divalent cations and polyphosphates is known, and their possible involvement in membrane phenomena has been discussed (*1*).

The present studies lend further credence to the concept that Ca^{2+}–ATP–phospholipid complexes can occur in biological membranes. It would also appear that the presence of a nucleotide such as ATP may be

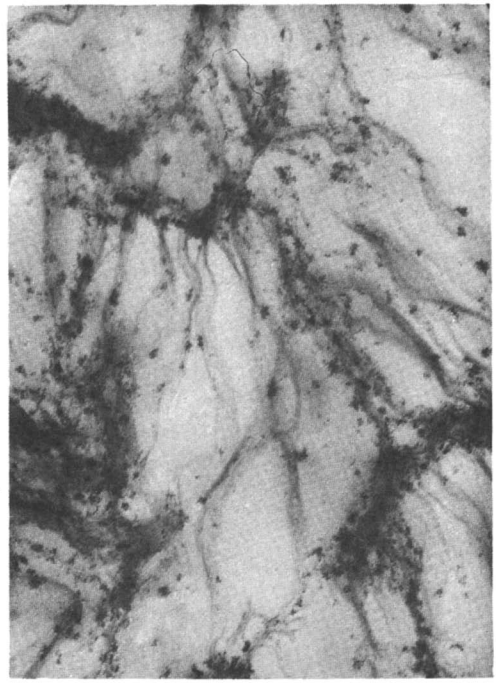

Figure 11. Same as Figure 10 except magnification × *50,000*

Figure 12. Electron micrograph of brain lipid surface film formed in presence of Ca^{2+} alone, × 22,500

a factor in forming cellular membranes, particularly of the laminar structure observed in myelin and other neural membranes. ATP, by virtue of its chelating and sequestering action, may also regulate the association of Ca^{2+} with the membrane and thus control ionic permeability and the level of excitability (*1*).

Literature Cited

(1) Abood, L. G., *Intern. Rev. Neurobiol.* **9**, 223 (1966).
(2) Abood, L. G., Biel, J. H., *Intern. Rev. Neurobiol.* **4**, 217 (1962).
(3) Abood, L. G., Koyama, I., Kimizuka, H., *Nature* **197**, 367 (1963).
(4) Abood, L. G., Koyama, I., Thomas, V., *Am. J. Physiol.* **207**, 1435 (1964).
(5) Aniasson, G., Lamm, O., *Nature* **165**, 357 (1950).
(6) Betts, J. J., Pethica, B. A., *Trans. Faraday Soc.* **52**, 1581 (1956).
(7) Biel, J. H., Sprengeler, E. P., Leiser, H. A., Horner, J., Drukker, A., Friedman, H. L., *J. Am. Chem. Soc.* **77**, 2250 (1955).
(8) Davies, J. T., Rideal, E. K., "Interfacial Phenomena," Academic Press, New York, 1961.
(9) Goddard, E. D., Ackilli, J. A., *J. Colloid Sci.* 18, 585 (1963).
(10) Lawrence, A. C. S., "Membrane Transport and Metabolism," A. Kleinzeller, A. Kotyk, eds., p. 35, Academic Press, New York, 1961.

(11) Manery, J. F., *Federation Proc.* **25**, 1804 (1966).
(12) Nilsson, G., *J. Phys. Chem.* **61**, 1135 (1957).
(13) Rogeness, G., Abood, L. G., *Arch. Biochem. Biophys.* **106**, 483 (1964).
(14) Rogeness, G., Krugman, L. G., Abood, L. G., *Biochem. Biophys. Acta* **125**, 319 (1966).
(15) Shah, D. O., Schulman, J. H., *J. Lipid Res.* **6**, 341 (1965).
(16) Stahl, E., "Thin Layer Chromatography," Springer-Verlag, New York, 1965.
(17) Tanaka, R., Abood, L. G., *Arch. Biochem. Biophys.* **108**, 47 (1964).
(18) Ward, A. F. H., Tordai, L., *J. Chem. Phys.* **14**, 453 (1946).
(19) Yamins, H. G., Zisman, W. A., *J. Chem. Phys.* **1**, 656 (1933).

RECEIVED May 8, 1967. Research supported by USPH grants NB-05856 and NB-06827.

16

Influence of Induced Dipoles, Metal Ions, and Cholesterol on the Characteristics of Phospholipid Monolayers

DINESH O. SHAH[1] and JACK H. SCHULMAN[2]

Stanley-Thompson Laboratory, School of Engineering, Columbia University, New York, N. Y. 10027

The interaction of metal ions and cholesterol with various phospholipid monolayers was studied by measuring the surface pressure, potential, and rheology of mixed monolayers. The concept of intermolecular cavities has been proposed to explain the apparent condensation of mixed monolayers and the structure of liquid-expanded monolayers. The unsaturation of fatty acyl chains strikingly influences the ionic structure, binding with metal ions, association with cholesterol, and enzymic hydrolysis of lecithin monolayers. It is possible to distinguish various types of interactions—ion-ion, ion-dipole, hydrocarbon-hydrocarbon—or their combinations by measurement of surface pressure, potential, and viscosity of mixed films. The surface rheology of cholesterol-phospholipid monolayers suggests that cholesterol may act as a biological plasticizer, increasing the distensibility of the membrane.

Phospholipids, cholesterol, and metal ions are important components of the cell membrane, which is generally believed to be composed of a bimolecular lipid leaflet or, alternatively, of lipoprotein subunits (*4*). Phospholipid monolayers afford a physical system suitable for studying lipid-lipid, lipid-protein, and lipid-metal ion interactions that may be analogous to those occurring at the cell surface. Using this approach, previous workers (*1, 2, 3, 7, 9, 10, 12, 13, 14, 15, 16, 20, 23, 26, 27, 28, 34,*

[1] Present address, Laboratory of Surface Chemistry, Marine Biology Division, Lamont Geological Observatory of Columbia University, Palisades, N. Y. 10964.
[2] Deceased.

35, 36, 39, 40, 41, 42, 43, 44, 45, 48, 50, 54, 55) have obtained valuable information about physicochemical aspects of reactions occurring at a lipid–water interface. Similar studies in our laboratory showed that the unsaturation of fatty acyl chains strikingly influences the ionic structure (*43*), binding of metal ions (*41*), association with cholesterol (*42*), and enzymic hydrolysis of pure lecithin monolayers (*40*). This paper presents our studies on various phospholipid monolayers employing surface pressure and surface potential techniques.

Methods

The method of measuring surface pressure by a modified Wilhelmy plate and surface potential by an ionizing air electrode has been described (*41*). For surface potential measurements, the electrometer was calibrated with stearic acid monolayers on 0.01*N* HCl, for which a value of 395 to 400 mv. at 21 sq. A. per molecule is assumed to be standard (*17*).

Results and Discussion

Induced Dipoles in Phosphatidal Choline and Sphingomyelin. Hughes and Rideal (*25*) showed from surface potential measurements that a dipole is induced in a double bond if it is situated in the α-position but not if it is further away. In phosphatidal choline (plasmalogen), an induced dipole in the vinyl ether linkage strikingly reduces the surface dipole of the molecule and hence the surface potential (*41*). In contrast, the presence of a double bond in the 4-5 carbon position of sphingomyelin increases the surface dipole and hence the surface potential of the monolayer (*44*). The known difference between the surface dipole of lecithin and plasmalogen in relation to the observation that beef-heart lecithin (containing about 40% plasmalogen) is unable to form stable bilayers (*24*) suggests that the induced dipole may influence the stability and organization of lipid bilayers.

Phospholipid Monolayers

Lecithin Monolayers. We have shown from surface pressure–area and surface potential–area curves of various lecithins that the molecular area increases and the interaction with metal ions decreases with increasing unsaturation of the fatty acyl chains (*41, 43*).

On the basis of the interaction of metal ions and ΔV-pH and ΔV-log C plots (*41, 43*), we propose ionic structures for dioleoyl, egg, and dipalmitoyl lecithin monolayers represented in Figure 1. Schematically shown in Figure 1A is the internal salt linkage between the phosphate and trimethylammonium groups in dioleoyl lecithin, preventing the inter-

action of metal ions with the phosphate group. Increasing saturation of the fatty acyl chains progressively decreases the intermolecular spacing which weakens the internal salt linkage (because of increase in ionic repulsion between similar charges), and thereby increases the binding of calcium.

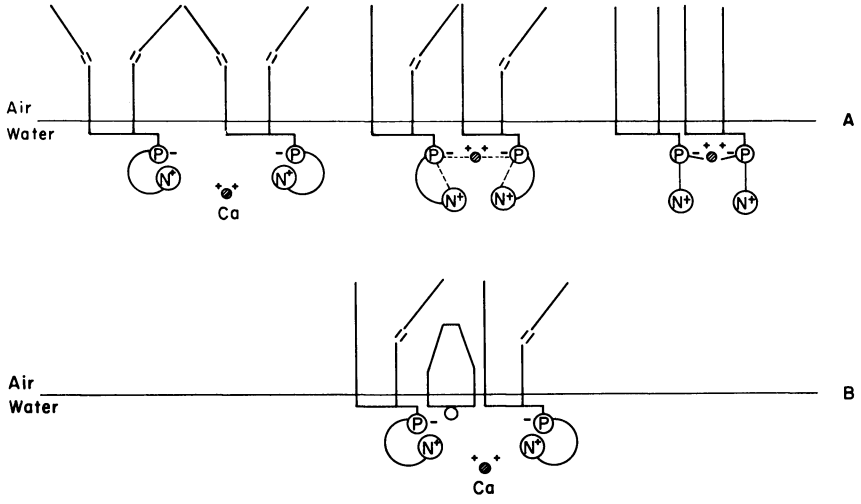

Figure 1. Schematic of interaction of calcium ion with dioleoyl, egg, and dipalmitoyl lecithins, and of egg lecithin–cholesterol monolayers

A: Dioleoyl lecithin shows internal salt linkage between phosphate and trimethylammonium groups. Broken lines in egg lecithin diagram represents weak interactions of phosphate with Ca^{2+} and trimethylammonium group. Solid line between Ca^{2+} and phosphate group in dipalmitoyl lecithin diagram represents strong interaction

B: Egg lecithin-cholesterol monolayers. Increased spacing between phosphate groups results in strong internal salt linkage preventing binding of Ca^{2+}

We have shown (*42*) that monolayers of egg lecithin interact with Ca^{2+}, whereas those of egg lecithin–cholesterol do not. A comparison of Figure 1B with the middle diagram of Figure 1A illustrates the explanation of this effect. In egg lecithin, the phosphate group interacts with a calcium ion and also with the adjacent trimethylammonium group (Figure 1A). However, the presence of cholesterol causes (statistically) a small net increase in the spacing between phosphate groups, which reduces the ionic repulsion between the polar groups, thereby strengthening the internal salt linkage (Figure 1B). Consequently, mixed monolayers of egg lecithin–cholesterol do not bind Ca^{2+}. Figure 1 (A, B) is a static representation of average kinetic states of molecules at the interface and is meant to illustrate the increase in effective molecular area with increase in unsaturation of fatty acyl chains.

Phosphatidic Acid Monolayers. Phosphatidic acid, prepared from egg lecithin by the action of phospholipase D, forms considerably more expanded monolayers than egg lecithin, presumably because of ionic repulsion between the phosphate groups in the phosphatidic acid monolayers (*42*). Phosphatidic acid monolayers showed about four times more increase in surface potential when $CaCl_2$ is substituted for NaCl in the subsolution than did egg lecithin monolayers (*43*). This again supports the conclusion that the trimethylammonium group competes with Ca^{2+} for the anionic phosphate group in egg lecithin monolayers (Figure 1*A*).

Cardiolipin Monolayers. Among various phospholipids studied by monolayer techniques, only cardiolipin (*41*) and phosphatidylserine (*36*) monolayers show significant condensation of their surface pressure–area curves in the presence of divalent as compared with monovalent cations in the subsolution. The condensation of cardiolipin is explained by the decrease in molecular area caused by the attraction between a divalent cation and the two phosphate groups in the molecule. This condensation is eliminated when the ratio of monovalent to divalent cations is greater than 5 to 1. At high surface pressures, the difference in the compressibility of cardiolipin monolayers correlates with the ionic radii of the metal ions ($Mg^{2+} < Ca^{2+} < Sr^{2+} < Ba^{2+}$).

Sphingomyelin Monolayers. The surface pressure–area curve of sphingomyelin is similar to that of dipalmitoyl lecithin in that both have approximately the same limiting areas (42 to 44 sq. A. per molecule). However, the interaction of metal ions with sphingomyelin monolayers is considerably smaller, as shown by the increase in the surface potential (*44*). The ΔV-log C plot of sphingomyelin suggests that the monolayer has a net positive surface charge (*39*). Thus, the weak interaction with metal ions and the positive surface charge of sphingomyelin can be explained satisfactorily by an ion-dipole association between the hydroxyl group and ionic oxygen of the phosphate group of sphingomyelin (Figure 2). This association in sphingomyelin molecules reduces the unit negative charge of the oxygen of phosphate group to a partial ionic charge, $\delta-$, which consequently decreases the interaction of the phosphate group with metal ions and the trimethylammonium group, leaving a net positive surface charge.

Position of Metal Ions in Monolayer Lattice. The surface potential is an important parameter for studying the ionic structure of monolayers, including the position of metal ions in the monolayer lattice. The interaction of cations with anionic groups in a monolayer results in a formation of ionic dipoles which influence the surface potential. If the polarity of the ionic dipole is in the same direction as that of the rest of the molecule, the surface potential of the monolayer increases; if the polarities are opposite, the surface potential decreases. It is known (*21*, *41*, *46*)

that the surface potential of fatty acid monolayers decreases, whereas that of alkyl phosphates and sulfates increases because of interaction with metal ions—*e.g.*, Ca^{2+}, Mg^{2+}. Using the above reasoning, the position of Ca^{2+} in various monolayers is proposed as shown in Figure 3.

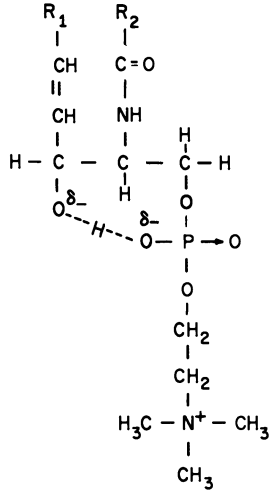

Figure 2. Ion-dipole association between hydroxyl group and ionic oxygen of phosphate group of sphingomyelin

δ—: Partial ionic charge on oxygen atoms

Influence of Intermolecular Spacing on Enzymic Hydrolysis of Lecithin Monolayers. When snake venom phospholipase A is injected under a lecithin monolayer, it splits lecithin into lysolecithin and free fatty acid. The change in polar groups of the monolayer results in a change of surface potential. However, if prior to injection of enzyme into the subsolution, a lecithin monolayer is compressed to such a surface pressure that the active site of the enzyme is unable to penetrate the monolayer, hydrolysis does not proceed. For monolayers of dipalmitoyl, egg, soybean, and dioleoyl lecithins the threshold surface pressure values at which hydrolysis does not proceed are 20, 30, 37, and 45 dynes per cm., respectively (*40*). This is also the same order for area per molecule in their surface pressure–area curves, indicating that enzymic hydrolysis of lecithin monolayers is influenced by the unsaturation of the fatty acyl chains and hence the intermolecular spacing in monolayers (*40*).

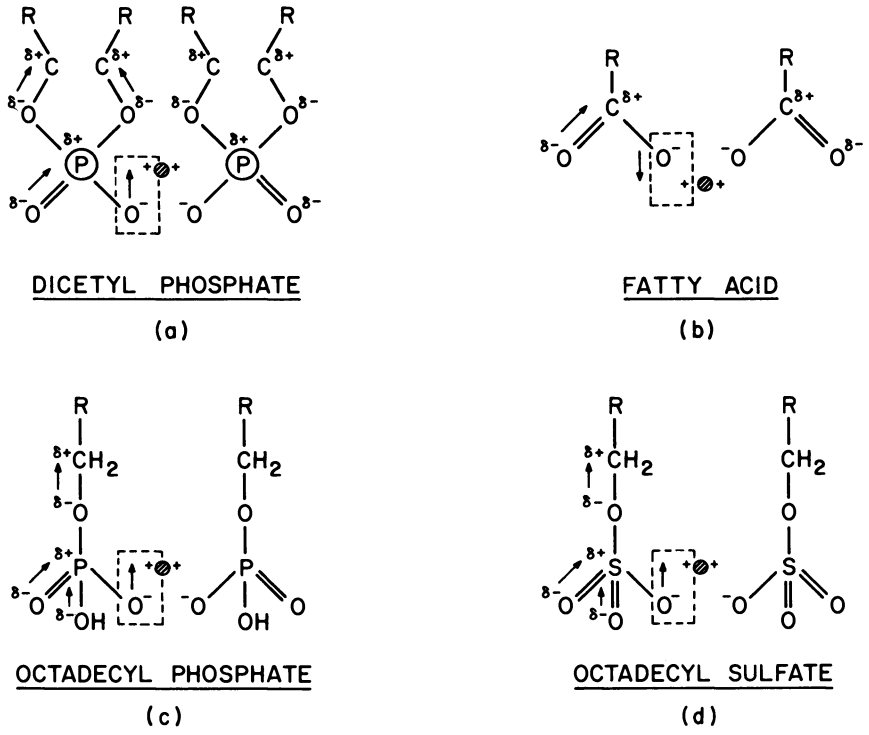

Figure 3. Position of calcium in relation to anionic oxygen in monolayers

→ Electric dipoles derived from covalent linkages
- - - Ionic dipole caused by divalent cation
δ+, δ−. Partial ionic charges on atoms

Mixed Monolayers

Concept of Intermolecular Cavities in Mixed Monolayers. In mixed monolayers a deviation in average area per molecule occurs if one component forms expanded and the other condensed monolayers. This reduction in average area per molecule has been attributed by previous workers to an interaction between components in the mixed monolayer. However, this need not be true in all cases where condensation occurs. In several instances the condensation can be explained on the basis of steric considerations in the mixed monolayers. Although the following discussion is based on lecithin-cholesterol monolayers, it is equally applicable to other mixed monolayers.

To understand the concept of intermolecular cavities we should consider the structure of an expanded monolayer. Since the hydrocarbon chains in an expanded monolayer are in the liquid state, they have greater

freedom to oscillate, rotate, and vibrate than in a condensed monolayer (*see* Figure 4a, representing a liquid-expanded monolayer of dipalmitoyl lecithin). The fatty acyl chains, because of their thermal motion, occupy an effective volume represented by a cone with its apex at the interface and base at the terminal end of the fatty acyl chains (Figure 4b). This would result in a "cavity" or vacancy between molecules. If molecules having dimensions smaller than or equal to those of the cavity are added to the lecithin monolayer, they may partially occupy these cavities to form a two-dimensional solution without causing a proportional increase in area of the monolayer (*see* Figure 4c, representing a mixed monolayer in which cholesterol partially occupies the cavity and reduces the average area per molecule). Furthermore, the liquid expanded monolayers of myristic acid, palmitic acid, and ethyl palmitate also show a reduction in the average area per molecule in the presence of cholesterol (*1, 16, 30*), which can be explained on the basis of intermolecular cavities. When the fatty acyl chains of lecithin are shorter—*e.g.*, C_{10}—the height of the intermolecular cavity is less than that of cholesterol (Figure 4d). Therefore, the presence of cholesterol causes a proportional increase in area; hence, such a mixed monolayer follows the additivity rule. The failure of cholesterol to condense highly expanded monolayers of lecithins containing polyunsaturated fatty acyl chains can also be explained on the basis of intermolecular cavities. For example, the monolayers of egg phosphatidic acid (*42*) or lecithins containing polyunsaturated fatty acyl chains (*48*) are more expanded than those of dipalmitoyl or egg lecithins. The greater area per molecule in these monolayers causes a larger intermolecular spacing, which results in a cavity of smaller height which does not accommodate a cholesterol molecule (Figure 4e). Therefore, such mixed monolayers follow the additivity rule of molecular areas.

Surface Pressure, Potential, and Fluidity Characteristics for Various Interactions in Mixed Monolayers. It is possible to distinguish various types of interactions which occur in mixed monolayers by measuring the surface pressure, surface potential, and surface fluidity of the monolayers. Deviation from the additivity rule of molecular areas indicates either an interaction between components or the "intermolecular cavity effect" in mixed monolayers.

Surface potential, ΔV, can be expressed (*37*) as $\Delta V = Kn\mu$ where K is a constant, n is the number of molecules per square centimeter of film, and μ is the surface dipole of the molecule. Thus $\Delta V/n = K\mu$, where the term on the left side of the equation, representing the surface potential per molecule (mv. per molecule), is proportional to the surface dipole, μ, of the molecule. When $\Delta V/n$ is plotted against mole fraction of the components, deviation from the additivity line indicates ion-ion or ion-dipole interaction between components (*42*).

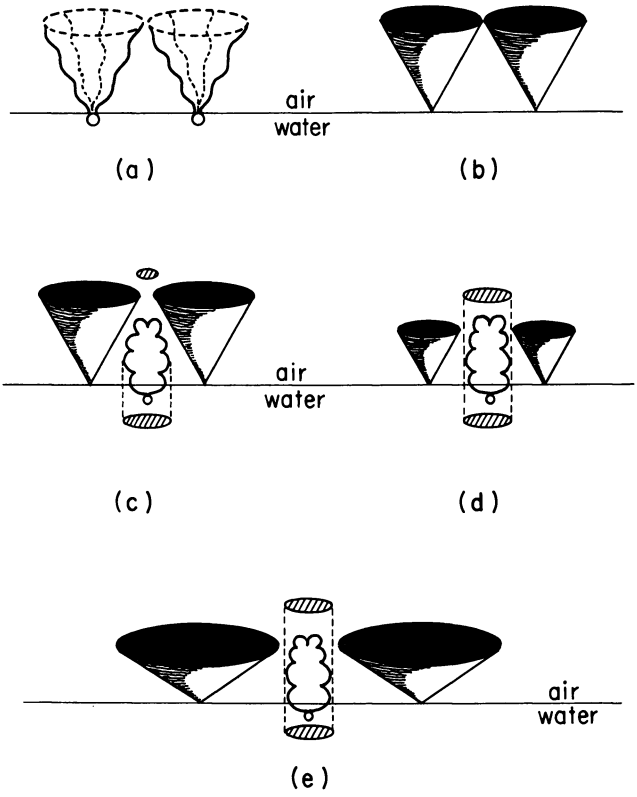

Figure 4. Schematic representation of structure of monolayers

a: Liquid-expanded monolayers. Broken lines indicate kinetic states of chains
b: Average space occupied by molecules at interface
c: Mixed monolayer—e.g., dipalmitoyl lecithin-cholesterol—in which true molecular area (cross-lined region) is shown below cholesterol and apparent increase in area above molecule
d: Mixed monolayer of short-chain lecithin, showing intermolecular cavity of smaller height. Cross-lined regions below and above cholesterol indicate true molecular area and increase caused in film area
e: Mixed monolayer of cholesterol with phosphatidic acid or lecithin having polyunsaturated fatty acyl chains whose intermolecular cavity is smaller in height. Cross-lined regions below and above cholesterol indicate true molecular area and increase in film area

Boyd and Vaslov (*6*) showed that the curve of log ϕ_s *vs.* mole fraction (where ϕ_s is the surface fluidity) for mixed monolayers exhibits additivity for mixed films of miscible components, positive deviation for immiscible components, and negative deviation for components having molecular interactions. Figure 5 shows various interactions which occur

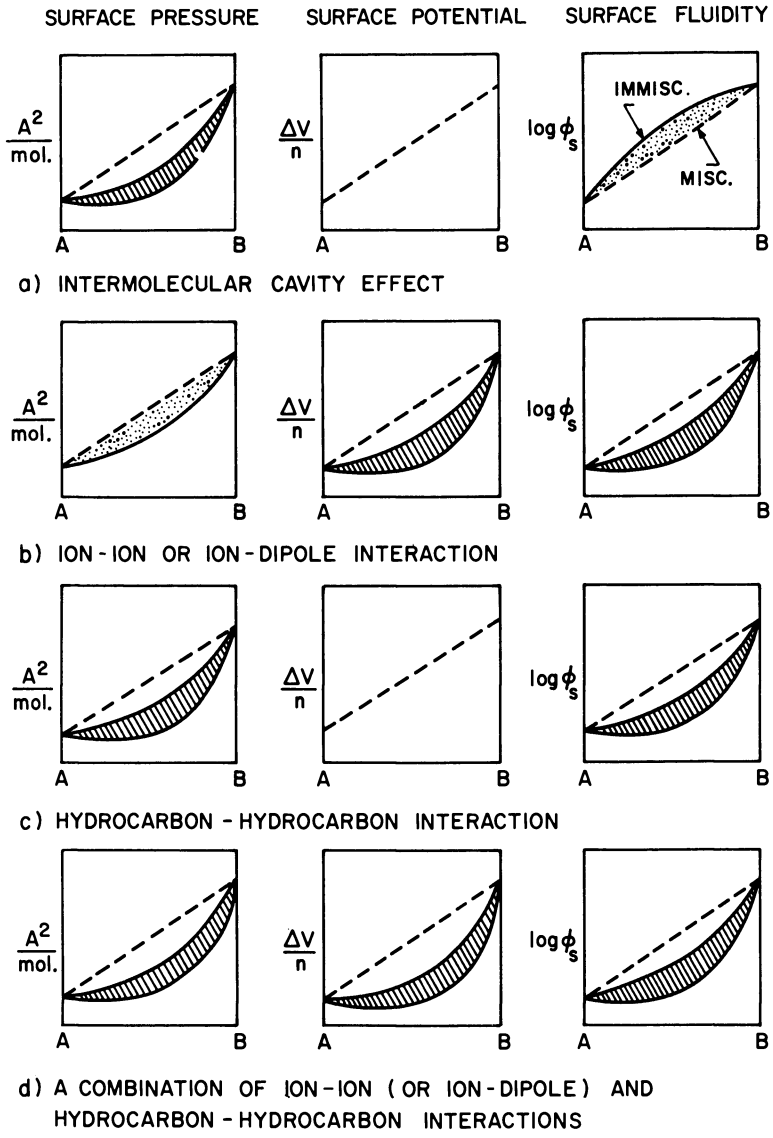

Figure 5. Interactions in mixed monolayers and their surface pressure, potential, and fluidity characteristics
--- Ideal additivity. A and B indicate pure components. Abscissa indicates mole fraction

in mixed monolayers and their characteristic changes in surface pressure, potential, and fluidity.

INTERMOLECULAR CAVITY EFFECT. Figure 5a shows the general characteristics of mixed monolayers in which the "intermolecular cavity effect"

occurs—*e.g.*, lecithin–cholesterol monolayers. The average area per molecule shows deviation, whereas surface potential per molecule ($\Delta V/n$) follows the additivity rule. Log ϕ_s can either follow the additivity rule (miscible components) or show positive deviation (immiscible components) (*6*). The cross-lined region in these diagrams represents obligatory deviation, whereas the stippled region represents optional deviation.

ION-ION OR ION-DIPOLE INTERACTION. Figure 5b, shows the general characteristics of mixed monolayers in which ion-ion or ion-dipole interaction takes place—*e.g.*, alkyl phosphate–alkyl trimethylammonium, or steric acid–octadecanol monolayers. The average area per molecule may or may not show a deviation from the "additivity rule" line, depending upon whether the two components form expanded or condensed monolayers. However, surface potential per molecule must show a deviation from the additivity line since ion-ion or ion-dipole interactions reduce the average surface dipole of the molecules in mixed monolayers (*31*, *42*). These interactions result in a negative deviation in the plot of log ϕ_s *vs.* mole fraction (*6*).

HYDROCARBON-HYDROCARBON INTERACTION. Figure 5c shows the general characteristics of mixed monolayers in which hydrocarbon-hydrocarbon interaction occurs—*e.g.*, trimyristin–myristic acid monolayers (*16*). The average area per molecule shows a deviation, whereas the surface potential per molecule follows the additivity rule. Hydrocarbon-hydrocarbon interaction also increases the cohesive force in the lipid layer and therefore reduces the fluidity of the mixed monolayer. It is evident from Figures 3a and 3c that surface fluidity is the only parameter which distinguishes an intermolecular cavity effect from hydrocarbon-hydrocarbon interaction.

ION-ION (OR ION-DIPOLE) AND HYDROCARBON-HYDROCARBON INTERACTION. Figure 5d shows the general characteristics of mixed monolayers in which ion-ion (or ion-dipole) and hydrocarbon-hydrocarbon interactions occur. The average area per molecule, the surface potential per molecule, and log ϕ_s all show deviations from the additivity rule.

Dicetyl Phosphate–Cholesterol Monolayers. Dicetyl phosphate, cholesterol, and their mixed monolayers are highly condensed—*i.e.*, steep surface pressure–area curves. However, their surface fluidity is strikingly different. Mobility of talc particles sprinkled on the monolayer indicates that dicetyl phosphate monolayers are solid, whereas cholesterol and all their mixed monolayers are liquid (*42*). The presence of 10 to 15 mole % of cholesterol is enough to liquefy the monolayers of dicetyl phosphate, indicating that cholesterol is a strong liquefying agent in these mixed monolayers. Work is in progress to determine whether these liquid films are Newtonian or non-Newtonian.

Monolayers of dicetyl phosphate–cholesterol follow the additivity rule for average area per molecule at all surface pressures, whereas surface potential per molecule shows deviation (Figures 6 and 7) (*42*). Thus, the surface potential measurements indicate that there is ion-dipole interaction between the ionic oxygen of phosphate and the hydroxyl group of cholesterol in the mixed monolayers (Figure 10a). The presence of Ca^{2+} in the subsolution neutralizes some of the phosphate groups and hence reduces the ion-dipole interaction in the mixed monolayer. Therefore, smaller deviations occur on subsolutions containing $CaCl_2$.

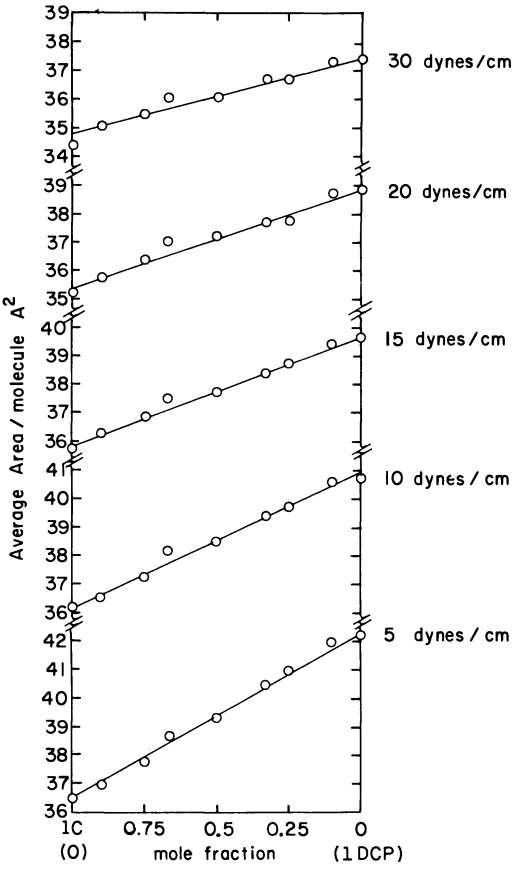

Figure 6. Average area per molecule of dicetyl phosphate–cholesterol monolayers at various surface pressures

Subsolution 0.02M NaCl or 0.01M $CaCl_2$, pH 5.6, at 25°C.

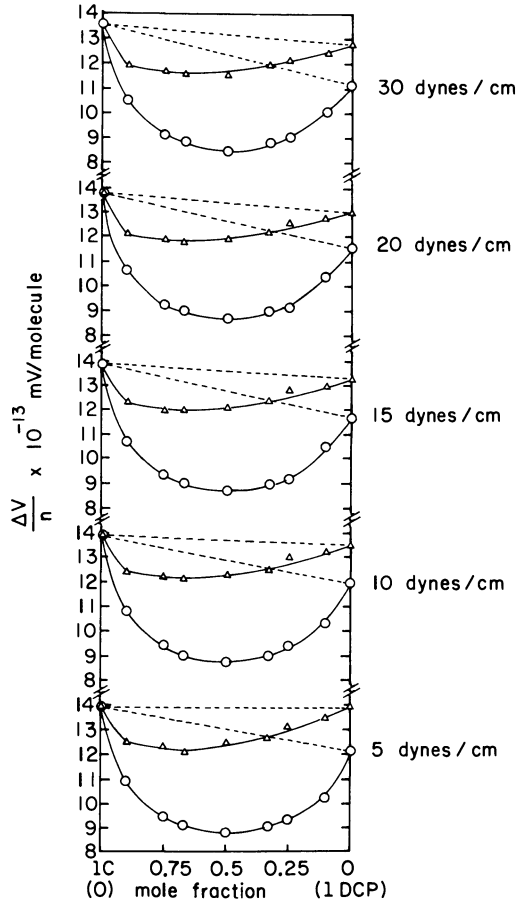

Figure 7. Average potential per molecule of dicetyl phosphate–cholesterol monolayers at various surface pressures

Subsolutions.....
○ *0.02M NaCl*
△ *0.01M $CaCl_2$*
--- *Line that would be followed if additivity rule held*

Dipalmitoyl Lecithin–Cholesterol Monolayers. The average area per molecule in dipalmitoyl lecithin–cholesterol monolayers shows deviation at low surface pressures, whereas at 30 dynes per cm. it follows the additivity rule (Figures 8 and 9) (*42*). The surface pressure–area curve of dipalmitoyl lecithin monolayers is liquid-expanded up to 30 dynes per cm., whereas above this surface pressure it is relatively incompressible (*42*). Figures 10b and c represent the structures of the dipalmitoyl

lecithin monolayer at low and high (> 30 dynes per cm.) surface pressures. At low surface pressures, a dipalmitoyl lecithin monolayer has intermolecular cavities which can be partially occupied by cholesterol molecules (Figure 10e). At high surface pressures (> 30 dynes per cm.) the fatty acyl chains are vertically oriented in the dipalmitoyl lecithin monolayer (Figure 10c); therefore, addition of cholesterol causes a proportional increase in area (Figure 10f).

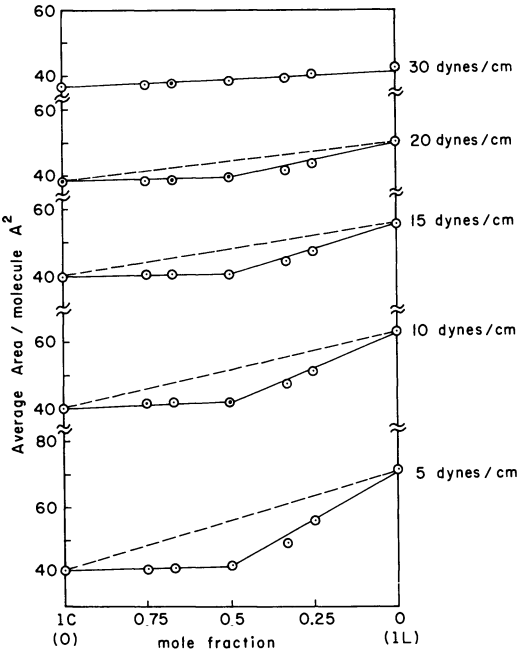

Figure 8. Average area per molecule of dipalmitoyl lecithin–cholesterol monolayers at various surface pressures

--- Additivity rule line

Van Deenen has reported (*48*) that the mixed monolayers of didecanoyl lecithin–cholesterol follow the additivity rule of molecular areas even though this lecithin forms expanded monolayers. This can be explained similarly by an intermolecular cavity of smaller height, which cannot accommodate cholesterol (Figures 10d and 4d).

The concept of ion-dipole interaction between lecithin and cholesterol has been suggested by many workers for the packing of these lipids in myelin or in the cell membrane (*18, 19, 51*). This concept is not supported by the surface potential measurements of mixed monolayers of lecithin and cholesterol. In contrast to dicetyl phosphate–cholesterol

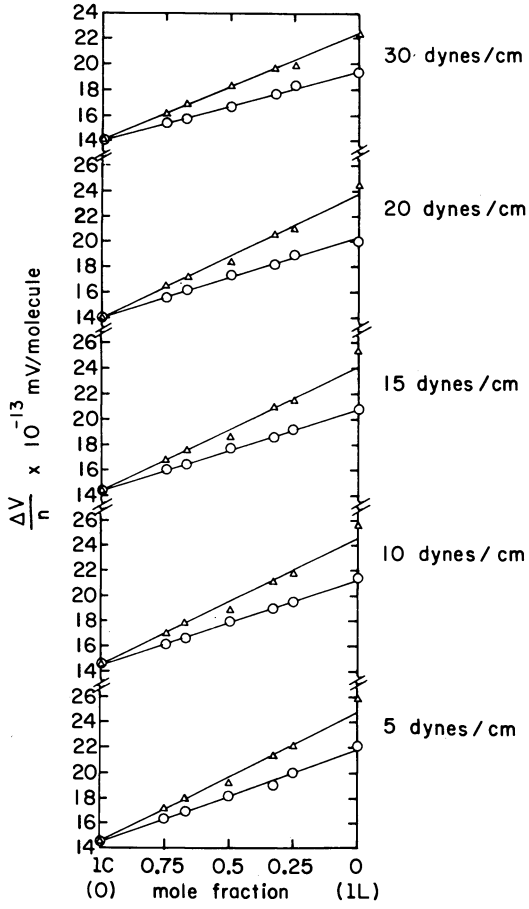

Figure 9. Average potential per molecule of dipalmitoyl lecithin–cholesterol monolayers at various surface pressures

Subsolutions
○ *0.02M NaCl*
△ *0.01M CaCl₂*
Points follow additivity rule

monolayers, the lecithin–cholesterol monolayers follow the additivity rule of average potential per molecule even at high surface pressures (*42*).

Egg Lecithin–Cholesterol Monolayers. The average area per molecule in egg lecithin–cholesterol monolayers shows deviation from the additivity rule at all surface pressures (*42*). The deviation in this case could be explained by the presence of molecular cavities caused by the kink in the oleoyl chain of egg lecithin, which would reduce the average area per molecule at low as well as high surface pressures (Figure 10g).

Similar reasoning accounts for the condensation of monolayers of dioleoyl lecithin by cholesterol reported by Van Deenen (*48*) (Figure 10h).

Even though 1,2-dilinoleoyl and 1-palmitoyl-2-linolenoyl lecithins form more expanded monolayers than egg lecithin, their mixed monolayers with cholesterol follow the additivity rule (*48*). This can be explained as follows. At low surface pressures, these lecithins have greater intermolecular spacing and hence form intermolecular cavities of smaller height which cannot accommodate cholesterol molecules (Figure 4e). At high surface pressure, the linoleoyl and linolenoyl chains, as opposed to oleoyl chains, do not form cavities in the monolayer (Figure 10i).

The optimum condensation at molecular ratios of 3 to 1 and 1 to 3 in egg lecithin–cholesterol monolayers and 1 to 1 in dipalmitoyl lecithin–cholesterol monolayers (*42*) do not imply complex formation between lecithin and cholesterol but rather suggest average geometrical arrangements of these molecules.

Recently Bourges, Small, and Dervichian (*5*) reported that a paracrystalline lamellar structure of egg lecithin can solubilize cholesterol up to a maximum of one molecule of cholesterol per molecule of lecithin. However, they conclude that this should not be considered as a molecular association but rather the consequence of the relative arrangement of the molecules in the lamellar structure which is a mutual (solid) solution of lecithin and cholesterol. They also reported that the state of compression in the lamellar structure corresponds to that of a highly compressed mixed monolayer of lecithin–cholesterol. The NMR results of Chapman and Penkett (*8*) also appear to indicate that solubilization of cholesterol in egg lecithin dispersions results in a highly packed structure in which fatty acyl chains possess little molecular motion. Our results from lecithin–cholesterol monolayers also suggest that these mixed monolayers are two-dimensional solutions with no specific interaction and that the apparent condensation in some instances is caused by the steric factors of the fatty acyl chains and not by the interaction or association between lecithin and cholesterol.

Phosphatidic Acid–Cholesterol Monolayers. In contrast to egg lecithin–cholesterol monolayers, the average area per molecule in phosphatidic acid–cholesterol monolayers shows a smaller deviation from the additivity rule at low surface pressures and a larger deviation at high surface pressures (*42*). The explanation for this is that at low surface pressure the large area per molecule in phosphatidic acid monolayers results in a cavity, but of a decreased height which cannot accommodate a cholesterol molecule (Figure 4e). At high surface pressures—*i.e.*, smaller area per molecule—the molecular cavity formed by the oleoyl chains of phosphatidic acid would have sufficient height to allow cholesterol to occupy partially these molecular cavities. Further in contrast

to lecithin–cholesterol monolayers, the average potential per molecule in phosphatidic acid–cholesterol monolayers shows a deviation from the additivity rule (*42*). This indicates ion-dipole interaction between the hydroxyl group of cholesterol and the ionic phosphate of phosphatidic acid.

Thermodynamics of Mixed Monolayers. Goodrich (*22*) considered mixed monolayers as "two-dimensional solutions" and derived an expression for excess free energy of mixing, G_{xs}, which is given as

$$G_{xs} = \int_{\pi^*}^{\pi} (\sigma_{12} - N_1\sigma_1 - N_2\sigma_2)d\pi \qquad (1)$$

where N_1 and N_2 are mole fractions of components 1 and 2 with $N_1 + N_2 = 1$; σ_1 and σ_2 are the areas of the respective monolayers; and σ_{12} is the area of the mixed monolayer. It is evident from Equation 1 that if $\sigma_{12} = N_1\sigma_1 + N_2\sigma_2$, then G_{xs} is zero. In other words, if a mixed monolayer follows the additivity rule of molecular areas at all surface pressures, it represents ideal mixing of components with no specific interaction between them. However, Goodrich's treatment is unsatisfactory and contradictory when applied to mixed monolayers of dicetyl phosphate–cholesterol. These mixed monolayers follow the additivity rule of molecular areas at all surface pressures (Figure 6), which indicates that G_{xs} is zero and that there is no specific interaction between dicetyl phosphate and cholesterol. However, surface potential measurements (Figure 7) clearly indicate ion-dipole interaction between dicetyl phosphate and cholesterol (*42*). Similarly, negative values of G_{xs} have been reported for lecithin–cholesterol monolayers (*15, 55*) where no specific interaction is found on the basis of surface potential (*42*) and viscosity measurements (*11, 12, 13*). This contradiction of experimental results to Goodrich's theoretical treatment points out the need for further experimental data and refinement of theoretical treatment in this area.

Figure 10. Molecular arrangement in various monolayers by space filling Fischer-Hirschfelder-Taylor molecular models

a: Dicetyl phosphate and cholesterol
--- Ion-dipole interaction between hydroxyl group of cholesterol and ionized oxygen of phosphate group
b: Dipalmitoyl lecithin at low surface pressures (< 30 dynes per cm.)
c: Dipalmitoyl lecithin at high surface pressures (> 30 dynes per cm.)
d: Didecanoyl lecithin and cholesterol
e: Dipalmitoyl lecithin and cholesterol at low surface pressures (< 30 dynes per cm.)
f: Dipalmitoyl lecithin and cholesterol at high surface pressures (> 30 dynes per cm.)
g: Egg lecithin and cholesterol monolayers
h: Dioleoyl lecithin and cholesterol monolayers
i: 1-Palmitoyl-2-linolenoyl lecithin and cholesterol

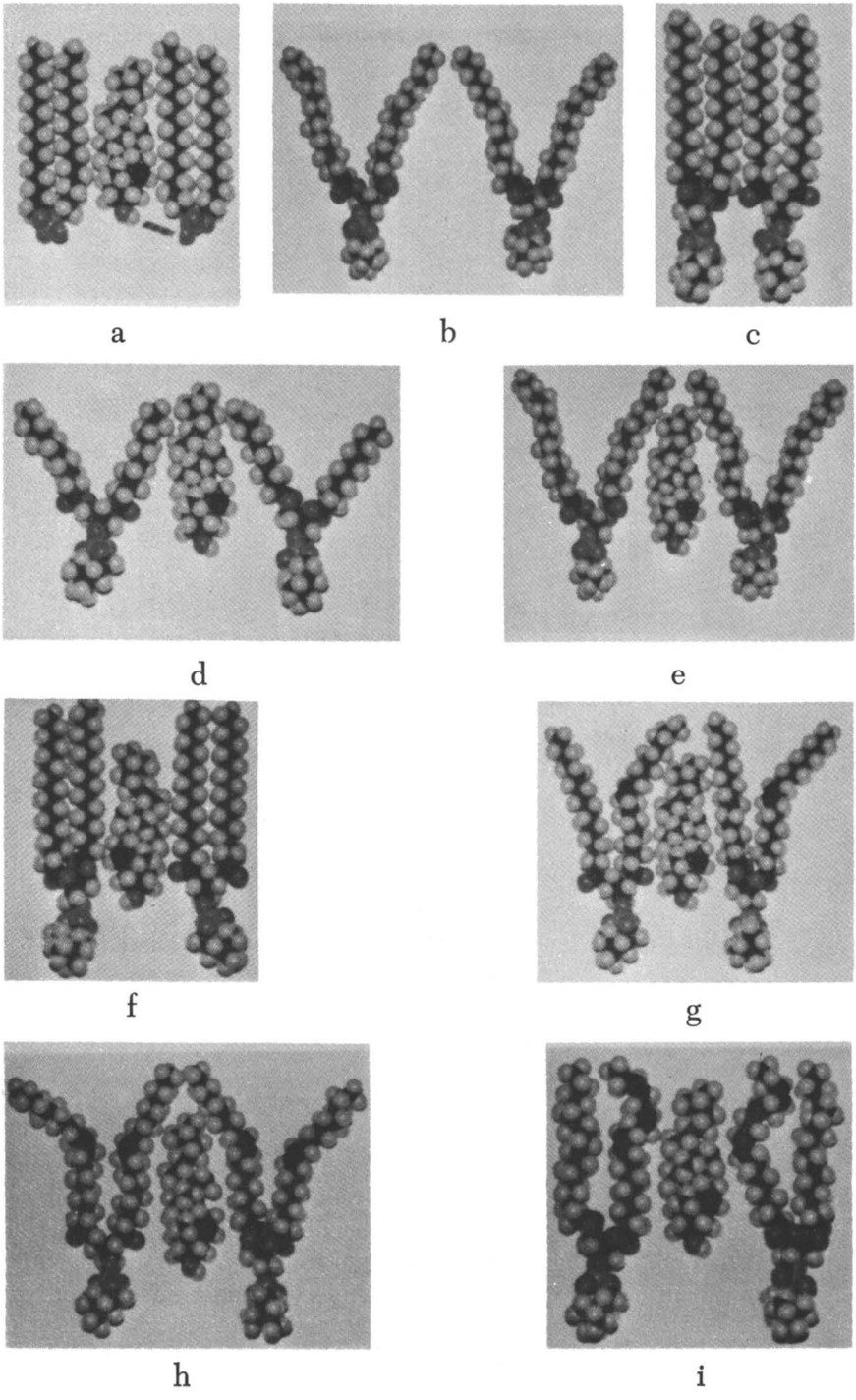

Correlation of Surface Properties of Cholesterol with Biomembranes. From the early work on condensation of lecithin monolayers in the presence of cholesterol (*13, 48*), it has been assumed generally that cholesterol increases the cohesive force in the lipid layer and thereby stabilizes the membrane. In contrast, we find that the two striking surface properties of cholesterol are its ability to liquefy lipid layers, even when present as a small fraction (10 to 15 mole %), and to occupy the molecular cavities between the fatty acyl chains. This agrees with the findings of Langmuir and Schaefer (*29*), who showed that the presence of cholesterol in C_{23} acid monolayers markedly increases the rate of evaporation through the monolayers, possibly because of an increase in the fluidity of the monolayer. In brain tissue, the high percentage of phospholipids with monounsaturated chains, and of cholesterol (*33, 53*) may lead to effects similar to those reported in the present work. Schulman, Waterhouse, and Spink (*38*) showed that addition of cholesterol to a lubricant reduces the frictional force between two metal surfaces by 80%, which can be attributed to increasing fluidity of the lipid layer. Hence the high cholesterol content of the erythrocyte membrane (*49*) suggests that cholesterol may play a role as a biological plasticizer, increasing the distensibility of the membrane.

Fluidity of the hydrocarbon chains is essential for the existence of lecithin bilayers (*24, 32, 47*). Bilayers of egg lecithin–cholesterol (molar ratio 1 to 1) are as stable as those of egg lecithin alone (stability being the time between formation and collapse of a bilayer), suggesting the liquid state for the fatty acyl chains (*47, 52*). If cholesterol had increased the cohesive force and hence the solidity of the bilayer, its stability would have been reduced considerably. Fluidity rather than rigidity is important for stability of thin films. A fluid film can adjust itself against thermal and mechanical fluctuations in the environment and thereby exhibit greater stability than rigid films. Cholesterol is unusual, in that its monolayers are highly incompressible but have low surface viscosity (*11, 12, 42*). Therefore, the liquefying property of cholesterol is presumably caused by its rigid, planar, asymmetrical molecular shape, which can act as a disordering agent, reducing the cohesive force between fatty acyl chains and thereby increasing the fluidity of the lipid layer.

Summary

The interaction of metal ions with lecithin monolayers, as measured by the increase in surface potential, decreases with increasing unsaturation of fatty acyl chains. The phosphate and trimethylammonium groups of a lecithin molecule form an internal salt linkage which dissociates upon

increasing saturation of fatty acyl chains, or upon increasing electrolyte concentration in the subsolution.

The double bond adjacent to the polar group strongly influences surface potentials of plasmalogen and sphingomyelin. In sphingomyelin, an ion-dipole association between the hydroxyl and ionic phosphate groups of the molecule results in a net positive surface charge.

The position of metal ions in a monolayer lattice has been proposed from surface potential measurements.

Enzymic hydrolysis of lecithin monolayers is strikingly influenced by the degree of unsaturation of fatty acyl chains and hence by the intermolecular spacing in monolayers.

Monolayers of dicetyl phosphate–cholesterol follow the additivity rule for average area per molecule, whereas lecithin–cholesterol monolayers deviate from it. The reverse is true for the additivity rule of average potential per molecule. Thus, the surface potential indicates that there is no interaction (or complex formation) between lecithin and cholesterol, but there is ion-dipole interaction between dicetyl phosphate and cholesterol as well as between phosphatidic acid and cholesterol.

The apparent condensation of mixed monolayers of lecithin in the presence of cholesterol is explained by a consideration of molecular cavities or vacancies caused by thermal motion of fatty acyl chains, the height of these cavities being influenced by the length, inclination, and degree of unsaturation (especially the proportion of monounsaturation) of the fatty acyl chains and the extent of compression of the monolayer. Monolayers are liquefied by the presence of unsaturated fatty acyl chains or by the addition of cholesterol.

Various types of molecular interactions which occur in mixed monolayers can be distinguished by simultaneous measurements of the surface pressure, potential, and fluidity of monolayers. Limitations of Goodrich's thermodynamic treatment of mixed monolayers are mentioned. Surface properties of cholesterol have been correlated with its function in biomembranes.

Acknowledgment

We thank R. W. Capps for many helpful suggestions and for assistance in preparing the manuscript. The authors gratefully acknowledge the financial support given by the National Science Foundation (Grant No. GB-5273) to carry out this work.

The untimely death of Jack H. Schulman, a truly brilliant and creative scientist, is reported with profound regret. Those who worked with him share a deep sorrow in this tragic event.

Literature Cited

(1) Adam, N. K., Jessop, G., *Proc. Roy. Soc. (London)* **A120,** 473 (1928).
(2) Anderson, P. J., Pethica, B. A., "Biochemical Problems of Lipids," G. Popjak and E. Le Breton, Eds., pp. 24-29, Butterworth & Co., London, 1956.
(3) Bangham, A. D., Papahadjopoulos, D., *Biochim. Biophys. Acta* **126,** 181 (1966).
(4) Benson, A. A., *J. Am. Oil Chemists' Soc.* **43,** 265 (1966).
(5) Bourges, M., Small, D. M., Dervichian, D. G., *Biochim. Biophys. Acta* **137,** 157 (1967).
(6) Boyd, G. E., Vaslov, F., *J. Colloid Sci.* **13,** 275 (1958).
(7) Chapman, D., Owens, N. F., Walker, D. A., *Biochim. Biophys. Acta* **120,** 148 (1966).
(8) Chapman, D., Penkett, S. A., *Nature* **211,** 1304 (1966).
(9) Colacicco, G., Rapport, M. M., *J. Lipid Res.* **7,** 258 (1966).
(10) Dawson, R. M. C., *Biochem. J.* **98,** 35C (1966).
(11) Deamer, D. W., Ph.D. thesis, Ohio State University, 1965.
(12) Deamer, D. W., Cornwell, D. G., *Biochim. Biophys. Acta* **116,** 552 (1966).
(13) De Bernard, L., *Bull. Soc. Chim. Biol.* **40,** 161 (1958).
(14) Demel, R. A., Van Deenen, L. L. M., *Chem. Phys. Lipids* **1,** 68 (1966).
(15) Demel, R. A., Van Deenen, L. L. M., Pethica, B. A., *Biochim. Biophys. Acta* **135,** 11 (1967).
(16) Dervichian, D. G., "Surface Phenomena in Chemistry and Biology," J. F. Danielli, K. G. A. Pankhurst, A. C. Riddiford, Eds., pp. 70-87, Pergamon Press, New York, 1958.
(17) Dreher, K. D., Sears, D. F., *Trans. Faraday Soc.* **62,** 741 (1966).
(18) Finean, J. B., *Circulation* **26,** 1151 (1962).
(19) Finean, J. B., *Experientia* **9,** 17 (1953).
(20) Galdston, M., Shah, D. O., *Biochim. Biophys. Acta* **137,** 255 (1967).
(21) Goddard, E. D., Ackilli, J. A., *J. Colloid Sci.* **18,** 585 (1963).
(22) Goodrich, F. C., Proceedings of 2nd International Congress on Surface Activity, J. H. Schulman, ed., Vol. 1, p. 85, Butterworth & Co., London, 1957.
(23) Hauser, H., Dawson, R. M. C., *European J. Biochem.* **1,** 61 (1967).
(24) Huang, C., Wheeldon, L., Thompson, T. E., *J. Mol. Biol.* **8,** 148 (1964).
(25) Hughes, A., Rideal, E. K., *Proc. Roy. Soc. (London)* **A140,** 253 (1933).
(26) Hyono, A., Kuriyama, S., *Nature* **210,** 300 (1966).
(27) Kimizuka, H., Koketsu, K., *Nature* **196,** 995 (1962).
(28) Kimizuka, H., Nakahara, T., Uejo, H., Yamauchi, A., *Biochim. Biophys. Acta* **137,** 549 (1967).
(29) Langmuir, I., Schaefer, V. J., "Surface Chemistry," F. R. Moulton, Ed., *AAAS Publ.* **21,** 17-39 (1943).
(30) Leathes, J. B., *Lancet* **208,** 853 (1925).
(31) Marsden, J., Schulman, J. H., *Trans. Faraday Soc.* **34,** 748 (1938).
(32) Mueller, P., Rudin, D. O., Tien, H. T., Wescott, W. C., "Recent Progress in Surface Science," J. F. Danielli, K. G. A. Pankhurst, A. C. Riddiford, Eds., Vol. 1, p. 384, Academic Press, New York, 1964.
(33) O'Brien, J. S., Sampson, E. L., *J. Lipid Res.* **6,** 545 (1965).
(34) Rogeness, G. A., Krugman, L. G., Abood, L. G., *Biochim. Biophys. Acta* **125,** 319 (1966).
(35) Rojas, E., Lettvin, J. Y., Pickard, W. F., *Nature* **209,** 886 (1966).
(36) Rojas, E., Tobias, J. M., *Biochim. Biophys. Acta* **94,** 394 (1965).
(37) Schulman, J. H., Rideal, E. K., *Proc. Roy. Soc. (London)* **A130,** 284 (1931).

(38) Schulman, J. H., Waterhouse, R. B., Spink, J. A., *Kolloid Z.* **146**, 77 (1956).
(39) Shah, D. O., Schulman, J. H., *Biochim. Biophys. Acta* **135**, 184 (1967).
(40) Shah, D. O., Schulman, J. H., *J. Colloid Interface Sci.* **25**, 107 (1967).
(41) Shah, D. O., Schulman, J. H., *J. Lipid Res.* **6**, 341 (1965).
(42) *Ibid.*, **8**, 215 (1967).
(43) *Ibid.*, p. 227.
(44) Shah, D. O., Schulman, J. H., *Lipids* **2**, 21 (1967).
(45) Shimojo, T., Ohnishi, T., *J. Biochem. (Japan)* **61**, 89 (1967).
(46) Spink, J. A., Sanders, J. V., *Nature* **175**, 644 (1955).
(47) Thompson, T. E., "Cellular Membranes in Development," M. Locke, Ed., p. 87, Academic Press, New York, 1964.
(48) Van Deenen, L. L. M., "Progress in the Chemistry of Fats and Other Lipids," R. T. Tolman, Ed., Vol. 8, Part 1, pp. 14, 59, Pergamon Press, New York, 1965.
(49) Van Deenen, L. L. M., Gier, J. D., "Red Blood Cell," C. Bishop, D. M. Surgenor, Eds., pp. 243-307, Academic Press, New York, 1964.
(50) Van Deenen, L. L. M., Houtsmuller, U. M. T., de Haas, G. H., Mulder, E., *J. Pharm. Pharmacol.* **14**, 429 (1962).
(51) Vandenheuvel, F. A., *Ann. N.Y. Acad. Sci.* **122**, 57 (1965).
(52) Van Zutphen, H., Van Deenen, L. L. M., Kinsky, S. C., *Biochem. Biophys. Res. Commun.* **22**, 393 (1966).
(53) Veerkamp, J. H., Mulder, I., Van Deenen, L. L. M., *Biochim. Biophys. Acta* **57**, 299 (1962).
(54) Villallonga, F., Altschul, R., Fernandez, S., *Biochim. Biophys. Acta* **135**, 406 (1967).
(55) *Ibid.*, p. 557.

RECEIVED May 22, 1967.

17

Effect of pH and Nature of Monovalent Cations on Surface Isotherms of Saturated C_{16} to C_{22} Soap Monolayers

ARIS P. CHRISTODOULOU and HENRI L. ROSANO

The City College of the City University of New York, New York, N. Y. 10031

Specific cation effects on surface pressure, potential, and viscosity vs. *molecular area isotherms of palmitic, stearic, arachidic, and behenic acid monolayers at the air–water interface have been investigated at high pH and 30°C. Surface pressure–area isotherms for stearic acid films were expanded over 0.5N hydroxides in the order: Cs > Rb > K > Na > Li, NH_4 > H. High surface viscosities and small, negative surface potentials for the alkali metal series suggest close proximity or penetration of the counterion into the interfacial plane. The unusual behavior of NH_4^+ substrates led to an investigation of a proposed counterion–hydrogen ion competition, and this effect was shown with K^+ substrates to be enhanced with increasing monolayer compression, and/or with increasing carboxyl chain length of the film molecule.*

The force-area (π-A), surface potential–area (ΔV-A), and surface viscosity–area (η-A) characteristics of long-chain fatty acid monolayers at the air–water interface have been extensively investigated over acid and neutral aqueous solutions (*17*). Studies of fatty acid monolayer isotherms at high pH and the specific cation effect on the isotherms are less numerous. The difficulties inherent in working at high pH are:

The fatty acid monolayer becomes increasingly solubilized into the aqueous substrate.

Traces of polyvalent ions—Ca^{2+} or Mg^{2+}, for example—affect the results drastically.

Competition at high pH from the hydrogen ion for the soap carboxylate anion at the interface can be expected. This would tend to confound investigations, of specific effects of cations other than hydrogen.

These difficulties can be overcome by using an automated Langmuir trough to assure reproducible compression, adding a complexing agent (Versene) to the aqueous substrate, and working at sufficiently high pH.

Surface pressures, potentials, and viscosities of stearic acid films on hydroxides of Li, Na, K, Rb, Cs, and NH_4 have been determined to characterize the specific cation effect. The first observation was that of expansion of the isotherms at high pH related to the nature of the cation. In addition, unexpected results were evident with NH_4OH substrates, notably high viscosity and reversal in the sign of the surface potential with compression.

Therefore, we decided to investigate further the surface potential reversal observed with NH_4OH. The effect may be explained by postulating enhanced competition between the hydrogen ion and the salt cation at the monolayer-air interface with increasing monolayer compression, leading to the formation of fatty acid or acid-soap in the monolayer at maximum compression. For this part of the study, the π-A and ΔV-A isotherms of monolayers of palmitic(C_{16}), stearic(C_{18}), arachidic(C_{20}), and behenic(C_{22}) acids have been determined over aqueous substrates of varying pH and containing K^+.

Experimental

The experimental apparatus for measuring surface pressures, potentials, and viscosities is shown in Figure 1. The aqueous substrates used to investigate the specific cation effect were all at a constant cation concentration of 0.5*N*. The pH's of the substrates in each case were: LiOH (12.90), NaOH (13.20), KOH (13.45), RbOH (13.52), CsOH (13.62), and NH_4OH (11.35), all at 30°C. For comparison, the case of 0.1*N* HCl (substrate pH 1.2) was also investigated. The competition between the monovalent soap counterion and the hydrogen ion in the interfacial region was studied by determining the π-A and ΔV-A isotherms at 30°C. of the C_{16} to C_{22} fatty acids over aqueous substrates containing KOH and KCl, at constant (K^+) concentration of 0.5*N* and with pH of the aqueous substrate varying from 5.6 to 12.9. The pH was changed by adding HCl or KOH. The region from 20 to about 80 sq. A. per molecule was investigated. All experiments were conducted within a Faraday box.

The fatty acid solution in *n*-hexane was deposited onto the aqueous surface with an Agla micrometer syringe (Burroughs Wellcome and Co., Tuckahoe, N. Y.). The substrate and film were retained in a fused silica trough (31.2 × 13.6 × 2.5 cm.) of 1-liter capacity. For the experiments with cesium and rubidium substrates, a shallow Teflon trough (26.9 × 14.3 × 0.4 cm.) of 150-ml. capacity was used. Temperature of the substrate was regulated by circulating water from a constant-temperature bath through a glass cooling coil submerged in the substrate. A thermometer was placed inside the substrate. Temperature control was good, within ± 0.2°C.

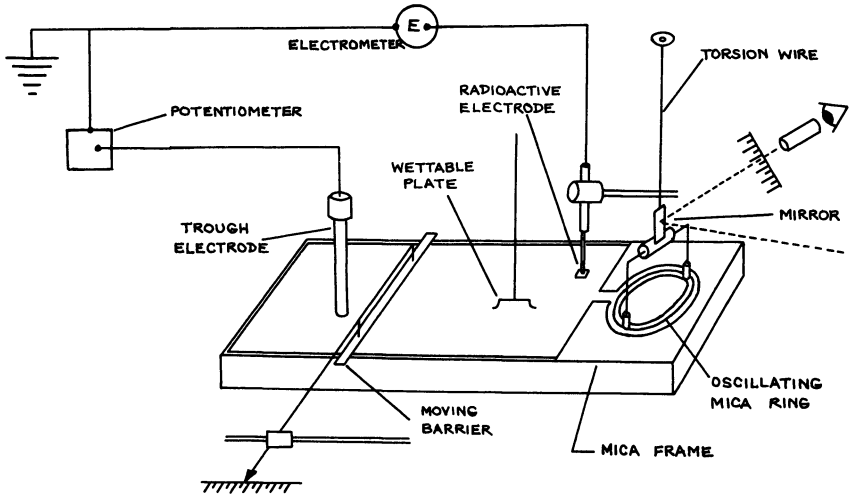

Figure 1. Experimental apparatus for measuring surface pressure, potential, and viscosity

The surface was cleaned by dusting calcinated talcum powder onto it and removing it with the aid of a hollow glass tip connected to an aspirator.

Surface Isotherms. Surface pressures were determined from surface tension measurements, which were made by suspending a sandblasted platinum blade from a transducer-amplifier (Model 311A, The Sanborn Co., Waltham, Mass.). The transducer output was recorded continuously on a recorder (Sargent, Model SR, E. H. Sargent and Co., Springfield, N. J.). The surface tensions were reproducible within ± 0.2 dyne.

Surface potentials were measured with an air-ionizing electrode (*16, 50*) (a radium-226 source, U. S. Radium Corp., Morristown, N. J.) placed 1 to 2 mm. above the surface of the liquid substrate and connected to a precision potentiometer (Model 2730, Honeywell, Denver Division), a high-input resistance electrometer (Model 610B, Keithley Instruments, Inc., Cleveland, Ohio), and a trough electrode (Ag/AgCl or calomel) dipped into the bulk of the aqueous substrate. The radioactive electrode was connected to the input terminal of the electrometer with Amphenol low-noise graphitized shielded cable and connectors. The entire circuit was grounded. The e.m.f. of the cell composed of the radioactive electrode, trough electrode, potentiometer, and electrometer, all connected in series, was measured immediately after cleaning the surface of the aqueous substrate (V_o), and compared with the e.m.f. obtained after spreading a film on the surface (V). The difference between the two e.m.f.'s ($V - V_o$) is the surface potential. The potentiometer opposed a convenient fraction of the cell e.m.f., and the electrometer output was recorded continuously on a recorder (Sargent Model SR). Sensitivity of the surface potential measurements was about ± 1 mv., and reproducibility of the data was within about ± 5 mv.

An automatic barrier drive with variable speed control permitted determination of an optimum compression rate and reproducible π-A and ΔV-A isotherms. A compression rate of 0.34 cm. per second was optimum for this study since below that level the palmitate films desorbed appreciably before compression was complete; compression rates as low as 0.13 cm. per second provided similar and reproducible results for the other chain lengths. The continuous reduction of the surface area by such rapid compression rates results in measured surface pressures for stable films which are considerably above their "equilibrium spreading pressures" (ESP), but still below their "monolayer stability limit" (MSL), which is defined (*17*) as the maximum pressure attainable in the film without collapse. The overcompressed monolayers above the ESP but below the MSL are not in thermodynamic equilibrium with respect to the bulk phase of the surfactant, but they are in equilibrium with a freshly collapsed monolayer, and they can be stable against any apparent changes for long times. Hysteresis effects in the compression and expansion of fatty acid monolayers (*17*) have suggested that the collapsed monolayer has a higher energy than the stable bulk phase, which explains the difference between these two equilibrium surface pressures.

Surface viscosities were measured by a damping method (*16, 32–36, 56*) with a torsion pendulum device, which consisted of a floating frame of paraffined mica placed on one end of the silica trough. The mica frame enclosed a rectangular area connected to a circular area by a narrow channel. A mica ring suspended from a torsion wire was allowed to oscillate in the circular area. Using a light beam reflected from a mirror on the wire, it was possible to measure the decrement of oscillations of the ring on the clean surface and on the film-spread surface. The damping of the oscillations, which depends on the concentration and nature of the surface film, was used to calculate the surface viscosity of the monolayer, according to Equation 1 (*56*):

$$\eta = \frac{(EI)^{1/2}}{2\pi}\left[\frac{1}{R_1^2} - \frac{1}{R_2^2}\right]\left[\frac{\lambda}{(4\pi^2+\lambda^2)^{1/2}} - \frac{\lambda_o}{(4\pi^2+\lambda_o^2)^{1/2}}\right] \qquad (1)$$

where

η = surface viscosity, poises
E = torsion modulus of wire
R_1 = radius of outer ring (fixed)
R_2 = radius of inner ring (moving)
λ = (natural) logarithmic decrement of oscillations with film
λ_o = (natural) logarithmic decrement of oscillations without film
I = moment of inertia of the free system

The monolayer was compressed manually and in stages for this part of the study, and the surface viscosity was determined at every stage of the compression. Surface tensions were monitored with a Rosano tensiometer (Federal Pacific Electric Co., Newark, N. J.). The time required for determining surface viscosity at a single surface concentration was 2 to 3 minutes.

The calculation of surface viscosity by this method had a maximum sensitivity and precision of $\pm 3 \times 10^{-5}$ and $\pm 1 \times 10^{-4}$ surface poise, respectively, in the low viscosity range, and 1×10^{-3} and 1×10^{-2} surface poise, respectively, in the high viscosity region. The method offers extreme simplicity in construction and operation, and is more adaptable to high viscosity films (greater than 10^{-2} surface poise) than the canal or slit viscometer. Recent work (*31*) with the canal viscometer indicates an inability to measure film viscosities of palmitic and stearic acid monolayers over pH 9.0 to 9.5 KOH substrates.

Reagents. The fatty acid solutions were prepared by dissolving about 25 mg. of the fatty acid per 25 ml. of spectrograde *n*-hexane solvent (Fisher Scientific Co.). Arachidic and behenic acids were dissolved in a 98 to 2 mixture of hexane and acetone, both solvents being spectroquality grade. Versene [disodium(ethylenedinitrilo)tetraacetate, reagent grade, Fisher Scientific Co.] was added to the basic substrates at at level of 10^{-3} and $10^{-4}M$, and Calgon (sodium metaphosphate, purified grade, Fisher Scientific Co.) to the acidic substrates at a level of 10^{-3} and $10^{-4}M$ to sequester any polyvalent cations present. No change in monolayer characteristics could be detected between the two concentrations of sequestering agents used.

The fatty acids were commercial samples of highest purity, used without further purification. The palmitic acid was provided by Fisher Scientific Co. (m.p. 61.0–62.0°C.), the stearic (m.p. 68.0–69.5°C.), arachidic (m.p. 76.0–77.0°C.), and behenic (m.p. 80.5–81.5°C.) acids were from the Hormel Institute, Austin, Minn., and were of > 98% purity as shown by GLC. The range in melting points indicates that there may be homologs present which could distort the quantitative relations of this study somewhat. Pellets of NaOH and KOH, concentrated HCl and NH_4OH solutions, and KCl crystals were all reagent grade (J. T. Baker Chemical Co., Phillipsburg, N. J.). Best available grades of anhydrous LiOH (99.3%) and RbOH (99.8%) were obtained from Amend Drug and Chemical Co., New York, N. Y., and CsOH (99.5%) from A. D. MacKay, Inc., New York, N. Y. All of the above reagents were used without further purification.

The water for the substrate was distilled from a Stokes still and foamed in a 600-ml. medium porosity sintered glass funnel; the foam was removed several times by sweeping the surface. The water gave adequately stable base line readings for both the surface potential and surface pressure measurements.

Results

The experimental results are shown in Figures 2 to 11. Each curve represents an average of two or more experiments.

Specific Cation Effect. The π-*A* curves (*see* Figure 2) for stearic acid films are expanded at 50 sq. A. per molecule in the order: Cs > Rb > K > Na > Li, NH_4 > H. The trends confirm the results of Sears and

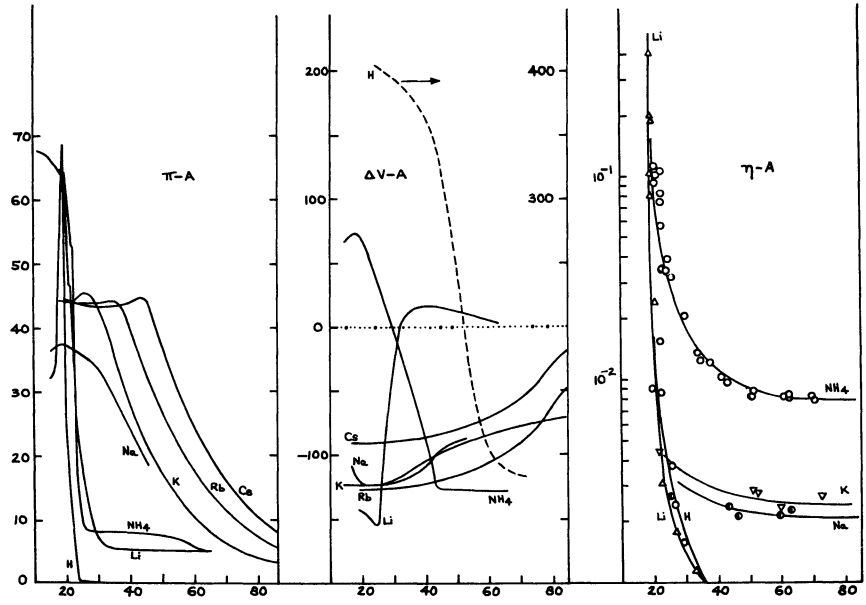

Figure 2. Surface pressure, potential, and viscosity vs. *molecular area of stearic acid monolayers spread at air–water interface over substrates containing ammonium and alkali metal cations (0.5N). 30°C., rapid compression*

Schulman (*51*) on Li, Na, and K stearates. The NH_4OH and LiOH curves are similar in shape to the HCl curve. The CsOH, RbOH, KOH, and NaOH curves are highly expanded, with lower collapse pressures. The NaOH curve seems to exhibit unusually pronounced solubility effects at low surface areas. At areas greater than 50 sq. A. per molecule, the surface pressures for the soaps are still substantial (greater than 5 dynes per cm.), while they fall to near zero for the unionized fatty acid.

The ΔV-A results (*see* Figure 2) indicate that with 0.1*N* HCl substrates, the surface potentials are always positive and increase with compression. At high pH, the surface potentials with Cs, Rb, K, and Na substrates are all small and always negative (air with respect to water). This is confirmed for stearic acid films over sodium-containing substrates by several investigators (*5*, *18*, *20*, *51*, *53*). Increasingly more negative surface potentials are obtained with increasing compression. The Li curve, originally indicating very small ΔV values close to zero, demonstrates the largest change in ΔV with increasing compression. At areas below 25 to 30 sq. A. per molecule, the ΔV-A curves for the alkali metal substrates become horizontal or reverse their downward trend; the reversal is only partial, however, and does not reach positive surface potentials. This behavior is confirmed for behenic acid over sodium-containing

substrates by the data of Goddard, Smith, and Kao (*21*). For stearic acid films, however, Sears and Schulman (*51*) report increasingly less negative ΔV values with compression over NaOH and KOH substrates; at miximum compression, their NaOH curve for 25°C. reaches $\Delta V = 0$. The order of positives of the surface potentials at 50 sq. A. per molecule (*see* Figure 2) is:

$$H > Li > Cs > Rb, K, Na > NH_4$$

while the order at 20 sq. A. per molecule becomes:

$$H > NH_4 > Cs > Rb, K, Na > Li$$

The ΔV-A results for NH_4OH substrates exhibit a unique behavior not seen with the other basic subsolutions. At 60 sq. A. per molecule, the ΔV values are negative and remain so with compression up to 40 sq. A. per molecule. Beyond this point, the curves rise sharply toward positive surface potentials; at maximum compression, potentials of +75 mv. are recorded for stearic acid. Montagne reports +40 mv. for stearic acid films at maximum compression over NH_4OH solutions at pH 11 (*41*).

The surface viscosities (Figure 2) for stearic acid monolayers are highest over NH_4OH substrates at areas greater than 30 sq. A. per molecule; the next highest viscosities in this region are for NaOH and KOH solutions. Viscosities with HCl and LiOH are the lowest at areas greater than 50 sq. A. per molecule; below 30 to 50 sq. A. per molecule, viscosities increase very sharply and approach the values obtained with NH_4OH, KOH, and NaOH. The effect of chain length on film viscosity is shown in Figure 3 for NaOH substrates; viscosities increase with chain length.

The film viscosities of stearic acid on HCl substrates agree with those reported by Boyd and Harkins (*6*), who used the method of damped oscillations but are at least an order of magnitude higher than those obtained by canal viscometers by Jarvis (*31*) and Deamer (*12*). It is expected (*16, 31*) that the method of damped oscillations will give viscosities higher by this amount from those obtained by the canal viscometer. This is especially true in the condensed region of the monolayer, where the concentrated surface charge of dipoles tends to orient water molecules adjacent to the interface and increases the drag on the moving element of the torsion pendulum viscometer; this drag is compensated for in canal viscometers by an absolute viscosity correction factor (*16*). Comparisons in the highly condensed region are complicated also by the increasing non-Newtonian behavior of the fatty acid film in this region (*17*).

Monovalent Cation *vs.* Hydrogen Ion Competition in Surface Phase. The π-A and ΔV-A curves *vs.* bulk pH for palmitic (C_{16}), stearic (C_{18}), arachidic (C_{20}), and behenic (C_{22}) acid monolayers on KOH + KCl sub-

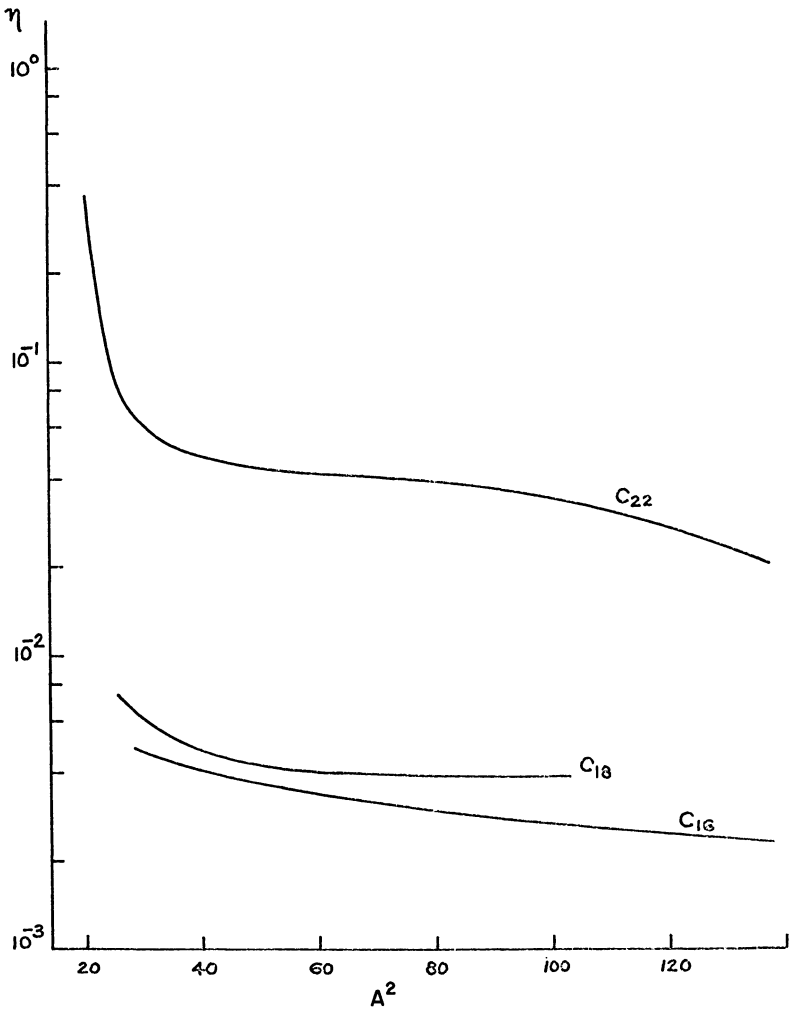

Figure 3. Surface viscosity vs. *molecular area for palmitic, stearic, and behenic acid monolayers spread on 0.5N NaOH substrates at 30°C.*

strates are shown in Figures 4 to 11. The force–area curves indicate greater monolayer condensation with increasing chain length of the film molecule. This trend is confirmed in the literature for acidic substrates (*1, 39, 42*), and for basic substrates at surface areas over 150 sq. A. per molecule (*22*).

For palmitic acid films (Figures 4 and 5), the π-*A* curves for pH 5.6 to 10.3 exhibit "close-packed heads" and "close-packed tails" regions which are absent at higher pH. At pH 7.4 and 10.3, there is evidence of a phase

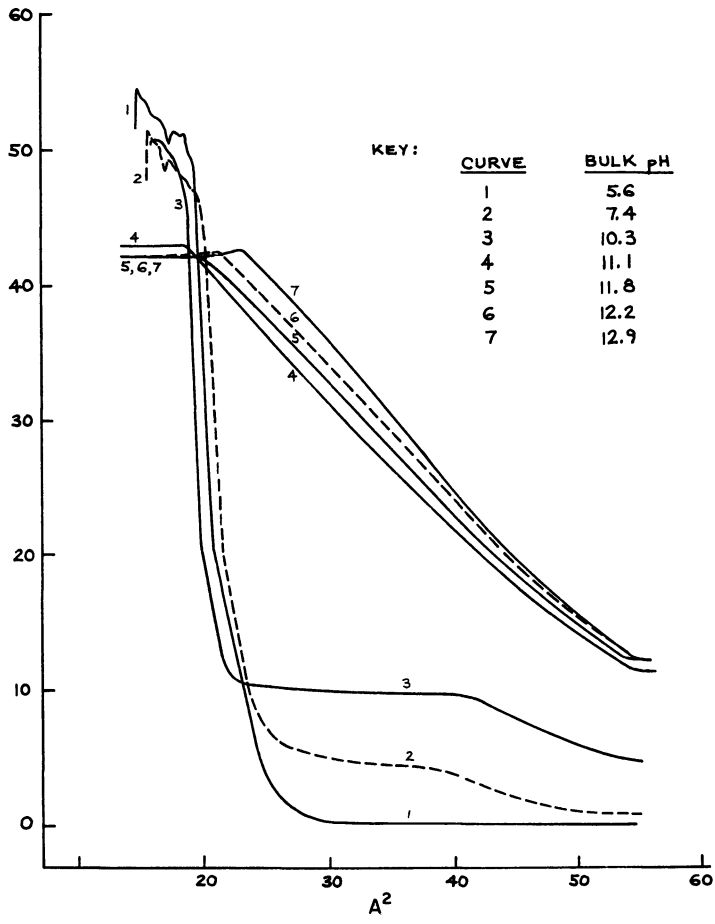

Figure 4. Surface pressure vs. *molecular area for palmitic acid monolayers spread on aqueous substrates of varying pH at 30°C. and 0.5N total cation concentration (KOH + KCl). Rapid compression*

change at about 40 sq. A. per molecule, which disappears at higher pH. Above pH 10.3, there is a large expansion in the π-A isotherm and, at areas $\leqslant$ 35 sq. A. per molecule, there is a reversal in the sign of the surface potential from positive to negative. Above pH 11.1, the π-A curves are almost coincident, with only slight expansion evident with increasing pH; in this same region, the ΔV-A curves are also coincident, decrease slightly with compression, and eventually attain a constant negative value.

Stearic acid films (Figures 6 and 7) show similar behavior except that the point at which the ΔV-A curve becomes horizontal and unaffected by compression is at higher pH—*i.e.*, 12.3. The π-A curves indicate con-

siderable expansion above pH 10.1, with phase changes evident at pH 10.1 to 11.8. Above pH 12.3, the curves are almost coincident, the phase changes are absent, and collapse occurs at a much lower surface pressure.

For arachidic acid films (Figures 8 and 9), the results are similar to stearic acid, except that the π-A isotherms are more condensed, with the collapse for pH above 12.3 occurring at a surface pressure only about one half that at lower pH.

Behenic acid films (Figures 10 and 11) show the most condensed π-A isotherms.

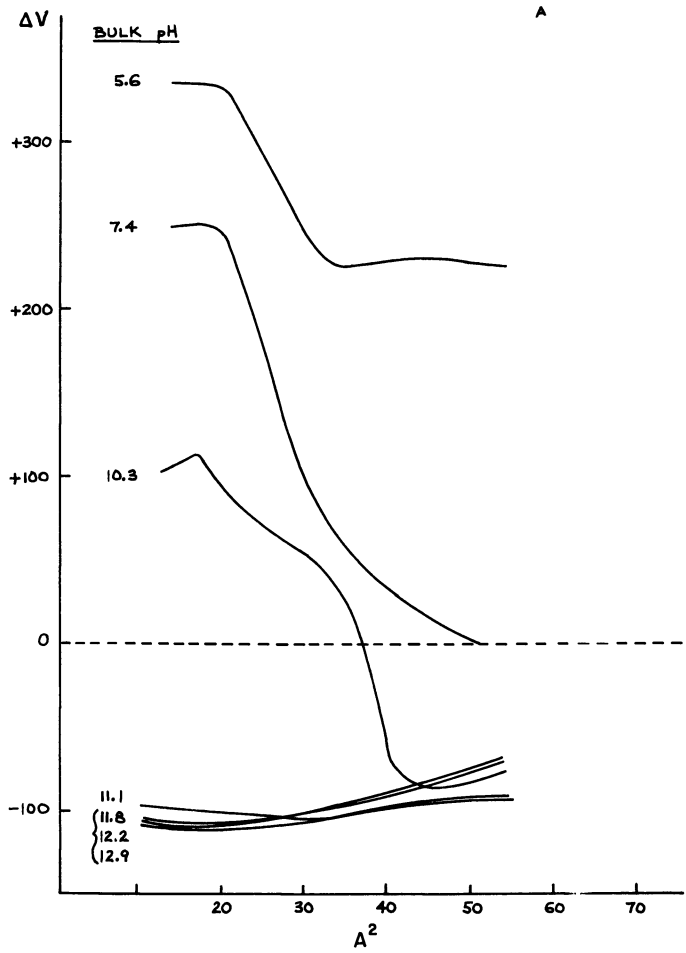

Figure 5. Surface potential vs. *molecular area for palmitic acid monolayers spread on aqueous substrates of varying pH at 30°C. and 0.5N total cation concentration. Rapid compression*

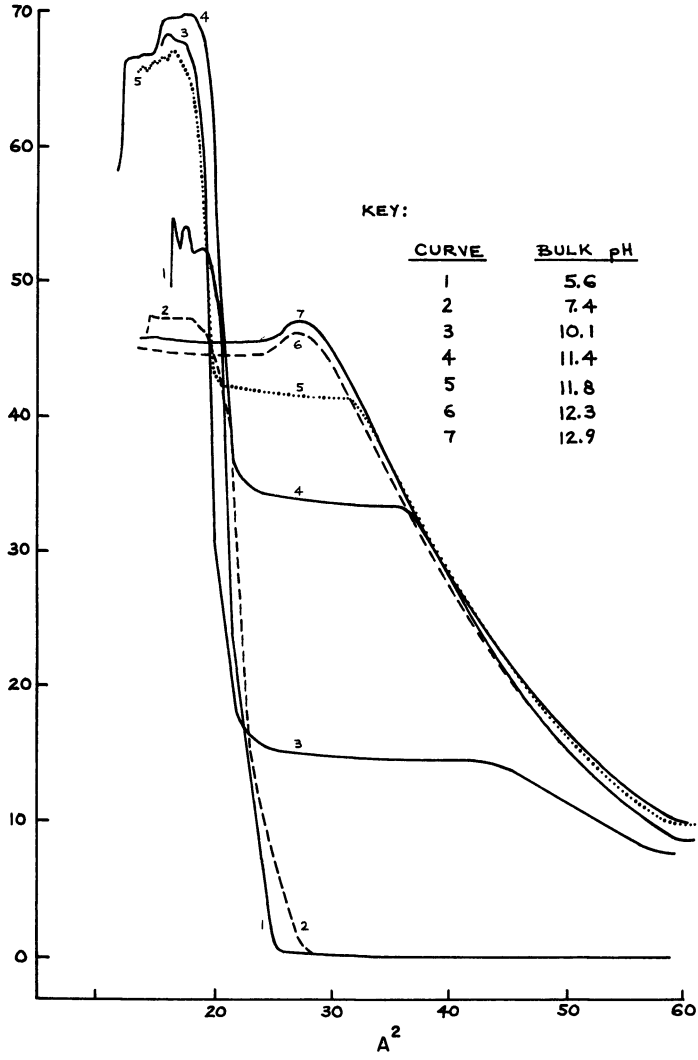

Figure 6. Surface pressure vs. *molecular area for stearic acid monolayers spread on aqueous substrates of varying pH at 30°C. and 0.5*N *total cation concentration. Rapid compression*

The π-A curves above pH 12.3 retain the phase change which is noticed at lower pH, unlike the behavior at lower chain lengths. The ΔV-A curves, in addition, do not attain a horizontal value with compression, even at pH 12.9; they continue to manifest a tendency towards less negative surface potentials with increasing compression.

Discussion

π-A and ΔV-A. Expansion in the π-A isotherms of C_{14} to C_{20} fatty acids over substrates varying from pH 2 to 12 have been reported (*2, 24*), but the specific cation effect on the expansion was not investigated. Goddard and Ackilli (*20*) studied the monolayer properties of stearic acid (C_{18}) on substrates of pH 2 to 11.1, varied by adding HCl or NaOH. Force-area data did not vary appreciably with pH up to pH 8.5; at pH 9, the film started to solubilize and expand. Spink (*53*) reported a slightly higher pH of expansion for stearic acid monolayers. Goddard, Smith, and Kao (*21*) conducted a similar study on the monolayer properties of behenic acid (C_{22}) upon substrates from pH 2 to 14; the films began to expand at pH 10.

The ΔV-A relationships for fatty acid monolayers were first investigated over a wide range of pH by Schulman and Hughes (*49*), who found that for myristic acid (C_{14}) films over substrates of pH 0 to 13, ΔV decreased with pH; HCl or NaOH was added to vary pH. Similar results were reported for stearic acid films over substrates whose pH was varied from 2 to 10 with HCl and NH_4OH (*48*), and over substrates ranging from pH 2 to 12, containing 0.01*M* sodium ions (*5, 18, 20, 53*).

The compositions of stearic and behenic acid films over substrates containing 0.1*M* sodium ions in the pH range 4 to 9.7 have been determined (*3*) by skimming the fatty acid film off the surface and determining carboxylate content by infrared analysis. The evidence of the present study, however, suggests that even at bulk pH 9.7, stearic and behenic acid films are not completely saponified.

The influence of the hydrophobic chains on π-A and ΔV-A isotherms of fatty acid monolayers has been studied in the past but generally only on acid or neutral solutions (*1, 17, 42*). The high pH region was investigated with respect to chain length over sodium-containing substrates but only in the expanded area region from 150 to 2000 sq. A. per molecule (*22*). In a recent study in our laboratory on the binding of K^+ and Na^+ counterions to the surfaces of soap micelles (*15, 47*), the apparent degree of binding of potassium increased with increasing aliphatic chain length of the soap anion (from C_{10} to C_{14}), indicating that increasing chain length increases the attractive forces acting on the cations. Lucassen-Reynders (*38*) considered the surface ideality of fatty acid films and suggested that it is the interaction between the hydrophobic chains rather than electrical interactions of the head groups at the interface which makes surfaces nonideal.

Specific Cation Effect. Adam and Miller (*2*) noted a specific expansion in the π-A isotherms of behenic acid on 2*N* solutions of NaOH and KOH. They attributed the expansion of the ionized monolayer to cou-

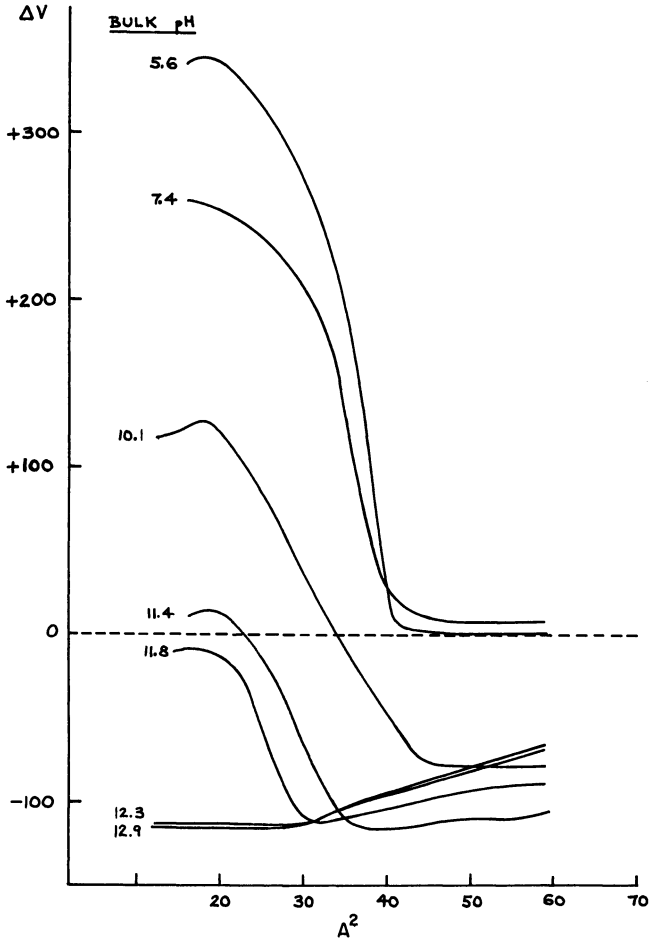

Figure 7. Surface potential vs. *molecular area for stearic acid monolayers spread on aqueous substrates of varying pH at 30°C. and 0.5*N *total cation concentration. Rapid compression*

lombic repulsion between the similar electric charges on the adjacent polar end groups of the fatty acid molecules.

Sears and Schulman (*51*) measured surface pressures and potentials *vs.* molecular area (20 to 110 sq. A. per molecule) for the alkali metal stearates over 0.5*N* solutions of LiOH, NaOH, and KOH. Like Adam and Miller, they detected a specific cation effect on the π-*A* and ΔV-*A* isotherms of the ionized monolayer at high pH; the π-*A* curves were expanded in the order of the crystalline sizes of the alkali metal cations: K > Na > Li. The sequence is the reverse observed for the long-chain

alkyl sulfates (*45, 58*). Sears and Schulman concluded that electrostatic repulsion (and the degree of surface ionization) was not important in determining expansion of the monolayer, as compared with the specific cation effect. No model of the interface was presented, however, indicating the relationship of the hydrated cation to the charged head groups of the fatty acid in the plane of the interface. In addition, no explanation was given for the reversal of the sulfate and carboxylate series.

Measurements of surface viscosity are included in the present study to supplement those of surface pressure and potential in an attempt to characterize better the relationship of the salt cation to the film anion at the interface. The demonstration in this study of the existence of a specific cation effect on the surface isotherms of ionized fatty acid monolayers conflicts with the two popular molecular models for such interfaces. The Helmholtz model (*29, 49*), for example, implies that the charged surface is impenetrable, the charge is uniformly spread over the surface, and the counterions are point charges contained in a plane parallel to the plane of the long-chain head group anions. The Gouy model of the diffuse double layer involves the same assumptions, except that the counterions are distributed in a Boltzmann distribution in the subsurface phase. The expectation with both the Helmholtz and the Gouy-Davies models (*9, 10*) for ionized films is: no change in the surface pressure with changing counterion size, at the same ionic strength; a relatively large surface potential, negative in sign for soap monolayers; and a relatively low surface viscosity, of the order of 10^{-4} surface poise. The expansion of the ionized film would be attributed to repulsion of adjacent like charges at the interface (*2*). Our study demonstrates that the surface potentials are small, indicating close proximity of the cation to the plane of the interface. Surface viscosities are high because of the influence of the cation charges on the film molecules at short distances. The influence on surface pressures, potentials, and viscosities may be caused by a direct penetration of the counterion into the plane of the interface, induced orientation of water dipoles near the interface, changes in surface pH and the degree of surface ionization of the fatty acid, or a combination of the above.

For completely ionized monolayers, the Gouy-Davies model predicts lower π and less negative ΔV with increasing ionic strength. These trends are confirmed for behenic acid films at high pH but only in the expanded area region ($>$ 90 sq. A. per molecule for π-A and $>$ 47 sq. A. per molecule for ΔV-A) (*21*). Experiments on octadecyl sulfate films (*40*) suggest that the Gouy theory seems applicable only for areas above about 5000 sq. A. per molecule. Nevertheless, the model has been used beyond its formal working range—*i.e.*, for closely packed monolayers—because of various compensating factors (*10, 27*). Goddard, Smith, and Lander

(*22*) discuss several modifications to the Gouy-Davies equation of state, including correction of the cohesive term (*8, 23, 52*), and of the electrical repulsion term by a "fluctuation potential" (*4, 40*); comparison is also made with alternative electrical models of Stern (*11*) and van Voorst Vader (*40, 57*), which are difficult to use because they require information on the distance of closest approach of the counter ion and the depth of the surface region, respectively.

Interfacial Penetration of Counterions and Hydrogen Ion Competition. In a study with cationic ionized monolayers $C_{18}H_{37}N(CH_3)_3^+$, Davies and Rideal (*10, 11*) predicted that penetration of the counterions into the interface leads to increases in surface viscosity if the packing of the surface molecules is sufficiently close; a two-dimensional salt lattice is formed, made up of ions of opposite sign attracting each other strongly. At 85 sq. A. per molecule, increases in surface viscosity were observed with an increase in salt concentration [this occurs also with stearic acid films over H_2O substrates to which 1*M* NaCl is added (*12*)]. The less hydrated counterions in bulk solution like chloride and iodide were more effective in penetration than the more hydrated fluoride ion. At 170 A., the viscosity plot did not rise with higher salt concentration but decreased continuously; at these large areas, penetration of the ions cannot cause the close linking required to raise the surface viscosity. The specific counterion (anion) effect was also observed with π-*A* isotherms up to 70 sq. A. per molecule (*45*).

The counterions involved in the present study decrease their degree of hydration in bulk solution in the following order: $Li^+ > Na^+ > K^+ > NH_4^+ > Rb^+ > Cs^+$ (*19, 25, 54*), so that Cs^+, having the least hydration, could penetrate furthest into the plane of the interface as the monolayer is compressed, following the argument of Davies and Rideal. The maximum penetration of Cs^+ is confirmed by expansion in the π-*A* curves and by the small (less negative) values of surface potential in the ΔV-*A* curves. In the same scheme, the Li^+ would have to be pictured as least penetrating, implying that ΔV values should be most negative for LiOH among the alkali metal hydroxides. This is so at 20 sq. A. per molecule, but not at larger areas. The explanation may depend on the role of the water dipoles near the interface, which would tend to undergo strong ion-dipole interactions with Li^+ at expanded areas, thus neutralizing the surface charge in the monolayer. That the effect of the water dipoles can be important was shown in recent work (*14*) on stearic acid films between 15° to 37°C., in which surface viscosities, potentials, and pressures were determined over H_2O and D_2O substrates at p H2.

The case of NH_4OH can be treated at first in a similar manner. Thus, the relatively unhydrated NH_4^+ at an area of about 70 sq. A. per molecule could be pictured as having penetrated the plane of the ionized car-

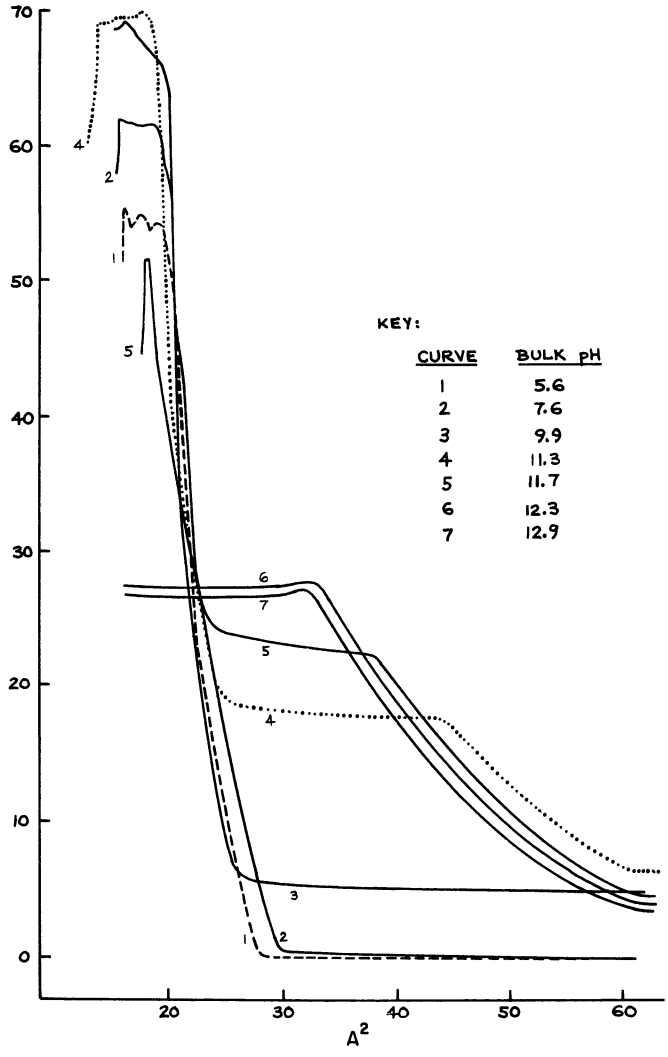

Figure 8. Surface pressure vs. *molecular area for arachidic acid monolayers spread on aqueous substrates of varying pH at 30°C. and 0.5*N *total cation concentration. Rapid compression*

boxylate head groups. With compression, the cation could be squeezed to a position slightly above the plane of the head groups; this maximum degree of penetration would explain the very large surface viscosities obtained with NH_4OH, especially at expanded areas larger than 50 sq. A. per molecule, and the unusual positive surface potentials at maximum compression. This reasoning is not adequate, however, in that it does

not explain why the expansion series of the π-A isotherms is not in the same order as the cation penetration series suggested earlier. It is difficult in any case to relate the monolayer properties (π, ΔV, and η) to a molecular model of the interface which includes counterion penetration, without considering the effect of water on the surface solution, of the acidic (or basic) strength of the surfactant, or of polarization energies of the amphipathic ion and its counter ion.

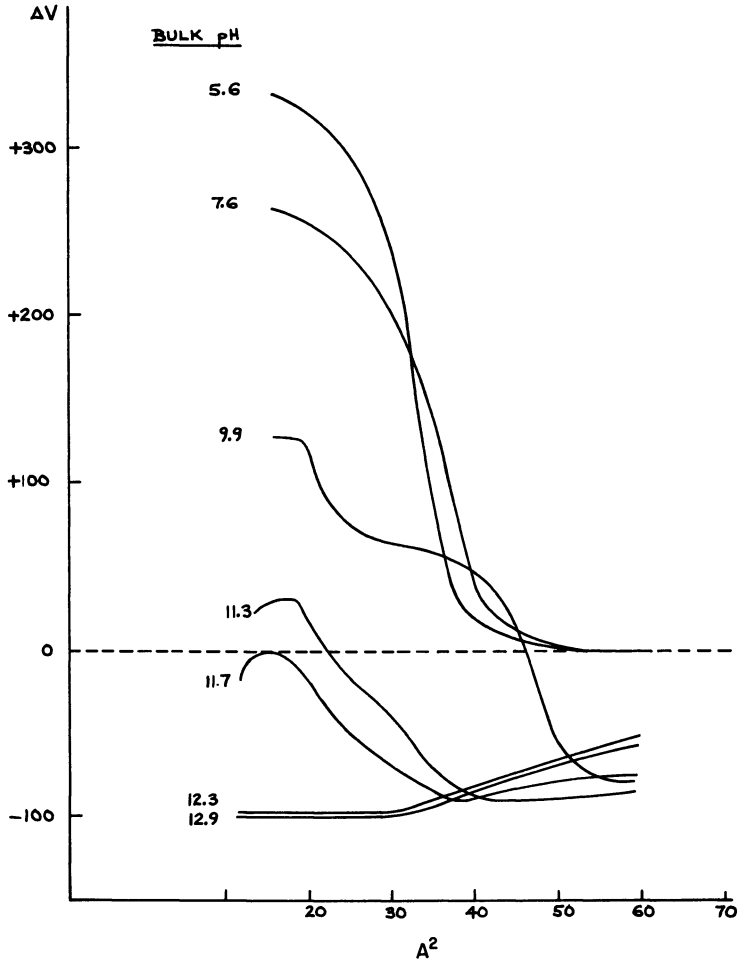

Figure 9. Surface potential vs. molecular area for arachidic acid monolayers spread on aqueous substrates of varying pH at 30°C. and 0.5N total cation concentration. Rapid compression

An alternative explanation of the NH_4OH results suggests itself; at maximum film compression, enhanced competition between H^+ and NH_4^+

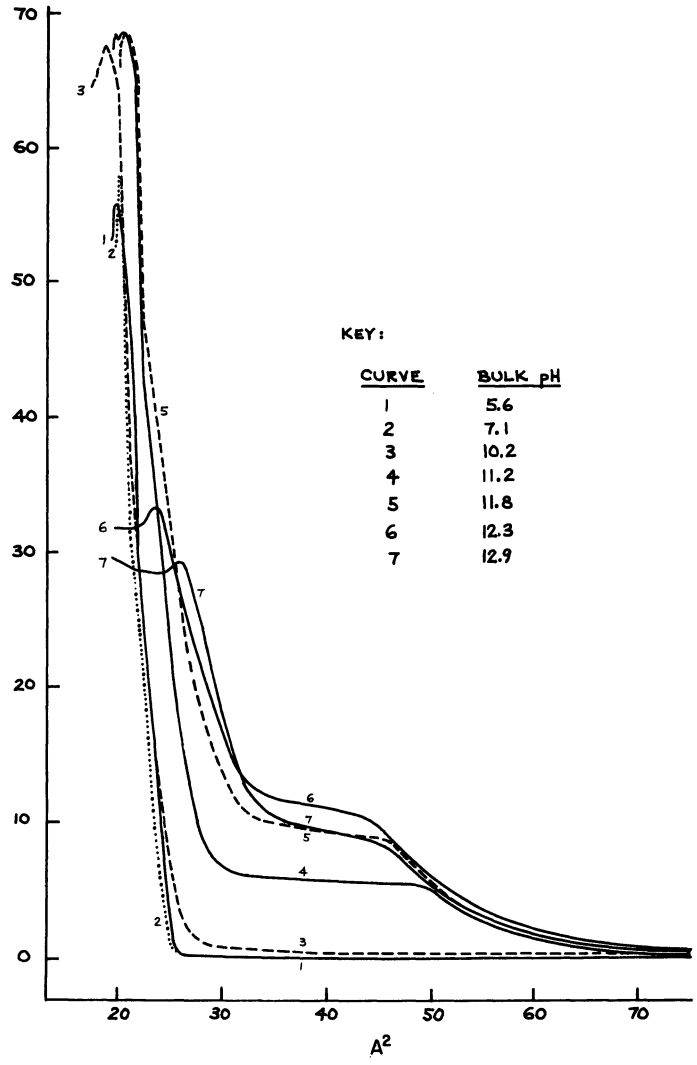

Figure 10. Surface pressure vs. *molecular area for behenic acid monolayers spread on aqueous substrates of varying pH at 30°C. and 0.5N total cation concentration. Rapid compression*

for the carboxylate anion may prevail. This competition should be more intense with NH_4OH than with the alkali metal hydroxides because the substrate pH with the former is only 11.35, while with the latter it is $\geqslant$ 12.9. The concentration of H^+ ions at the interface is thus greater with NH_4OH, permitting the possibility of discharge of the ionized interface,

the formation of acid soap (*21*) or fatty acid on the surface, and the concomitant rise of the surface potential to positive values. Recent studies on bulk potentiometric titrations of soap solutions suggest that no acid-soap or fatty acid exists at bulk pH greater than about 12.3 (*46*). Goddard, Smith, and Kao (*21*), however, claim that surface ionization may not be complete for compressed behenic acid films even up to bulk pH 14 since the ΔV values continue to change between pH 13 and 14. This conclusion agrees with the results of our study. The ΔV-A curves for behenic acid films (*see* Figure 11) at varying substrate pH suggest that even up to bulk pH 12.9, hydrogen ion is still an effective competitor for the soap anion at the interface. The competition diminishes as the chain length decreases, at a given substrate pH. Increasing the chain length results in greater attractive forces among the associated chains drawing the end groups closer together, thus increasing the field strength and the binding of the counterions. This increase in the attractive forces acting on the cations confirms our recent results on counterion binding to micelle surfaces (*15, 47*). The attraction for the smaller hydrogen ions is expected to be greater than for the larger monovalent cations, because the "field strength" or polarizing power increases with decreasing ionic size.

The surface potential-area curves *vs.* pH (*see* Figures 5, 7, 9, and 11) can be treated, as a first approximation only, by the Helmholtz formula for a partially charged weak acid monolayer (*5, 10, 20*):

$$\Delta V = 12\pi[n_1\mu_1 + n_2\mu_2] \qquad (2)$$

where ΔV is the surface potential in millivolts; n_1 and n_2 are the number of dipoles per square centimeter in the monolayer of fatty acid and soap, respectively; and μ_1 and μ_2 are the surface dipole moments (in milliD) for the uncharged fatty acid and charged soap forms of the molecules, respectively. Goddard and co-workers (*21*) have added a third term to the above expression to account for the possible formation of acid-soap on the surface at intermediate pH. If the electrical contribution of the diffuse layer is effectively incorporated in the μ_2 term (it will be only a small contribution at the high ionic concentrations used in this study), and μ_1 and μ_2 are assumed constant with pH at a given molecular area, the values of n_1 and n_2 can be calculated. The μ_1 and μ_2 values used are for the extreme conditions of pH at each molecular area (where the contribution of only one term in Equation 2 remains). The results are plotted as fraction of soap molecules present in the monolayer *vs.* pH of substrate, for molecular areas of 20 and 30 sq. A. (*see* Figure 12). As expected from the interpretation given above, the behenic acid films show less soap formation than the smaller chain lengths, at areas of 20 sq. A. per molecule and at a given bulk pH above 5.6. This is explained as being

caused by enhanced competition by hydrogen for the soap anion at the air–water interface, which is increased as chain length increases. At larger molecular areas (30 sq. A.), at a given pH and chain length of surfactant molecule, the results indicate enhanced soap formation on the surface due to a decrease in the hydrogen ion–soap cation competition.

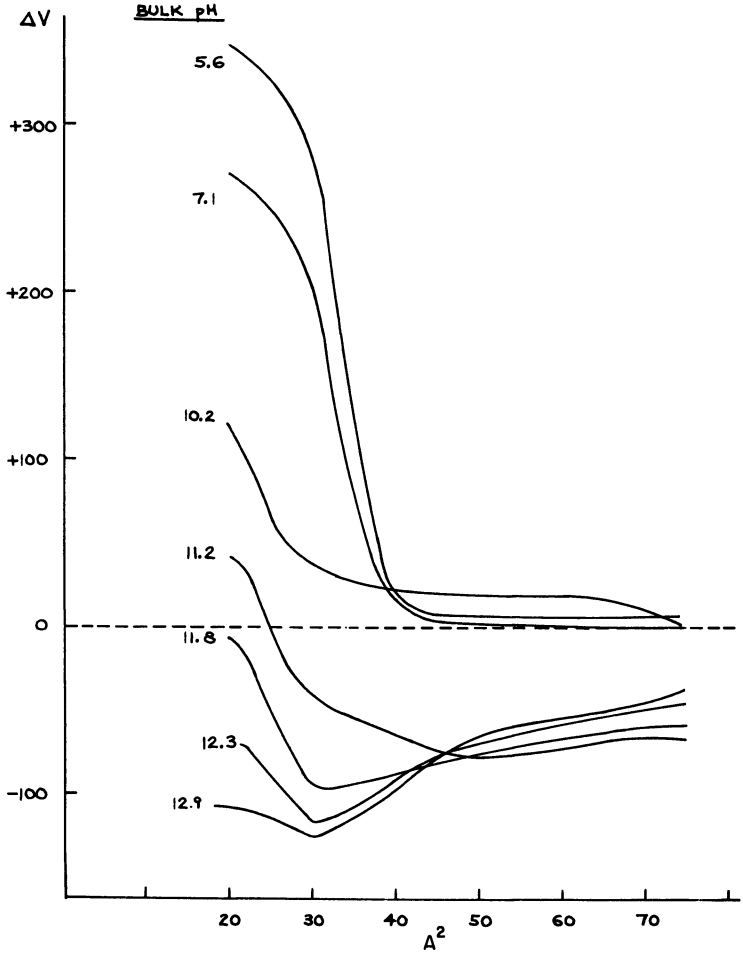

Figure 11. Surface potential vs. *molecular area for behenic acid monolayers spread on aqueous substrates of varying pH at 30°C. and 0.5*N *total cation concentration. Rapid compression*

Reversal of Specific Cation Effect in π-A Isotherms. The reversal of the specific cation effect on the π-A curves for the long-chain carboxylic acids (*51*) and the alkyl sulfates (*45, 58*) can be related to a model sug-

gested by Teunissen and Bungenberg de Jong (*55*) and discussed by Bregman (*7*) and Kruyt (*37*) to account for the reversal of selectivities of ionized cationic exchange resins. For the colloidal resins, a charge reversal is assumed to occur at the ionized interface, caused by fixation of a sufficient number of cations on the ionized groups. The affinity of cations and the colloidal anions depends upon the valence and polarizing power of the cation (decreases with increasing ionic size), and on the polarizability of the colloidal anionic group and that of the solvent, water. The calculated order of polarizability of the anionic group is (*7*, *37*, *55*):

$$PO_4^{3-} > COO^- > H_2O > SO_4^{2-}$$

For anionic monolayers, the reversal of the π-A isotherms can be explained in terms of a competition between the anionic head groups and the alkali metal cations for molecules of water. If a modified Stern-type model of the plane interface is assumed, this interface will be composed of distinct adsorption sites, with counterions (cations) of finite size that can adsorb on these sites if the standard free energies of adsorption are favorable. If the anionic head group is more polarizable than water, as with carboxylic acids or phosphates, the hydration shell of the cation is incompletely filled, and the order of cation sizes near the interface is $K^+ > Na^+ > Li^+$. When the polarizability of the anionic group is less than that of water, as with the sulfates, the lithium cation becomes the most hydrated one, and the order of cation sizes becomes $Li^+ > Na^+ > K^+$.

As the counterion penetrates the plane of the interfacial head groups, the surface pressure will be affected as a first-order effect; thus, the expansion of the π-A isotherms for the fatty acid monolayers is in the same sequence as the cation sizes noted above. The penetrated counterions must be held with an energy at least comparable to KT since they are not expelled during the kinetic movement of the film molecules, but remain in place and increase the surface pressure. To penetrate the plane of the head groups in the monolayer, the counterions must possess sufficient adsorption energy to overcome the work against the kinetic surface pressure π_K, such that, according to Davies and Rideal (*10*):

$$\lambda_p > \pi_K A^*$$

where λ_p is the polarization energy of the counterion, and A^* is the actual area of the (hydrated) counter ion entering the film. Polarization energies of counterions in many colloidal and monolayer system have been calculated (*10*).

It would be interesting to test the reversal of the π-A isotherms with monolayers of long-chain phosphates, but the only data available to our knowledge are for octadecyl phosphates and phosphoric acids over

sodium-containing substrates (*43, 44*). Of further interest with the long-chain phosphates would be the investigation of the positions of Cs and Rb^+ in the π-*A* expansion series; for the carboxyl and sulfate colloids, the position of Cs^+ and Rb^+ in an affinity series is reported by Kruyt (*37*) as being regular relative to Li^+, Na^+, and K^+ but not regular with phosphate colloids. The explanation offered is that the Cs^+ and Rb^+ ions have too large an ionic radius, and hence too small a field strength to show polarizing action; an irregular sequence of π-*A* expansion—$K^+ > Na^+$, Rb^+, $Cs^+ > Li^+$—can therefore be expected.

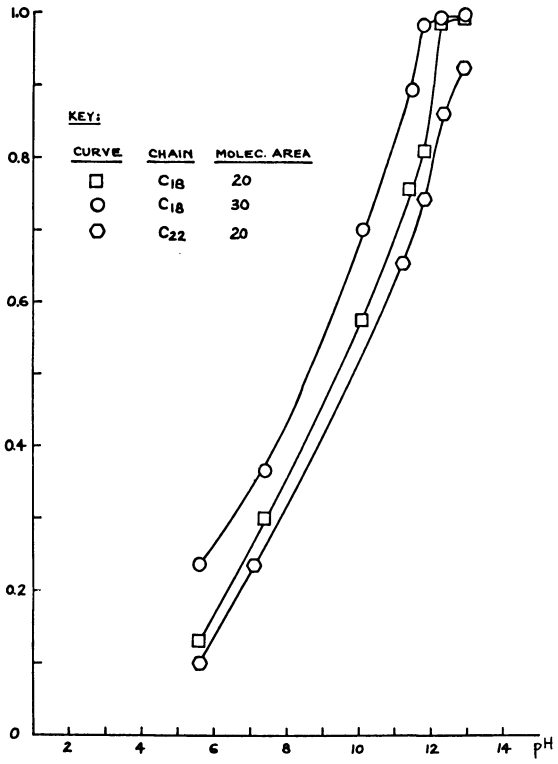

Figure 12. Fraction of soap molecules present in monolayer vs. *pH of substrate at 30°C. and 0.5N total cation concentration (KOH + KCl). Stearic and behenic acids at 20 and 30 sq. A. per molecule*

There is evidence in the case of anionic exchange resins (*7, 28*) that an increase in temperature (to 130°C.) causes a reversal of selectivity for the alkali metal counterion; the higher temperature increases thermal motion and perhaps partially dehydrates the counterion. Demonstration

of this effect by monolayer technique is complicated by the high temperatures required.

Similarities between reversal of charge spectra for colloids with solubility sequences of salts in bulk solution have been indicated (*7, 37*)—for example, for salts possessing different cations but the same anion, the solubility sequence of the phosphates is $K^+ > Na^+ > Li^+$, while it is the reverse for the sulfates (*7, 30*). In view of this similarity, it is natural to introduce this fact as another possible link to explain the reversal of the specific cation effect in π-*A* isotherms, though the precise relationship to monolayers is not clear at this time.

A better method for studying the alkali metal cation–soap anion interaction on the surface, according to Weil (*58*), is to assume a similarity between surface behavior and solution behavior and to use the activity coefficient of the solute in the solution as the parameter to account for surface behavior. By plotting activity coefficients as a function of the molality for the salts of the alkali metals (*7, 26*), the resulting order of the curves of the weak acids (formates, acetates, hydroxides) is the reverse of that found for the strong acids (chlorides, bromides, nitrates, chlorates, sulfates). The activity curves of the acetate salts can be used as the counterparts for the long-chain fatty acid salts, while those for the chlorides can be the analogs of the alkyl sulfates. The scheme is speculative in that the fatty acid and alkyl sulfate salts micellize, and acetate and chloride do not.

The concept of the reversal of the π-*A* isotherms being related to acidic (or basic) strength is suggested for long-chain anionic surfactants by the data of Sears and Schulman (*51*). Whereas the π-*A* expansion series at bulk pH $\geqslant$ 12.6 is in the order $K^+ > Na^+ > Li^+$ for the stearate soap, the order reverses ($Na^+ > K^+$) at bulk pH 8.5, where the stearate, which is a "weak acid," is not fully ionized (*46*). By contrast, the "strong acid" octadecyl sulfates, which are fully ionized over H_2O solutions, expand in the same order ($Li^+ > Na^+ > K^+$) over neutral (*45*) and strongly basic substrates greater than pH 12.6 (*13*). These trends were confirmed for weak acid (carboxylic, phosphonic) and strong acid (sulfonic) colloidal exchange resins and are discussed by Bregman (*7*).

Monolayers of the cationic surfactant stearyl trimethylammonium bromide (STAB), which is a "strong base," would be expected to exhibit no reversal at low pH, analogous to the behavior of the alkyl sulfates at high pH, but no data are available on this point. The expansion series for the π-*A* isotherms of STA^+ is reported by Rogers and Schulman (*45*) to be $F^- > Cl^- > I^-$, or in the order of increasing (unhydrated) ionic size, analogous to the sulfate series $Li^+ > Na^+ > K^+$. The "weak base" *n*-stearylamine (*17*) spread on acidic substrates ($10^{-3}M$ H_2SO_4, $10^{-2}M$ HCl) shows specific π-*A* expansion in the order $Cl^- > SO_4^{2-}$, which is the same rela-

tive sequence of counterion sizes as occurs with the "strong base" STAB. Apparently, the relationship between acidic (or basic) strength and π-A expansion which was evident with the anionic surfactants does not hold for the cationics. Admittedly, however, the evidence is scanty and incomplete; in particular, the data on stearylamine (*17*) are not all at the same counterion concentration.

Rogers and Schulman (*45*) report the existence of both a specific cation and a specific anion effect on π-A isotherms for the anionic octadecyl sulfates. The anionic fatty acids have indicated a specific cation effect, but no demonstration of an anion effect has been attempted. However, the long-chain cationic surfactants STA^+ exhibit a specific anion effect only.

Acknowledgment

The authors acknowledge the financial support of The City College Research Fund, and the helpful suggestions of E. D. Goddard and the late J. H. Schulman. APC thanks the NSF Graduate Traineeship Program for additional financial support. The help of J. Forkosch with the numerical calculations is appreciated.

Literature Cited

(1) Adam, N. K., Harding, J. B., *Proc. Roy. Soc. (London)* **A138**, 411 (1932).
(2) Adam, N. K., Miller, J. G. F., *Proc. Roy. Soc. (London)* **A142**, 401 (1933).
(3) Bagg, J., Haber, M. D., Gregor, H. P., *J. Colloid Interface Sci.* **22**, 138 (1966).
(4) Bell, G. M., Levine, S., Pethica, B. A., *Trans. Faraday Soc.* **58**, 904
(5) Betts, J. J., Pethica, B. A., *Trans. Faraday Soc.* **52**, 1581 (1956).
(6) Boyd, E., Harkins, W. D., *J. Am. Chem. Soc.* **61**, 1188 (1939).
(7) Bregman, J. I., *Ann. N. Y. Acad. Sci.* **57**, 125 (1953).
(8) Chattoraj, D. K., Chatterjee, A. K., *J. Colloid Interface Sci.* **21**, 159 (1966).
(9) Davies, J. T., *Proc. Roy. Soc. (London)* **A224**, 208 (1951).
(10) Davies, J. T., Rideal, E. K., "Interfacial Phenomena," Academic Press, New York, 1961.
(11) Davies, J. T., Rideal, E. K., *J. Colloid Sci. Suppl.* 1, 1 (954).
(12) Deamer, D. W., Jr., Ph.D. thesis, Ohio State University, 1965.
(13) Dreher, K., personal communication, Jan. 10, 1967.
(14) Dreher, K. D., Sears, D. F., *Trans. Faraday Soc.* **62**, 741 (1966).
(15) Feinstein, M. E., Rosano, H. L., *J. Colloid Interface Sci.* **24**, 73 (1967).
(16) Gaines, G. L., Jr., "Insoluble Monolayers at Liquid-Gas Interfaces," Chap. 3, Interscience, New York, 1966.
(17) *Ibid.*, Chap. 4, 5.
(18) Glazer, J., Dogan, M. Z., *Trans. Faraday Soc.* **49**, 448 (1953).
(19) Glueckauf, E., *Trans. Faraday Soc.* **51**, 1235 (1955).
(20) Goddard, E. D., Ackilli, J. A., *J. Colloid Sci.* **18**, 585 (1963).
(21) Goddard, E. D., Smith, S. R., Kao, O., *J. Colloid Interface Sci.* **21**, 320 (1966).

(22) Goddard, E. D., Smith, S. R., Lander, L. H., Proceedings of 4th International Congress on Surface Activity, Brussels, 1964, Paper B/II-6, Gordon and Breach Publications, 1966.
(23) Guastalla, J., *Cahiers Phys.* **10,** 30 (1942).
(24) Guastalla, J., "Surface Chemistry," p. 145, Butterworth, London, 1949.
(25) Gurney, R. W., "Ionic Processes in Solution," Dover Publications, New York, 1962.
(26) Harned, H. S., Owen, B. B., "Physical Chemistry of Electrolyte Solutions." 3rd ed., Reinhold, New York, 1958.
(27) Havinga, E., Den Hertog-Polak, M., *Rev. Trav. Chim.* 71, 64, 72 (1952).
(28) Helfferich, F., "Ion Exchange," McGraw-Hill, New York, 1962.
(29) Helmholtz, H. L. F. Von, *Ann. Physik* **7,** 337 (1879); translated in Engineering Research Bull. **33,** Engineering Research Institute, University of Michigan, Ann Arbor, Mich., 1951.
(30) "International Critical Tables," 1st ed., McGraw-Hill, New York, 1926.
(31) Jarvis, N. L., *J. Phys. Chem.* **69,** 1789 (1965).
(32) Joly, M., *J. Chim. Phys.* **36,** 285 (1939).
(33) *Ibid.*, **44,** 206 (1947).
(34) Joly, M., *Kolloid-Z.* **89,** 26 (1939).
(35) *Ibid.*, **126,** 35 (1952).
(36) Joly, M., "Recent Progress in Surface Science," J. F. Danielli *et al.*, eds., Vol. 1, p. 1, Academic Press, New York, 1964.
(37) Kruyt, H. R., "Colloid Science," Vol. II, p. 276, Elsevier, New York, 1949.
(38) Lucassen-Reynders, E. H., *J. Phys. Chem.* **70,** 1777 (1966).
(39) Lundquist, M., *Finska Kemistsamf. Medd.* **72,** 14 (1963).
(40) Mingins, J., Pethica, B. A., *Trans. Faraday Soc.* **59,** 1892 (1963).
(41) Montagne, J. B., Ph.D. thesis, Columbia University, New York, 1961.
(42) Nutting, G. C., Harkins, W. D., *J. Am. Chem. Soc.* **62,** 3155 (1940).
(43) Parreira, H. C., Pethica, B. A., Proceedings 2nd International Congress on Surface Activity, London, 1956, Vol. 1, p. 44, Butterworth, London, 1957.
(44) Payens, T. A. J., *Ibid.*, Vol. 1, p. 64.
(45) Rogers, J., Schulman, J. H., Proceedings 2nd International Congress on Surface Activity, London, 1956, Vol. 3, p. 243, Butterworth, London, 1957.
(46) Rosano, H. L., Breindel, K., Schulman, J. H., Eydt, A. J., *J. Colloid Interface Sci.* **22,** 58 (1966).
(47) Rosano, H. L., Feinstein, M. E., *Rev. Franc. Corps Gras* **13,** 661 (1966).
(48) Sanders, J. V., Spink, J. A., *Nature* **175,** 644 (1955).
(49) Schulman, J. H., Hughes, A. H., *Proc. Roy. Soc. (London)* **A138,** 430 (1932).
(50) Schulman, J. H., Rideal, E. K., *Proc. Roy. Soc. (London)* **A130,** 259 (1931).
(51) Sears, D. F., Schulman, J. H., *J. Phys. Chem.* **68,** 3529 (1964).
(52) Smith, T., *J. Colloid Interface Sci.* **23,** 27 (1967).
(53) Spink, J. A., *J. Colloid Sci.* **18,** 512 (1963).
(54) Stokes, R. H., Robinson, R. A., *J. Am. Chem. Soc.* **70,** 1870 (1948).
(55) Teunissen, P. H., Bungenberg de Jong, H. G., *Kolloid-Beihefte* **48,** 33 (1939).
(56) Tschoegl, N. W., *Kolloid-Z.* 181, 19 (1962).
(57) van Voorst Vader, F., Proceedings of 3rd International Congress on Surface Activity, Cologne, 1960, Vol. 2, p. 309, University of Mainz Press, 1960.
(58) Weil, I., *J. Phys. Chem.* **70,** 133 (1966).

RECEIVED June 12, 1967.

Structure of the Caffeine–Pyrogallol Complex

A. ARNONE[1] and R. H. MARCHESSAULT

State University of New York, College of Forestry, Syracuse, N. Y.

The co-crystallization of caffeine and pyrogallol produces thin needle-like crystals capable of gelling the solution. Spectroscopic analysis has shown a 1 to 1 molar composition of these crystals. An x-ray fiber diagram from a parallel bundle of needles grown in a fine capillary tube yielded unit cell (tetragonal) dimensions, and by combining this with density data it was deduced that the asymmetric unit had five water molecules associated with it. Single crystal data were recorded on a Weissenberg camera from a very narrow crystal (0.01 mm.), and a Fourier analysis was performed, leading to direct evidence that the caffeine and pyrogallol were stacked alternately in infinite columns about a fourfold axis parallel to the needle axis. General van der Waals forces seem to be responsible for the association of caffeine and pyrogallol in the crystalline complex.

The complexing of virtually all purines with aromatic molecules seems to have far-reaching biological significance. For example, it is known that caffeine affects the rates of many enzymatic reactions (*e.g.*, 0.01, 0.05, and 0.10*M* caffeine will inhibit salivary amylase 29, 54, and 72% respectively) (*12*), and purine can decrease the helix-coil transition temperature of the proteins bovine serum albumin and lysozyme (*2*). It is not unreasonable to expect the involvement of caffeine-aromatic and purine-aromatic complexes because caffeine derivatives and purine complex with the aromatic amino acids tyrosine, phenylalanine, and tryptophan (*2*). (In fact tryptophan forms a stable 1 to 1 crystalline complex in 0.5*M* theophylline glycol.)

[1] Present address: Chemistry Department, Massachusetts Institute of Technology, Cambridge, Mass. 02139.

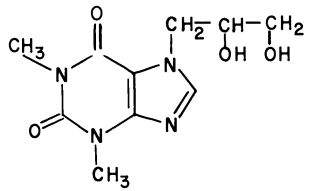

Theophylline Glycol

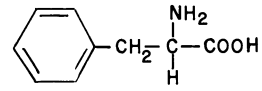

Phenylalanine

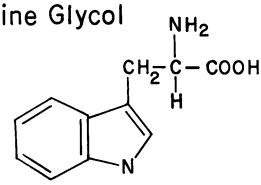

Tryptophan

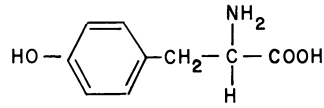

Tyrosine

Possible Bonding Forces

The intramolecular forces usually involved in complexing are charge-transfer, van der Waals, and hydrogen bonding. At present the generally accepted theory of charge-transfer complexing is the result of theoretical work done by Mulliken (9). To describe the ground state of the complex, Mulliken uses a linear combination of a no-bond structure (D,A) and a dative structure (D^+–A^-), in which an electron has been transferred from the donor (D) to the acceptor (A), to give a resonance hybrid of the two. That is, the ground state Ψ_N of the complex can be approximately written as:

$$\Psi_N \approx a\Psi_0(\mathrm{D,A}) + b\Psi_1(\mathrm{D^+ - A^-})$$

where a and b are weighting coefficients with $a^2 >> b^2$ in a loosely bound complex. Likewise, the excited state of the complex, Ψ_E can be written as the linear combination:

$$\Psi_E \approx a^*\Psi_1(\mathrm{D^+ - A^-}) - b^*\Psi_0(\mathrm{D,A})$$

with $a^* >> b^*$. In complexes ascribed to charge-transfer forces a new peak usually appears in the ultraviolet or visible absorption spectrum, and this is attributed to the transition from the ground state, N, to the excited state, E. Mulliken's theory also predicts that the stability of the complex will depend on the overlap of the highest filled molecular orbital of the donor and the lowest unfilled molecular orbital of the acceptor molecule. To obtain maximum overlap between molecules of similar symmetry, such as in aromatic-aromatic complexes, the molecular orbitals must be superimposed plane to plane. Thus, if charge-transfer forces are important in the caffeine-pyrogallol complex we might expect the

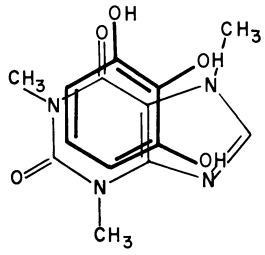

I

molecules to be oriented with the hexagonal molecular orbital of the pyrogallol directly above and superimposed on the hexagonal molecular orbital of caffeine, as in I, for example.

Van der Waals forces can be grouped into three major classes: dipole-dipole, dipole-induced dipole, and dispersion or London forces. Complexes stabilized by van der Waals forces should be characterized by the juxtaposition of dipoles. In caffeine, resonance structures such as:

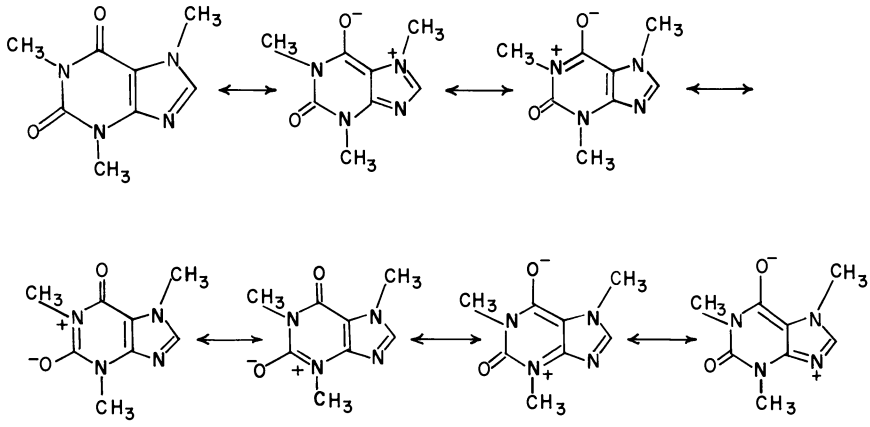

all contribute to the hybrid structure having dipoles as in II.

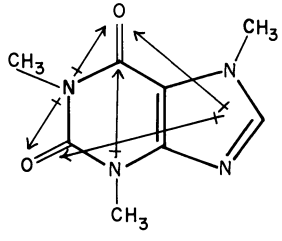

II

In general we can say caffeine's permanent dipole of 3.4 D (*10*) will be directed from the relatively positive five-membered ring to the relatively negative six-membered ring, III; the exact orientation remains to be established by appropriate quantum chemical calculations.

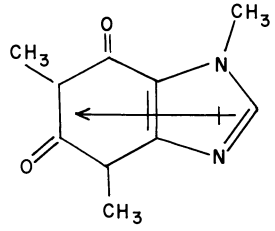

III

Pyrogallol also has a permanent dipole which is obviously directed along its axis of symmetry, IV.

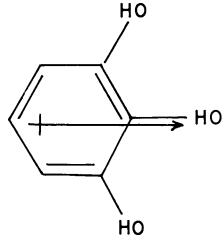

IV

Thus, if van der Waals forces are responsible for the stability of the caffeine-pyrogallol complex we would expect the molecules to be oriented as in V. Bearing in mind, however, the uncertainty as to the exact orientation of caffeine's dipole vector, the superposition of molecular planes might in the final analysis not be so different from I. In that case one would have to look to other evidence to establish whether or not charge transfer forces were involved.

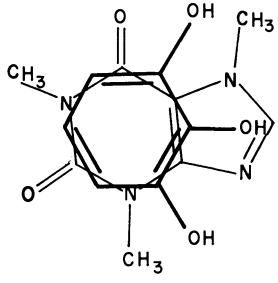

V

Hydrogen bonding might contribute to the stability of the complex, in which case the orientation between the two molecules would be such that distances between bonding groups are of the proper magnitude, ~2.7A. A recent study (*7*) of the crystal structure of the complex between 9-ethylhypoxanthine and 5-fluorouracil illustrates this factor, hydrogen-bonding being exclusively "in-plane."

Evidence of charge-transfer forces in crystalline aromatic-aromatic complexes has been reported by Wallwork (*13*). For example, in the *N,N,N',N'*-tetramethyl-*p*-phenylenediaminechloranil complex (VI) Wallwork reports the orientation of the molecules as shown in VI:

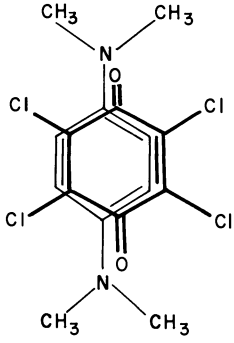

VI

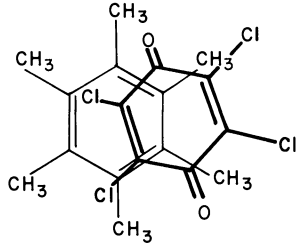

VII

which is the most suitable for overlap of molecular π-orbitals. However, other forces such as steric hindrance can affect the degree of π-orbital overlap (*13*) as in the hexamethylbenzenechloranil complex (VII). Briegleb and Czeckalla (*4*) have examined the spectra of some aromatic-aromatic complexes involving *s*-trinitrobenzene and have concluded that approximately half the energy of stabilization of the ground state of these complexes arises from charge-transfer forces.

Pullman (*10*) has studied several complexes involving 3,4-benzpyrene and various purines and pyrimidines. He was able to predict the order of complexing power of the bases by calculating the force of interaction considering only van der Waal forces. The infrared and ultraviolet absorption spectra of a number of purine-aromatic complexes were studied by Booth, Boyland, and Orr (*3*). They observed small changes in the infrared spectra and a bathochromic shift in the ultraviolet spectra (but did not find a charge-transfer band); hence, they concluded, "these facts support the suggestion that the complexes owe their formation to forces of attraction between the two components arising from their mutual polarization." Similar findings were also reported by Sond-

heimer, Covitz, and Marquisee (*11*) in a study of complexes between caffeine and aromatic compounds related to chlorogenic acid.

The only purine-aromatic complex crystal structure published thus far is the tetramethyluric acid-pyrene structure (*6*). The orientation of the molecules in this complex is shown below in VIII.

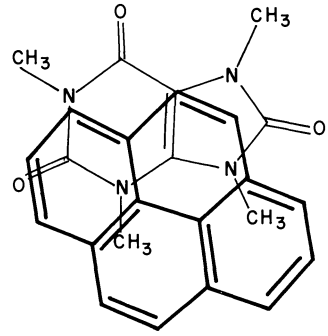

VIII

From the small degree of overlap in this case the authors concluded that charge-transfer forces must be weak, if present at all; hence van der Waals forces seem to be responsible for the stability of the complex.

Experimental and Results

If 0.01 mole of caffeine and 0.01 mole of pyrogallol are dissolved in 100 ml. of water at 60°C., a 1:1 crystalline complex will appear as the solution cools. Long needle-shaped crystals "growing" radially from central nuclei cause the entire solution to solidify into a "gel-like" structure with the fibrous appearance of mold (Figure 1).

To determine the ratio of caffeine to pyrogallol in the complex, the following spectrophotometric technique was employed.

First, 0.02 mole of each component was dissolved in 100 ml. of water. The precipitating complex was then vacuum filtered before the precipitation was complete and dried over P_2O_5 under vacuum.

The ultraviolet spectra of the precipitate can be seen in Figure 2 along with the spectra of pure caffeine and pure pyrogallol solutions. With such low concentrations it is assumed that the caffeine and pyrogallol are completely dissociated and that their ultraviolet spectra will be additive. Hence, if we let the ratio of pyrogallol with respect to caffeine be 1:P, then the extinction coefficient of the complex is:

$$\epsilon_{\text{complex}} = \epsilon_{\text{caffeine}} + P\epsilon_{\text{pyrogallol}}$$

where

$$\epsilon = \frac{(\text{optical density})\,(\text{mol. wt.})}{(\text{light path})\,(\text{conc. in grams/liter})}$$

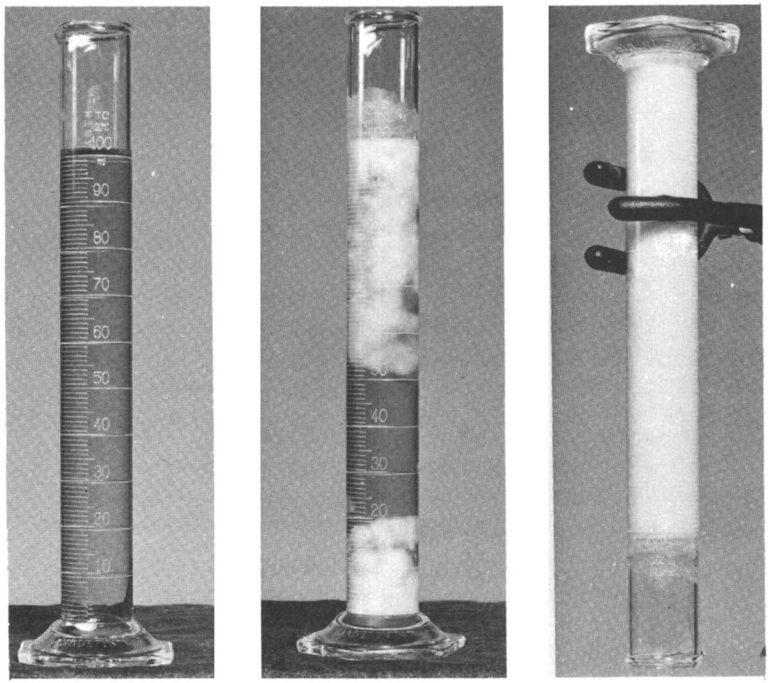

Figure 1. Formation of caffeine-pyrogallol crystalline complex by cooling a saturated aqueous solution from above room temperature. Left, homogeneous solution, 0.1M in each component, above room temperature; center, preliminary crystallization near room temperature; right, gel-like structure of complex crystals after standing at room temperature for one day

We also know that the molecular weight (MW) of the complex is:

$$MW_{complex} = MW_{caffeine} + P(MW)_{pyrogallol}$$
$$= 194.2 + 126.1\,P$$

From the data in Figure 2 we have, $\epsilon_{caffeine} = 10{,}100$ and $\epsilon_{pyrogallol} = 728$ at 272 mμ, light path = 1 cm., the concentration of complex = 0.05609 grams per liter of water, and the corresponding optical density = 1.90. Therefore,

$$\epsilon_{complex} = 10{,}100 + 728P \text{ and}$$

$$10{,}100 + 728P = \frac{(1.90)(194.2 + 126.1P)}{(1)(0.05609)} = 6{,}570 + 4{,}270P$$

$$3{,}542P = 3{,}530$$

$$\text{or } P = 0.996 \approx 1$$

Thus, we have a 1:1 complex. (The same result is observed when the complex is precipitated from a *non*-1:1 mixture of caffeine and pyrogallol (*e.g.*, 1:2 mixture).

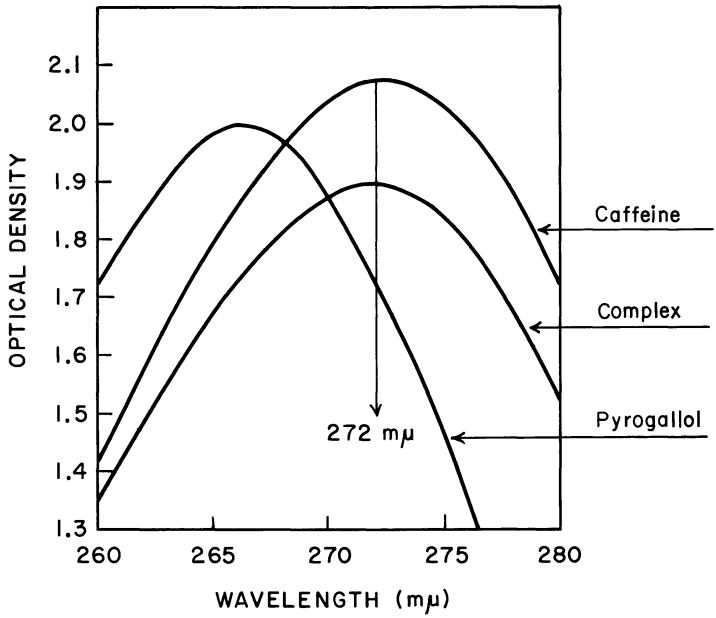

Figure 2. Ultraviolet spectra of complex and its components using a 1-cm. light path. Concentrations (grams/liter): complex, 0.0561; caffeine, 0.0399; pyrogallol, 0.306

Crystal Preparation. Attempts to grow a single crystal of the caffeine-pyrogallol complex were not successful at first. However, it was possible to obtain a good "fiber diagram" (Figure 3) using the following method.

First a mixture of 0.01 mole of each component was dissolved in 30 ml. of water by heating to approximately 60°C. This solution was then drawn up into a fine capillary (*ca.* 0.1 mm. in diameter) and seeded with crystalline complex at one end. Under these conditions the growing needle-shaped crystals oriented their long axes parallel to that of the tube. The phenomenon was observed under a microscope (Figure 4).

After many attempts to grow the complex crystals in very fine capillary tubes, it was found that occasionally one crystal would grow past the meniscus of the mother liquor and isolate itself from the mass of crystals behind it (Figure 5). In this way a single crystal was obtained, allowing the use of single crystal equipment to gather much more intensity data (Figure 6).

It was deduced from the fiber diagram and confirmed later by the single crystal photographs that the unit cell of the caffeine-pyrogallol complex is tetragonal with sides $a = b = 23.26$ A. and $c = 6.99$ A., and the space group is $P4/n$. The latter was deduced from systematic absences in the observed reflections including 00l reflections which were observed by recording equi-inclination rotation diagrams.

Density. To determine the number of complex moieties per unit cell, n, the density of the single crystals must be known since

$$\text{density} = \frac{n \times (\text{MW of Complex})}{\text{volume of unit cell} \times N_A}$$

where N_A is Avogadro's number.

The fact that the complex has a great affinity for water presents a problem in determining its density. However, by placing the samples of the complex in desiccators at different relative humidities it could be determined when the "free" (or adsorbed) water had been lost and when the water of hydration (or crystallization) had been lost. That is, by watching the weight loss in the samples as the relative humidity varied (Table I) and by comparing this with the x-ray powder

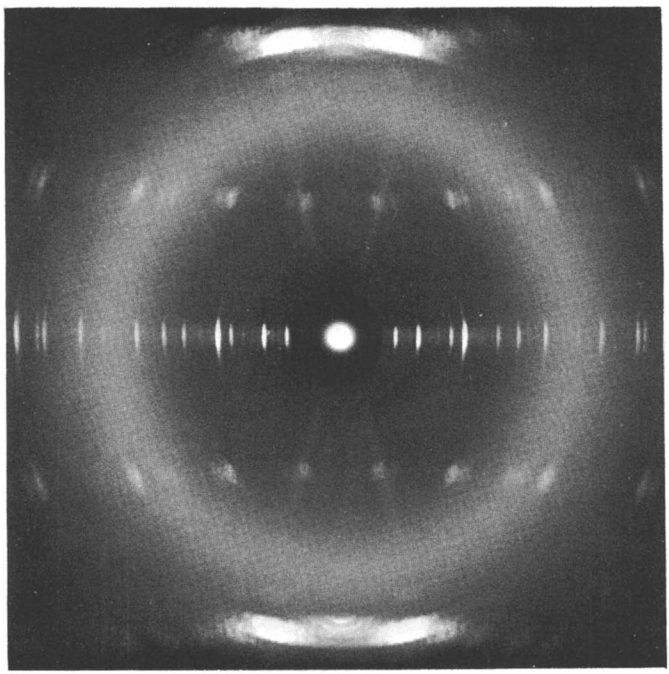

Figure 3. X-ray diffraction diagram of an oriented bundle of complex crystals in a fine glass capillary. Needle axis is vertical, and pattern was recorded with flat plate camera

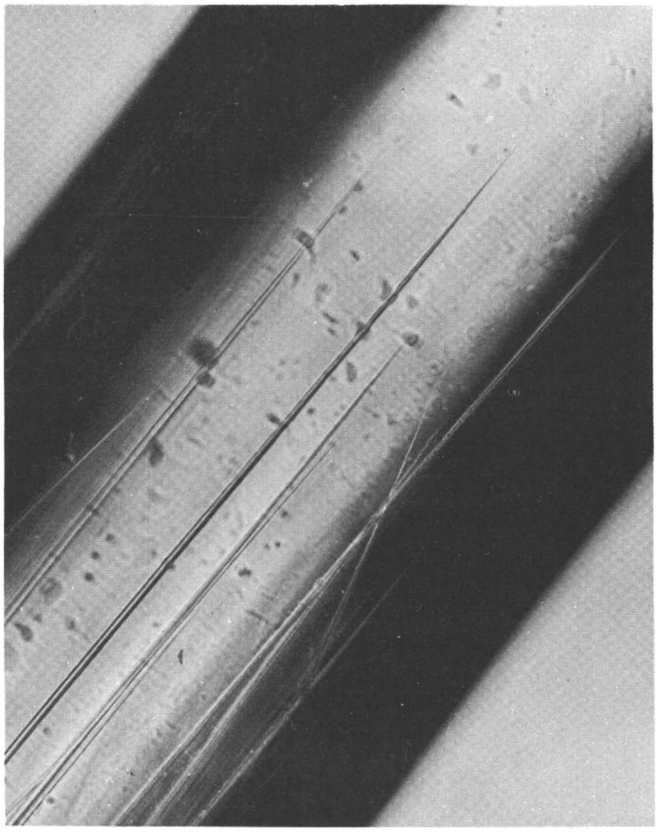

Figure 4. Needle-shaped crystals of molecular complex growing in glass capillary

diagrams of the same samples (Figure 7), it was possible to select the relative humidity leaving just enough water to form the complex. Of course, it is the density under these conditions which is of most interest. Adding water in excess of the minimum amount simply produces a gel, changing the morphology but not the crystal structure of the complex. It is the density of the single crystals which must be used to determine n. Density measurements were made by titrating with hexane and CCl_4 until the complex sample floated. Then the density of the liquid medium was measured and taken to be equal to the solid sample. Figure 7 shows a plot of complex density *vs.* relative humidity.

Determination of n. Using the aforementioned ultraviolet spectrum relationship

$$\epsilon = \frac{(\text{optical density})\,(\text{MW})}{(\text{light path})\,(\text{concentration})}$$

it is possible to determine the molecular weight of the complex at various humidities (Figure 8). The x-ray powder pattern changes at 93% R.H.; hence, the molecular weight of the complex dried between 95 and 93% R.H. is the molecular weight closest to that of the single crystals. This gives a molecular weight of about 410, which corresponds to one caffeine (MW = 194), one pyrogallol (MW = 126), and five water molecules (MW = 90). Similarly a density intermediate between that observed at 95% R.H. and 93% R.H. is assumed to be the density of the single crystals. With this density, 1.382 grams/cc., and a molecular weight of 410 we can calculate n using:

$$n = \frac{\text{volume of unit cell} \times \text{density} \times N_A}{\text{MW of asymmetric unit}}$$

where N_A is Avogadro's number

$$\text{or } n = \frac{(23.263)(23.263)(6.989) \times 10^{-24} \text{ cc.}}{(410)/(6.025 \times 10^{23}) \text{ grams}} \times (1.382 \text{ grams/cc.})$$

$$n = 7.68$$

Owing to symmetry, a tetragonal unit cell can have values of only $n = 4$, 8, 16, 32; hence, we choose $n = 8$.

Fourier Analysis. A standard intensity scale was used to measure the intensities of the reflections in Figure 6 (bottom) (5). From the intensity data, the structure factor was calculated from the relation

$$F_{hkl} = I_{hkl}/K(Lp)^{1/2}$$

where K is a scaling constant, and Lp is a correction factor caused by the depolarization of the incident x-ray beam and the geometry of the x-ray camera. Thus, from the experimental data, the intensities of the diffraction spots, only the magnitude of F_{hkl} can be extracted; its phase remains undetermined. This is known as the "phase problem," and the solution of crystal structures by x-ray diffraction amounts to solving the phase problem. One method of attacking this problem starts by assuming a

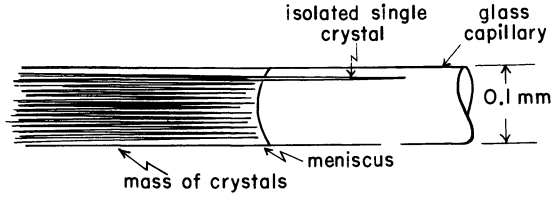

Figure 5. Schematic of growing needle-shaped crystals in capillary tube. One needle outpaces the others and is first to cross the meniscus boundary which recedes in opposite direction owing to evaporation

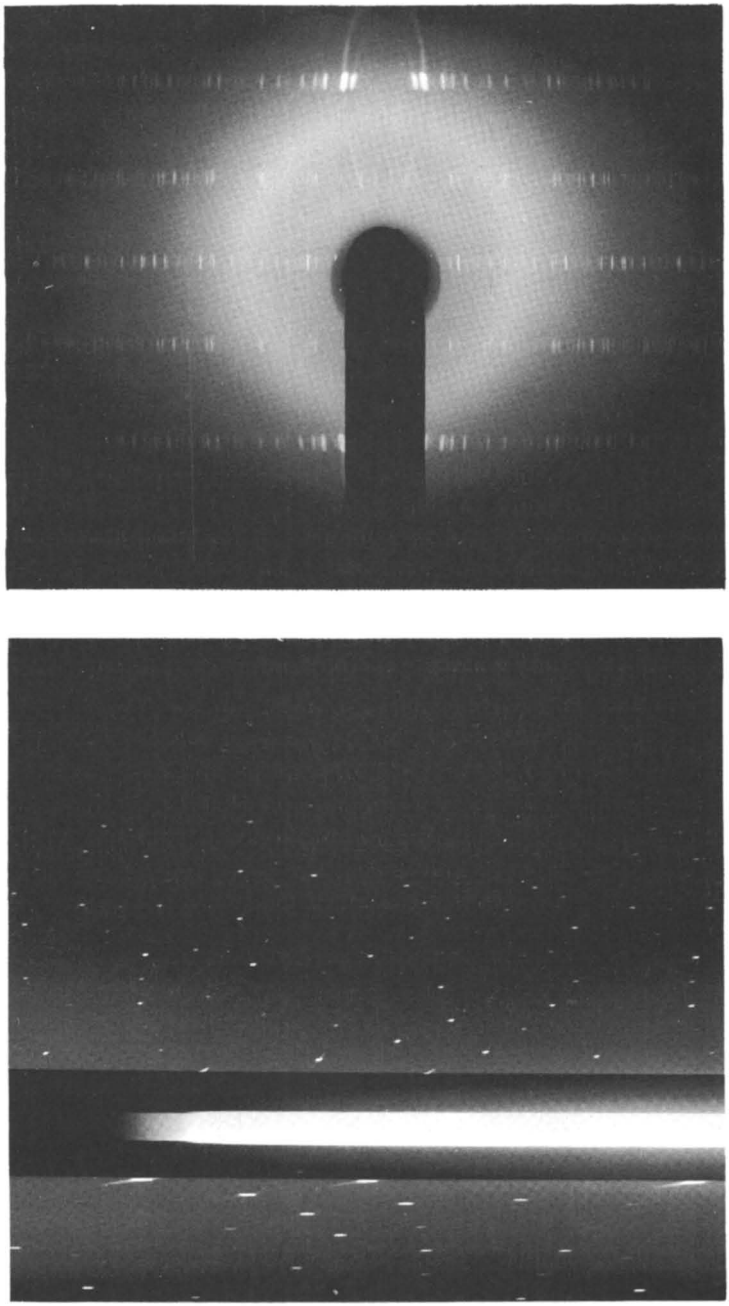

Figure 6. Top: single-crystal rotation diagram recorded on Weissenberg camera from a single crystal inside a glass capillary. Bottom: second layer line of Weissenberg photograph of a single crystal

crystal structure—*i.e.*, the *x,y,z* coordinates of all the atoms in the unit cell are determined by an initial "guess." This is an educated guess since all the chemical and physical information known about the crystal and any knowledge of similar crystal structures which have been solved is used to make the guess. The structure factors corresponding to this model can be calculated completely (*i.e.*, both the magnitude and phase can be calculated). The phases from the assumed model are then assigned to a few of the strong, measured magnitudes in the hope that the model is close enough to the correct structure so that most of the calculated phases will be nearly correct. The measured F_{hkl} with their newly assigned phases are now substituted into an equation which yields the electron density at a point. When enough points in the unit cell are considered, this yields an electron density distribution. The calculated electron density in the unit cell will not be correct because only a few of the larger F_{hkl} were used in summing and because the phases are at best only close to the correct phases. However, this calculated electron density distribution can be used to propose a new model of crystal structure which is different from the initial model and hopefully closer to the correct structure. Iteration of this procedure may result in the convergence of the initial model to the correct structure depending on how close the initial "guess" was to the correct structure. Convergence occurs when the electron density maximums become progressively better defined (*i.e.*, the resolution improves) and when the calculated magnitudes, $F_{hkl,\,calc.}$, correlate to a high degree with the measured magnitudes $F_{hkl,\,obs.}$. If convergence does not occur, a new initial model must be chosen and the iteration process begun anew.

The first step in the Fourier synthesis of the caffeine-pyrogallol complex was to choose an initial model so an electron density projection could be calculated. From the previous results it was determined that the unit cell was tetragonal measuring $23.26 \times 23.26 \times 6.99$ A., and that eight caffeine-pyrogallol complex moieties reside in the unit cell. This information alone does not give any indication of the way in which the molecules are packed inside the unit cell, but the symmetry operations of the space group can be used to eliminate many models. For example, one of the symmetry operators in the unit cell is a fourfold axis.

If an asymmetric unit is placed at (x_1,y_1), then the fourfold axis places three more asymmetric units at $(-y_1,x_1)$, $(-x_1,-y_1)$, $(y_1,-x_1)$. Thus, if caffeine is our asymmetric unit, it can not be placed too close to the fourfold axis since this would result in an overlap of the van der Waals radii with the three other caffeine molecules generated by the fourfold axis. By taking all of the symmetry operations of the space group P4/*n* into consideration there is only a "limited area" in which the initial projected model can be placed.

From other planar structures which have been studied, specifically planar complexes such as the tetramethyluric acid-pyrene complex, it is known that the molecules tend to stack plane to plane at a distance of about 3.4 A. (*6*). One unit cell dimension in this case is 6.99 A. Thus, it would be reasonable to expect the caffeine and pyrogallol molecules to be stacked with their planes roughly perpendicular to this short axis, and it would be likely that a projection of the caffeine-pyrogallol complex down this axis to the *x,y* plane would result in a two-dimensional picture of the complex with a small amount of distortion owing to the tilt of the planes of the molecules with respect to the *x,y* plane.

Table I. Percent Weight Loss as a Function of Relative Humidity for 1:1 Caffeine-Pyrogallol Crystalline Complex

Percent Relative Humidity	*Percent Weight Lost*
100	−4.8
99	6.65
97	56.5
95	59.0
93	58.2
71	59.1

At this point nothing was known about the orientation of the caffeine with respect to the pyrogallol; hence, as a starting point an orientation was assumed. The two components were then placed on the *xy* plane in a number of ways all of which were inside the "limited area" created by the symmetry operators of P4/*n*. These models were then used to predict the signs of 15 of the strongest (*h,k*,0) reflections. The strongest reflections were chosen because they contribute the most to the electron density.

One of these models yielded an electron density map wherein the outline of caffeine could be detected. At this stage of resolution the pyrogallol molecule was masked by the caffeine, and only one water molecule could be detected.

To obtain coordinates for a three-dimensional model the two-dimensional (2D) projection was used to locate roughly the *x*, *y* coordinates of the caffeine molecule. The *z* coordinate of each atom in caffeine was calculated by assuming the planar molecule was positioned in the 1,2,2 plane. (The 1,2,2 was selected because it was the strongest reflection observed.) The orientation of pyrogallol was assumed to be as in I. (There was no justification for this assumption other than it appeared to give the least steric hindrance.) The *z* coordinates of pyrogallol were calculated by assuming it to be parallel to caffeine and $\frac{1}{2}$ unit cell above the plane of caffeine. The water molecule uncovered in the 2D projec-

tion was arbitrarily placed in the plane of the pyrogallol molecule.

With these coordinates as a model, the structure factor of any reflection, F_{hkl}, could be calculated. The standard iterative process of Fourier analysis was used to converge on the correct structure. Figure 9 gives the electron density map of 1/8 of the unit cell (the other 7/8 is generated by the symmetry of the space group). Each section in the 3D electron density map represents a slice through the unit cell at a constant z value. Thus, the section labeled $z = 0.40$ gives the electron density at this level of the unit cell in the x,y plane (units are fractions of a unit cell), x (the vertical direction) between 0.00 and 0.50 and y (the horizontal direction) between 0.00 and 0.25. (The increment between letters or data in the x or y direction is 0.01 of a unit cell and the increment between sections in the z direction was 0.05 unit cell.) The two sections shown in Figure 9 were those where the outline of the caffeine and pyrogallol molecules were most pronounced.

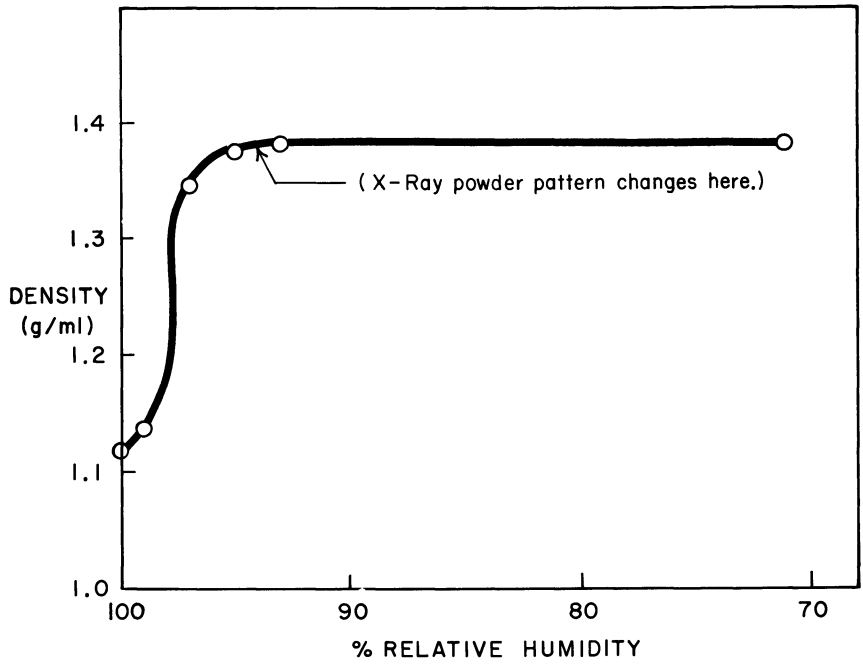

Figure 7. Flotation density of crystalline caffeine-pyrogallol complex measured after sample was equilibrated at various relative humidities

Table II lists the atomic coordinates of the atoms in 1/8 of the unit cell which were used in the final model. This model was used to calculate the structure factors in Table II, and the signs from these calculated F_{hkl}'s

were then assigned to the observed F_{hkl}'s which are also listed in Table II. A necessary criteria for a model structure to be an accurate representation of real crystal is for the calculated $F_{hkl,\,calc}$ to correlate with the observed magnitudes $F_{hkl,\,obs}$. A number of parameters have been used as a measure of this correlation. The most common is the reliability index, R, given by the formula,

$$R = \frac{\Sigma\,||F_{obs}| - |F_{calc.}||}{\Sigma|F_{obs}|}$$

where the summation is over all the structure factors. The model given in Table II yields a reliability index of 0.52. This indicates the need for more refinement since a refined structure usually has a reliability index of less than 0.25.

Discussion

Normally, if the assumed model for a crystal structure has an R value of 0.5 and resists attempts to refine to a lower residual, then the model structure is rejected as false, and a new model is tried until a fit between the observed and calculated structure factors yields an acceptable residual ($R < 0.25$). (Other models were tried for this complex, but they either gave Fourier maps which were uninterpretable or they converged to the present model). However, the "normal" crystal structure is solved with data obtained from crystals which have dimensions of the order of 0.1 mm. In the crystals available for this experiment, two of the dimensions were of the order of 0.01 mm. Thus, long exposures were required to give a small number of relatively weak diffraction spots. (Each Weissenberg photograph was exposed for five days with Cuk$_\alpha$ radiation: 50 kv., 20 ma. loading, in a helium atmosphere).

The results of this crystal structure analysis should then be viewed as having a reliability intermediate between standard single crystal structures where R is often 0.1, and crystalline polymer structures where only qualitative agreement is expected between observed and calculated structure factors.

Table II includes a projection of one asymmetric moiety on the x,y plane (*i.e.*, just the x,y coordinates are plotted). From this projection, it is clear that the dipoles of caffeine and pyrogallol are oriented in opposite directions, which definitely indicates the presence of attractive dipole-dipole forces or in general, van der Waals forces.

However, this orientation does not indicate the existence or non-existence of charge-transfer forces. At this stage of refinement there does not appear to be much overlap of the hexagonal molecular orbitals of

caffeine and pyrogallol. This does not exclude the possibility of charge-transfer forces contributing to the stability of the complex because further refinement could show more or less overlap of the two six-membered rings. The absence of a charge-transfer band in the absorption spectra of this complex, however, would indicate charge-transfer forces are weak if present at all. This conclusion is supported by other investigators (*3, 11*), who have failed to find any new band in the absorption spectra of purine-aromatic complexes.

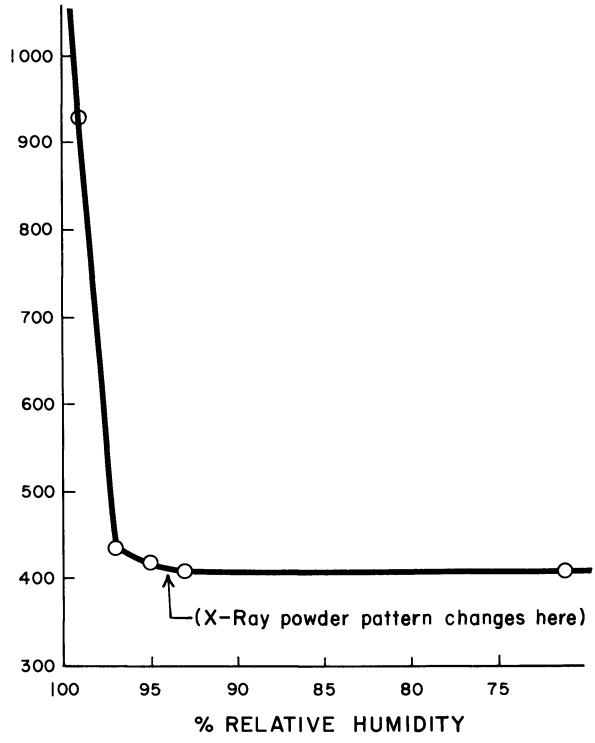

Figure 8. Molecular weight of the caffeine-pyrogallol complex determined by optical density measurement after sample was equilibrated at various relative humidities

The Fourier maps in Figure 9 tend to indicate that the caffeine and pyrogallol molecules are roughly parallel to the *x,y* plane and separated from each other by half of a unit cell in the *z* direction which amounts to approximately 3.5 A. The closest approach between these two molecules occurs between the nitrogen atom labeled 3 (Table II) in the caffeine

molecule and the oxygen atom labeled VIII in the pyrogallol molecule. The calculated distance between these two atoms is therefore about 3.05 A. Since these two atoms do not constitute a particularly good pair for hydrogen bonding and since more likely hydrogen bonding sites are further apart (*e.g.*, the caffeine carbonyl oxygen, atom 11, and the pyrogallol hydroxyl oxygen atom IX, are separated by 3.7 A.), this force probably plays no part in the attraction between caffeine and pyrogallol.

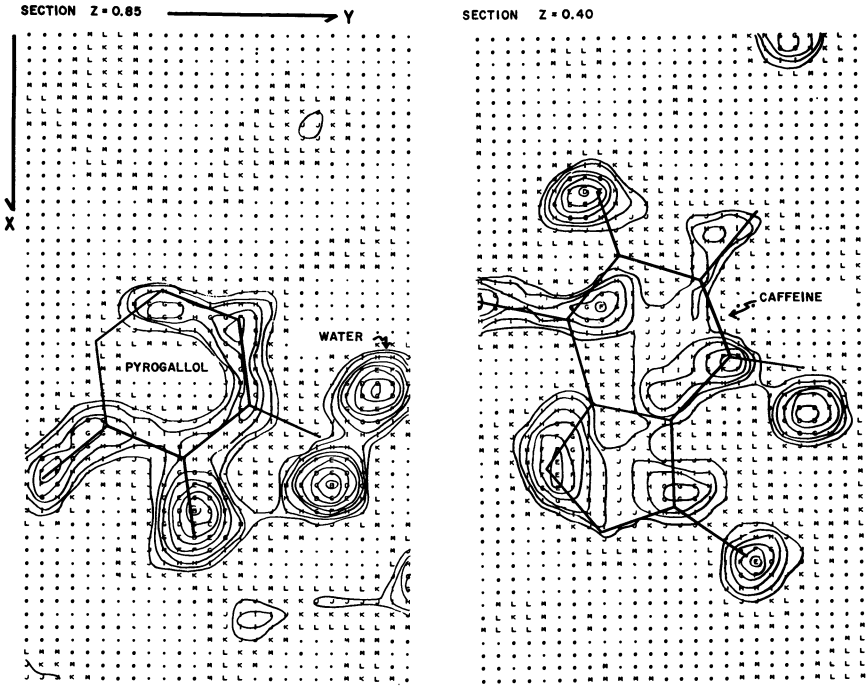

Figure 9. Electron density sections of the caffeine-pyrogallol crystalline complex. The sections show 1/8 of unit cell (the other 7/8 is generated by the symmetry of the space group) at the present stage of refinement. Each section corresponds to a slice through the unit cell at a constant z *value with the* x *coordinate running from 0.00 to 0.50 and* y *from 0.00 to 0.25 (units are in fractions of unit cell dimensions)*

Figure 10 is a projection of the entire unit cell on the *x,y* plane. The interesting feature here is the abundance of water molecules. The dotted lines indicate possible hydrogen bonds involving these water molecules.

The disturbing features of the present model (such as the unacceptably short hydrogen bond distances of 2.0 A.) will hopefully improve on refinement when more data of better quality become available.

Table II. Atomic Coordinates of Model Structure and the Observed and Calculated Structure Factors

$R = 0.5205$, $R_2 = 0.3161$, Scale Factor = 12.738, Temperature Factor = 1.000

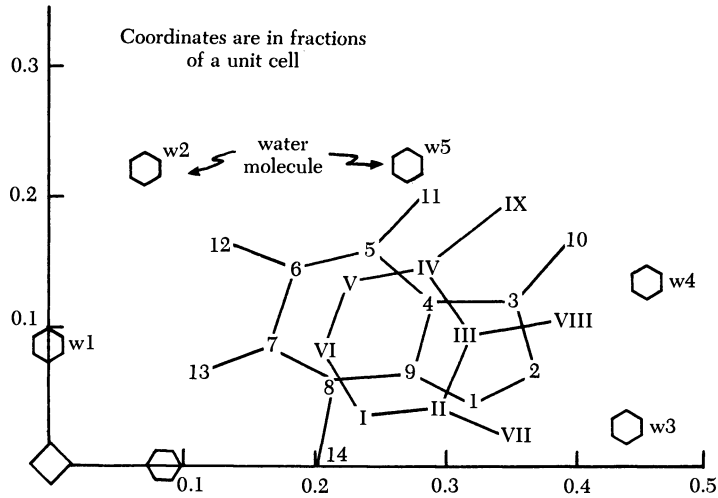

	Atomic Coordinates		
	X	*Y*	*Z*
1	.3250	.0450	.4500
2	.3750	.0700	.4500
3	.3600	.1250	.4350
4	.2950	.1250	.3900
5	.2500	.1650	.3800
6	.1900	.1500	.3900
7	.1700	.0900	.4100
8	.2200	.0650	.4400
9	.2800	.0700	.4550
10	.4050	.1750	.4250
11	.2950	.2150	.3400
12	.1400	.1700	.3400
13	.1200	.0700	.4500
14	.2050	-.0050	.4800
I	.2420	.0360	0.0000
II	.3000	.0430	.9250
III	.3250	.1000	.9000
IV	.2900	.1500	.9000
V	.2300	.1400	.9000
VI	.2100	.0850	.8750
VII	.3500	.0200	.9400
VIII	.3850	.1100	.8500
IX	.3500	.2000	.8600
W1	0.0000	.0900	.0700
W2	.0800	.2250	.1500
W3	.4450	.0250	.2500
W4	.4600	.1400	.7750
W5	.2750	.2300	.8500

Table II. Continued

H	K	L	$F_{calc.}$	$F_{obs.}$	H	K	L	F_{calc}	$F_{obs.}$
3	1	0	293.54	262.95	16	4	0	-83.19	-35.75
2	0	0	161.63	141.90	7	5	0	65.91	38.20
1	1	0	152.19	73.08	11	5	0	81.80	31.26
3	7	0	77.05	198.98	4	6	0	116.41	18.37
3	9	0	182.79	161.01	12	6	0	-19.45	-55.03
1	5	0	47.42	106.98	14	6	0	-34.56	-39.94
2	2	0	-51.08	-74.48	9	7	0	-7.64	-38.77
2	6	0	68.03	114.32	11	7	0	-84.50	-42.61
2	4	0	-19.04	-87.77	4	8	0	-8.17	-41.83
5	5	0	137.20	99.90	6	8	0	24.37	38.90
6	4	0	-26.37	-101.05	8	8	0	-73.93	-17.24
4	0	0	-70.21	-72.79	1	9	0	-36.43	-42.16
7	7	0	49.22	122.22	9	9	0	54.39	45.88
8	6	0	50.41	123.02	6	10	0	43.80	46.59
9	1	0	-91.25	-117.84	10	10	0	26.82	20.22
12	2	0	72.09	125.01	12	10	0	-55.21	-43.49
1	3	0	-134.08	-54.84	9	11	0	48.78	24.85
5	11	0	130.97	114.17	15	11	0	-31.26	-45.66
7	3	0	122.37	84.84	4	12	0	45.77	47.54
5	9	0	103.14	99.13	12	12	0	28.77	39.94
1	7	0	-126.83	-71.51	14	12	0	37.72	54.31
10	4	0	66.15	89.83	5	13	0	43.08	24.49
5	1	0	-50.05	-52.40	13	13	0	25.81	29.70
6	6	0	-22.81	-67.91	17	13	0	49.80	36.02
7	1	0	-38.51	-53.73	4	14	0	-112.61	-38.64
10	0	0	-5.83	-61.51	10	14	0	121.70	49.37
3	5	0	-18.63	-44.59	12	14	0	75.61	45.44
2	12	0	-46.81	-70.25	2	2	1	38.63	89.88
4	10	0	102.02	63.52	5	5	1	125.56	110.78
6	2	0	44.57	41.74	1	0	1	-119.92	-47.64
2	10	0	108.41	54.55	1	5	1	-5.73	-77.04
7	11	0	86.21	61.75	3	4	1	-28.34	-85.35
4	2	0	11.67	32.30	5	7	1	-60.21	-112.45
10	6	0	-82.53	-55.69	5	1	1	36.71	73.08
8	0	0	-4.06	-42.58	1	3	1	113.12	59.42
1	11	0	114.30	50.90	1	9	1	23.93	95.49
3	13	0	-138.93	-58.13	3	3	1	-12.40	-63.41
8	16	0	63.89	63.13	2	7	1	-.72	-79.54
12	0	0	-72.55	-40.17	6	7	1	-44.29	-90.63
14	0	0	-106.19	-73.74	3	0	1	-33.46	-47.50
13	1	0	-108.29	-33.00	7	4	1	-99.21	-68.60
8	2	0	-21.41	-22.24	8	2	1	-32.18	-69.46
20	2	0	9.97	35.68	1	1	1	22.83	33.09
3	3	0	32.27	18.13	1	8	1	-9.41	-66.86
5	3	0	53.75	19.94	4	2	1	55.86	50.01
11	3	0	55.10	47.48	7	0	1	22.63	62.01
17	3	0	9.10	49.48	10	4	1	116.07	79.22
19	3	0	-34.02	-39.24	12	4	1	55.54	87.93
					10	6	1	48.17	81.12

Table II. Continued

H	K	L	$F_{calc.}$	$F_{obs.}$	H	K	L	$F_{calc.}$	$F_{obs.}$
1	7	1	-20.55	-59.66	7	19	1	53.55	42.97
4	3	1	24.17	48.28	8	4	1	-27.55	-28.16
7	5	1	-96.04	-61.59	8	8	1	72.16	30.23
6	9	1	-65.22	-68.18	8	10	1	-21.50	-36.38
5	3	1	-14.80	-46.80	10	5	1	5.97	32.23
1	6	1	-60.07	-46.67	10	10	1	-9.67	-42.42
8	3	1	-14.37	-55.78	11	2	1	-57.63	-32.23
4	9	1	-101.84	-60.58	11	4	1	46.33	29.69
9	0	1	32.36	56.52	11	17	1	36.83	39.53
4	6	1	53.33	49.63	12	15	1	-16.60	-42.32
8	7	1	-50.03	-61.39	14	2	1	-16.62	-46.68
11	6	1	99.27	68.27	14	3	1	-75.82	-32.55
5	6	1	-119.89	-50.90	14	4	1	-53.33	-35.80
11	8	1	69.47	67.01	14	12	1	-85.93	-36.45
2	6	1	.76	42.72	14	15	1	41.07	39.61
9	10	1	82.13	65.16	15	13	1	-8.20	-53.06
9	7	1	-84.97	-56.53	17	1	1	-27.37	-39.74
5	8	1	76.66	50.31	17	8	1	-34.35	-36.77
1	4	1	23.01	31.31	18	5	1	-38.35	-36.68
9	2	1	71.99	49.08	18	6	1	.46	36.93
9	8	1	87.80	51.65	1	2	2	444.97	303.37
11	1	1	100.73	48.85	2	1	2	-202.09	-214.51
7	11	1	25.08	54.47	2	2	2	-176.62	-154.02
13	6	1	-32.38	-53.77	1	1	2	-69.94	-90.82
9	9	1	-32.50	-49.62	3	1	2	202.83	99.52
12	3	1	-107.30	-48.68	3	2	2	103.33	95.91
7	3	1	21.17	33.25	3	6	2	89.66	111.72
10	2	1	14.16	39.29	4	2	2	41.85	87.78
13	5	1	105.54	48.16	1	7	2	-87.84	-92.46
11	0	1	9.24	36.83	5	1	2	-74.58	-68.59
10	0	1	-15.81	-32.94	5	9	2	-94.47	-96.17
1	15	1	-8.93	-37.98	1	5	2	86.04	67.01
2	3	1	-25.95	-20.90	3	8	2	57.44	82.89
2	4	1	-37.75	-40.40	5	5	2	-45.45	-73.58
2	9	1	49.55	30.51	3	0	2	59.75	51.08
3	5	1	59.05	26.60	3	10	2	57.28	83.69
3	6	1	103.82	45.74	5	3	2	-15.91	-61.89
3	10	1	62.12	35.65	8	2	2	14.46	72.80
4	4	1	-106.38	-29.72	7	7	2	80.65	75.04
4	7	1	45.91	31.43	3	12	2	153.21	75.77
4	10	1	72.37	34.48	9	1	2	-42.63	-61.62
4	11	1	11.84	38.33	6	5	2	-49.77	-56.01
5	12	1	64.56	41.09	7	5	2	-39.55	-58.82
5	2	1	41.39	20.15	1	9	2	-26.22	-60.42
5	18	1	-6.27	-55.63	9	4	2	47.89	60.00
6	20	1	42.14	44.75	2	7	2	-34.47	-53.03
7	1	1	-33.95	-27.13	7	6	2	-33.00	-57.87
7	2	1	14.09	25.15	12	2	2	-.85	-58.97
7	9	1	54.42	32.63	6	1	2	-73.81	-41.10

Table II. Continued

H	K	L	$F_{calc.}$	$F_{obs.}$	H	K	L	$F_{calc.}$	$F_{obs.}$
11	0	2	28.07	53.88	1	3	3	-53.33	-102.20
9	3	2	-45.49	-49.56	1	4	3	9.09	29.92
4	1	2	-44.02	-32.96	2	2	3	48.00	37.77
8	4	2	73.64	46.50	2	3	3	17.28	36.54
7	2	2	-19.17	-40.50	2	5	3	-61.50	-30.75
11	2	2	-108.06	-49.96	2	7	3	12.01	22.75
4	9	2	-29.59	-50.59	2	8	3	-24.22	-27.79
3	3	2	-10.42	-34.41	2	9	3	34.11	25.38
5	12	2	103.28	54.74	3	1	3	-21.83	-19.48
4	10	2	28.92	48.89	3	3	3	-72.86	-41.36
9	6	2	-15.79	-44.24	3	6	3	12.23	28.36
10	5	2	43.38	45.10	3	7	3	24.98	32.83
8	0	2	.32	32.06	3	8	3	31.21	31.59
1	3	2	-69.40	-21.21	3	9	3	23.02	39.32
1	6	2	-12.15	-35.24	4	2	3	-3.13	-28.76
1	10	2	40.61	31.33	4	4	3	-32.80	-51.63
1	15	2	18.25	51.54	4	7	3	-33.89	-36.38
2	5	2	9.99	29.91	5	1	3	67.46	50.94
2	13	2	71.54	36.75	5	3	3	-21.25	-43.21
4	4	2	.20	23.66	5	5	3	-8.37	-53.49
4	5	2	-47.74	-24.98	5	11	3	-76.23	-44.58
4	6	2	16.20	26.39	6	2	3	-51.35	-30.32
4	13	2	29.58	37.53	6	3	3	42.71	38.06
5	2	2	-18.83	-22.18	6	5	3	-41.22	-38.34
5	4	2	62.22	23.91	6	6	3	-50.23	-34.49
6	4	2	-31.74	-30.48	6	9	3	-43.51	-35.53
6	8	2	34.82	34.93	7	1	3	71.59	31.77
7	3	2	3.87	33.19	7	4	3	-8.28	-43.49
7	4	2	-61.59	-35.08	7	6	3	-58.88	-32.77
7	10	2	-39.26	-35.10	7	8	3	-36.73	-44.54
8	6	2	-58.24	-38.27	7	9	3	59.29	43.22
9	5	2	56.66	36.67	8	6	3	-69.11	-43.16
10	3	2	-16.33	-39.21	8	7	3	-45.62	-38.57
10	4	2	-23.73	-32.59	8	8	3	-4.37	-46.01
10	7	2	-36.14	-33.61	9	3	3	12.90	39.32
12	1	2	-58.52	-42.64	9	9	3	-30.56	-34.65
13	3	2	3.93	45.41	10	4	3	-30.90	-35.45
3	0	3	-88.52	-38.39	11	5	3	-25.01	-44.58
6	0	3	-91.27	-54.21	12	6	3	-16.00	-35.64
8	0	3	-10.76	-36.25	13	5	3	-29.28	-44.52
13	0	3	-57.36	-46.36	12	12	3	59.35	48.65

Conclusions

The results indicate that caffeine and pyrogallol form a 1:1 crystalline complex in which five water molecules associate with each caffeine-pyrogallol pair.

The electron density maps need further refinement, but the gross features are distinguishable. These maps show that caffeine and pyrogallol alternate in "infinite" columns parallel to the *c* axis of the crystal. This association could be characterized as a "linear polymer" held together by weak (compared with primary valence forces) intermolecular forces.

Fourier analysis revealed the orientation of the complex to be that which might be expected for dipole-dipole interactions. The absence of any charge-transfer band in the absorption spectra of this or any other purine-aromatic complex indicated that charge-transfer forces are weak if present at all. Also, no significant hydrogen bonding was found between caffeine and pyrogallol molecules. Thus, the major forces operating

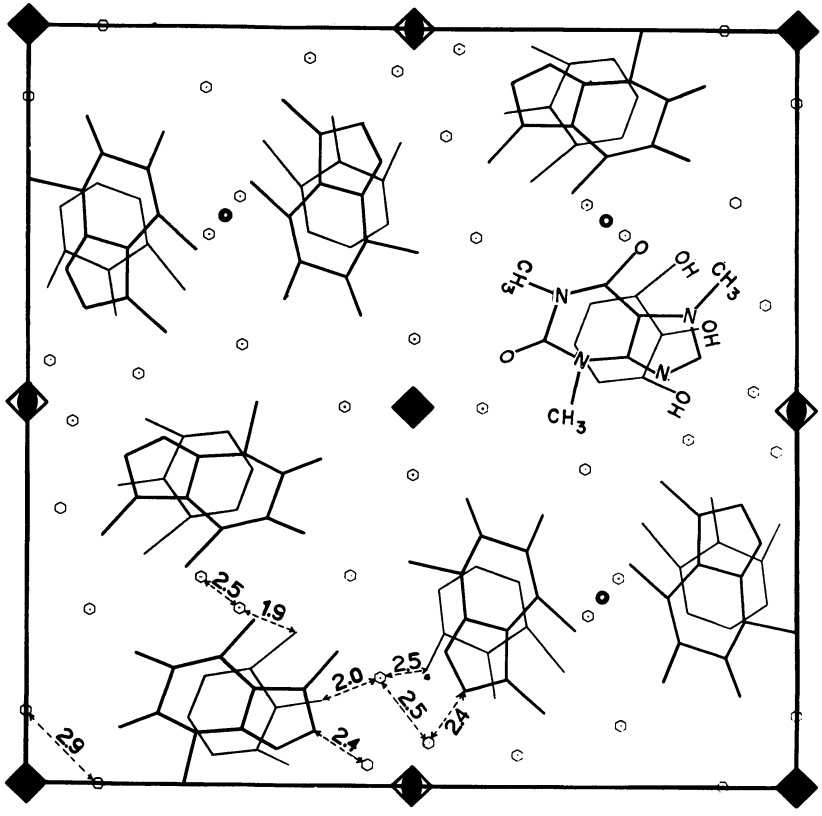

Figure 10. Projection of entire unit cell on the xy *plane. Filled squares indicate centers of fourfold symmetry, while the small, dark, unfilled circles are inversion points. Small hexagons are H_2O positions; dotted lines are possible hydrogen bonds. Three-dimensional distances are indicated in angstroms*

along the c axis of the crystal appear to be solely dipole-dipole, dipole-induced dipole, and dispersion forces.

Laterally these "infinite" columns seem to be held together by weak hydrogen bonding, with the abundant water molecules acting as a "cement." The speculation that these forces along the x and y directions are weak is supported by the dimensions of the crystal. That is, the crystals grow to only about 0.01 mm. in the x and y directions, while the z direction often reaches several centimeters.

Literature Cited

(1) Akinrimisi, E. O., Ts'o, P. O. P., *Biochemistry* **3**, 619 (1964).
(2) Booth, J., Boyland, E., Mason, D., Wiltshire, G. H., *Rep. Brit. Emp. Cancer Campn.* **29**, 27 (1951).
(3) Booth, J., Boyland, E., Orr, S. F. D., *J. Chem. Soc.* **1954**, 598.
(4) Briegleb, Czeckalla, Z., *Elektrochem.* **59**, 184 (1955).
(5) Buerger, M. J., "Crystal-Structure Analysis," Wiley, New York, 1960.
(6) Damiani, A., De Santis, P., Giglio, E., Liquori, A. M., Puliti, R., Ripamonti, A., *Acta Cryst.* **19**, 340 (1965).
(7) Kim, Sung-Hou, Rich, A., *Science* **158**, 1048 (1967).
(8) Liquori, A. M., De Lerma, B., Ascoli, F., Botre, C., Trasciatti, M., *J. Mol. Biol.* **5**, 521 (1962).
(9) Mulliken, R. S., *J. Am. Chem. Soc.* **72**, 600 (1950).
(10) Pullman, B., Claverie, P., Caillet, J., *Science* **147**, 1305 (1965).
(11) Sondheimer, E., Covitz, F., Marquisee, M. J., *Arch. Biochem. Biophys.* **93**, 63 (1961).
(12) Vincent, D., Lagreu, R., *Compt. Rend. Soc. Biol.* **144**, 1658 (1950).
(13) Wallwork, S. C., *J. Chem. Soc.* **1961**, 494.

RECEIVED July 19, 1967.

Spectroscopic and Calorimetric Studies of Biological Membrane Structure

JOSEPH M. STEIM

Brown University, Providence, R. I. 02912

Optical rotatory dispersion spectra of membranes are characteristic of partially helical polypeptides, except that the Cotton effect is red shifted by several mμ. Studies of lipid-free membrane proteins suggest that the shift may arise from protein-protein association. Differential scanning calorimetry shows that for M. laidlawii *both membranes and water dispersions of membrane lipids undergo a thermotropic phase transition characteristic of lipids in the bilayer conformation. Infrared spectroscopy indicates that most of the amide protons in erythrocyte ghosts exchange in deuterium oxide. Pronase treatment of ghosts removes 75% of the protein and most of the helicity, and although the treated ghosts appear intact under the microscope, most of the amide protons of the remaining polypeptides exchange. Nuclear magnetic resonance is useful for some lipoproteins, but for membranes interpretation is difficult.*

One of the most dramatic and important recent developments in biology has been the revelation of cell ultrastructure by electron microscopy. The emergence of the cell as a compartmented multimembrane system has emphasized that an understanding of the structure and function of biological membranes is fundamental to the understanding of cellular function. Membranes are intimately involved in the transport of ions and metabolites, in nerve impulse transmission and synapse function, and in the action of some pharmaceuticals. They are the site of much of the protein synthesis in the cells of higher organisms, they are basic to the production of ATP in mitochondria, they constitute the myelin sheath of nerve axons and the apparatus of chloroplasts in plants and photoreceptors in animals, and in the form of lysosomes they con-

tain the enzymes for the cell's self-destruction. Yet despite the importance of biological membranes and the considerable work done on the problem, our understanding of the structure and function of membranes on the molecular level is scanty. The problem seems to be not with a paucity of models but rather with insufficient data to choose between them.

The most commonly accepted model for cellular membranes has been the Davson-Danielli concept of a phospholipid bilayer bounded on each side by protein (*5, 18*). Although originally proposed before the advent of electron microscopy, the bilayer idea has been extended and generalized by Robertson to the "unit membrane" concept (*65*). Myelin has played an important role in the development of the bilayer model since low-angle x-ray diffraction of wet myelin shows electron-dense repeat distances that agree reasonably well with the spacings of the dark lines observed in fixed and stained specimens in the electron microscope (*28*). The bilayer architecture of myelin has been extrapolated to the generalized unit membrane by electron microscopy, largely by studies of the developing nerve sheath (*22*). Indirect evidence for the bilayer hypothesis has come from numerous studies of phospholipid behavior in water (*1, 20*). The formation of liquid-crystalline myelin forms by phospholipids swollen by water is well known, and the lamellar appearance in the electron microscope of these paracrystalline phospholipid-in-water systems is tantalizingly similar to the appearance of cell membranes. Numerous attempts have been made to correlate biological properties with the behavior of lipid monolayers (*19*) and more recently, with the behavior of synthetic bilayer systems (*57, 81*). However, the bilayer concept is not firmly established. Some investigators question the basic foundations of the bilayer model and suggest hydrophobic interaction between protein and lipid (*2, 36*), while others suggest less drastic modifications of the bilayer structure (*45*). Superimposed on the uncertainty in the nature of protein-lipid association there is both biochemical (*35*) and electron microscopic (*70*) evidence that membranes may be a planar mosaic of fairly uniform lipoprotein subunits.

A hindrance to the elucidation of membrane structure is, of course, the material itself. Membranes are rather intractable lipoprotein systems. Their lipid, protein, and carbohydrate contents are variable both quantitatively and qualitatively; since they cannot be crystallized, a detailed analysis by x-ray diffraction is impossible, and since they do not form solutions, the use of hydrodynamic or light-scattering techniques is quite limited. Electron microscopy has been the major physical method, but it is becoming increasingly clear that the electron microscope, at least at present, is incapable by itself of clarifying membrane structure on the molecular level (*47*). Despite an extensive literature, there is no general

agreement on the chemistry of fixation and staining. Gross alterations of structure could be caused by the drastic techniques used for specimen preparation, but even if the molecular architecture of the membrane were not changed, it is not difficult to imagine several models which might give rise to the doublet of dark lines often observed in micrographs. The recently introduced technique of freeze fracturing, however, appears quite promising (*6, 55, 59*).

Knowledge of the composition and dynamic changes of the lipid portion of membranes has increased spectacularly in recent years owing to newly developed techniques in lipid chemistry, and chemical studies of membrane protein have been carried out on a more limited scale. Data bearing upon the problem of the conformation of membrane protein and lipid *in situ* are badly needed, and new experimental approaches are necessary. Recently, several techniques used by physical chemists have been brought to bear upon the problem of protein and lipid conformation in membranes. They require the isolation of membrane preparations, but membranes from a variety of organisms can now be prepared in a reasonably pure state. Among these methods are optical rotatory dispersion, circular dichroism, infrared spectroscopy, nuclear magnetic resonance spectrometry, and calorimetry. I shall discuss some studies we have carried out in my own laboratory using these methods, together with some other published work having a direct bearing upon the interpretation of the data obtained.

Protein Conformation: Optical Rotatory Dispersion and Circular Dichroism

Principles of the Methods. Both optical rotatory dispersion (ORD) and circular dichroism (CD) depend upon the presence of one or more optically active absorption bands. ORD experiments measure the rotation of a plane-polarized light beam as a function of wavelength. At wavelengths removed from an absorption band the rotation increases or decreases monotonically and produces a plain dispersion curve, resembling an exponential function. In the neighborhood of an isolated optically active absorption band the function resembles, but is not identical with, the derivative of the absorption curve and crosses the axis of zero rotation at a wavelength near the middle of the band. The behavior of the ORD curve in the region of absorption is termed a negative Cotton effect if the extremum on the longer wavelength side of the crossover is negative; it is a positive Cotton effect if this first extremum is positive. The nature of the Cotton effects in polypeptides is valuable for determining the conformation of the polypeptide "backbone." Figure 1 illustrates the

Cotton effects which result from the random coil and α-helical forms of polylysine (*37*). The ordinate is the reduced mean residue rotation, which is defined as

$$[m'] = \frac{[\alpha]M_o}{100} \frac{3}{n^2 + 2}$$

where $[\alpha]$ is the specific rotation, M_0 is the mean molecular weight of an amino acid residue in a polypeptide or protein, and n is the index of refraction of the solvent at the frequency at which $[\alpha]$ is measured. The term $3/(n^2 + 2)$ takes into account the bulk polarizability of the solvent.

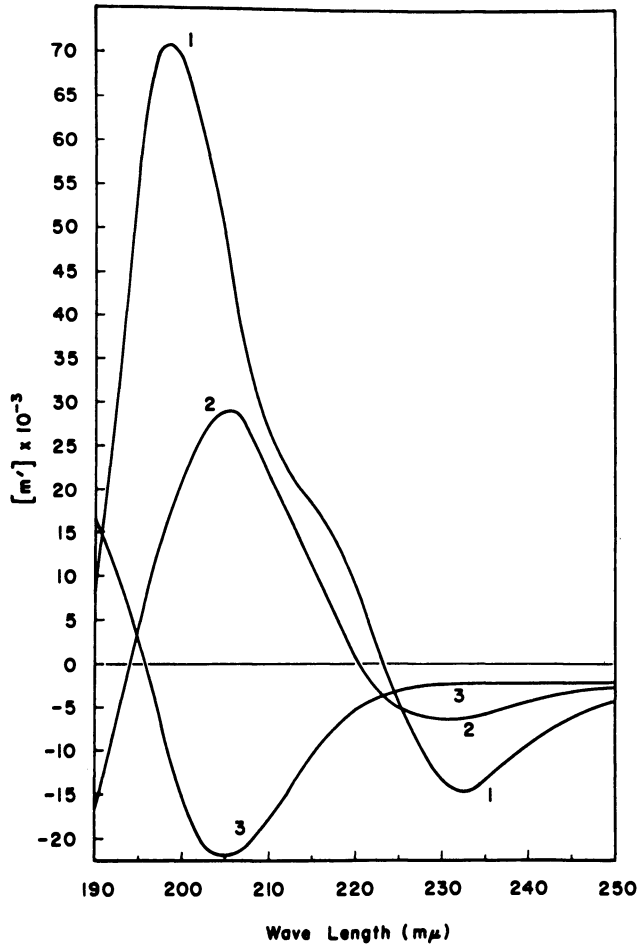

Figure 1. ORD spectra of poly-L-lysine in the (1) α-helical, (2) beta, and (3) random coil conformations (37). *The ORD of biological membranes resembles Curve 1 but is shifted toward longer wavelengths*

Similar curves are obtained with other synthetic polypeptides, and in most cases they are reasonably independent of the nature of the amino acid side chains. In synthetic polypeptides and proteins the observed Cotton effects do not arise from isolated chromophores but are composite curves resulting from several transitions assigned to the amide bonds in the 200-mμ region. The α-helical curve, for example, results from three optically active absorption bands. One around 222 mμ arises from an $n \rightarrow \pi^*$ transition of nonbonding electrons, and the other two at 208 and 191 mμ are attributed to $\pi \rightarrow \pi^*$ transitions parallel and perpendicular to the axis of the helix. These transitions of the α-helix and the resulting Cotton effects characteristic of the α-helix are at present of great interest in interpreting ORD curves of membranes.

Circular dichroism arises from the same optically active transitions responsible for the Cotton effects observed in ORD curves, but unlike ORD it is an absorption, not a dispersion, phenomenon. Hence, the CD effect is restricted to the region of the transition and can be interpreted more straightforwardly. Both ORD and CD can best be understood if one imagines the incident plane-polarized beam resolved into two in-phase circularly polarized beams whose vectors rotate in opposite directions. A difference in index of refraction between the left and right circularly polarized beams results in rotation of the transmitted plane polarized beam while differential absorption of the two circularly polarized beams results in depolarization of the transmitted beam, so that an incident plane-polarized beam whose frequency is within that of an optically active absorption band becomes both rotated and elliptically polarized upon passage through the sample. This depolarization effect is CD, and the measured parameter is $(\epsilon_l - \epsilon_r)$, the difference in extinction coefficient between the left and right circularly polarized beams. The data is usually recorded as the specific ellipticity, defined as:

$$[\psi] = \frac{330}{cl} (\epsilon_l - \epsilon_r)$$

where c is the concentration in grams/ml., and l is the path length in cm., or more commonly as the mean residue ellipticity:

$$[\theta] = \frac{[\psi] M_o}{100}$$

where M_o is the mean residue weight of an amino acid, usually taken as 115. CD is often the method of choice because a CD curve, like any absorption curve, is a direct indication of the position and band width of the optically active transitions. (For more detailed descriptions of ORD and CD and their application to proteins and synthetic polypeptides *see* Refs. *3, 8, 9, 25, 82, 85, 87.*) CD's for the α and random conformations

of polylysine (*84*) are shown in Figure 2, where the curves are quite different from those in Figure 1. For example, for the α-helix the three transitions at 222, 208, and 191 mμ are resolved. Again for membranes these transitions are the ones of major importance.

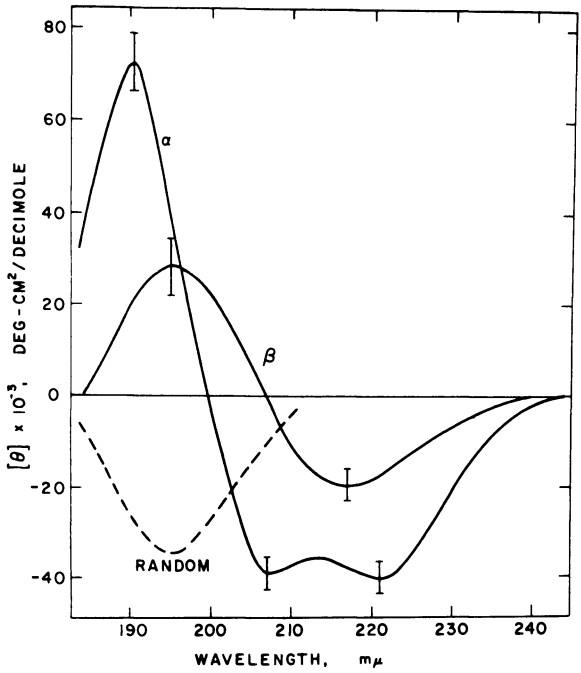

Figure 2. CD of poly-L-lysine in the α-helical, random coil, and β conformations (84). *The separate transitions responsible for the ORD can be resolved*

Thus, both ORD and CD are functions of protein structure and are quite responsive to minor differences in secondary and even tertiary conformation. At constant temperature and solvent composition, a change in rotational parameters indicates a conformation change. Difficulties arise, however, in determining the absolute amounts of α, β, and random structures present. Although quantification is reasonably satisfactory for some well-defined synthetic polypeptides, for proteins the methods are only semiquantitative. Limits can be set on the percentage helicity, for example, but calculations cannot be taken literally. The preferred method for calculating helical content is to fit the dispersion data to the Moffitt-Yang equation, which yields a parameter, b_o, assumed to be a linear function of percentage helicity. The procedure depends upon empirical calibrations, and there is disagreement on the proper choice of b_o for a

completely helical system (*85*). Dispersion data for the Moffitt-Yang treatment do not extend into the region of the Cotton effect. For membranes, however, attention has been centered upon the region of the Cotton effects from 190 to 300 mμ. Helical content can also be estimated in this region by the amplitude of CD bands or the depth of the trough in the ORD in the neighborhood of 233 mμ. For ORD, trough depth is assumed to be a linear function of helicity, and again there is no general agreement on the choice of proper trough depth for a completely helical system (*64, 91*). Estimates range from −11,000° to −18,000° and seem to converge around −15,000°. However, despite uncertainties in absolute numbers the methods are capable of distinguishing between only a little helicity and a considerable amount of helicity and of detecting minor conformational changes. In combination with infrared absorption their scope is also increased. For biological membranes certain other features of ORD and CD, such as the frequencies of the troughs and peaks of Cotton effects and the changes which occur upon removal of lipid or addition of detergent, are certainly as important as the extraction of quantitative data.

Properties of the ORD and CD Spectra of Biological Membranes. In 1965 Maddy and Malcolm (*52*) reported ORD studies of butyl alcohol-extracted erythrocyte ghost protein, and by applying the Moffitt equation they calculated a helical content of 17%. This calculation of helicity agrees reasonably well with later estimates based upon direct observation of the Cotton effects, but the measurements were terminated at 246 mμ. Later Ke (*46*) published the ORD of spinach chloroplast fragments. Although the extrinsic Cotton effects of the photosynthetic pigments *in situ* were emphasized, the spectra were extended to 220 mμ. A negative extremum, or trough, characteristic of the α-helix appeared at 235 mμ rather than at the 232–233 mμ position characteristic of most other proteins and synthetic polypeptides.

In a study of plasma membrane vesicles prepared from Ehrlich ascites carcinoma cells, Wallach and Zahler (*89*) first recognized the unique character of the ORD spectra exhibited by cell membranes (Figure 3). Although the shape was generally the same as that produced by an α-helix, the trough and peak positions were located at 236–237 and 200–202 mμ, respectively. The crossover also occurred at comparatively high wavelengths. The usually accepted parameters for trough and peak for most other helical proteins and polypeptides are 232–233 and 198–199 mμ, although it should be noted that the ORD of proteins are generally more variable than for synthetic polypeptides. Addition of lysolecithin to the membrane suspension caused the trough to shift to 233 mμ and also displaced the crossover to shorter wavelength. Similar behavior has also been shown for human erythrocyte ghosts and *Bacillis*

subtilis membranes by Lenard and Singer (*50*), and for submitochondrial vesicles from heavy beef heart mitochondria by Urry *et al.* (*86*).

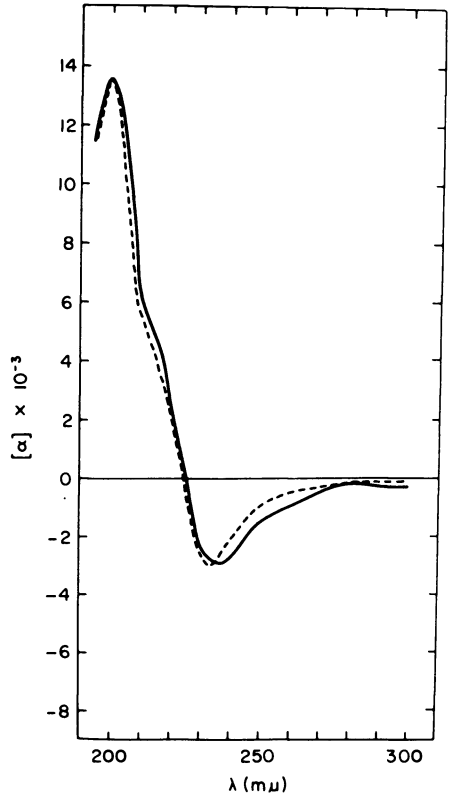

Figure 3. ORD of plasma membranes of Ehrlich ascites plasma membranes (solid line) in tris buffer, pH 8.2 (89). *Dotted line is helical poly-L-glutamic acid, plotted on a reduced scale. The trough and crossover of the membrane spectrum are red shifted. In other membranes the peak is red shifted as well*

In this laboratory we have examined the ORD of various membrane systems including heavy beef heart submitochondrial vesicles, rat liver submitochondrial vesicles, erythrocyte ghosts, and the membranes of *Micrococcus lysodeikticus, Halobacterium halobium, Halobacterium cutirubrum,* and *Mycoplasma laidlawii.* The optical behavior of all these materials is strikingly similar; the Cotton effects are similar to those produced by an α-helix but are red shifted to abnormally high wavelengths (*71*). Cotton effects arising from amide transitions in other

proteins often vary in form from protein to protein (*41*, *42*) and rarely exhibit troughs above 233 mμ. Solubilization of the membrane preparations by detergents such as sodium dodecyl sulfate or cetyltrimethylammonium bromide, or simply by dilution to low ionic strength in the case of the extreme halophiles, causes the red shift to vanish and the ORD curves to assume the wavelength parameters characteristic of the usual α-helix. Solubilization is also accompanied by an increase in rotational amplitude in every case. The wavelength parameters of several membranes are listed in Table I. Clearly the dispersion curves of all these systems behave in the same way—*i.e.*, the Cotton effects in the membrane preparations are red shifted to unusually high wavelengths under physiological conditions, but upon solubilization the Cotton effects shift toward lower wavelengths. Except for plasma membranes of Ehrlich ascites carcinoma cells, treatment with detergent results in a displacement of the entire Cotton effect—*i.e.*, trough, crossover, and peak—toward lower wavelengths.

The interpretation of the red-shifted ORD curves as a true reflection of α-helicity, and not some other structure stabilized by lipid, is supported by CD studies. As pointed out earlier, the CD minima for the usual α-helix occur at about 222 and 208 mμ. For human erythrocyte membranes (*50*), *B. subtilis* membranes (*50*), and submitochondrial vesicles from heavy beef heart mitochondria (*86*) the CD bands, like the ORD Cotton effects, are characteristic of the α-helical spectrum but are reported to be red shifted. For example, for red blood cell membranes in 0.008*M* phosphate at pH 7.7, CD minima occur at 224 and 210 mμ. In the presence of 0.05*M* sodium dodecyl sulfate the minima move to 221 and 207 mμ. For *B. subtilis* the corresponding parameters in the same buffer were 224 and 211–212 mμ, which shifted to 222 and 208 mμ in the sodium dodecyl sulfate. As far as can be judged from these data, the red-shifted ORD Cotton effects apparently reflect red shifts in the positions of the CD band rather than changes in CD band widths, and any explanation in terms of molecular structure would have to take into account the reduced energy of electronic transitions. However, CD indicates that in the plasma membranes of Ehrlich ascites cells although the $\pi \rightarrow \pi^*$ transitions are red shifted the $n \rightarrow \pi^*$ transition is not shifted but instead has increased band width (*88*). Such an increase in band width could account for the shifted trough observed in the ORD spectra. In contrast, the CD of sarcotubular vesicles has been reported to be normal—*i.e.*, not shifted—and evidence has been given which suggests that at least in some cases shifted CD bands might arise from partial denaturation of membrane structure during preparation (*54*). If, in fact, measurements on the same membrane preparation would yield an unperturbed CD but a shifted ORD, one would have to consider whether the ORD has physi-

cal significance. The results from Ehrlich ascites cells indicate that both CD and ORD are aberrant; hence, for this system an artifact can be ruled out. Clearly the issue of whether or not the CD bands of membranes are red shifted, broadened, or unperturbed is important in terms of the origin of the red shift in ORD spectra, and the point will not be settled until more data are gathered.

Table I. Wavelength Parameters of the Cotton Effect in Biological Membranes

Material	*Solvent*	*Wavelength, mμ*		
		Min.	*Crossover*	*Max.*
Spinach chloroplast fragments	Phosphate, pH 7.5	235	225	—
Ehrlich ascites plasma membranes	Tris-HCl, pH 8.2	236–237	225–227	200–202
	Tris-HCl + lysolecithin	233	223	200–202
Human erythrocyte ghosts	Phosphate, pH 7.7	235–235.5	225–227	201–202
	Na dodecyl sulfate	233	220–221	197–198
B. subtilis membranes	NaCl–phosphate, pH 7.7	235–237.5	227	201–203
	Na dodecyl sulfate	233	221–222	198–199
Heavy beef heart submitochondrial vesicles	Tris-HCl + sucrose, pH 7	237	227	202
	Tris-HCl, pH 8.0	237	226	204
	Na dodecyl sulfate	233	221	199
Rat liver submitochondrial vesicles	Tris-HCl, pH 8.0	237	225	203
	Na dodecyl sulfate	233	222	199
H. Cutirubrum envelopes	4.3*M* NaCl	235–237	225–226	—
	0.2*M* NaCl	233	220	198–199
H. Halobium envelopes	4.3*M* NaCl	235–237	225–226	—
	2% $MgSO_4$	236–237.5	225–226	202–203
	Distilled water	233	220	198–199
M. lysodeikticus membranes	Tris-HCl, pH 8	235	—	—
	Tris-HCl + Na dodecyl sulfate, pH 8	233	—	—
M. laidlawii membranes	Tris-HCl, pH 8	235	226	—
	Tris-HCl + Na dodecyl sulfate	233	224	—

In addition to red-shifted spectra and low rotational amplitude, Ehrlich ascites plasma membranes exhibit Cotton effects in the region of aromatic chromophores, 250–300 mμ (*89*). Similar behavior has been observed in other proteins, such as carbonic anhydrase (*34*) and lysozyme (*58*), and disappear upon denaturation. Ehrlich ascites plasma mem-

branes appear to be unique in this respect; no membranes examined by other workers or in this laboratory display such effects. Hence, it is unlikely that Cotton effects in the aromatic region, or any molecular conformations responsible for them, have any fundamental significance for membrane structure. The usual explanation for these effects is aromatic chromophores or disulfide bonds constrained in some asymmetric environment.

Interpretation of ORD and CD Spectra. LIGHT SCATTERING. Almost all published studies of conventional polypeptides or proteins have dealt with optically clear solutions. However, cell membrane preparations consist of turbid suspensions, and turbidity might introduce artifacts. Experimental evidence indicates that neither trough positions nor rotational amplitudes are affected by extraneous scattering particles in a solution of protein or polypeptide. We have shown that the addition of colloidal silica gel to a solution of helical poly-L-glutamic acid at pH 4.3 has no effect on the ORD spectrum except for an increase in noise level. Another type of check was provided by Lenard and Singer (*50*) by suspending cell membrane preparations in 90% glycerol. The high refractive index of glycerol greatly reduced light scattering but did not affect the position of the Cotton effect appreciably. Synthetic polypeptide systems also provide controls. For example, poly-L-lysine when heated at pH 7 assumes a β-conformation (*67*). The solution is optically clear if prepared at low concentrations and turbid at high concentrations, but turbidity has no effect upon trough position (*26*). The sodium dodecyl sulfate–polyornithine system studied by Grourke and Gibbs is also relevant (*39*). Addition of sodium dodecyl sulfate to poly-L-ornithine at pH 7 produces a transition from the random coil to the α-helix. Depending upon the method of preparation the trough appears either at 233 or 235–237 mμ, although both solutions are quite turbid (*38*). An example of the reverse situation—*i.e.*, a red shift accompanied by optical clarity—is shown by a study of aggregated poly-L-glutamic acid. Cassim and Yang (*10*) have shown that the entire Cotton effect and the CD bands of this helical polymer shift slightly (1 mμ) toward longer wavelengths when the pH is lowered from 4.3 to 3.8. Additional evidence for the reality of the red shift comes from studies of the reconstitution of *Mycoplasma laidlawii* membranes after solubilization with sodium dodecyl sulfate (*23, 73*). For native membranes we have shown that the trough of the ORD occurs at 235 mμ but shifts to 233 mμ when the suspension is cleared with sodium dodecyl sulfate. Upon dialysis against 0.05*M* Mg^{2+} membranous structures, with an ORD trough at 235 mμ, reappear. If the concentrations of detergent or Mg^{2+} are not optimal, amorphous aggregates of lipoprotein are obtained whose trough remains at 233 mμ. Both systems, however, are turbid.

ORD curves can be generated from CD spectra by applying the Kronig-Kramer transform, and if the experiments are done properly, the ORD obtained by transformation of the CD must be identical with the dispersion curve obtained by direct measurement. This test provides an additional criterion for authenticity because ORD and CD measure two different optical properties—*i.e.*, the former is a function of the differential refractive indices while the latter is a function of the differential absorptions of left and right circularly polarized light. As noted earlier, Wallach and Gordon (*88*) have carried out such calculations for the long wavelength $n \rightarrow \pi^*$ CD bands of Ehrlich ascites cell plasma membranes and erythrocyte ghosts, and they obtained red-shifted ORD troughs which agree with direct measurements.

Available evidence indicates, then, that ORD-CD studies reflect a real property of membrane protein. However, results from different laboratories vary. The lack of agreement may reflect true differences in protein conformation from membrane to membrane, but in some cases the effects observed might be artifacts arising, for example, from different preparative procedures or from some poorly understood property of scattering systems.

Conformational Assignment of the Red Shift. The ubiquitous appearance of strikingly similar red-shifted Cotton effects in the ORD of membrane systems suggests some structural feature common to all. There are three obvious possibilities in terms of molecular association: protein-protein interaction, protein-lipid interaction, and lipid-lipid interaction. All three have been suggested in the literature.

Let us consider first lipid-lipid interaction. Urry *et al.* showed the existence of a positive CD band at 218 mμ and a negative CD band at about 192 mμ in phosphatidyl choline and phosphatidyl ethanolamine dissolved in trifluoroethanol (*86*). The 192-mμ band was not characterized in detail, but the 218-mμ band is of such position and shape that the addition of lipid and protein CD bands could produce a composite CD band, and hence an ORD Cotton effect, which is red shifted. As noted by Urry, the 218-mμ CD extremum of lecithin must arise from $n \rightarrow \pi^*$ transitions in the fatty acid ester groups. Although the optical activities of solutions of deproteinized membrane phospholipids determined at the same concentration as in the intact membrane are negligibly small, in membranes an ordered array of lipids could greatly enhance rotation. Such an effect could yield information on the nature of lipid-lipid association. This can be tested experimentally. *Halobacterium cutirubrum* offers a unique system since Kates has shown that the lipids in this extreme halophile contain ether bonds rather than ester bonds (*43*, *44*). Hence, the $n \rightarrow \pi^*$ transition essential to the CD band at 218 mμ in phospholipids does not exist. Nevertheless, we found that the ORD

of the envelopes of *H. cutirubrum* exhibits an obvious red shift (trough at 237–237.5 mμ) in either 4.3*M* NaCl or 2% $MgSO_4$. Dilution of the suspension to low salt concentration, like the addition of detergent to other membranes, results in a loss of the red shift. A second kind of evidence comes from studies of lipid-free systems. If the optical activity of lipids is responsible for the red shift, then of course the effect should disappear when phospholipid is removed. However, when submitochondrial vesicles from heavy beef heart mitochondria are extracted in cold 90% acetone, the lipid-depleted material (2.3 μgrams P/mg. protein) still yields a red-shifted Cotton effect with trough at about 237 mμ (*31*). Another indication of the non-involvement of lipid is the recent demonstration by Steim and Fleischer (*75*) that aggregated lipid-free mitochondrial structural protein is red shifted (trough at about 239 mμ) in the physiological pH range. Hence, the presence of lipid is unnecessary for the red shift as observed in ORD spectra.

As a second possibility, lipid-protein interaction must be considered. The red shift might be explained in terms of hydrophobic interaction of the hydrocarbon chains of phospholipids with the protein in such a way that the amide chromophores are transferred to a less polar environment (*89*). Again, the hypothesis can be tested by removal of lipid. The existence of the red shift in lipid-depleted mitochondria and in lipid-free mitochondrial structural protein shows that lipid-protein interaction is not necessary to produce the ORD spectra characteristic of membranes. It is possible that if some molecular rearrangement occurs during the extraction process, a red shift caused by hydrophobic lipid-protein association could be replaced with a red shift arising from hydrophobic protein-protein association. Such an explanation is unlikely, especially in view of the retention of the "unit membrane" structure in electron micrographs taken of extracted vesicles (*30*). On the basis of ORD, then, the most reasonable conclusion is that the red shift need not be assigned to lipid-protein association.

The postulate of protein-protein association, suggested by Lenard and Singer (*50*), has been supported by the investigations of Steim and Fleischer on the effects of pH and detergents upon the ORD of lipid-free mitochondrial structural protein (*75*). At extremes of pH ($3 > pH > 11$), solutions of structural protein are optically clear, and the ORD shows α-helicity with trough at 232.5 and peak at 199 mμ. The usual calculations from trough depth indicate about one-fourth helical content. As the pH is lowered from 11 or raised from 3, turbidity progressively increases, and the trough, crossover, and peak become increasingly shifted toward longer wavelengths. The shift is accompanied by a decrease in rotational amplitude. These perturbations of the α-helical spectrum are maximal at about 7.5, where the trough occurs at 239 mμ

and the rotatory strength is reduced to about 75% of the value for the optically clear solution at high pH. This behavior, which is a reversible function of pH, is illustrated in Figures 4 and 5. We interpret the concurrent changes in turbidity and optical activity to indicate that the red shift is aggregation induced. In the presence of sodium dodecyl sulfate, cetyltrimethylammonium bromide, or lysolecithin, mitochondrial structural protein solutions remain optically clear, and the Cotton effects do not shift to the red over the entire pH range of 3 to 11. Similarly the addition of SDS to flocculated structural protein at pH 7.5 produces the same result: the red shifted Cotton effect reverts to the wavelength parameters shown by the disaggregated protein at pH 11 or pH 3. This detergent-induced loss of the red shift is accompanied by an increase in rotational amplitude similar to that observed when submitochondrial vesicles and other membranes are treated with surfactants. All these phenomena—*i.e.*, the red shift, the decrease in rotatory strength, and the response to detergent—mimic the ORD of membrane preparations. ORD data indicate that it is reasonable to assign the red shift in mitochondrial vesicles and intact mitochondria to intermolecular association of proteins. The possibility remains, however, that the red-shifted ORD observed with aggregated structural protein could originate from changes in the CD bands which are different from those observed in membranes. Experiments are in progress to evaluate this possibility.

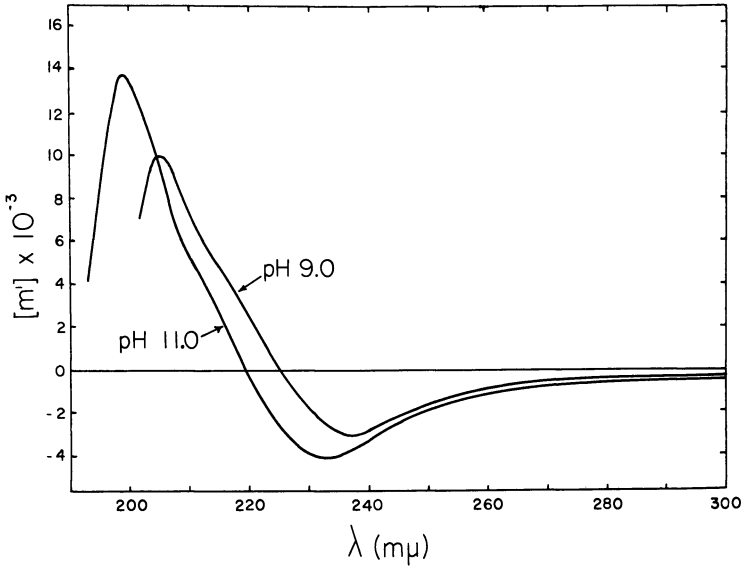

Figure 4. ORD of mitochondrial structural protein in the disaggregated state at pH 11 and the aggregated state at pH 9. Spectra were taken in distilled water, and pH was adjusted with HCl or KOH

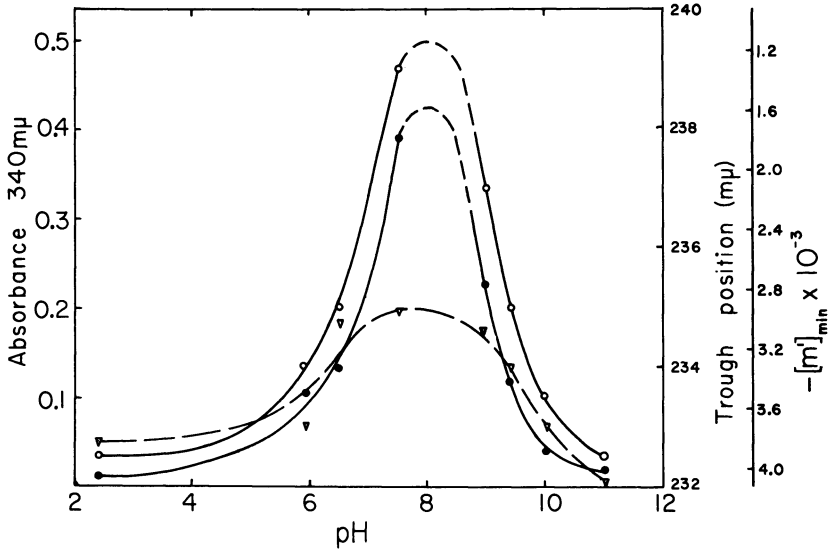

Figure 5. Effect of pH upon aggregation and ORD of mitochondrial structural protein in water. The curves are trough position (○), absorbance (●), and reduced mean residue rotation (▽). Dashed lines show region where precipitation prevented dependable measurements, but spectra of the precipitate in glycerol suggest that here the trough position may be at about 240 mμ

We found recently that protein prepared from beef erythrocyte ghosts by cold butyl alcohol extraction behaves in a similar fashion to mitochondrial structural protein (78). In 0.002*M* phosphate buffer at pH 7 and pH 3, where the protein solution is optically clear, the ORD parameters are those expected for an α-helix (trough at 233 mμ, crossover at 222 mμ, and peak at 199-200 mμ). In the pH range where the solution is visibly turbid, from about pH 6 to 3.5, the Cotton effects red shift and decrease in rotational amplitude. The phenomenon reaches a maximum at about pH 4.5, where the trough, crossover, and peak occur at 236, 225, and 203 mμ, respectively. Again, the effect of detergents on the lipid-depleted protein is the same as the effect upon intact erythrocyte ghosts: sodium dodecyl sulfate, cetyltrimethylammonium bromide, and lysolecithin prevent aggregation and cause the red shift to vanish. Little change occurs in the ORD of erythrocyte protein upon removal of lipid. The presence of lipid is unnecessary to stabilize much of the helical protein conformation in this system or in mitochondrial structural protein.

The shift to longer wavelengths of the ORD Cotton effects upon aggregation of lipid-free membrane protein must arise from a unique kind of association or an association which, if not qualitatively unique, is more dominant in membrane protein than in other proteins. Since the

parameters that show the shifts are those characteristic of the α-helix, the interaction may involve the peptide chromophores of the helical regions of the protein molecules. Although the mechanism responsible for aggregation and for perturbation of the ORD spectra will require elucidation, other materials have been reported which exhibit red-shifted spectra under conditions that promote aggregation. As pointed out, Cassim and Yang (*10*) reported that the ORD and CD spectra of aggregated helices of poly-L-glutamic acid at pH 4.3 are red shifted. Hydrodynamic and light scattering studies on this system indicate side-by-side association. The polyornithine–sodium dodecyl sulfate system of Grourke and Gibbs may have relevance to membranes (*39*). Addition of the detergent to the poly-L-ornithine at pH 7 results in turbidity and a transition from the random coil from of the polymer to an α-helix with a trough at 235-237 and a peak at 202-204 mμ. CD indicates an α-helix. These systems are poorly understood, but it is possible that similar mechanisms are responsible for perturbation of the spectra of both aggregated synthetic polymers and structural protein.

Significant differences may occur between red-shifted Cotton effects of the ORD of polypeptides and those of membranes. The poly-L-glutamic acid system of Cassim and Yang shows increased rotatory strength (which may arise simply from charge neutralization) upon aggregation, while aggregation of mitochondrial structural protein and erythrocyte ghost protein produces a decrease in rotation. ORD spectra of some membranes also show low rotational amplitudes based upon total protein content (*86, 89*). Such rotational changes might be a direct indication of changes in helical content accompanying aggregation, but they also might arise, for example, from changes in polarizability in the neighborhood of the peptide chromophores or from field effects from neighboring helices or even from instrumental artifacts.

QUANTIFICATION OF ORD AND CD DATA. In principle ORD and CD can be used to calculate the amounts of α, β, and random conformations in protein, but in practice such estimates are subject to large errors. The Moffitt-Yang plot is probably the best estimate of percentage of α-helicity, but it is unable to distinguish between the β and random structures. A detailed analysis of CD bands and their resultant Cotton effects, combined with infrared data, is the most promising approach; even here the limits of error are large (*82*). Traditional estimates have been based on combinations of α-helix and random coil, and attention has been centered upon estimation of helical content. Consideration of β structure has been introduced more recently. The technique must be calibrated empirically with synthetic polypeptides of known conformation, and the proper choice of reference is not obvious. The β structure seems to be particularly variable in its rotational properties (*27, 82*).

For membranes the difficulty is increased by the changes in rotatory strength which accompany aggregation as well as by the usual uncertainties in the choice of $[m']_{233}$ for a completely helical polypeptide (*91*). In fact, if the ORD curve is that of a miniaturized α-helix, as suggested by some (*86, 89*), a serious additional uncertainty is introduced into the selection of the proper reference value for trough depth. In addition, in some particulate membrane systems, and particularly in intact organelles, calculations based upon total protein content may not be realistic. Standard calculations based upon trough depth assuming a mixture of α-helix and random coil estimate that the helical content of membranes is not high (perhaps one-fourth). Percentage helicity estimated by the Moffitt-Yang treatment of the long wavelength dispersion for delipidized erythrocyte membrane protein (*52*) (17%) agrees reasonably well with the estimates determined from the Cotton effect in other membranes. If the value of one-fourth is incorrect, it is likely to be an underestimate. For CD spectra of Ehrlich ascites carcinoma cell plasma membranes, Wallach and Gordon have shown by curve fitting that the helical content may be about one-half (*88*). The remaining polypeptide is presumably random—*i.e.*, neither α nor β.

Protein Conformation: Infrared Spectroscopy

Infrared Spectra of Proteins. Because of the similarity of the ORD of the β conformations and the α-helix, ORD is limited in its ability to distinguish between these forms where present in protein. CD is less equivocal in this respect, but interpretation is still difficult. Recently it has become evident that the various β structures are more variable in their rotational properties than are either the α-helix or the random coil forms. Fortunately infrared spectroscopy nicely complements ORD and CD because it can distinguish between the β structure (parallel or antiparallel pleated sheet) on the one hand and the α-helix on the other (*82, 83*). The amide I band, arising mostly from carbonyl stretching, is of particular interest; it occurs at about 1650 $cm.^{-1}$ for the helix or random conformations and about 1630 $cm.^{-1}$ for the β forms. The position of the amide II band is also sensitive to conformation but is more variable than for the amide I band.

The usefulness of infrared spectroscopy of proteins and membranes is increased when spectra of dry films are compared with those taken in deuterium oxide. Exchange of protons for deuterons can affect both the amide I and amide II bands. For randomly coiled proteins in D_2O the amide I band is shifted down by about 10 $cm.^{-1}$ but for many proteins D_2O does not affect the frequency of the carbonyl stretch of either the β structure or the α-helix. In addition, upon complete exchange the amide

II band in the neighborhood of 1540 cm.$^{-1}$ disappears and is replaced by a band at about 1450 cm.$^{-1}$. The extent of diminution of the amide II band is, at least in principle, a measure of the extent of proton exchange. Little effect is observed in ordinary water since, of course, proton exchange does not occur. Table II summarizes some of the characteristic frequencies observed with proteins (*83*).

Table II. Amide I Wavenumbers for Protein Conformations (*83*)

Conformation	*Dry Film*	*In H_2O*	*In D_2O*
α-Helix	1650	1652	1650
Random coil	1658	1656	1643
β-Pleated sheet	1632	1632	1632
Aggregated β	—	1617	1617

Infrared Spectra of Cell Membranes in the 1400–1800 cm.$^{-1}$ Region. Maddy and Malcolm (*52, 53*) have reported the infrared spectra of dried films of beef erythrocyte ghosts, and of ghosts suspended in deuterium oxide. The amide I band was symmetrical about 1648 cm.$^{-1}$ (corrected from 1660 cm.$^{-1}$ reported in an earlier paper) in both wet and dry materials. No shoulder was visible in the 1630 cm.$^{-1}$ region. The lipid-extracted protein could be partially converted to the β from, however, by denaturation. After being heated in 50% ethyl alcohol, the protein gave an amide I absorption which was distinctly split into two bands, one at 1648 and one at 1632 cm.$^{-1}$. Sphingolipid absorption was negligible. Similar results were obtained by Chapman with dry human erythrocyte ghosts (*14*) and by Wallach and Zahler with dried films of Ehrlich ascites carcinoma cell plasma membranes (*90*). For the Ehrlich cells the amide I band appeared at 1652 cm.$^{-1}$, both in whole membranes and after extraction of lipids in chloroform–methanol. There was no absorption in the 1630 cm.$^{-1}$ region. After denaturation of the lipid-extracted protein in 0.1*M* HCl or by treatment with formic acid or 2-chloroethanol a second peak at 1632 cm.$^{-1}$ and a shoulder at 1690 cm.$^{-1}$ appeared. Absorption at these two frequencies indicates the antiparallel pleated sheet.

The observation by Maddy and Malcolm (*53*) that the amide I band of bovine erythrocyte ghosts in D_2O is not shifted is remarkable because it implies that all of the membrane protein is either deeply buried in an environment of hydrophobic lipids or exists in a tightly folded α-helical conformation. We have examined extensively the infrared spectra of bovine erythrocyte ghosts, both as dry films and as intact ghosts in D_2O and H_2O (*73*). The results for dry films essentially agree with those of other workers and show no evidence of β structure. Little change occurs in water. In D_2O, however, we consistently obtained a shift in the amide I band and a considerable decrease in absorption of the amide II band.

The spectra of dry films of intact ghosts prepared by lysis in 20 milliosmolal phosphate buffer (*21*) and of ghost protein prepared by cold butyl alcohol extraction (*51*) are shown in Figure 6. In both cases the amide I band occurs at 1651 cm.$^{-1}$ and shows no shoulder near 1630 cm.$^{-1}$, characteristic of β structure. The amide II band is also unaffected by removal of lipid and occurs at 1540 cm.$^{-1}$. As expected, extraction of lipid results in removal of the band at 1737 cm.$^{-1}$ assigned to lipid ester carbonyl stretch and a decrease of the band at about 1455 cm.$^{-1}$ arising from methylene and methyl bending.

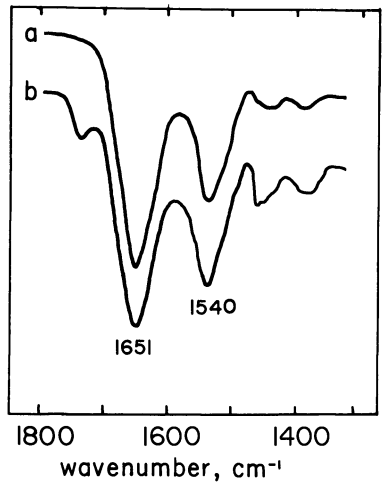

Figure 6. Infrared spectra of dried films of (a) butyl alcohol-extracted membrane protein and (b) beef erythrocyte membranes, taken on CaF_2 plates. No shoulder characteristic of the β conformation occurs at 1630 cm.$^{-1}$

When ghosts are transferred from water to 0.1*M* NaCl in D_2O, without drying, both of the amide absorptions change (Figure 7). The amide I band moves from 1651 to about 1640 cm.$^{-1}$, and simultaneously the amide II band at 1540 cm.$^{-1}$ diminishes. Such changes are characteristic of an appreciable content of randomly coiled protein, accessible to water. Note, however, that the amide I band becomes asymmetric after exchange and that some absorption remains at 1540 cm.$^{-1}$. This effect can be accounted for by the presence of some helical protein that neither exchanges nor shifts. In some preparations (Figure 8) a definite shoulder remains at 1651 cm.$^{-1}$ after exchange. After being heated in D_2O at 100°C. for 20 minutes to effect complete exchange, the membrane preparation shows no amide II band but an additional shift of the amide I

band to about 1634 cm.$^{-1}$, the position characteristic of the β structure. Occasionally heat denaturation produces a shoulder at about 1618 cm.$^{-1}$, which has been assigned by Timasheff (*83*) to an aggregated β conformation. In all of the spectra of ghosts in D_2O weak absorption occurs around 1575 cm.$^{-1}$, which is presumably caused by carboxylate absorption since it vanishes when the suspension is adjusted to pD 3 by DCl (*90*). Some of the spectral data are summarized in Table III.

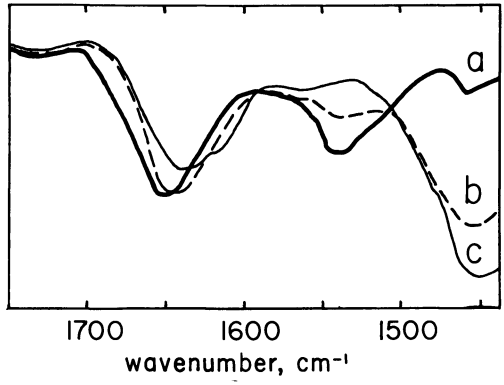

Figure 7. Infrared spectra of erythrocyte membranes (a) dry, (b) in D_2O–0.1M NaCl for 1.5 hours, and (c) heated to 100°C. in D_2O–0.1M NaCl for 10 minutes. Spectra were taken in CaF_2 cells. The residual amide II band at 1540 cm.$^{-1}$ indicates incomplete exchange in D_2O, and disappears on heating. The shoulder at 1618 cm.$^{-1}$ on the amide I band of heated membranes suggests aggregated β structure

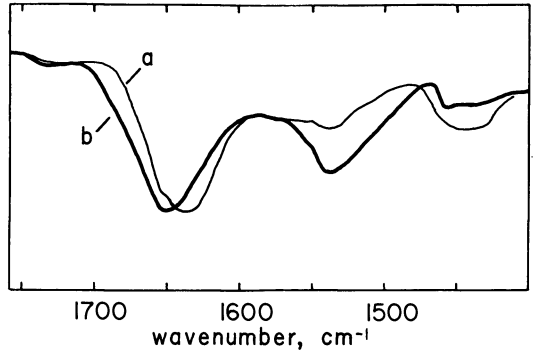

Figure 8. Infrared spectra of erythrocyte membranes (a) in D_2O–0.1M NaCl for 1.5 hours and (b) dry. The amide I band of the wet material shows a shoulder at 1650 cm.$^{-1}$, which may arise from α-helical protein

Table III. Amide I Wavenumbers for Erythrocyte Membranes

Treatment	*Dry Film*	*In H_2O*	*In D_2O*
None	1651	1648	1640
Heat to 100°C.	—	1630, 1616	1634, 1618
Formic acid	1630	—	—
Pronase	1650	—	1640
Pronase, heat to 100°C.	—	—	1633

The helical content of the membranes can be estimated roughly by comparing the amide II absorption of the dry film or the membrane in H_2O with the spectrum taken in D_2O (83). One must assume that the residual amide II absorption arises from helical polypeptides. A baseline can be established by heating the preparation to permit total exchange. This approach suggests a helical content of about one-fourth to one-third, in reasonable agreement with estimates based on ORD. Preliminary kinetic studies indicate that the majority of the exchangeable protons are exchanged rather rapidly (within 3 minutes) while the residual one-fourth to one-third of the protons do not exchange even after 24 hours. After freeze-drying and resuspension of the ghosts in D_2O, the amide II band is very weak, so that freeze-drying appears to increase the extent of proton exchange.

In an attempt to determine the distribution of helical protein in the membrane, pronase was used to remove accessible protein. Hydrolysis in pronase at pH 7.5 in tris-HCl buffer rapidly removes about 75% of the ghost protein without loss of phospholipid or cholesterol. The remaining protein is not attacked by pronase even after two days' incubation with the enzyme. Surprisingly, the pronase-treated ghosts are not destroyed by removal of most of the protein; their appearance in the phase contrast microscope is unchanged except for loss of contrast, and they behave as osmometers. Infrared spectra of dried films of the modified ghosts are very similar to those of native ghosts that have not been exposed to enzyme (Table III). In D_2O the same changes occur in the pronase-treated "core" as in the intact ghosts. As with the intact membranes, examination of the amide II band indicates that about one-third of the amide protons do not exchange. Measurements of the ORD trough depth also place the helical content at about one-third. It appears, then, that the conformation of the residual protein is not grossly different from that of the protein in the native membrane.

Interpretation of Infrared Spectra in Terms of Protein Conformation. With respect to β structure the interpretation of infrared spectra of wet and dry membranes is straightforward. There is no evidence for β conformation in any of the systems examined. Since the β structure can be produced by denaturation there appear to be no constraints

inherent to membrane protein which prevent it from assuming the β form, but it does not appear to be present under physiological conditions in the membrane. A small amount of β, say 15–20%, might be difficult to detect, but Maddy and Malcolm (*52*) have calculated that at least 35% of the total protein in erythrocyte membranes would be required to cover both sides of the membrane with a monolayer in the β conformation. Hence, if the β conformation is present at all, it is present in amounts below the limit of resolution of the infrared method. If such small amounts are present, they must not constitute a major feature of membrane structure. This result does not dismiss the possibility of a two-dimensional array of random protein chains.

The absence of β structure is also important for interpreting ORD spectra. It is important to establish that the ORD curves for membranes really reflect helicity rather than some other structure which is stabilized by lipid. As discussed earlier, CD studies support the concept of a helical conformation. Our demonstration of helicity in the absence of lipids in mitochondrial structural protein and in erythrocyte ghost protein also offers support. Without the additional evidence of CD and IR, rejection of the β structure on the basis of ORD alone would be questionable since in ORD the β structure is characterized by Cotton effects of low rotational amplitude and a red-shifted peak (*67*). The trough of the β curve is usually taken to be about 230 mμ, but β structures with troughs at higher wavelengths are known (*27*). However, ORD, CD, IR, and studies of lipid-free protein when taken together indicate that the Cotton effects of membranes are properly assigned to α-helices.

The use of infrared is not limited to β structure detection, however. The erythrocyte study reported here clearly illustrates the information available when spectra are taken in D_2O. Optical changes permit one to estimate the extent and rapidity of proton exchange in proteins and hence to estimate the availability of peptide bonds to water protons as well as the contributions from random coil and α-helical conformations. The results with erythrocytes indicate that about two-thirds to three-fourths of the protein amide groups are freely accessible to water and that most of the protein exists in an open, mostly random, conformation. The fraction of non-exchangeable protons agrees reasonably well with the helical content determined by ORD.

It appears that most of the protons that do not exchange are not shielded from water by hydrophobic interaction with lipids since the fraction of exchangeable protons in the amide bonds of residual protein after pronase treatment is approximately the same as in intact ghosts. Indeed this result, together with ORD data, suggests that there is no difference in the gross conformations of the enzymatically accessible and inaccessible protein. Proton exchange is probably inhibited because

much of the protein is in a tightly folded tertiary structure. Experiments are being carried out to examine proton exchange in lipid-free membrane protein.

Lipid Conformation: Calorimetric Studies

Rationale for the Technique. Although ORD, CD, and infrared spectroscopy have yielded valuable information concerning protein conformation in membranes, at present time none of these techniques seems capable of clearly establishing the state of lipids or the nature of lipid-protein interaction. In addition to searching for effects of lipid on protein conformation, the problem might be approached by directly examining the state of lipids. One promising approach is high resolution nuclear magnetic resonance (NMR), reported by Chapman and co-workers (*12, 13*). Although NMR can show that fatty acid hydrocarbons are constrained in membranes, identification of the molecular associations giving rise to the constraints is not always straightforward. One might hope to find a property of lipids in water, uniquely dependent upon their conformation and observable by a physical technique, which could also be found in membranes.

If, for example, lipids exist in membranes as bilayers, some unique property of the smectic mesophase might be detected by a direct physical technique. Such a property is the reversible thermotropic gel-liquid crystal phase transition observed in phospholipids in water. It has been studied by differential scanning calorimetry, differential thermal analysis, nuclear magnetic resonance, x-ray diffraction, and light microscopy and arises from melting of the hydrocarbon chains within the lipid bilayers (*11, 16, 48*). The transition temperature varies with unsaturation and length of the fatty acid hydrocarbon chains as well as with the nature of the polar heads of the phospholipids. No transition is observed when appreciable amounts of cholesterol are present (*48*). Since the phase change appears to be a melt of the hydrocarbon chains from a crystalline to a liquid-like state and like other melts involves cooperative association between hydrocarbon chains, it would vanish or be profoundly perturbed by apolar binding of lipids to proteins.

Various techniques might be used to detect such a two-dimensional "melt" in membranes, but differential scanning calorimetry (DSC) is particularly useful because membranes can be examined under physiological conditions and results can be made quantitative in a straightforward manner. In DSC a sample and a thermally inert reference (lacking a transition) are both heated at a constant rate. The measured parameter is the difference in power input between the sample and reference necessary to maintain identical heating rates for both. If no

transition occurs in the sample, a straight baseline is obtained; if a transition occurs, more heat must be supplied to the sample than to the reference, and a peak is recorded with area proportional to the heat of transition. Both the temperature scale and the peak areas can be calibrated with a compound of known melting point and heat of transition, such as stearic acid or water.

Pertinent Properties of the Gel-Liquid Crystal Transition. Figure 9 illustrates the effect of the nature of the polar end and of fatty acid chain length on the transition temperature of some synthetic saturated phospholipids (*76*). The smaller peak observed with the synthetic lecithins does not occur with the phosphatidyl ethanolamines and appears to be associated with the ionic portion of the lecithin. This lesser peak vanishes, for example, in 2.0*M* NaCl, 1.0*M* $MgSO_4$, or 50% ethylene glycol. It is present in the diether analog of lecithin in water but not when the choline moiety is replaced by *N,N*-dimethylethanolamine. It seems possible, then, that the "head" and "tail" transitions in synthetic lecithin may be useful in clarifying lipid-protein interaction in synthetic systems. For any given phospholipid, however, both the temperature and area of the calorimeter peak arising from the hydrocarbon tail transition are very nearly independent of the concentration of salt or the presence of ethylene glycol in the water. This invariance of the hydrocarbon transition temperature gives one some confidence that transitions of lipids in membranes might match those of the membrane lipids dispersed in water. In fact, this is the case for *M. laidlawii* membranes (shown below). Similar phase changes are observed in water for naturally occurring phospholipids (Figure 10). In natural systems the heat of transition is about 2–3 cal./gram, about one-third that of the synthetics.

Scanning Calorimetry of M. *laidlawii* Membranes. Since the transition temperature of phospholipids in water varies with unsaturation and chain length of the constituent fatty acids and since cholesterol interferes (*48*), to detect a thermotropic phase change in a membrane above the ice point an organism containing saturated fatty acids but little or no cholesterol must be chosen. *Mycoplasma laidlawii* fulfills these qualifications since Razin and co-workers (*61*, *62*) have shown that the membranes of the organism do not contain cholesterol when grown on a tryptose medium. *M. laidlawii* possesses the added advantage that the fatty acids in the membrane polar lipids can be changed at will over a wide range of saturation by supplying them in the growth medium (*61*, *62*). Since the cells do not possess a cell wall, membranes can be prepared simply by osmotic lysis. Biological evidence exists for a transition, including fatty acid-dependent changes in cell morphology, osmotic behavior, and temperature requirements for growth (*61*, *62*). Normal cells are filamentous but when forced to incorporate large amounts of saturated

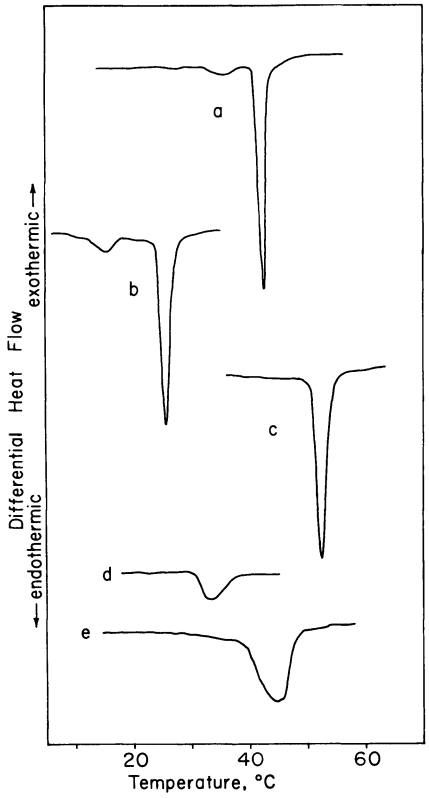

Figure 9. Scans of synthetic phospholipids in water taken with a Perkin-Elmer DSC 1B differential scanning calorimeter. Lipid concentrations were 10–15% by weight

(a) Dipalmitoyl-L-α-phosphatidylcholine
(b) Dimyristoyl-L-α-phosphatidylcholine
(c) Dimyristoyl-L-α-phosphatidylethanolamine
(d) 1:1 mixture by weight of (a) and (b)
(e) Dipalmitoyl-L-α-phosphatidylcholine sonicated above the transition temperature for 7 minutes. Samples a–d were not sonicated.

fatty acids (up to about 80%), they become swollen and rounded, possibly because accumulation of excess ions produces an abnormally high internal osmotic pressure. The temperature at which this effect occurs depends upon fatty acid chain length, and is lower for palmitic than stearic acid and much lower for oleic acid. Note that physically *M. laidlawii* membranes are the same as those from other organisms. The

optical rotatory dispersion (*50*) and infrared spectra (*73*) and the appearance in the electron microscope (*23*) are not abnormal, and reversible dissociation with detergents with the formation of apparent "subunits" has been demonstrated (*23*). Since the fatty acid composition of the membrane lipids can be varied, it should also be possible to vary the transition temperature observed in the calorimeter.

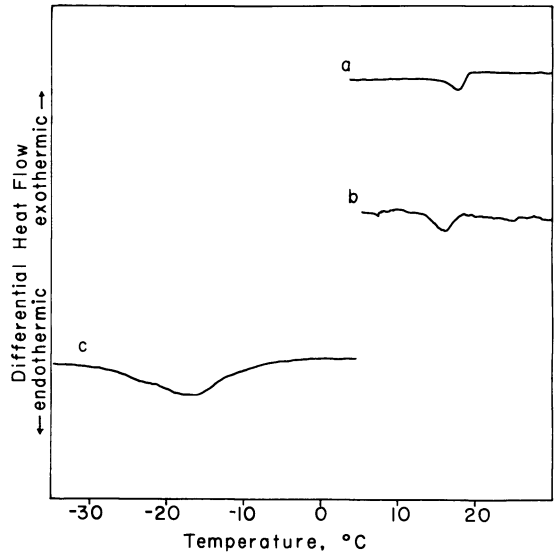

Figure 10. Calorimeter scans of some unsonicated dispersions of natural phospholipids

(a) Bacterial (E. coli) *phosphatidyl ethanolamine in water*
(b) Bacterial phosphatidyl ethanolamine in 50% ethlyene glycol
(c) Egg lecithin in 50% ethylene glycol.

We have observed such a transition in intact membranes of *M. laidlawii* which occurs at the same temperature as in the membrane lipids dispersed in water (*77*). Figure 11 shows representative endothermic transitions of membranes and lipids in water. Membranes were prepared for calorimetry by sedimenting at high speed, then 90–100 mg. of packed pellet were sealed in a stainless steel sample pan. The material was neither dried nor frozen before examination. Total membrane lipids were extracted with chloroform-methanol 2:1 v/v then dried and suspended in water. Lipids from the membranes of cells grown in the usual tryptose medium without added fatty acids are shown in a, while b and c are scans of intact membranes from the same cells. In b the membrane preparation had not been previously exposed to temperatures above 27°C. The smaller transition at higher temperature probably arises from

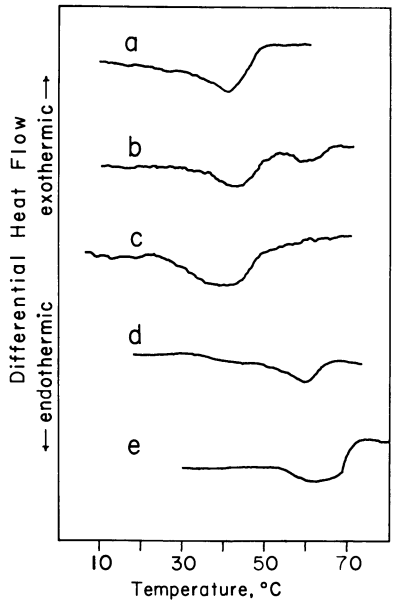

Figure 11. Calorimeter scans of M. laidlawii *membranes and membrane lipids in water. Membrane concentrations were 10–15% and lipid concentrations 20–25% dry weight*

(a) Total membrane lipids from cells grown in unsupplemented tryptose
(b) Initial scan of membranes from unsupplemented tryptose
(c) Same as (b), but subsequent scan
(d) Total membrane lipids from cells grown in tryptose with added stearate
(e) Membranes from stearate-supplemented tryptose.

protein denaturation (*72*) because it never appears on subsequent scans, such as c, and is temperature invariant for all membranes regardless of lipid composition. Lipid transitions in the membranes are reversible. Curves d and e are from lipids and membranes of cells grown in tryptose medium supplemented with stearate. Scan e was made after protein denaturation; in the initial scan a peak occurred at the same temperature but with larger area. The increased area on the first scan can be attributed to the addition of peaks arising from both the lipid transition and protein denaturation. For palmitate-enriched lipids and membranes the transition occurs between those shown for the unsupplemented and stearate-enriched systems. For membranes high in oleate the transition is below room temperature. As pointed out previously, cells with transitions above

or at growth temperature show obvious osmotic anomalies; those grown in oleate do not.

Because the area under the peaks in the scanning calorimeter is proportional to the heat of transition, the instrument can be calibrated by running a known amount of membrane lipid suspended in water. It is necessary to assume, of course, that all of the lipid is in the bilayer conformation in water. If the lipid content of the membranes is known, the fraction of the lipids contributing to the peak observed for the membranes can then be calculated by comparing peak areas for the membranes and the lipids in water. Our preliminary results using this approach indicate that at least 60% of the lipids in the membranes participate in the phase change. Work is in progress to obtain more precision.

Interpretation of the Calorimetric Results. There is little doubt that the transition observed in *M. laidlawii* membranes arises from the lipids since it occurs at the same temperature in both intact membranes and in water dispersions of membrane lipids. It is reasonable to conclude that in both membranes and membrane lipids the lipid hydrocarbon chains have the same conformation. The lamellar bilayer is well established for phospholipids in water (*1*, *20*, *29*) at the concentration of lipids used in these experiments. In the phase change the hydrocarbon core of the bilayer undergoes melting from a crystalline to a liquid-like state. Such a transition, like the melting of bulk paraffins, involves association between hydrocarbon chains and would vanish or be greatly perturbed if the lipids were apolarly bound to protein. We can reasonably conclude that most of the lipids in *M. laidlawii* membranes are not apolarly bound to protein.

The transition temperature for the membranes of cells grown in stearate occurs above the growth temperature, and even for cells grown in unsupplemented tryptose medium it is surprisingly high. This result does not imply, however, that such high transition temperatures are the usual case in cell membranes. As pointed out earlier, cells with transition temperatures within or above the growth temperature show osmotic anomalies which might be ascribed to abnormal ion transport. The cells examined in this study had ceased growth and in the case of the cells supplemented with stearate had begun to lyse. Cells supplemented with oleate were not in osmotic difficulties; for these membranes the transition temperature is well below growth temperature. For highly saturated membranes the cells first incorporate unsaturated fatty acids present in small quantities in the growth medium and then are forced to incorporate the saturated fatty acids. As the membranes become more highly saturated, the phase transition temperature would rise until finally it would reach that of the growth temperature, at which point transport would become perturbed and growth would cease.

Lipid Conformation: Nuclear Magnetic Resonance

Theory of the Method. One of the most promising techniques for elucidating lipid-protein association is high resolution NMR, introduced by Chapman and co-workers (*12, 13*). NMR has already been shown to be a powerful tool for studying the binding of small molecules to proteins (*33, 40*) because line widths of absorptions by individual groups of protons are functions of spatial constraints upon molecular motion. When molecules have freedom of motion, correlation times are short, local magnetic fields are time averaged, and the absorption lines are narrowed. When molecular motion is restricted, correlation times and line widths increase even to the point where the lines vanish. Broadened lines can result, for example, when solvent viscosity is very high or when molecular associations occur. Many globular proteins do not exhibit high-resolution spectra because the protons are constrained. Consequently the proton line widths of small molecules bound onto proteins are greatly increased. Thus, since NMR is capable of resolving resonance lines from individual groups of protons, and line width is a function of motional constraints, in some systems the technique is capable of showing which lipid protons are immobilized by binding onto proteins. Chapman *et al.* (*13*) have shown that although the hydrocarbon protons of total lipids from erythrocyte ghosts show a narrow resonance line when the phospholipids are sonicated into water, the fatty acid hydrocarbon proton resonances are not present in sonicated ghosts. The hydrocarbon chains appear to be considerably more immobilized in the membranes than in the sonicated lipids from the membranes. Such immobilization could arise from hydrophobic association of lipids with proteins *via* the fatty acid chains, but it could also arise because the motion of fatty acid chains is restricted within bilayers. Since NMR line widths can yield information on the nature of molecular motion but not directly on hydrophobic interaction between lipid and protein, it is necessary to understand the NMR properties of phospholipids.

Interpretation of the NMR Spectra of Membranes. Let us first consider a model system of lysolecithin and serum albumin (*74*), shown in Figure 12. Lysolecithin in D_2O is shown in Figure 12A, while the effect of increasing amounts of bovine serum albumin is shown in Figures 12B and 12C. When no protein is present, the lines for both the methylene protons on the lysolipid "tails" and the quaternary ammonium methyl protons on the choline moiety of the polar "heads" are narrow. Thus, the polar ends of the molecules are free to move, and the apolar hydrocarbons within the detergent micelles are in a liquid-like state (*24*). When protein is added, the hydrocarbon proton line broadens and shifts upfield slightly, but neither the width nor area of the quaternary ammonium line

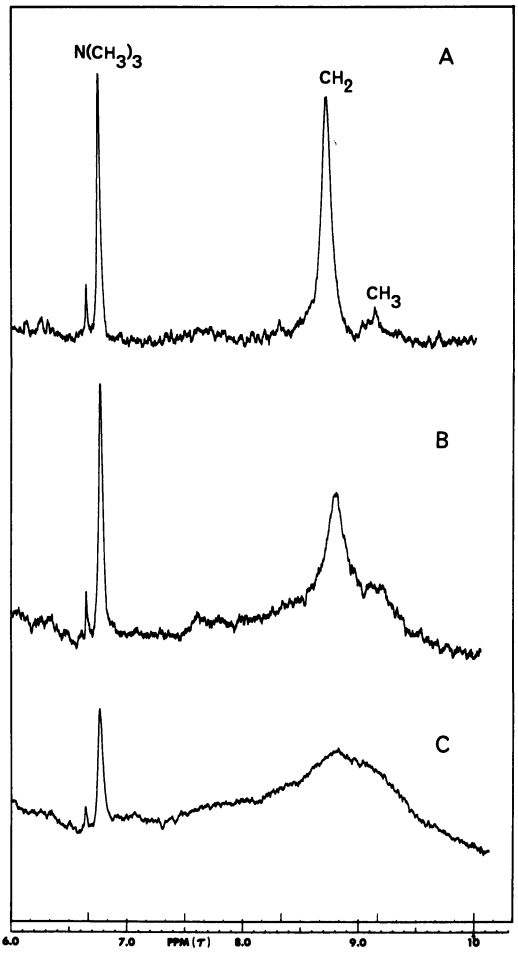

Figure 12. Effect of bovine serum albumin upon the NMR spectrum of 0.5 w/v% lysolecithin in 0.1M NaCl–D_2O at 40°C.

(a) No protein added
(b) 3 w/v% protein present
(c) 10 w/v% protein present
In (c) the spectrometer amplitude setting was half that of (a) and (b). All solutions were optically clear, with no evidence of precipitation. All high-resolution spectra illustrated were taken with a Varian A60A spectrometer at 60 megacycles.

increases. Such upfield shifts could arise from ring currents if the hydrocarbons were bound near aromatic amino acid residues on the surface of the serum albumin. With sufficiently high protein concentrations the methylene proton line vanishes even though that of the polar portion of

the lysolecithin remains unperturbed. The selective broadening of the hydrocarbon proton absorptions in the lysolecithin-serum albumin system indicates that the fatty acid chains are apolarly bound and consequently constrained while the polar ends are unbound and unconstrained. Thus, the binding of lysolecithin to serum albumin appears to be hydrophobic in this case.

A more complex case is the serum lipoprotein (*74*), shown in Figure 13. When sonicated into water, total lipids from both the low density (β) and high density (α) lipoproteins give rise to the high resolution spectra expected of molecules which have a high degree of motion. The spectra of the native lipoproteins show line widths nearly identical to those of the lipids alone, so that no additional motional constraints of the apolar portions of the phospholipids occur when the lipids are bound to the apoproteins of the blood lipoproteins. All the obvious peaks observed in the native lipoproteins can be accounted for by lipid protons, and no upfield shift of the methylene protons occurs. We can conclude that unlike the case of the lysolecithin-serum albumin system, the bonding of lipids to proteins is not apolar. In the serum lipoproteins the NMR results are consistent with a micellar structure and not with extensive apolar association of lipid with protein.

For biological membranes the situation is more complex. The results from erythrocyte ghosts and lipids (*13*) suggest nonpolar association through lipid hydrocarbon chains. As a test of the technique a membrane in which the bilayer conformation has been demonstrated by some independent technique is desirable. I have argued earlier from calorimetric evidence that the membrane of *M. laidlawii* is such a system. NMR spectra of *M. laidlawii* membranes taken in this laboratory do not, however, show discernible hydrocarbon proton resonance. We must consider, then, why the two techniques of calorimetry and NMR do not agree.

Unlike lysolecithin or other detergents, phospholipids do not reversibly associate in water to form isotropic micelles, and they do not show a critical micellar concentration. Instead phospholipids swell in water to produce myelin forms, which are lamellar arrays of lipid bilayers (*1, 20, 29*). The thermal properties of these systems have already been discussed. When myelin forms are dispersed in water by sonication above their thermal transition temperature, they yield high resolution proton NMR spectra similar to those observed with detergents (*13*). Most phospholipids which are merely swollen in water or dispersed by hand shaking do not, however, show any appreciable high resolution resonance signals for the hydrocarbon protons (Figure 14). For such systems broad line NMR signals are obtained with line widths of about 100 milligauss, as shown in Figure 15. Line widths of about 100 milligauss have also been reported for soaps in the neat phase (*49*). In fact, high resolution spectra

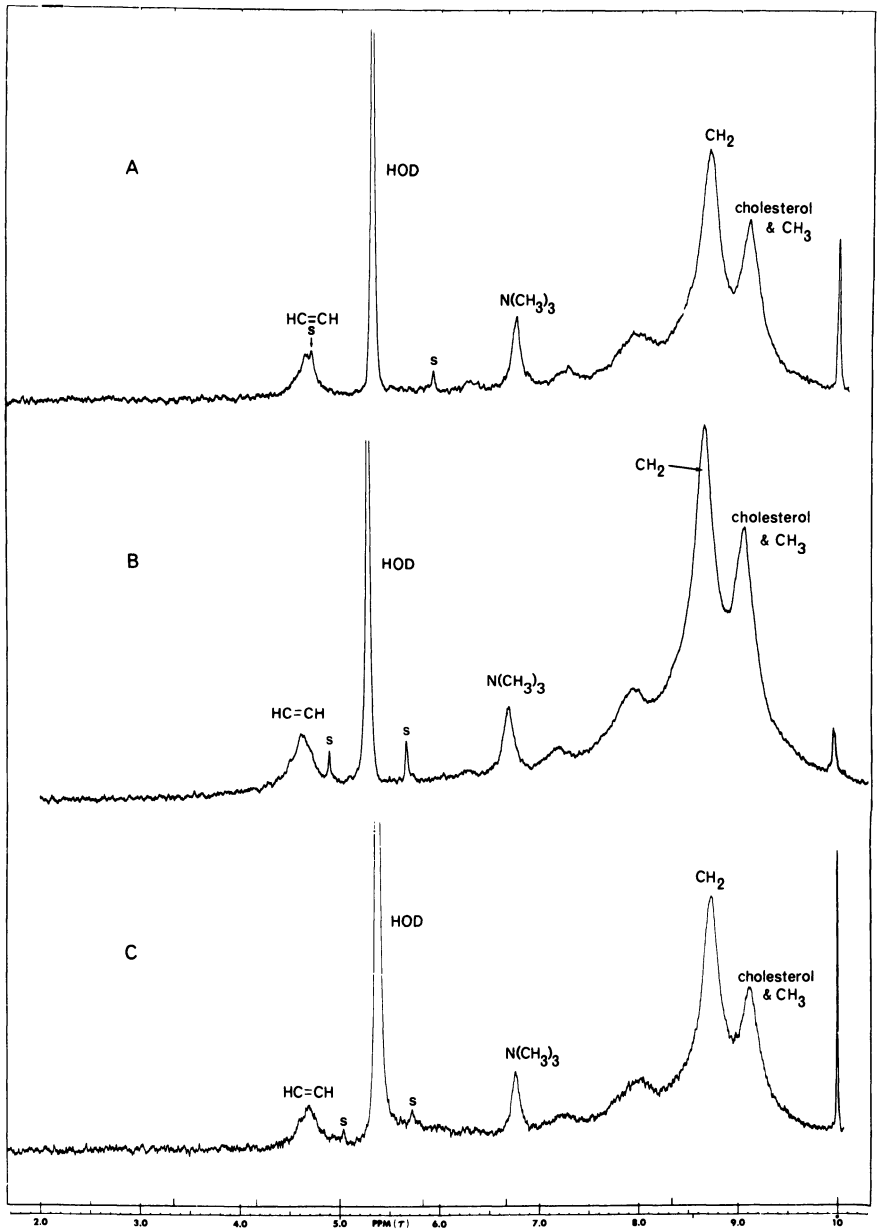

Figure 13. NMR spectra at 35°C. of (a) low density lipoprotein lipids dispersed in D_2O by sonication, 512 μgrams phosphorus/ml.; (b) low density serum lipoproteins in 0.1M NaCl–D_2O, 625 μgrams lipid phosphorus/ml.; (c) high density serum lipoproteins in 0.1M NaCl–D_2O, 832 μgrams lipid phosphorus/ml. Spectrum for high density lipoprotein lipids dispersed in water by sonication was essentially identical to (a). Spinning side bands are labeled S

of most unsonicated phospholipids in water resemble those of membranes, and if the spectra of membranes were compared with those of unsonicated phospholipids, one might conclude that high resolution NMR cannot distinguish between a membrane with a bilayer structure and one in which the lipid-protein association is nonpolar.

Hence, the most important point in interpreting high resolution NMR studies of membranes is whether membrane spectra should be compared with those of sonicated or of hand-shaken dispersions of the membrane lipids in water. If sonication merely breaks down myelin forms to particles of small dimensions without changing the internal correlation times for the molecules within the bilayers, then a reasonable choice for reference could be the sonicated lipid-water systems. One must explain, however, why sonication of myelin forms gives rise to high resolution spectra. One possibility is that the particles become small enough to tumble rapidly enough in the water to average magnetic field inhomogeneities. Calculations from accepted NMR theory indicated that for particles the size of sonicated phospholipids, which have molecular weights of several million and diameters of a few hundred angstroms (*60, 68*), the contribution to correlation times from over-all tumbling of the entire particle is completely negligible as far as high resolution NMR is concerned (*4, 24, 40*). Although correlation times of 10^{-5} second characterize the region in which broad line absorption begins to become narrowed, line widths in this region are still many thousands of c.p.s. wide and cannot be observed on a high-resolution instrument. Typical high resolution spectra, with line widths of only a few cycles, arise when correlation times are about 10^{-8} to 10^{-10} second. The correlation time for tumbling sphere of 500-A. diameter is on the order of 10^{-5} second. Thus, high resolution lines cannot be accounted for in terms of tumbling.

Another possibility could be that in the unsonicated case anisotropy in the magnetic field within the liquid-crystalline myelin forms could produce line broadening. Myelin forms are known to be strongly optically anisotropic. However, myelin forms of mitochondrial lipids (Figure 16), which are highly unsaturated, show high resolution spectra similar to those obtained by sonicating the more saturated systems. Since the myelin forms of mitochondrial lipids, like those of other phospholipids, are repeated anisotropic parallel arrays of bilayers, it is unlikely that high resolution signals are absent in the more saturated systems because of anisotropy. If these considerations are taken into account, the most reasonable conclusion is that sonication produces high resolution spectra in water dispersions of phospholipids because internal correlation times for the fatty acid chains within the bilayers are increased. In sonicated lipids, which appear to exist as closed vesicles bounded by one bilayer

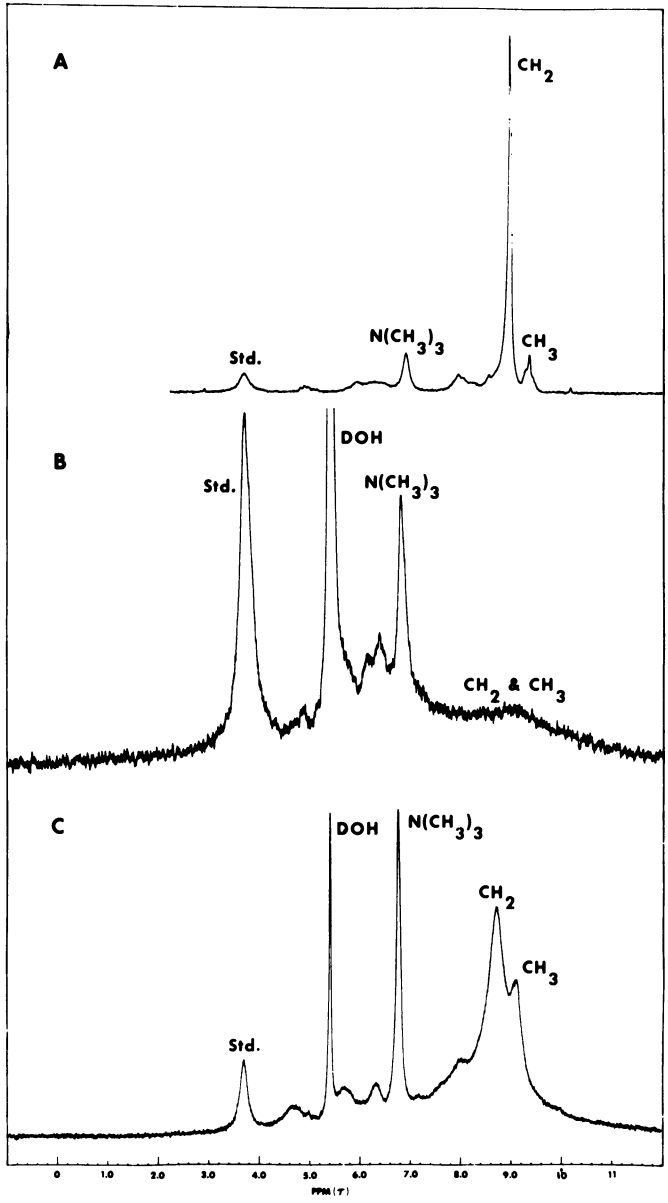

Figure 14. NMR spectra of egg lecithin at 40°C.: (a) 18 w/v% in $CDCl_3$, (b) 18 w/v% dispersed in D_2O without sonication, and (c) 28 w/v% sonicated 5 minutes in D_2O. Std. indicates an external integration standard of 30% H_2SO_4 and 1% $CuSO_4 \cdot 5H_2O$ in D_2O

(*60*), chains must be less tightly packed than in the hand-dispersed systems. A small radius of curvature might be responsible.

Hand-shaken dispersions of phospholipids thus may be a more reasonable choice for comparison with membranes, and except in rare cases of highly unsaturated systems the high resolution NMR spectra of such dispersions do not exhibit high resolution proton absorption. Hence, for most membranes, NMR can indicate immobilization of fatty acid chains but not whether chains are immobilized by binding onto proteins or by tight packing into bilayers. Broad line NMR may be useful, especially when a phase transition is present.

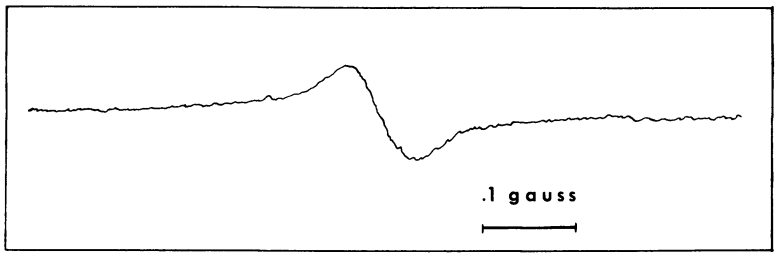

Figure 15. Broad line proton NMR spectrum of total lipids from bovine erythrocytes, dispersed in D_2O without sonication (15 w/v%). Spectrum was taken at 30°C. with a Varian V-4200 broad line NMR at 16 megacycles

Discussion

A promising beginning has been made in applying physical techniques to the problem of membrane structure. The use of these methods is growing rapidly and will become increasingly important. The number of systems that have been studied is limited, and generalizations must be made cautiously, but some important points have already been established. Since the data are sparse, a membrane model will not be suggested. Instead some of the implications of the experimental results will be discussed.

If preparative or instrumental artifact is ruled out, the universal occurrence of red-shifted Cotton effects with α-helical character in all the membranes studied points to a common property of the proteins in biological membranes. The ORD results from lipid-free mitochondrial structural protein and erythrocyte ghost protein are consistent with assigning the red shift in these membranes to aggregated protein. It is, therefore, reasonable that similar protein-protein association may occur in all membranes. Ionic requirements for membrane stability could then reflect in part the requirements for protein-protein association. To some extent the molecular associations which stabilize membranes, therefore, may be protein-protein as well as lipid-lipid in nature.

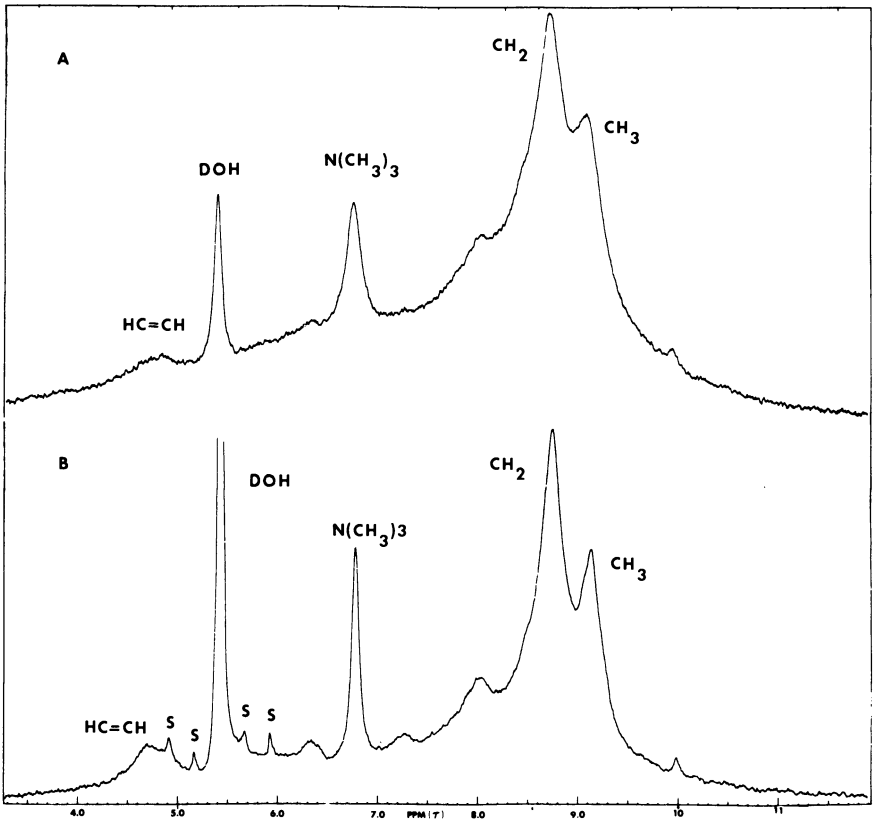

Figure 16. NMR spectra of total mitochondrial phospholipids at 40°C. in D_2O: (a) 15 w/v% lipids dispersed without sonication, (b) 8 w/v% lipids dispersed by sonication

If these ideas are correct, the solubilization of membranes by detergents may result in the disaggregation of protein as well as the disruption of associations between lipids. This point of view is consistent with the action of detergents upon the ORD of lipid-free membrane protein—*i.e.*, the turbid suspension of aggregated protein clears, and the red shift vanishes. For various membranes it has been suggested that treatment with detergents results in the disaggregation of lipoprotein subunits and that the intact membrane is fundamentally a two-dimensional array of such repeating subunits (*32, 35, 36*). However, although the production of lipid-protein-detergent complexes by the action of detergents might be a consequence of a subunit membrane architecture, it is not sufficient evidence that such a structure exists in intact membranes.

In fact, several recent experiments suggest that the mechanism of detergent solubilization should be re-examined, and that if repeating

subunits are present in membranes, they are not disaggregated intact by detergents. Although calorimetric evidence strongly suggests that most of the lipid in *M. laidlawii* membranes exists in a liquid-crystalline state and probably as a bilayer, reversible disaggregation of this system by detergents has been demonstrated. For the *M. laidlawii* system Engelman, Terry, and Morowitz (*23*) have shown that even though solubilization by sodium dodecyl sulfate appears to yield a lipid-protein-detergent complex which is monodisperse in the analytical ultracentrifuge, prolonged centrifugation in a sucrose gradient containing 9 m*M* sodium dodecyl sulfate gives two bands. The band of lower density is protein-free lipid, while the denser band is lipid-free protein. Similar results were obtained with a D_2O gradient. In this case the detergent completely displaces the lipid from the membrane protein. Dialysis of the solubilized membrane preparation against 0.05*M* Mg^{2+} results in removal of detergent and reconstitution of membranous structures (*23*). Solubilization and reconstitution has been demonstrated for several other membranes and for other detergents, notably deoxycholate and cholate (*35*). With these detergents as well as with sodium dodecyl sulfate, solubilization may result in partial or complete removal of lipid from protein rather than in the disaggregation of membrane subunits essentially in their native state. Separation of lipid from protein upon treatment of membranes with detergents has also been reported by other workers (*66*). In this laboratory we have found that when beef heart mitochondria are solubilized in sodium deoxycholate-cholate and passed through a column of Sephadex G-200 in the detergent solution, much of the phospholipid elutes as a single peak free of protein (*79*).

NMR offers a second kind of evidence bearing upon the nature of detergent action. Experiments reported by Chapman and his colleagues (*12, 13*) and also those done in this laboratory show that although membranes show little high resolution absorption by methyl and methylene protons, the addition of deoxycholate invariably results in greatly increased absorption by these hydrocarbon protons. The amplitude and line widths of these peaks are quite similar to those of lipid-detergent micelles in water. Thus, the NMR evidence also indicates that the lipid conformation in detergent-solubilized membranes is considerably different from that in the native state and is consistent with a mechanism of solubilization involving disaggregation of proteins with partial or complete removal of lipid from the protein with inclusion of the lipid in mixed micelles with the detergent.

For blood cell membranes the agreement of optical rotatory dispersion and infrared spectroscopy is reassuring. About one-third to one-fourth of the protons in the peptide bonds do not exchange in D_2O. This non-exchangeable fraction can be equated with the helical content of

about one-third measured by ORD (*82, 83*). The peptide bonds of the remaining two-thirds are quite accessible to water and are in the random coil conformation. We can draw some tentative conclusions concerning the location of helical and random regions of the polypeptide chains in the membrane by examining the pronase-resistant "core," which retains about 25% of the total ghost protein. The ORD and proton exchange properties of the residual protein and the intact ghosts are quite similar—approximately the same proportions of helical and random polypeptides are present in both systems. In the pronase-treated membranes as in the native ghosts most of the amide protons exchange rapidly, and the rest does not exchange after many hours. If it is assumed that molecular rearrangements do not occur upon treatment with pronase (and this assumption seems justified because the modified ghosts appear intact in the phase microscope), the resistant protein must be protected from enzyme attack by lipid. This argument is supported by the observation that neither phospholipid nor cholesterol are lost by treatment with the enzyme, and that after removal of the lipids by organic solvents, the digestion goes to completion (*73*). It appears, then, that in the core both random and helical polypeptides are rendered resistant to enzyme attack by close association with lipids. These resistant proteins or protein fragments could exist entirely in the interior of the membrane in apolar association with lipids, but they could also penetrate a lipid bilayer. In any case, the helical protein regions appear to be distributed uniformly throughout the membrane.

It might be possible that the non-exchangeable amide bonds are shielded from water by interaction with lipid. Experimental evidence does not support this concept. Approximately 75% of the non-exchangeable amide protons are removed by pronase, and hence are accessible to the enzyme. The remaining protein, although protected from enzyme attack by lipid, nevertheless rapidly exchanges most of its amide protons. In both intact and modified ghosts the lack of exchange can be more adequately explained by the existence of helical regions, many of which may exist in tightly folded globular conformations. The accessibility of most of the helical protein to pronase implies that lipids do not play a dominant role in stabilizing helical segments of membrane protein. Comparison of the Cotton effects of intact ghosts and butyl alcohol-extracted ghost protein supports this point of view. Calculations of helicity based on trough depth indicate that most (75%) of the helical content of the membrane is preserved in the lipid-free protein. Thus, if hydrophobic lipid-protein association occurs, it must occur in such a way that lipids do not exert much stabilizing effect upon helicity. These results are similar to those obtained by Scanu (*69*) with serum lipoproteins.

Just as ORD, CD, and infrared are useful to elucidate protein conformation in membranes, NMR and differential scanning calorimetry can give insight into the state of lipid. High resolution NMR is clearly applicable to studies of detergent-protein interaction and to such systems as the soluble serum lipoproteins, although we believe that the technique must be applied to membranes with caution. If narrow high resolution lines characteristic of mobile fatty acid chains were observed in membranes, they might confidently be assigned to phospholipids in a smectic mesophase, but when no absorption occurs, the reason for chain immobilization cannot be identified easily. Broad line NMR could prove useful, especially when a phase transition is present as in *M. laidlawii.*

Calorimetric evidence for a phase transition in *M. laidlawii* can be interpreted more straightforwardly. Since the transition involves melting of fatty acid chains from a crystalline state to a liquid-like state, it must imply lipid-lipid association and not lipid-protein association. The argument is based on recognized properties of the bilayer conformation. The calorimeter thus supplies a link between membranes and x-ray diffraction studies of phospholipids in water since if the melt occurs at the same temperature in both systems, the structures must be quite similar. Use of the calorimeter is restricted to membranes which are capable of showing transitions. Since the transition does not occur in phospholipids when appreciable amounts of cholesterol are present, myelin and mammalian plasma membranes probably cannot be used. Other membranes, such as those of bacteria, mitochondria, or chloroplasts may be suitable although in many cases the change, if present, would occur below the ice point. In these cases possible destructive effects of freezing should be considered. The combination of high resolution NMR, broad line NMR, and calorimetry may have sufficiently broad capabilities to clarify the state of lipids in most membranes.

Although the majority of the lipids in *M. laidlawii* membranes appear to be in a liquid-crystalline state, the system possesses the same physical properties that many other membranes possess. The ORD is that of a red-shifted α-helix; high resolution NMR does not show obvious absorption by hydrocarbon protons, and infrared spectroscopy shows no β structure. Like erythrocyte ghosts, treatment with pronase leaves an enzyme-resistant core containing about 20% of the protein of the intact membrane (*56*). This residual core retains the membrane lipid and appears membranous in the electron microscope (*56*). Like many others, *M. laidlawii* membranes are solubilized by detergents and can be reconstituted by removal of detergent. Apparently all of these properties can be consistent with a structure in which the lipids are predominantly in the bilayer conformation. The spectroscopic data are therefore insufficient to reject the concept of a phospholipid bilayer structure or to

establish the idea of a repeating subunit structure. The bilayer concept can be retained with some modifications to accommodate recent spectroscopic results. The membrane cannot be viewed as a continuous bilayer system bounded on each side by unfolded protein layers. In particular, infrared rules out the specific model of a β-pleated sheet covering the polar array of phospholipid heads. Inclusion of helical protein, much of it probably aggregated and in a folded conformation, would represent a minimal revision of the Danielli-Davson-Robertson membrane. Some of the helical protein appears to penerate the membrane and is resistant to enzyme attack.

It is possible that quite different molecular architectures may occur in membranes from different sources. Current research may result in a much more dramatic revision or complete rejection of the bilayer model for some membranes, especially in such systems as mitochondria (*30*) and chloroplasts (*2*). However, it is also possible that structural differences are only variations on the basic theme of the bilayer, from myelin at one extreme to mitochondria or chloroplasts on the other. One must not readily reject the fundamentals of the Danielli concept, especially in view of the present inadequate knowledge of the properties of phospholipids in water. Clearly the molecular architecture of membranes is speculative, but most aspects of the problem are amenable to direct experimental test by the new physical techniques. A consistent model for biological membranes will emerge quickly.

Summary

Spectroscopic and calorimetric techniques have been used to examine the structure of several biological membranes. Optical rotatory dispersion of all membranes examined resembles those obtained with α-helical proteins and synthetic polypeptides, except that the Cotton effects are shifted to abnormally high wavelengths. The ORD of membranes solubilized in detergents is not red shifted but still resembles that of an α-helix. Analysis of ORD data indicates a helical content of about one-third for most membranes. The similarity of ORD spectra from many membranes suggests structural features common to all. Controversy exists in the literature concerning the perturbations of the CD spectra which accompany changes in the ORD. We have shown that the red-shifted dispersion spectra do not arise from lipid-lipid association. Red-shifted ORD spectra are obtained, however, with aggregated lipid-free membrane protein, and the red shift vanishes upon disaggregation of the protein either by the proper choice of pH or by detergents. Therefore, the red shift in the ORD of membranes may be accounted for in terms of protein-protein association.

Infrared studies of the position and fine structure of the amide I band of both wet membranes and dried films show that although membrane protein can be converted to the β structure by denaturation, β structure is not present in the native material. The changes observed in the infrared spectra of erythrocyte membranes in D_2O and H_2O are compatible with ORD results. In D_2O approximately two-thirds of the amide protons exchange within minutes; the remainder does not exchange after many hours. Complete exchange is effected by heating to 100°C. The amide I band shifts from 1651 $cm.^{-1}$ in the dry film to 1640 $cm.^{-1}$ in D_2O and upon heating shifts further to 1634 $cm.^{-1}$. The shift in the amide I band in D_2O at room temperature appears to be assymetric, and in some cases a residual shoulder remains at 1651 $cm.^{-1}$. These spectral properties are consistent with about one-third helical content, with the remaining polypeptide chains random and accessible to water.

For those amide bands in erythrocyte membranes which do not exchange, the lack of exchange cannot be accounted for by association with lipid. Pronase treatment removes approximately 75% of the membrane protein, but the residual protein has essentially the same exchange properties and percentage helicity as the native membrane. The results strongly suggest that helical polypeptide chains are uniformly distributed among proteins associated with lipids and those free of lipids, and that it is not necessary to invoke hydrophobic interaction to explain the stability of helical segments in the membrane. This conclusion is supported by the observation that lipid-free membrane protein retains helicity. The protein of membranes, like most other proteins, appears to possess considerable tertiary structure, stabilized by intramolecular associations. On the basis of presently available data, this concept does not exclude the possibility that some of the protein molecules, or some parts of all the protein molecules, may be randomly unfolded in some planar conformation. Some of the folded protein resides in the interior of the membrane.

Comparson of the transitions observed by differential scanning calorimetry in membranes of *M. laidlawii* and in water dispersions of the lipids from the membranes support the concept that most of the lipids exist as a smectic mesophase in the membranes. The evidence for a bilayer structure is straightforward in this case. Lipid transition temperatures are a function of fatty acid composition and correlate well with biological properties. The calorimeter possesses advantages over high resolution NMR for *M. laidlawii,* and perhaps in many other systems, because the data can be interpreted less ambiguously. In *M. laidlawii* membranes the bilayer appears to be compatible with the same physical properties observed in other membranes—a red-shifted ORD, lack of β structure in the infrared, reversible dissociation by detergents, and poorly

defined high resolution NMR spectra. This system thus offers a unique opportunity for interpreting the results obtained from physical techniques.

With respect to the effects of detergents, the optical properties of membrane protein mimic those of intact membranes—detergents disaggregate structural protein. However, NMR and density gradient centrifugation indicate that detergents also have a profound effect upon membrane lipid conformation and lipid-protein interaction. It is, therefore, suggested that detergents have a two-fold effect upon membranes—the disaggregation of protein and the complete or partial displacement of lipid from protein with the conversion of the lipid from a rather constrained conformation to a much more liquid-like micellar state. For sufficiently active detergents, such as sodium dodecyl sulfate, the lipid is completely released from the protein and exists as separate micelles.

Acknowledgment

The author thanks S. Fleischer, J. H. Gibbs, E. S. Pysh, M. E. Tourtellotte, and M. J. Grourke for stimulating and helpful discussions. Much of the support came from U. S. Public Health Service Grants FR 07085 and GM 14696. The Cary 60 spectropolarimeter and the Varian A60A NMR spectrometer were purchased with National Science Foundation instrument grants.

Literature Cited

(1) Bangham, A. D., *Advan. Lipid Res.* 1, 65 (1964).
(2) Benson, A. A., *J. Am. Oil Chemists Soc.* **43**, 264 (1966).
(3) Beychok, S., *Science* **154**, 1288 (1966).
(4) Bloembergen, N., Purcell, E. M., Pound, R. V., *Phys. Rev.* **73**, 679 (1948).
(5) Brady, R. O., Trams, E. G., *Ann. Rev. Biochem.* **33**, 75 (1964).
(6) Branton, D., *Proc. Natl. Acad. Sci.* **55**, 1048 (1966).
(7) Brown, A. D., *J. Mol. Biol.* **12**, 491 (1965).
(8) Carver, J. P., Shechter, E., Blout, E. R., *J. Am. Chem. Soc.* **88**, 2550 (1966).
(9) *Ibid.*, p. 2562.
(10) Cassim, J. Y., Yang, J. T., *Biochem. Biophys. Res. Commun.* **26**, 58 (1967).
(11) Chapman, C., Byrne, P., Shipley, G. G., *Proc. Roy. Soc. (London)* **A290**, 115 (1966).
(12) Chapman, D., Kamat, V. B., de Gier, J., Penkett, S. A., *Nature* **213**, 74 (1967).
(13) Chapman, D., Kamat, V. B., de Gier, J., Penkett, S. A., *J. Mol. Biol.* **31**, 101 (1968).
(14) Chapman, D., Kamat, V. B., Levene, R. J., *Science* **160**, 314 (1968).
(15) Chapman, D., Penkett, S. A., *Nature* **211**, 1304 (1966).
(16) Chapman, D., Williams, R. M., Ladbrooke, B. D., *Chem. Phys. Lipids* 1, 445 (1967).

(17) Criddle, R. S., Bock, R. M., Green, D. E., Tisdale, H., *Biochemistry* 1, 827 (1962).
(18) Davson, H. A., Danielli, *J. Cell. Comp. Physiol.* **5**, 495 (1935).
(19) Demel, R. A., van Deenen, L. L. M., Pethica, B. A., *Biochim. Biophys. Acta* **135**, 11 (1966).
(20) Dervichian, D. C., *Progr. Biophys. Mol. Biol.* **14**, 263 (1964).
(21) Dodge, J. T., Mitchell, C., Hanahan, D. J., *Arch. Biochem. Biophys.* **100**, 119 (1963).
(22) Elbers, P. F., "Recent Progress in Surface Science," J. F. Danielli, K. G. A. Pankhurst, A. C. Riddiford, Eds., Vol. 2, p. 443, Academic Press, New York, 1964.
(23) Engelman, D. M., Terry, T. M., Morowitz, H. J., *Biochim. Biophys. Acta* **135**, 381 (1967).
(24) Eriksson, J. C., *Acta Chem. Scand.* **17**, 1478 (1963).
(25) Fasman, G. D., *Methods in Enzymology* **6**, 928 (1963).
(26) Fasman, G. D., personal communication (1968).
(27) Fasman, G. D., Potter, J., *Biochem. Biophys. Res. Commun.* **27**, 209 (1967).
(28) Fernandez-Moran, Finean, J. B., *J. Biophys. Biochem. Cytol.* **3**, 725 (1957).
(29) Finean, J. B., "Biological Ultrastructure," 2nd ed., Academic Press, New York, 1967.
(30) Fleischer, S., Fleischer, B., Stoecknius, W., *J. Cell. Biol.* **32**, 193 (1967).
(31) Fleischer, S., Steim, J. M., unpublished data.
(32) Gent, W. L. G., Gregson, N. A., Gammack, D. B., Raper, J. H., *Nature* **204**, 553 (1964).
(33) Gerig, J., *J. Am. Chem. Soc.* **90**, 2681 (1968).
(34) Glazer, A. N., Simmons, N. S., *J. Am. Chem. Soc.* **87**, 2287 (1965).
(35) Green, D. E., Allman, D. W., Bachmann, E., Baum, H., Kopaczyk, K., Korman, E. F., Lipton, S., MacLenna, D. H., McConnell, D. G., Perdue, J. F., Pieske, J. S., Tzagoloff, A., *Arch. Biochem. Biophys.* **119**, 312 (1967).
(36) Green, D. E., Perdue, J. F., *Proc. Natl. Acad. Sci.* **55**, 1295 (1966).
(37) Greenfield, N. B. Davidson, Fasman, G. D., *Biochemistry* **6**, 1630 (1967).
(38) Grourke, M., personal communication (1968).
(39) Grourke, M., Gibbs, J. H., *Biopolymers* **5**, 586 (1967).
(40) Jardetzky, O., *Advan. Chem. Phys.* **7**, 512 (1964).
(41) Jirgensons, B., *J. Biol. Chem.* **240**, 1064 (1965).
(42) *Ibid.*, **241**, 147 (1966).
(43) Kates, M., Palameta, B., Perry, M. P., Adams, G. A., *Biochim. Biophys. Acta* **137**, 213 (1967).
(44) Kates, M., Palameta, B., Yengoyan, L. S., *Biochemistry* **4**, 1595 (1965).
(45) Kavanaugh, J. L., "Structure and Function of Biological Membranes," Holden-Day, San Francisco, 1965.
(46) Ke, B., *Arch. Biochem. Biophys.* **112**, 554 (1965).
(47) Korn, E. D., *Science* **153**, 1491 (1966).
(48) Ladbrooke, B. D., Williams, R. M., Chapman, D., *Biochim. Biophys. Acta* **150**, 333 (1966).
(49) Lawson, K. D., Flautt, T. J., "Liquid Crystals," G. H. Brown, G. J. Dienes, M. M. Labes, Eds., pp. 37-58, Gordon and Breach, New York, 1966.
(50) Lenard, J., Singer, S. J., *Proc. Natl. Acad. Sci.* **56**, 1828 (1966).
(51) Maddy, A. H., *Biochim. Biophys. Acta* **117**, 193 (1966).
(52) Maddy, A. H., Malcolm, B. R., *Science* **150**, 1617 (1965).
(53) *Ibid.*, **153**, 213 (1966).
(54) Mommaerts, W. F. H. M., *Proc. Natl. Acad. Sci.* **58**, 2476 (1967).
(55) Moor, H., Muhlethaler, K., *J. Cell Biol.* **17**, 609 (1963).

(56) Morowitz, H., personal communication (1968).
(57) Mueller, P. D., Rudin, D. O., Tien, H. T., Wescott, W. G., "Recent Progress in Surface Science," Vol. 1, Chap. 11, Academic Press, New York, 1964.
(58) Myers, D. V., Edsall, J. T., *Proc. Natl. Acad. Sci.* **53**, 169 (1964).
(59) Northcote, D. H., *British Med. Bull.* **25**, 107 (1968).
(60) Papahadjopoulos, D., Miller, N., *Biochim. Biophys. Acta* **135**, 624 (1967).
(61) Razin, S., Cosenza, B. J., Tourtellotte, M. E., *J. Gen. Microbiol.* **42**, 139 (1966).
(62) Razin, S., Tourtellotte, M. E., McElhaney, R. N., Pollack, J. D., *J. Bacteriol.* 91, 609 (1966).
(63) Richardson, S. H., Hultin, H. O., Fleischer, S., *Arch. Biochem. Biophys.* **105**, 254 (1964).
(64) Riddiford, L. M., *J. Biol. Chem.* **241**, 2792 (1966).
(65) Robertson, J. J., *Symp. Biochem. Soc. (Cambridge)* **16**, 3 (1959).
(66) Salton, M. R. J., Schmitt, M. D., *Biochem. Biophys. Res. Commun.* **27**, 529 (1967).
(67) Sarkar, P. K., Doty, P., *Proc. Natl. Acad. Sci.* **55**, 981 (1966).
(68) Saunders, L., *Biochim. Biophys. Acta* **125**, 70 (1966).
(69) Scanu, A., *Proc. Natl. Acad. Sci.* **54**, 1699 (1965).
(70) Sjostrand, F. S., *J. Ultrastruc. Res.* **9**, 340 (1967).
(71) Steim, J. M., "Abstracts of Papers," 153rd Meeting, ACS, April 1967, H59.
(72) Steim, J. M., *Arch. Biochem. Biophys.* 112, 599 (1965).
(73) Steim, J. M., Kaufman, S., Gibbs, J. H., unpublished data.
(74) Steim, J. M., Edner, O. J., Bargoot, F. G., *Science*, in press.
(75) Steim, J. M., Fleischer, S., *Proc. Natl. Acad. Sci.* **58**, 1292 (1967).
(76) Steim, J. M., Reinert, J. C., unpublished data.
(77) Steim, J. M., Reinert, J. C., Tourtellotte, M. E., Rader, R. L., McElhaney, R. N., *Nature*, in press.
(78) Steim, J. M., Swanton, J. R., unpublished data.
(79) Steim, J. M., Webster, W., unpublished data.
(80) Terry, T. M., Engelman, D. M., Morowitz, H. J., *Biochim. Biophys. Acta* **135**, 391 (1967).
(81) Tien, H. T., Diana, A. L., *Chem. Phys. Lipids* **2**, 55 (1968).
(82) Timasheff, S. N., Gorbunov, M. J., *Ann. Rev. Biochem.* **36**, 13 (1967).
(83) Timasheff, S. N., Susi, H., Townend, R., Stevens, L., Gorbunov, M. J., Kumosinski, T. F., "Conformation of Biopolymers," G. N. Ramachandran, Ed., Vol. 1, p. 173, Academic Press, New York, 1967.
(84) Townend, R., Kumosinski, T. F., Timasheff, S. N., *Biochem. Biophys. Res. Commun.* **23**, 163 (1966).
(85) Urnes, P., Doty, P., *Advan. Protein Chem.* **16**, 401 (1961).
(86) Urry, D. W., Mednieks, M., Bejnarowicz, E., *Proc. Natl. Acad. Sci.* **57**, 1043 (1967).
(87) Velluz, L., Legrand, M., Grosjean, M., "Optical Circular Dichroism," Academic Press, New York, 1965.
(88) Wallach, D. F. H., Gordon, A., personal communication (1968).
(89) Wallach, D. F. H., Zahler, P. H., *Proc. Natl. Acad. Sci.* **56**, 1552 (1966).
(90) Wallach, D. F. H., Zahler, P. H., *Biochim. Biophys. Acta* **150**, 186 (1968).
(91) Yang, J. T., McCabe, W. J., *Biopolymers* **3**, 209 (1965).

RECEIVED September 27, 1967.

INDEX

R

S

T

U

V

W